JOURNAL OF RESEARCH

OF THE U.S. GEOLOGICAL SURVEY

JULY–AUGUST 1977
VOLUME 5, NUMBER 4

Scientific notes and summaries of investigations in geology, hydrology, and related fields

U.S. DEPARTMENT OF THE INTERIOR

UNITED STATES DEPARTMENT OF THE INTERIOR
CECIL D. ANDRUS, Secretary
GEOLOGICAL SURVEY
V. E. McKelvey, Director

For sale by Superintendent of Documents, U.S. Government Printing Office, Washington, DC 20402. Annual subscription rate, $18.90 (plus $4.75 for foreign mailing). Make check or money order payable to Superintendent of Documents. Send all subscription inquiries and address changes to Superintendent of Documents at above address.

Purchase single copy ($3.15) from Branch of Distribution, U.S. Geological Survey, 1200 South Eads Street, Arlington, VA 22202. Make check or money order payable to U.S. Geological Survey.

Library of Congress Catalog-card No. 72-600241.

The Journal of Research is published every 2 months by the U.S. Geological Survey. It contains papers by members of the Geological Survey and their professional colleagues on geologic, hydrologic, topographic, and other scientific and technical subjects.

Correspondence and inquiries concerning the Journal (other than subscription inquiries and address changes) should be directed to Anna M. Orellana, Managing Editor, Journal of Research, Publications Division, U.S. Geological Survey, 321 National Center, Reston, VA 22092.

Papers for the Journal should be submitted through regular Division publication channels.

The Secretary of the Interior has determined that the publication of this periodical is necessary in the transaction of the public business required by law of this Department. Use of funds for printing this periodical has been approved by the Director of the Office of Management and Budget through June 30, 1980.

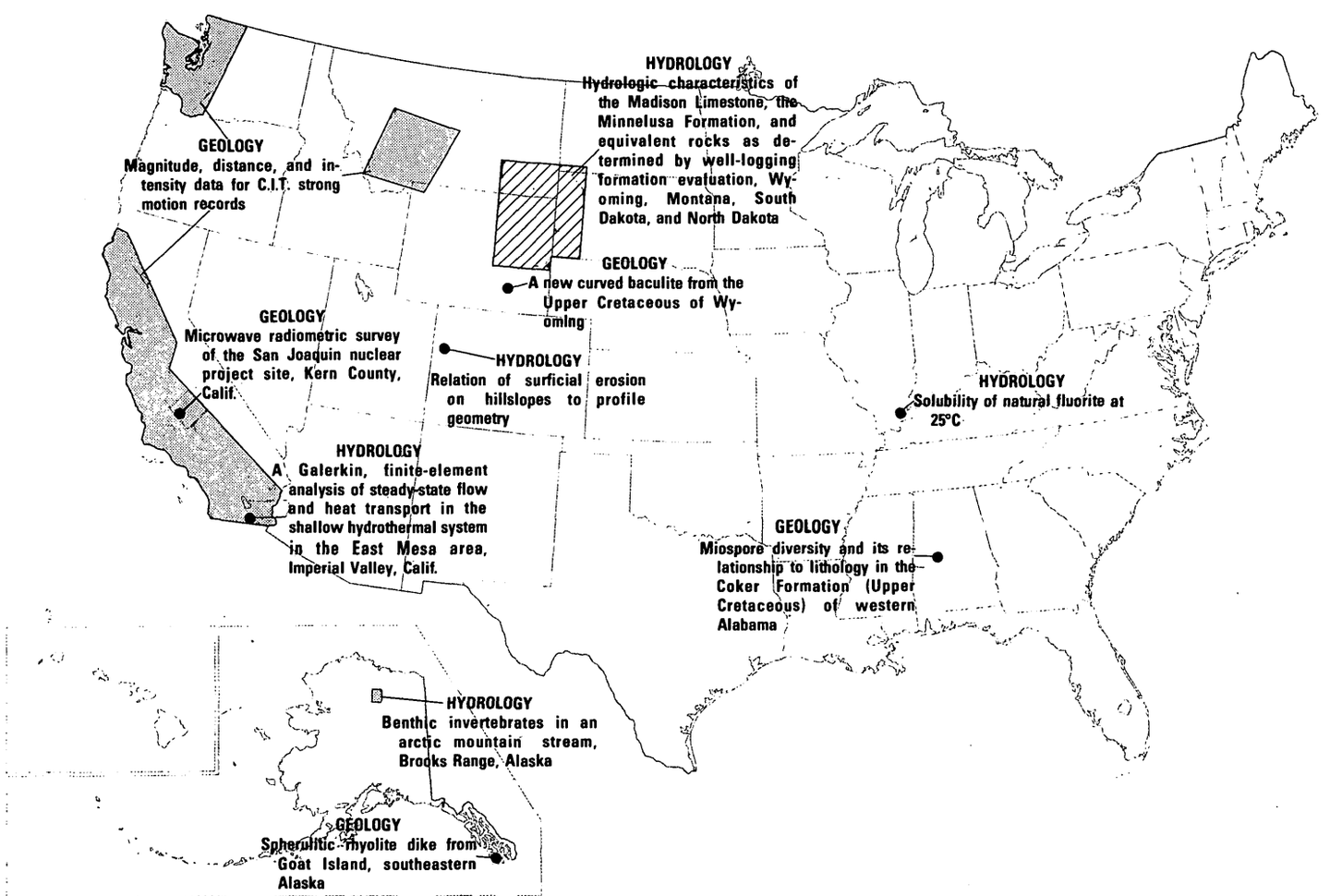

GEOGRAPHIC INDEX TO ARTICLES

See "Contents" for articles concerning areas outside the United States and articles without geographic orientation.

JOURNAL OF RESEARCH

of the

U.S. Geological Survey

Vol. 5 No. 4 July–August 1977

CONTENTS

SI UNITS AND U.S. CUSTOMARY EQUIVALENTS

[SI, International System of Units, a modernized metric system of measurement. All values have been rounded to four significant digits except 0.01 bar, which is the exact equivalent of 1 kPa. Use of hectare (ha) as an alternative name for square hectometer (hm^2) is restricted to measurement of land or water areas. Use of liter (L) as a special name for cubic decimeter (dm^3) is restricted to the measurement of liquids and gases; no prefix other than milli should be used with liter. Metric ton (t) as a name for megagram (Mg) should be restricted to commercial usage, and no prefixes should be used with it. Note that the style of $meter^2$ rather than square meter has been used for convenience in finding units in this table. Where the units are spelled out in text, Survey style is to use square meter]

SI unit		U.S. customary equivalent	
Length			
millimeter (mm)	=	0.039 37	inch (in)
meter (m)	=	3.281	feet (ft)
	=	1.094	yards (yd)
kilometer (km)	=	0.621 4	mile (mi)
	=	0.540 0	mile, nautical (nmi)
Area			
$centimeter^2$ (cm^2)	=	0.155 0	$inch^2$ (in^2)
$meter^2$ (m^2)	=	10.76	$feet^2$ (ft^2)
	=	1.196	$yards^2$ (yd^2)
	=	0.000 247 1	acre
$hectometer^2$ (hm^2)	=	2.471	acres
	=	0.003 861	section (640 acres or 1 mi^2)
$kilometer^2$ (km^2)	=	0.386 1	$mile^2$ (mi^2)
Volume			
$centimeter^3$ (cm^3)	=	0.061 02	$inch^3$ (in^3)
$decimeter^3$ (dm^3)	=	61.02	$inches^3$ (in^3)
	=	2.113	pints (pt)
	=	1.057	quarts (qt)
	=	0.264 2	gallon (gal)
	=	0.035 31	$foot^3$ (ft^3)
$meter^3$ (m^3)	=	35.31	$feet^3$ (ft^3)
	=	1.308	$yards^3$ (yd^3)
	=	264.2	gallons (gal)
	=	6.290	barrels (bbl) (petroleum, 1 bbl=42 gal)
	=	0.000 810 7	acre-foot (acre-ft)
$hectometer^3$ (hm^3)	=	810.7	acre-feet (acre-ft)
$kilometer^3$ (km^3)	=	0.239 9	$mile^3$ (mi^3)
Volume per unit time (includes flow)			
$decimeter^3$ per second (dm^3/s)	=	0.035 31	$foot^3$ per second (ft^3/s)
	=	2.119	$feet^3$ per minute (ft^3/min)
Volume per unit time (includes flow)—Continued			
$decimeter^3$ per second (dm^3/s)	=	15.85	gallons per minute (gal/min)
	=	543.4	barrels per day (bbl/d) (petroleum, 1 bbl=42 gal)
$meter^3$ per second (m^3/s)	=	35.31	$feet^3$ per second (ft^3/s)
	=	15 850	gallons per minute (gal/min)
Mass			
gram (g)	=	0.035 27	ounce avoirdupois (oz avdp)
kilogram (kg)	=	2.205	pounds avoirdupois (lb avdp)
megagram (Mg)	=	1.102	tons, short (2 000 lb)
	=	0.984 2	ton, long (2 240 lb)
Mass per unit volume (includes density)			
kilogram per $meter^3$ (kg/m^3)	=	0.062 43	pound per $foot^3$ (lb/ft^3)
Pressure			
kilopascal (kPa)	=	0.145 0	pound-force per $inch^2$ (lbf/in^2)
	=	0.009 869	atmosphere, standard (atm)
	=	0.01	bar
	=	0.296 1	inch of mercury at 60°F (in Hg)
Temperature			
temp kelvin (K)	=	[temp deg Fahrenheit (°F)+459.67]/1.8	
temp deg Celsius (°C)	=	[temp deg Fahrenheit (°F)−32]/1.8	

The policy of the "Journal of Research of the U.S. Geological Survey" is to use SI metric units of measurement except for the following circumstance:

When a paper describes either field equipment or laboratory apparatus dimensioned or calibrated in U.S. customary units and provides information on the physical features of the components and operational characteristics of the equipment or apparatus, then dual units may be used. For example, if a pressure gage is calibrated and available only in U.S. customary units of measure, then the gage may be described using SI units in the dominant position with the equivalent U.S. customary unit immediately following in parentheses. This also applies to the description of tubing, piping, vessels, and other items of field and laboratory equipment that normally are described in catalogs in U.S. customary dimensions.

S. M. LANG, *Metrics Coordinator,*
U.S. Geological Survey

Jour. Research U.S. Geol. Survey
Vol. 5, No. 4, July–Aug. 1977, p. 403–404

APPLICATION OF A SELENIUM HYDRIDE–ATOMIC ABSORPTION TECHNIQUE TO TEST FOR HOMOGENEITY OF USGS STANDARD ROCKS

By L. P. GREENLAND and E. Y. CAMPBELL, Reston, Va.

Abstract.—After acid decomposition of the sample, selenium hydride was generated by means of sodium borohydride, and the gas was swept through a resistance-heated quartz cell mounted in an atomic absorption spectrometer to determine as little as 5 ng/g selenium in 0.25 g rock sample. One-way analyses of variance of data from nine USGS standard rocks indicated no significant differences in selenium content among bottles of any of these rocks.

Studies of the geochemistry of selenium have been limited largely to selenium's occurrence in sulfide minerals and in soils because of the lack of sufficiently sensitive analytical methods. Sindeeva (1964) in his comprehensive investigation of selenium relied on chemically concentrating the element from very large samples to obtain detection limits of 0.1 μg/g selenium, which is barely adequate for most rocks. Neutron-activation techniques (Brunfelt and Steinnes, 1967; Lavrakas and others 1974) are very sensitive, but the need for radiochemical separations apparently has precluded the routine analysis of large numbers of samples.

Hydride generation–atomic absorption techniques are being used for the rapid determination of submicrogram amounts of selenium in simple (mostly organic) matrices (Vijan and Wood, 1976; Fiorino and others 1976). The present paper describes the application of these techniques to the analysis of rocks in an investigation of the variability of selenium among bottles of the USGS standard rocks.

EXPERIMENTAL METHOD

Hydride apparatus.—The apparatus has been described in detail elsewhere (Greenland and Campbell, 1976). A 25-mL generating flask, having a side arm which allows injection of the borohydride solution, is connected by a spray trap (a 50-mL test tube) to a resistance-heated quartz cell mounted in the light path of an atomic absorption spectrometer. The cell temperature is maintained at about 1000°C by means of a variable transformer. A nitrogen stream (4–4.5 L/min) is passed through the system continuously.

Borohydride solution.—5 g sodium borohydride is dissolved in 100 mL water which contains two pellets of sodium hydroxide.

Selenium standard solution.—100 mg selenium metal is dissolved in a minimal volume of aqua regia with heating and diluted to 100 mL with 6 *M* hydrochloric acid. Just before use, an aliquot of the stock solution is diluted with 6 *M* hydrochloric acid to provide a 200 ng/mL selenium standard solution.

Procedure.—5 mL nitric acid is added to 0.25 g silicic rock, or 0.1 g basalt, in a Teflon beaker and evaporated to dryness on a hotplate at 150°C. The evaporation is repeated, first with 5 mL nitric plus 5 mL hydrofluoric acids and then with 1 mL nitric plus 5 mL hydrofluoric plus 0.5 mL perchloric acids. The residue is dissolved in 5 mL 6 *M* hydrochloric acid. The entire rock solution is decanted into the hydride generating flask, and an automatic pipet containing 1 mL of the borohydride solution is inserted through the side neck of the flask. When the recorder has returned to a stable baseline, the borohydride is injected and the peak height of the transient selenium absorbance signal is measured from the recorder trace. Standards, 2–25 ng selenium in 5 mL of 6 *M* hydrochloric acid, are measured similarly and sample concentrations are obtained by direct comparison.

RESULTS AND DISCUSSION

Most of the apparatus and procedure described here is the same as we used previously (Greenland and Campbell, 1976) for the determination of tellurium. The major difference is in the decomposition of the sample. Preliminary experiments with ^{75}Se tracer demonstrated that losses of selenium occurred when rocks were evaporated with hydrofluoric acid and that these losses could be avoided by a prior evaporation with nitric acid. Interestingly, losses did not take place when ^{75}Se tracer was evaporated with hydrofluoric acid in the absence of rock powders; further, analysis of rock solutions from which most of the tracer had been lost showed that selenium originally in the rock was retained. Selenium was apparently volatilized only during the initial reaction of the acid with rock powder and before selenium dissolved from the sample. The

^{75}Se tracer was not lost during the nitric acid attack, or subsequently, and thus prior evaporation of the sample with nitric acid is recommended.

This procedure has been applied to the determination of selenium in some USGS standard rocks. A one-way analysis of variance experiment (Flanagan, 1976) permitted a test of the homogeneity of the bottles as well as estimates of the analytical error and mean content of selenium.

For this purpose, three bottles of each of nine standard rocks were selected at random. Four portions of each bottle were randomized among the set of 108 samples and analyzed to provide the data shown in table 1. The analyses of variance (table 2) showed no significant differences among bottles of any of the standard rocks at the 95-percent confidence level.

In table 3, the mean and analytical error derived from the analyses of variance are compared with neutron-activation analyses of Brunfelt and Steinnes (1967), and of Lavrakas and others (1974). Except for GSP-1, the two independent techniques are in satisfactory agreement. For GSP-1, our value is distinctly greater than that of Brunfelt and Steinnes but agrees well with Lavrakas and others.

The agreement of the two independent analytical methods, the wide variance of selenium content, and the absence of demonstrable bottle heterogeneity make the USGS standard rocks ideal controls for geochemical studies, whereas the simplicity and sensitivity of the hydride-generation technique make such studies feasible.

TABLE 1.—*Selenium, in nanograms per gram, in nine USGS standard rocks*

Rock	Bottle		
	A	B	C
SDC–1, schist	38.8	43.4	41.1
	39.9	43.0	37.6
	39.6	39.6	36.5
	37.3	30.5	41.1
RGM–1, rhyolite	6.4	7.5	7.5
	2.9	6.4	1.0
	4.5	6.7	6.1
	1.1	4.5	5.6
QLO–1, quartz latite	9.9	9.9	11.0
	11.3	7.5	4.9
	11.3	9.9	10.7
	12.4	8.4	6.6
GSP–1, granodiorite	82.1	72.3	76.9
	78.1	73.4	78.7
	73.6	64.5	81.0
	69.0	74.7	83.8
STM–1, nepheline syenite	9.9	7.2	13.3
	11.0	10.7	3.8
	9.0	6.1	9.5
	6.7	9.0	8.4
BHVO–1, basalt	128	134	138
	137	142	145
	135	137	134
	121	150	128
G–2, granite	12.2	8.7	11.8
	8.4	10.7	14.1
	10.1	10.1	6.7
	5.6	7.9	11.3
AGV–1, andesite	15.6	8.7	10.7
	12.2	7.2	11.8
	7.2	9.0	9.0
	6.7	14.7	10.1
BCR–1, basalt	93.5	101	98.5
	105	102	96.6
	98.5	102	107
	98.1	96.6	92.4

TABLE 2.—*Analyses of variance of data obtained from the determination of selenium content of nine USGS standard rocks*

[d.f., degrees of freedom]

Rock	Sum of squares		F ratio [1]	Mean (ng/g Se)	Analytical error (ng/g Se)
	Among bottles (d.f.=2)	Within bottles (d.f.=9)			
GSP–1	157.5	185.9	3.8	75.7	4.5
STM–1	1.627	68.19	.1	8.7	2.8
QLO–1	18.98	34.86	2.4	9.5	2.0
RGM–1	13.01	43.98	1.3	5.0	2.2
SDC–1	.1117	129.0	.003	39.0	3.8
G–2	8.435	57.98	.7	9.8	2.5
AGV–1	.7017	90.89	.03	10.2	3.2
BHVO–1	222.0	458.2	2.2	135.8	7.1
BCR–1	7.752	200.0	.2	99.3	4.7

[1] $F_{0.95}(2,9)=4.3$.

TABLE 3.—*Comparison of selenium determinations, in nanograms per gram, of five USGS standard rocks*

Rock	This work (table 2)	Neutron activation	
		Brunfelt and Steinnes (1967)	Lavrakas and others (1974)
STM–1	8.7±2.8	12, 8	----------
GSP–1	75.7±4.5	63, 55	87, 84, 66
G–2	9.8±2.5	5	8, 6, 5
BCR–1	99.3±4.7	112, 93	----------
AGV–1	10.2±3.2	9, 7	9, 9, 8, 7

REFERENCES CITED

Brunfelt, A. O., and Steinnes, Eiliv, 1967, Determination of selenium in standard rocks by neutron activation analysis: Geochim. et Cosmochim. Acta, v. 31, p. 283–285.

Fiorino, J. A., Jones, J. W., and Capar, S. G., 1976, Sequential determination of arsenic, selenium, antimony, and tellurium in foods via rapid hydride evolution and atomic absorption spectrometry: Anal. Chemistry, v. 48, p. 120–125.

Flanagan, F. J., 1976, Descriptions and analyses of eight new USGS rock standards: U.S. Geological Survey Prof. Paper 840, 192 p.

Greenland, L. P., and Campbell, E. Y., 1976, Rapid determination of nanogram amounts of tellurium in silicate rocks: Anal. Chim. Acta. (In press.)

Lavrakas, V., Golembeski, T. J., Pappas, G., Gregory, J. E., and Wedlick, H. L., 1974, Modified approach for submicrogram determination of selenium in United States Geological Survey standard rocks: Anal. Chemistry, v. 46, p. 952–954.

Sindeeva, N. D., 1964, Mineralogy and types of deposits of selenium and tellurium: New York, Interscience, 363 p.

Vijan, P. N., and Wood, G. R., 1976, An automated submicrogram determination of selenium in vegetation by quartz-tube furnace atomic-absorption spectrophotometry: Talanta, v. 23, p. 89–94.

Jour. Research U.S. Geol. Survey
Vol. 5, No. 4, July–Aug. 1977, p. 405–408

DETERMINATION OF ARSENIC, ANTIMONY, AND SELENIUM IN COAL BY ATOMIC ABSORPTION SPECTROMETRY WITH A GRAPHITE TUBE ATOMIZER

By PHILIP ARUSCAVAGE, Reston, Va.

Abstract.—Submicrogram quantities of antimony, arsenic, and selenium in coal samples are determined by an atomic absorption procedure using an electrically heated graphite atomizer. The samples are decomposed in a mixture of nitric, sulfuric, and perchloric acids and are separated and concentrated by extraction from sulfuric acid-iodide solution into toluene. The results obtained on several intralaboratory reference samples and the National Bureau of Standards coal 1632 are compared with results from other methods. The determination can be made routinely for concentrations as small as 0.1 parts per million for arsenic, antimony, and selenium in the coal.

Environmental concerns have stimulated interest in the determination of trace elements in coal, especially the toxic elements, such as mercury, selenium, arsenic, and antimony. This has caused a reevaluation of older methods and an attempt to develop new methods which are not only sensitive but able to handle many samples on a routine basis. (Lehmden and others, 1974). Methods for the determination of antimony, arsenic, and selenium have been described recently, (Mesman and Thomas, 1975; Ondov and others, 1975; Golembeski, 1975; Schnepfe, 1974; Byrne and Gorenc, 1972; Thompson and Thomerson, 1974).

The electrically heated graphite-furnace accessory to the atomic absorption spectrometer, because of its very low detection limits for most elements and its small sample volume requirement, is finding increased applications. Because of the high atomization temperatures obtained with the furnace, elements which can be determined only with difficulty by flame methods can be readily determined with this technique. (Mesman and Thomas, 1975; Shaw and Ottaway, 1975).

The method described here, utilizing the graphite-furnace technique, is rapid (about 75 samples per day per element) and sufficiently sensitive to determine 0.1 parts per million of arsenic, antimony, or selenium in a 100-milligram sample of coal.

REAGENTS AND APPARATUS

Antimony standard solution (100 ppm Sb): Dissolve 0.1200 gram of reagent grade Sb_2O_3 in 50 milliliters of 2*N* NaOH. Dilute to 1000 mL with H_2O and store in a plastic bottle. Prepare a 1.0-ppm antimony standard by dilution of the above with 1 *N* NaOH.

Selenium standard solution (100 ppm Se): Dissolve 0.100 g of reagent grade selenium metal with 10 mL of nitric acid. Evaporate to near dryness on a steam bath and transfer to a 1-liter volumetric flask with 1 *N* HCl. Prepare a 1.0-ppm selenium standard by dilution of the above with H_2O.

Arsenic standard solution (100 ppm As): Dissolve 0.1320 reagent grade As_2O_3 in 50 mL of 2 *N* NaOH. Dilute to 1000 mL with H_2O and store in a plastic bottle. Prepare a 1.0-ppm arsenic standard by dilution of the above with 0.1 *N* NaOH.

Nickel nitrate solution (1 mg/mL): Dissolve 2.47 g of $Ni(NO_3)_2 \cdot 6H_2O$ in 500 mL of 0.5-percent nitric acid.

Sodium iodide solution (6 *M*): Dissolve 90 g of reagent grade NaI in H_2O and dilute to 100 mL. Prepare a 0.06 *M* NaI solution by a 1 to 100 dilution of the above.

Atomic absorption spectrophotometer: A Perkin Elmer model 303 equipped with a Perkin Elmer graphite tube furnace, model HG–2100 controller, and Perkin Elmer electrodeless discharge lamps was used for all measurements. The instrument settings are given in table 1.

Test tubes: Ground glass 17×180 millimeters.

Air condensers: 20-mm-long 19/38 inner ground joints.

Aluminum heating block: A 30×30×8-cm aluminum block with 64 holes, 18 mm diameter, to accept the above test tubes.

TABLE 1.—*Atomic absorption spectrophotometer instrument settings for the determination of antimony, arsenic, and selenium in coal samples*

	Antimony	Arsenic	Selenium
Slit	3	5	4
Wavelength, nm	217.6	193.6	196.0
Scale expansion	3X	3X	3X
Gas flow	Interrupt	Interrupt	Interrupt
Gas	Argon	Argon	Argon
Dry temperature, °C/s	110/30	110/30	110/30
Charring temperature, °C/s	500/40	900/40	900/40
Atomization temperature, °C/s	2500/6	2500/6	2500/6

PROCEDURE

To 0.100 g of powdered coal in a test tube, and 5 mL of concentrated HNO_3 and 3 mL of concentrated H_2SO_4. To separate test tubes, add 0.02 to 0.5 μg of As, Sb, and Se from the 1.0-ppm standard solutions, add the above acids, and process along with samples. Add an alundum boiling stone to prevent bumping, fit with an air condenser, and heat in an aluminum block on a hot plate at 200°C for 30 min. Cool; add 3 mL of concentrated $HClO_4$ and heat at 200°C until the nitric acid is removed (about 3 hours). Remove the air condenser and continue heating overnight to remove perchloric acid. Cool; add 5 mL of H_2O and 2 mL of 20-percent ascorbic acid, and mix. Add 1 mL of 0.06*M* NaI and mix. Add 2 mL of toluene and extract for 1 min. Using a 20-microliter Eppindorf pipet, or equivalent, take an aliquot of the toluene layer and pipet into the graphite furnace. Immediately start the cycle and record the peak height under the conditions set up for antimony (table 1). Determine the amount of antimony by comparison with the standard solutions. For the determination of arsenic or selenium, add 1 mL of 6*M* NaI to the same solutions and reextract for 1 min. Pipet 20 μL of the nickel nitrate solution into the graphite furnace and dry manually for 15 s. Pipette a 10-μL aliquot of the toluene layer into the graphite furnace and record the peak height using the settings in table 1 for either arsenic or selenium. Determine the amount of arsenic or selenium by comparing with processed standard solutions.

RESULTS AND DISCUSSION

The toluene extraction of arsenic, antimony ,and selenium as iodides from sulfuric acid–iodide media has been described in detail previously (Byrne and Gorenc, 1972). From data given, conditions were chosen for the extraction of arsenic, antimony, and selenium to insure complete extraction. Ascorbic acid was added to initially reduce those elements which may rapidly oxidize the iodide and possibly cause low extraction yields. The yield for antimony through the entire procedure was checked by means of an Sb^{125} tracer added to 0.1 g of coal. A yield of greater than 97 percent was obtained, indicating no significant losses for antimony either during the digestion or upon extraction. Also, processed standards agree with unprocessed standards, thereby further verifying that no significant losses of As, Sb, or Se took place during digestion.

The speed and reliability of the decomposition were increased by using the test tube–aluminum block combination. This arrangement provides good refluxing without the need for transferring the sample prior to extraction.

The optimum conditions for the graphite furnace were determined from experimental curves of charring temperature versus absorption signal. The highest charring temperature before appreciable losses took place was used. The use of $Ni(NO_3)_2$ solution, as described in the Perkin Elmer manual, was found to prevent the losses of arsenic and selenium and to allow charring up to 900°C. Without the nickel nitrate solution, the losses of arsenic and selenium were significant at 500°C. With the conditions outlined in the procedure, background correction was not necessary for any of these elements, and the curves for each of the three elements were linear to as much as approximately 1.5 ng. Samples which were greater than this amount were diluted with additional toluene in order to be on the linear part of the working curve.

The pipetting of the small volumes of organic solvent with the disposable plastic-tipped pipet is one of the most significant sources of error in the determination. Reproducibility was significantly improved by reaming the graphite tube to allow the plastic tip to touch the bottom and thus remove the droplet by capillary action.

Tables 2–4 show the results of determinations of arsenic, antimony, and selenium in replicate on several coal samples. They compare favorably with results of determinations by other techniques on most of the samples. The poor precision on some of these coal samples may be due to the lack of homogenity for certain elements when only a 100-mg sample is taken.

TABLE 2.—*Estimate of antimony content, in parts per million*
[Instrumental neutron activation analysis: J. J. Rowe, written commun., 1975. Colorimetric: M. M. Schnepfe, written commun., 1975]

Coal sample	This method	Mean ± σ	Instrumental neutron activation analysis	Colorimetric
24D --------	1.2, 1.1, 1.2, 1.1	1.2 ± 0.06	2.3	2.4, 1.7
31 --------	0.4, 0.2, 0.2, 0.2	0.3 ± 0.10	0.4	0.3, 0.4
1A --------	0.1, 0.1, 0.2, 0.2	0.2 ± 0.06	0.4	0.1, 0.3
10 --------	0.8, 0.7, 0.7, 0.9	0.8 ± 0.10	0.7, 2.0	1.2, 1.3, 1.7
26 --------	0.5, 0.5, 0.5, 0.5	0.5 ± 0	0.9	1.2, 1.6
30 --------	0.2, 0.1, 0.2, 0.1	0.2 ± 0.06	0.3	0.7, 0.3
8 --------	0.2, 0.2, 0.1, 0.1	0.2 ± 0.06	0.5, 0.3, 0.4	1.4, 1.0
14 --------	0.2, 0.2, 0.2, 0.3	0.2 ± 0.05	0.6	0.3, 0.5
NBS-1632 ---	1.8, 1.1, 3.0, 1.1	1.8 ± 0.9	5.6, 0.9, 2.1, 2.0	2.3 to 5.8

TABLE 3.—*Estimate of arsenic content, in parts per million*
[Instrumental neutron activation analysis: J. J. Rowe, written commun., 1975. Colorimetric: M. M. Schnepfe, written commun., 1975]

Coal sample	This method	Mean ± σ	Instrumental neutron activation analysis	Colorimetric
24D --------	5.8, 5.0, 5.4	5.4 ± 0.40	5.9	5.1, 5.5
31 ---------	2.4, 2.5, 2.2, 2.0	2.3 ± 0.22	2.2	2.0, 2.4
1A ---------	0.3, 0.5, 0.5, 0.5	0.5 ± 0.10	0.7	0.6, 0.5
10 ---------	11.1, 10.8, 12.5, 10.8	11.3 ± 0.81	11.2, 12.2	11.1, 10.8
26 ---------	1.9, 1.8, 2.1, 2.2	2.0 ± 0.18	1.8	2.1, 1.9
30 ---------	3.6, 3.6, 3.8, 3.7	3.7 ± 0.10	3.6	3.5, 3.4
8 ---------	1.5, 1.7, 1.7, 1.6	1.6 ± 0.10	1.6, 1.9	1.7, 1.5
14 ---------	2.3, 2.4, 2.9, 3.1	2.7 ± 0.39	2.8, 2.4, 2.6	2.5, 2.8
NBS-1632 ---	5.8, 5.9, 5.1, 5.6	5.6 ± 0.36	5.8, 5.4, 5.3, 5.8, 5.8	5.6, 5.5, 5.8, 4.6, 5.5

TABLE 4.—*Estimate of selenium content, in parts per million*

[Instrumental neutron activation anaysis: J. J. Rowe, written commun., 1975. X-ray analysis: J. S. Wahlberg, written commun., 1975, NBS–1632 Certificate value, 2.9±0.3 ppm]

Coal sample	This method	Mean ± σ	Instrumental neutron activation analysis	X-ray analysis
24D --------	3.1, 3.1, 3.8, 3.6	3.4 ± 0.36	4.9	5.0
31 --------	4.3, 4.8, 4.1, 4.4	4.4 ± 0.29	3.7	4.3
1A --------	4.0, 3.8, 3.8, 4.0	3.9 ± 0.11	4.1	3.7
10 --------	5.9, 6.2, 5.8, 5.6	5.9 ± 0.25	6.9, 6.7, 7.1	6.3
26 --------	1.7, 1.9, 1.9, 1.9	1.9 ± 0.10	----------	2.0
30 --------	2.2, 2.5, 2.4, 2.7	2.5 ± 0.21	2.5	2.2
8 --------	1.1, 1.0, 1.0, 1.1	1.1 ± 0.06	1.5, 1.3	.8
14 --------	4.0, 3.4, 3.7, 4.5	3.9 ± 0.47	4.3, 4.0, 4.1	3.3
NBS-1632 ---	2.4, 2.6, 2.6, 2.8	2.6 ± 0.16	----------	2.9, 2.6, 3.1, 3.1

This is especially evident in the National Bureau of Standards coal 1632 where poor precision for antimony was observed by many methods in a variety of laboratories (Ondov and others, 1975).

REFERENCES CITED

Byrne, A. R., and Gorenc, D., 1972, The toluene extraction of some elements as iodides from sulfuric acid-potassium iodide media—Application to neutron activation analysis: Anal. Chim. Acta, v. 59, p. 81–89.

Golembeski, T., 1975, Determination of submicrogram amounts of selenium in rocks by atomic absorption spectroscopy: Talanta, v. 22, p. 547–549.

Lehmden, D. J., von, Jungers, R. H., and Lee R. E., 1974, Determination of trace elements in coal, fly ash, fuel oil and gasoline—preliminary comparison of selected analytical techniques: Anal. Chemistry, v. 46, no. 2, p. 239–245.

Mesman, B. B., and Thomas, T. C., 1975, A study of two atomic absorption methods for the determination of submicrogram amounts of arsenic and selenium: Anal. Letters, v. 8, no. 7, p. 449–459.

Ondov, J. M., Zoller, W. H., Olmez, I., Aras, N. K., Gordon, G. E. Rancitelli, L. A., Abel, K. H. Filby, R. H., Shah, K. R., and Ragaini, R. C. 1975. Elemental concentrations in the National Bureau of Standards environmental coal and fly ash reference materials: Anal. Chemistry, v. 47, no. 7, p. 1102–1109.

Schnepfe, M. M., 1974, Spectrofluorometric procedure using 2,3-naphthalenediamine for determining selenium in rocks: U.S. Geol. Survey, Jour. Research, v. 2, no. 5, p. 631–636.

Shaw, F., and Ottaway, J. M., 1975, The determination of trace amounts of aluminum and other elements in iron and steel by atomic absorption spectrometry with carbon furnace atomization: Analyst, v. 100, no. 1189, p. 217–228.

Thompson, K. C., and Thomerson, D. R., 1974, Atomic absorption studies on the determination of antimony, arsenic, bismuth, germanium, lead, selenium, tellurium, and tin by utilizing the generation of covalent hydrides: Analyst, v. 99, p. 595–601.

Jour. Research U.S. Geol. Survey
Vol. 5, No. 4, July–Aug. 1977, p. 409–412

CHEMICAL DISSOLUTION OF SULFIDE MINERALS

By T. T. CHAO and R. F. SANZOLONE, Denver, Colo.

Abstract.—Chemical dissolution treatments involving the use of aqua regia, 4 *N* HNO_3, H_2O_2-ascorbic acid, oxalic acid, $KClO_3$+HCl, and $KClO_3$+HCl followed by 4 *N* HNO_3 were applied to specimens of nine common sulfide minerals (galena, chalcopyrite, cinnabar, molybdenite, orpiment, pyrite, stibnite, sphalerite, and tetrahedrite) mixed individually with a clay loam soil. The resultant decrease in the total sulfur content of the mixture, as determined by using the Leco induction furnace, was used to evaluate the effectiveness of each chemical treatment. A combination of $KClO_3$+HCl followed by 4 *N* HNO_3 boiling gently for 20 min has been shown to be very effective in dissolving all the sulfide minerals. This treatment is recommended to dissolve metals residing in sulfide minerals admixed with secondary weathering products, as one step in a fractionation scheme whereby metals in soluble and adsorbed forms, and those associated with organic materials and secondary oxides, are first removed by other chemical extractants.

Many of the ore-forming metals are major constituents of sulfide minerals in rocks. During the course of weathering, sulfide minerals undergo disintegration and decomposition, releasing the metals to the secondary environment. The dispersion patterns of these metals are influenced to varying degrees by chemical parameters of the surroundings and by absorption-desorption reactions between metal ions and solid components of stream sediments and soils. A knowledge of the distribution of a given metal or metals in different chemical forms in the secondary environment may provide information that is valuable at two levels of the geochemical exploration process: (1) during the orientation phase, such knowledge assists the researcher to select sample media and extraction procedures for a given problem and area and (2) during the followup phase, it helps the researcher to evaluate the significance of metal anomalies. A scheme detailing metal distribution may be constructed if a fractionation procedure can be developed to distinguish metals in various, specific forms: (1) soluble-exchangeable metals (usually only a very small portion), (2) metals specifically adsorbed on clays, (3) metals chelated by soluble and humified organic matter, (4) metals associated with manganese-, iron-, and aluminum-oxides or with amorphous materials, (5) metals residing in sulfide minerals, and (6) metal constituents of a silicate matrix. This paper is concerned with chemical dissolution of sulfide minerals that may be residual or mechanically transported away from their original sites, as related to the fifth category in the above procedure.

Several chemical reagents have been employed for the dissolution of sulfide minerals, including aqua regia (Stanton, 1966), nitric and tartaric acids (Rubeška, 1968), hydrogen peroxide–ascorbic acid (Smirnova and others, 1968; Lynch, 1971), water-bromine (Czamanske and Ingamells, 1970), and a solution of bromine in carbon tetrachloride and nitric acid (Hubert and Lakin, 1973). The potassium chlorate–hydrochloric acid method described by Dolezal, Povondra, and Sulcek (1968) was recently evaluated by Olade and Fletcher (1974) for its selectivity in dissolving sulfide minerals from rocks.

Chemical dissolution of sulfide minerals generally relies on the oxidation of sulfide to sulfate, which renders the associated metals soluble. In the present study, nine common sulfide minerals were finely ground and individually mixed with a clay loam soil to approximate their occurrence in natural samples which had been ground in the preparation process. The mixtures were then subjected to various chemical treatments (detailed below), and the sulfate ion generated in these processes was removed by replacement with phosphate. The decrease in the total sulfur content as a result of a chemical treatment is a measure of the treatment's effectiveness in dissolving a given sulfide mineral.

Acknowledgments.—The authors thank H. W. Lakin, U.S. Geological Survey, for furnishing the sulfide minerals used in this study and Z. E. Stephenson, U.S. Geological Survey, for assisting with the total sulfur determination.

MATERIALS AND METHODS

Nine sulfide minerals (table 1) were ground and mixed individually at a 1:9 ratio with a clay loam soil.

TABLE 1.—*Sulfide minerals used in this study*

Sulfide mineral	Description
Galena	PbS with small amounts of sphalerite and dolomite.
Chalcopyrite	$CuFeS_2$, yellow copper ore.
Cinnabar	HgS with pyrite and basaltic volcanic rock.
Molybdenite	MoS_2 with ferrimolybdite, quartz, and feldspar.
Orpiment	As_2S_3 with small amounts of realgar and calcite.
Pyrite	FeS_2 with small amounts of feldspar and clay.
Stibnite	Sb_2S_3 with quartz and clay.
Sphalerite	(Zn, Fe) S with chalcedony and dolomite.
Tetrahedrite	$(Cu, Fe, Zn, Ag,)_{12}Sb_3S_{13}$.

The mixtures were further homogenized in a ceramic-plate mill to a fineness of −150 mesh (105 μm). Half-gram samples of the mixtures were subjected to various chemical treatments. These treatments include not only digestion techniques that have been recommended in the literature but also previously untried procedures for the dissolution of sulfide minerals. Each treatment was applied to duplicate samples of all nine minerals.

These treatments follow:

1. Aqua regia: 500-mg samples were mixed with 12.5 mL aqua regia (3 vol HCl + 1 vol HNO_3) in 50-mL beakers and heated to dryness. The residues were washed with 5 mL concentrated HCl plus 5 mL H_2O into 50-mL polypropylene tubes, and the wash solutions were separated at 18 000 r/min for 10 min in a Sorvall RC2–B centrifuge.
2. 4 *N* HNO_3, 10 min boil: 500-mg samples were gently boiled with 4 *N* HNO_3 in 50-mL beakers for 10 min. The contents of the beakers were transferred with 10 mL H_2O to polypropylene tubes and centrifuged as in treatment 1.
3. 4 *N* HNO_3, dryness: Same as in treatment 2, except that the suspensions of samples in 4 *N* HNO_3 were boiled until dry.
4. H_2O_2-ascorbic acid: 500-mg samples were reacted in polypropylene tubes with 35 mL H_2O_2-ascorbic acid solution (prepared by adding 200 mL 30 percent H_2O_2 to 500 mL 2 percent ascorbic acid) for about 18 h (overnight) with occasional mixing (Lynch, 1971). After treatment, the solution was separated by centrifugation.
5. Oxalic acid: 500-mg samples were gently boiled with 10 mL 3 percent oxalic acid for 10 min and then were transferred with 10 mL H_2O to polypropylene tubes for centrifugation.
6. $KClO_3$ + HCl once: 500-mg samples were weighed into polypropylene tubes, and an equal weight of $KClO_3$ was added, followed by 10 mL concentrated HCl. After standing for 30 min, the solution was diluted with 10 mL H_2O, was mixed, and then was centrifuged to separate the supernatant solution (Olade and Fletcher, 1974).
7. $KClO_3$ + HCl twice: 500-mg samples were treated with $KClO_3$ + HCl twice.
8. $KClO_3$ + HCl followed by 4 *N* HNO_3, 10-min boil: 500-mg samples were treated with $KClO_3$ + HCl as in treatment 6, and the resulting residue was gently boiled with 4 *N* HNO_3 for 10 min as in treatment 2.
9. $KClO_3$ + HCl followed by 4 *N* HNO_3, 20-min boil: Same as treatment 8, except that the 4 *N* HNO_3-boil was for 20 min.
10. $KClO_3$ + HCl followed by 4 *N* HNO_3, dryness: Essentially treatment 6 plus treatment 3 in sequence.

After a given chemical treatment was completed, residues were equilibrated by occasional shaking on a tube vibrator for 10 min with 10 mL KH_2PO_4 (500 μg/mL P) to replace the sulfate ion (Chao and others, 1962) and were then washed with 10 mL 0.50 M $CaCl_2$. The samples left in the tubes after washing were dried at 70°C for about 4 h and then were weighed to determine weight losses caused by the chemical treatment. They were then ground in a mortar, and duplicate analyses for total sulfur as sulfide were performed by the Leco induction-furnace method, whereby the generated SO_2 was titrated with potassium iodate. The effectiveness of each chemical treatment was measured by the decrease in the total sulfur content as compared to that of the untreated but washed samples.

The limit of determination of sulfur by the Leco induction-furnace method was 0.01 percent. Because a 100-mg sample was taken for analysis, this percentage was equivalent to 10 μg or 0.01 mg S. Before each batch of determinations, the method was standardized against samples of known sulfur content. A relative standard deviation of 1–2 percent was obtained from 10 replicate analyses of samples containing 0.02–1.00 percent S.

RESULTS AND DISCUSSION

The percentage of sulfur dissolution from sulfide-soil mixtures by various chemical treatments and ratings of the effectiveness of each treatment are given in table 2. Four ratings were arbitrarily established for the convenience of discussion as follows:

1. Not effective—0- to 40-percent dissolution.
2. Moderately effective—41- to 70-percent dissolution.
3. Effective—71- to 80-percent dissolution.
4. Very effective—86- to 100-percent dissolution.

Aqua regia was very effective in dissolving orpiment, was moderately effective in dissolving galena, cinnabar, and tetrahedrite, and was effective in dissolving the other five sulfides. The chemical treatments using 4 *N* HNO_3 heated to boiling, whether for 10 min or until dry, were not effective in dissolving galena; each dissolved less than 40 percent S. These two treatments were moderately effective in dissolving chalcopyrite, cinnabar, and tetrahedrite. However, heating of the 4 *N* HNO_3-sample suspensions to dryness produced greater dissolution of molybdenite, orpiment, and stibnite than did the 10-min boil.

The H_2O_2-ascorbic acid treatment, probably the least destructive to the silicate lattice of all the chemical reagents used, was not effective in dissolving orpiment and stibnite but was moderately effective in dissolving galena, chalcopyrite, cinnabar, molybdenite, pyrite, sphalerite, and tetrahedrite.

The oxalic acid dissolution was used originally to dissolve secondary hydrous iron and aluminum oxides from soil-profile samples (Ball and Beaumont, 1972) and from weathering products of soils (Gallagher and Walsh, 1943). As expected, this treatment was not effective in dissolving any one of the nine sulfide minerals.

The $KClO_3$+HCl treatment was not effective in dissolving molybdenite, was moderately effective in dissolving chalcopyrite and pyrite, was effective in dissolving orpiment, and was very effective in dissolving galena, cinnabar, stibnite, sphalerite, and tetrahedrite. One additional $KClO_3$ + HCl treatment increased the dissolution of pyrite from the moderate to the effective level and that of chalcopyrite and orpiment to the very effective level. The dissolution of molybdenite, though enhanced by the additional treatment, still amounted to only 15 percent. Two treatments of $KClO_3$ + HCl would cause greater destruction of the silicate matrix than one treatment.

Effectiveness of dissolution increased greatly if residue from the $KClO_3$ + HCl treatment was treated with 4 *N* HNO_3. Whether the 4 *N* HNO_3 solution was boiled for just 20 min or heated to dryness, all sulfides were dissolved completely. The single advantage of this combination is a greater ability to dissolve molybdenite. Inasmuch as heating of 4 *N* HNO_3 to dryness after $KClO_3$ + HCl dissolution is a more lengthy procedure, the treatment $KClO_3$ + HCl followed by 4 *N* HNO_3 with a 20-min boil (treatment 9) is suggested as a general method of sulfide dissolution. For samples containing galena, cinnabar, stibnite, sphalerite, and tetrahedrite, the $KClO_3$ + HCl method of Olade and

TABLE 2.—*The dissolution of sulfide minerals by various chemical treatments*

[Each sample initially consisted of 500 mg of a clay loam soil mixture containing 50 mg of the specified mineral. (N)=not effective, 0- to 40-percent dissolution; (M)=moderately effective, 41- to 70-percent dissolution; (E)=effective, 71- to 86-percent dissolution; (V)=very effective, 86- to 100-percent dissolution]

Sulfide mineral	Total sulfur in untreated, washed sample[1] (mg)	Percent of total sulfur dissolved by various chemical treatments[2]							
		Aqua regia	4 *N* HNO_3		H_2O_2–ascorbic acid	Oxalic acid	$KClO_3$ + HCl		$KClO_3$ + HCl followed by 4 *N* HNO_3	
			10-minute boil	Boiled until dry			Once	Twice	10-minute boil	20-minute boil	Boiled until dry
Galena	5.57	45.2 (M)	38.4 (N)	36.3 (N)	42.9 (M)	7.4 (N)	89.9 (V)	96.9 (V)	95.9 (V)	99.3 (V)	99.6 (V)
Chalcopyrite	12.15	72.6 (E)	52.7 (M)	62.0 (M)	65.9 (M)	8.6 (N)	65.6 (M)	94.7 (V)	81.8 (E)	99.2 (V)	99.7 (V)
Cinnabar	2.29	63.3 (M)	59.8 (M)	47.6 (M)	55.0 (M)	13.1 (N)	92.1 (V)	93.4 (V)	96.1 (V)	99.1 (V)	99.1 (V)
Molybdenite	5.68	71.3 (E)	61.6 (M)	93.8 (V)	63.6 (M)	0.4 (N)	6.0 (N)	15.0 (N)	69.9 (M)	88.7 (V)	98.8 (V)
Orpiment	11.08	89.2 (V)	81.3 (E)	98.2 (V)	2.4 (N)	-1.0 (N)	72.2 (E)	89.9 (V)	90.5 (V)	99.6 (V)	99.5 (V)
Pyrite	15.00	80.7 (E)	97.3 (V)	75.4 (E)	49.2 (M)	15.9 (N)	59.9 (M)	83.3 (E)	97.9 (V)	99.6 (V)	98.8 (V)
Stibnite	6.83	79.8 (E)	58.6 (M)	89.0 (V)	38.9 (N)	1.6 (N)	91.5 (V)	88.7 (V)	92.1 (V)	99.4 (V)	99.4 (V)
Sphalerite	7.27	76.5 (E)	75.4 (E)	64.2 (M)	45.1 (M)	7.0 (N)	97.7 (V)	99.4 (V)	98.9 (V)	99.4 (V)	99.2 (V)
Tetrahedrite	1.91	46.1 (M)	44.0 (M)	57.1 (M)	42.9 (M)	10.8 (N)	97.1 (V)	96.8 (V)	97.0 (V)	100.0 (V)	97.9 (V)

[1]Total sulfur in sample = sulfur concentration x sample weight

[2]Percent of dissolution = $\left(1 - \frac{\text{S in chemically treated sample}}{\text{S in untreated but washed sample}}\right) \times 100$.

Fletcher (1974), adapted from Dolezal, Povondra, and Sulcek (1968), is satisfactory.

The treatment $KClO_3$ + HCl followed by 4 *N* HNO_3 with a 20-min boil can be used to dissolve metals in residual sulfides from secondary weathering products. It is best suited for use in a fractionation scheme after sequential extraction of metals in soluble and adsorbed forms and of metals in association with organic materials and secondary oxides. When so applied, it probably will cause partial destruction of the silicate matrix, especially along edges, corners, and surfaces. However, it is emphasized that, if a metal of interest is not a major constituent in the silicate structure, the danger of confounding a metal residing in the sulfide with that from the silicate will be minimal. In areas of sulfide mineralization, the proportion of metal contamination from the silicate structure as a result of the treatment is even less significant.

The specimens used here are sulfide minerals that have not gone through extensive alteration and weathering and therefore are resistant to chemical attack. It would be difficult to extrapolate laboratory data on specimen sulfide minerals to natural field samples. However, it is apparent that the above chemical treatments would be more effective when applied to residual sulfide in natural samples.

CONCLUSION

A combination of $KClO_3$ + HCl followed by 4 *N* HNO_3 boiling for 20 min has been shown to be an effective treatment in dissolving the sulfide minerals galena, chalcopyrite, cinnabar, molybdenite, orpiment, pyrite, stibnite, sphalerite, and tetrahedrite. For galena, cinnabar, stibnite, and tetrahedrite, the $KClO_3$ + HCl method of Olade and Fletcher (1974), adapted from Dolezal, Povondra, and Sulcek (1968), is satisfactory. Although the combined treatment of $KClO_3$ + HCl and 4 *N* HNO_3 will probably cause partial destruction of the silicate matrix, it is emphasized that there is little danger of confounding a metal in the sulfide with that from the silicate in an area of sulfide mineralization, if the metal of interest is not a major constituent in the silicate structure. This treatment is useful in dissolving metals residing in sulfide minerals admixed with secondary weathering products as one step in a fractionation scheme whereby metals in soluble and adsorbed forms, and those associated with organic materials and secondary oxides, are first removed by other chemical extractants.

REFERENCES CITED

Ball, D. F., and Beaumont, P., 1972, Vertical distribution of extractable iron and aluminum in soil profiles from a brown earth-peaty podzol association: Jour. Soil Sci., v. 23, no. 3, p. 298–308.

Chao, T. T., Harward, M. E., and Fang, S. C., 1962, Adsorption and desorption phenomena of sulfate ions in soils: Soil Sci. Soc. America Proc., v. 26, no. 3, p. 234–237.

Czamanske, G. K., and Ingamells, C. O., 1970, Selective chemical dissolution of sulfide minerals—a method of mineral separation: Am. Mineralogist, v. 55, nos. 11 and 12, p. 2131–2134.

Dolezal, J., Povondra, P., and Sulcek, Z., 1968, Decomposition techniques in inorganic analysis: London, Iliffe, 224 p.

Gallagher, P. H., and Walsh, Thomas, 1943, The solubility of soil constituents in oxalic acid as an index to the effects of weathering: Royal Irish Acad. Proc., ser. B, v. 49, p. 1–26.

Hubert, A. E., and Lakin, H. B., 1973, Atomic absorption determination of thallium and indium in geologic materials, *in* Geochemical exploration 1972: Internat. Geochem. Explor. Symposium, 4th, London 1952, Proc., p. 383–387.

Lynch, J. J., 1971, The determination of copper, nickel, and cobalt in rocks by atomic absorption spectrometry using a cold leach, *in* Boyle, R. W., and McGerrigle, J. I., eds., Geochemical exploration: Canadian Inst. Mining and Metallurgy Spec. Vol. 11, p. 313–314.

Olade, M., and Fletcher K., 1974, Potassium chlorate–hydrochloric acid—a sulphide selective leach for bedrock geochemistry: Jour. Geochem. Explor., v. 3, no. 4, p. 337–344.

Rubeška, I., 1968, The determination of trace elements in sulphide minerals by atomic absorption spectrophotometry with absorption tubes: Anal. Chim. Acta, v. 40, no. 2, p. 187–194.

Smirnova, N. P., Nesterenko, G. V., and Almukamedov, A. I., 1968, The mode of occurrence of nickel and cobalt in mafic rocks: Geochem. Internat., v. 5, p. 363–372.

Stanton, R. E., 1966, Rapid methods of trace analysis for geochemical applications: London, Edward Arnold, 96 p.

Jour. Research U.S. Geol. Survey
Vol. 5, No. 4, July–Aug. 1977, p. 413–429

ENTHALPIES OF FORMATION OF LOW ALBITE ($NaAlSi_3O_8$), GIBBSITE ($Al(OH)_3$), AND $NaAlO_2$; REVISED VALUES FOR $\Delta H^\circ_{f,298}$ AND $\Delta G^\circ_{f,298}$ OF SOME ALUMINOSILICATE MINERALS

By BRUCE S. HEMINGWAY and RICHARD A. ROBIE, Reston, Va.

Abstract.—The enthalpies of formation from the elements ΔH°_f, of low albite, analbite, $NaAlSi_3O_8$ glass, gibbsite ($Al(OH)_3$), and $NaAlO_2$, have been determined by hydrofluoric acid solution calorimetry from measurements of the heats of solution, ΔH_{soln}, of low albite, $NaAlO_2$, SiO_2, $Al(OH)_3$, Al, H_2O, NaCl, and $HCl \cdot 12.731H_2O$ in 20.1 weight percent HF(aq) at temperatures between 303.15 and 348.15 K. At 298.15 K the enthalpies of formation, $\Delta H^\circ_{f,298}$, for low albite, analbite, $NaAlSi_3O_8$ glass, gibbsite ($Al(OH)_3$), and $NaAlO_2$ are $-3\,935\,115 \pm 3415$, $-3\,924\,235 \pm 3640$, $-3\,875\,455 \pm 3700$, $\pm 1\,293\,130 \pm 1190$, and $1\,135\,990 \pm 1255$ J mol^{-1}, respectively. Our values for the enthalpies of formation of low albite, analbite, and for $NaAlSi_3O_8$ glass are approximately 13 810 J mol^{-1} more negative than the values calculated by D. R. Waldbaum in 1968. Our value for the enthalpy of formation of gibbsite at 298.15 K is 11 234 J more negative than the value of R. Barany and K. K. Kelley obtained in 1961. The standard Gibbs free energies of formation, $\Delta G^\circ_{f,298}$ for low albite, analbite, and gibbsite calculated from the above enthalpies and the appropriate entropy data are $-3\,711\,715 \pm 3435$, $-3\,706\,500 \pm 3660$, and $-1\,154\,890 \pm 1200$ J mol^{-1}, respectively. The enthalpy of solution of Standard Reference Material 1654, α-quartz (37 to 74 μm), in 20.1 wt percent HF(aq) is $-137\,737 \pm 209$ J mol^{-1} at 333.15 K. This value is approximately 1255 J less negative than the value obtained by King in 1951 and 1952 for material that has a mean particle diameter of less than 5 μm and that has been used by the U.S. Bureau of Mines in their determinations of the enthalpies of formation of many silicates. Revised values of the enthalpies and Gibbs free energies of formation are presented for some aluminosilicate minerals, based upon this new data for $\Delta H^\circ_{f,298}$ of gibbsite and the heat of solution of α-quartz.

Waldbaum (1968) estimated the enthalpies of formation of the different structural modifications of $NaAlSi_3O_8$ and $KAlSi_3O_8$ on the basis of measurements of the heat of solution of low albite, analbite, microcline, and sanidine in aqueous HF at 322.8 K (Waldbaum, 1968; Waldbaum and Robie, 1971). Waldbaum's (1968) estimate was adopted by Robie and Waldbaum (1968) in their compilation of thermodynamic data for minerals as the best available values for $\Delta H^\circ_{f,298}$ of the alkali feldspars at the time. Because of the large number of auxiliary reactions utilized by Waldbaum (1968), none of which were determined with the same calorimeter as the heats of solution of the feldspars, we felt that a more direct measurement of ΔH°_f for the alkali feldspars was desirable.

During the early stages of the present investigation, it became obvious that a serious discrepancy existed in the value of ΔH°_f for low albite ($NaAlSi_3O_8$) depending upon whether $AlCl_3 \cdot 6H_2O$, $Al(OH)_3$, or $NaAlO_2$ was used as a component in the reactions used to obtain ΔH°_f. It thus became necessary to expand our studies to include new determinations of ΔH°_f for $Al(OH)_3$ and $NaAlO_2$ in order to find the source of this discrepancy.

Acknowledgments.—We wish to thank R. C. Coleman and D. B. Stewart, U.S. Geological Survey, and the late Prof. D. R. Waldbaum, Department of Geological and Geophysical Sciences, Princeton University, Princeton, N.J., for providing us with the analyzed samples of low albite used for our studies; J. R. Fisher, U.S. Geological Survey, for a sample of gibbsite; D. B. Stewart and M. E. Mrose, U.S. Geological Survey, for their X-ray studies of the low albite and $NaAlO_2$; and E. J. Dwornik and R. R. Larson, U.S. Geological Survey, for electron microscopic studies of the finely divided quartz. Donald Wagman and V. B. Parker of the National Bureau of Standards kindly provided us with their preliminary evaluation of the thermodynamic properties of the aluminum oxides and hydroxides, which was most helpful, and the late Dr. P. Gross, Fulmer Research Institute, Stoke Poges, Buckinghamshire, England, sent us his unpublished results of ΔH°_f of $Al(OH)_3$. Kenneth Krupka of the Pennsylvania State University, University Park, Pa., made measurements of the heats of solution of gibbsite and α-quartz. Prof. S. Savin, Case Western Reserve University, Cleveland,

TABLE 1.—*X-ray unit-cell parameters for calorimetric samples of low albite*
[A, angstrom (1 A=0.1 nanometer]

Sample No. and locality	*a*	*b*	*c*	α	β	γ	Cell volume (A^3)	Number of lines used
	Angstroms							
6306 Rutherford mine, Amelia, Va.[1]	8.141 4 ±0.001 6	12.783 6 ±0.002 0	7.157 1 ±0.001 1	94°14.0′ ±1.0′	116°35.5′ ±0.7′	87°40.8′ ±0.9′	663.82 ±0.15	30
49–69 Floras Creek, Oreg.[2]	8.135 ±0.002	12.781 ±0.002	7.159 ±0.001	94°14.0′ ±1.1′	116°34.7′ ±0.9′	87°41.8′ ±1.1′	663.78 ±0.16	30
57–69 Floras Creek, Oreg.[2]	8.134 ±0.002	12.782 ±0.002	7.159 ±0.001	94°19.2′ ±1.1′	116°36.7′ ±0.8′	87°40.1′ ±1.1′	663.55 ±0.14	32
Amelia, albite[3]	8.138 ±0.002	12.786 ±0.009	7.159 ±0.003	94°17.3′ ±3.2′	116°33.7′ ±2.0′	87°39.1′ ±3.0′	664.55 ±0.20	24

[1] Waldbaum and Robie (1971).
[2] Source: R. G. Coleman, U.S. Geol. Survey. X-ray refinement by D. B. Stewart, U.S. Geol. Survey.
[3] Stewart and von Limbach (1967). This sample is believed to be from the material studied by Kracek and Neuvonen (1952). NaCl, a= 5.641 19 A at 26° internal standard.)

Ohio, made available unpublished measurements of the heat of solution of α-quartz as a function of particle size. The work reported in this study was supported by the Office of Saline Waters, U.S. Department of Interior, under agreement number 14–30–3040 with the U.S. Geological Survey.

MATERIALS

Low albite ($NaAlSi_3O_8$)

Four samples of low albite were used in our heat-of-solution measurements. R. G. Coleman (U.S. Geol. Survey, Menlo Park, Calif.) kindly provided us with two samples of low albite (sample identification 49–69 and 57–69), of very low total CaO plus K_2O (<0.04 wt percent), −100 mesh (0.149 mm). The albite samples were separated from veins in blueschist tectonic blocks near Floras Creek, Langlois quadrangle, Oregon. The associated minerals were colorless amphibole, sphene, chlorite, epidote, glaucophane, and lawsonite. The geologic setting of the albite veins has been described by Coleman and Lanphere (1971).

The late D. R. Waldbaum, Princeton University, kindly sent us a low-albite specimen (No. 6306, —200 to +325 mesh) from Amelia, Va., which had been previously studied by Waldbaum and Robie (1971).

D. B. Stewart (U.S. Geol. Survey) provided us with a purified sample of Amelia, Va., albite (C–801), which had been used for thermal-expansion measurements by Stewart and von Limbach (1967). This sample is believed to be part of the material (U.S. Natl. Mus. 5390) used by Kracek and Neuvonen (1952) in their heat-of-solution studies.

The unit-cell parameters of the low-albite samples used in this investigation, those of samples used by Waldbaum and Robie (1971), and those of the albite samples used in the heat-of-solution studies by Kracek and Neuvonen (1952) are listed in table 1. Chemical analyses of these samples are given in table 2. X-ray and microscopic observations by D. B. Stewart indicated the presence of about 1 percent quartz in sample 49–69. Inasmuch as the heat of solution per gram of quartz and low albite in 20.1 percent HF are the same within 3 percent (—2322 and —2397 J g^{-1} at 333.15 K), 1 percent of quartz in the sample would lead to an insignificant error (0.03 percent in ΔH). Earlier measurements of the heat of solution of low albite (No. 6306) from Amelia, Va., in a very similar calorimeter at 322.85 K have been described by Waldbaum and Robie (1971).

α-Quartz (SiO_2)

The quartz sample used was NBS SRM (Natl. Bur. Standards, Standard Reference Material) 1654 α-quartz. It was used as received from the NBS with-

TABLE 2.—*Chemical analyses of low-albite samples used for heat of solution measurements*

	1	2	3	4	5	6
SiO_2	68.82	68.78	68.68	67.84	68.76	68.74
Al_2O_3	19.31	19.48	20.26	19.65	19.50	19.44
Fe_2O_3	*.02	*.02	----	.03	-----	-----
FeO	-----	-----	----	.02	.13	-----
MgO	.02	.003	----	.04	-----	-----
CaO	.04	.03	----	.00	.13	-----
Na_2O	11.80	11.77	----	11.07	11.51	11.82
K_2O	.02	.04	.16	.29	.13	-----
P_2O_5	-----	-----	----	----	.02	-----
H_2O+	-----	-----	----	.56	.08	-----
H_2O-	.00	.00	----	.30	-----	-----
	100.03	100.12	----	99.80	100.26	100.00

* All iron as Fe_2O_3.
1. Floras Creek, Oreg.; R. G. Coleman sample 49–69. X-ray analyses indicate presence of about 1 percent quartz. USGS analysis M109109 by S. T. Neil.
2. Floras Creek, Oreg.; R. G. Coleman sample 57–69. USGS analysis M109110 by S. T. Neil.
3. Amelia, Va.; Waldbaum and Robie (1971) sample 6306. Analysts (U.S. Geol. Survey), J. J. Fahey, Robena Brown, and H. J. Rose.
4. Amelia, Va.; USNM sample 5390, Kracek and Neuvonen (1952). Analyst, E. Chadborn (Univ. of Minnesota). X-ray studies by D. B. Stewart (U.S. Geol. Survey) indicated presence of approximately 2 percent muscovite in this sample.
5. Varutrask, Sweden; Kracek and Neuvonen (1952). Analyst, E. G. Zies (Geophys. Lab., Washington, D.C.).
6. $NaAlSi_3O_8$ (ideal low albite).

out further grinding or heating. The particle size of the sample was —200 to +400 mesh (37 to 74 μm).

Halite (NaCl)

The sodium chloride used for these studies was Fisher Scientific Co. certified reagent (S–271), lot number 791274. The maximum impurities were Ca, Mg, and Pb, present to the extent of 0.001 percent each. The sample was heated at 475 K for 2 hours and then stored in a desiccator over fresh Drierite prior to use.

$NaAlO_2$

$NaAlO_2$ was prepared by sintering an equimolar mixture of reagent grade $Al_2O_3 \cdot 3H_2O$ (Fisher A–581) and Na_2CO_3 (Fisher S–263) in a platinum crucible at 1325±10 K for 6 hours. The sample was removed from the furnace, cooled to room temperature, ground and mixed in a Diamonite mortar, and returned to the furnace for 2 hours at 1573 K. While still at a temperature above 700 K, it was placed in a desiccator filled with fresh Drierite for storage. Loading and weighing of the sample into the sample holder was done in less than 5 minutes.

Aluminum metal

Two samples of aluminum were used for our heat-of-solution measurements: certified aluminum metal (Fisher A–557) in the form of American Wire Gauge No. 19 wire (99.85 percent Al) and Alfa Products (Ventron Corp.) inorganics reagent 00008 aluminum foil (0.0025 cm thick, 99.997 percent Al). The impurities in the wire were Si 0.07 percent, Cu 0.006 percent, Fe 0.03 percent, Ti 0.01 percent, and 0.037 percent insoluble in dilute HCl. The wire was filed (with a new degreased file) to form a powder. The foil was cut into thin strips about 2 mm wide by 2.0 cm long.

Gibbsite ($Al(OH)_3$)

The samples of aluminum hydroxide used for the heat-of-solution measurements were Fisher reagent $Al_2O_3 \cdot 3H_2O$ (A–581) and a sample prepared from J. T. Baker Chemical Co.'s chemically pure reagent aluminum hydroxide (Hemingway, Robie, J. R. Fisher, and W. H. Wilson, unpub. data, 1976). They gave X-ray diffractometer patterns identical with gibbsite. The unit-cell parameters for the latter gibbsite are $a = 8.664 \pm 0.002$, $b = 5.069 \pm 0.001$, $c = 9.719 \pm 0.001$, $\beta = 94°30.0'$, using $a = 6.1971 \pm 0.0001$ of BaF_2 as the internal standard, and are in good agreement with the values of Saalfeld (1960). The particle size of the material ranged from 3 to 90 μm in diameter, with a mean diameter of about 30 μm (J. R. Fisher, written commun., 1972), and the material is insoluble in HCl. The material used for the calorimetric measurements was heated for 6 hours at 423 K prior to use. Previous investigations had determined that the material underwent no significant weight loss (that is, decomposition) as a result of this heat treatment. Results from scanning calorimetric measurements in our laboratory (Hemingway, Robie, and J. A. Kittrick, unpub. data, 1976) indicate that decomposition of gibbsite takes place at 490 K.

HCl, HF, and H_2O

The HCl(aq) and HF(aq) used were Fisher reagents A–144 and A–147, respectively, diluted to the appropriate concentration with distilled water passed through an ion-exchange column.

The formula weights used in the stoichiometric calculations are based on the 1971 values of the atomic weights (Commission on Atomic Weights, 1972). The values used were: $NaAlSi_3O_8$ 262.224, $KAlSi_3O_8$ 278.337, SiO_2 60.085, HCl 36.461, H_2O 18.0154, KCl 74.555, NaCl 58.443, $Al(OH)_3$ 78.0037, Al_2O_3 101.9612, Al 26.9815, $HCl \cdot 12.731\ H_2O$ 265.812, and $NaAlO_2$ 81.970 (g mol^{-1}).

APPARATUS AND PROCEDURES

The solution calorimeter used in these investigations and the methods of data reduction have been described by Robie and Hemingway (1972). After the measurements on quartz and $NaAlO_2$ had been completed, the calibration of the copper resistance thermometer was checked at the ice point, 273.15 K. The resistance at 273.15 K was 109.688 ohms; it differed by 0.017 ohms from the initial calibration of 109.705 ohms made in August 1966. This corresponds to a possible change of 0.04 K over the 6 years between calibrations of the thermometer and would cause only negligible error.

For the measurements described in this report, the calorimeter was operated under constant pressure conditions (that is, open to the atmosphere), and, accordingly, our measured heats of solution are enthalpy changes at 10^5 pascals pressure.

REACTION SCHEMES

The reaction schemes used to determine the heats of formation of the alkali feldspars are complex because α-Al_2O_3 (corundum) is insoluble in concentrated HF(aq) and because it is difficult to prepare Na_2O as a pure single phase (O'Hare, 1972). Furthermore, metallic sodium is difficult to handle and along with aluminum requires a large correction because the

hydrogen gas evolved during the dissolution of the metal escapes from the colorimeter.

Previous studies of the enthalpies of formation of the alkali-aluminum silicates have utilized NaCl and $AlCl_3 \cdot 6H_2O$ or $Al(OH)_3$ as the soluble reactant for Na and Al. Because $NaAlO_2$ is easily prepared and because an independent value for ΔH_f° for $NaAlO_2$ is available (Coughlin, 1957), we initially decided to study the reactions

$$3SiO_2(\alpha\text{-quartz}) + [1849HF + 8163H_2O](aq) = [3H_2SiF_6 + 1831HF + 8169H_2O](aq), \quad (1)$$

$$NaAlO_2(c) + [3H_2SiF_6 + 1831HF + 8169H_2O](aq) = [3H_2SiF_6 + NaF + AlF_3 + 1827HF + 8171H_2O](aq), \quad (2)$$

and

$$NaAlSi_3O_8(\text{low-albite}) + [1849HF + 8163H_2O](aq) = [3H_2SiF_6 + NaF + AlF_3 + 1827HF + 8171H_2O](aq) \quad (3)$$

to obtain ΔH° for the reaction

$$3SiO_2(\alpha\text{-quartz}) + NaAlO_2(c) = NaAlSi_3O_8(\text{low albite}). \quad (4)$$

By combining the results for ΔH° of equation 4 with the ΔH_f° value of Coughlin (1957) for $NaAlO_2$ and the ΔH_f° value of α-quartz (Robie and Waldbaum, (1968), we can obtain the enthalpy of formation, ΔH_f°, for low albite, that is, for the reaction

$$Na(c) + Al(c) + 3Si(c) + 4O_2(g) = NaAlSi_3O_8(\text{low albite}) \quad (5)$$

The actual reactions studied were stoichiometric for the solution of 0.005 mol of $NaAlSi_3O_8$ in 920.0 g of 20.1 wt percent HF(aq). The experimental data for reactions 1, 2, and 3 were determined at 333.15 K. Our initial results disagreed with the value of ΔH_f° for low albite calculated by Waldbaum (1968) and indicated that further studies were necessary.

Waldbaum's result was based upon his value for the heat of solution of low albite (see Waldbaum and Robie, 1971) and upon heat-of-solution measurements reported by the U.S. Bureau of Mines for $AlCl_3 \cdot 6H_2O$, NaCl, $HCl \cdot 12.731H_2O$, $SiO_2(\alpha\text{-quartz})$, and H_2O, using a different design of calorimeter. Although Waldbaum (1968) did not give the exact reaction scheme that he used, or all of the numerical data, we can reconstruct his calculation from the references that he gave and can arrive at essentially the same value that he did, —3 921 060 J mol^{-1}.

Zen (1972) showed that a discrepancy existed between the thermodynamic data calculated from equilibrium data and those obtained from calorimetric measurements for several aluminum silicates. Zen originally believed that ΔH_f° of corundum (α-Al_2O_3) was the source of the differences but has since concluded that the data for $AlCl_3 \cdot 6H_2O$ was in error (Zen, written commun., July 1972). Gross, Christie, and Hayman (1970) suggested that, on the basis of their determination of ΔH_f° of gibbsite, the value of ΔH_f° for $AlCl_3 \cdot 6H_2O$ given by Coughlin (1957) was incorrect.

The value of ΔH_f° for gibbsite, obtained by Barany and Kelley (1961) involved both the heat of solution of $AlCl_3 \cdot 6H_2O$ and its enthalpy of formation (Coughlin, 1957) in the reaction scheme used to obtain ΔH_f°. An independent value of ΔH_f° for either gibbsite or $AlCl_3 \cdot 6H_2O$ is clearly desirable.

In order to resolve this discrepancy, we have redetermined the enthalpy of formation of gibbsite, using a more direct set of reactions than those used by Barany and Kelley (1961) and by Gross, Christie, and Hayman (1970). The reactions studied to obtain ΔH_f°, for gibbsite were:

$$Al(c) + [1849HF + 8163H_2O](aq) = [AlF_3 + 1846HF + 8163H_2O](aq) + \tfrac{3}{2}H_2(g), \quad (6)$$

$$3H_2O(l) + [AlF_3 + 1846HF + 8163H_2O](aq) = [AlF_3 + 1846HF + 8166H_2O](aq), \quad (7)$$

and

$$Al(OH)_3(c) + [1849HF + 8163H_2O](aq) = [AlF_3 + 1846HF + 8166H_2O](aq). \quad (8)$$

Inasmuch as we wished to use $NaAlO_2$ as one of the reactants in our scheme to obtain ΔH_f° of low albite, we also measured the heats of the reactions

$$14.73H_2O(l) + [AlF_3 + 1846HF + 8163H_20](aq) = [AlF_3 + 1846HF + 8177.73H_2O](aq), \quad (9)$$

$$NaCl(c) + [AlF_3 + 1846HF + 8177.73H_2O](aq) = [NaF + HCl + AlF_3 + 1845HF + 8177.73H_2O](aq), \quad (10)$$

$$NaAlO_2(c) + [1849HF + 8163H_2O](aq) = [NaF + AlF_3 + 1845HF + 8165H_2O](aq), \quad (11)$$

and

$$HCl \cdot 12.73H_2 + [NaF + AlF_3 + 1845HF + 8165H_2O](aq) = [NaF + AlF_3 + HCl + 1845HF + 8177.73H_2O](aq) \quad (12)$$

from which ΔH_f° of $NaAlO_2$ may be obtained.

Reactions 6 through 12 were measured at 303 K. The actual measurements all corresponded to a stoichiometry of 0.005 mol of aluminum metal in 920.0 g of 20.1 wt percent HF(aq).

HEATS OF SOLUTION

α-Quartz (SiO_2)

The heat of solution of α-quartz in HF(aq) is the single most important quantity in the determination of the enthalpies of formation of complex silicates by reaction calorimetry. The heat of solution of α-quartz in HF(aq) has been measured by many investigators using several different designs of calorimeter, and HF(aq) concentrations of 9.8 to 39 percent by weight, for particle sizes ranging from <2 μm to >100 μm. Recently the National Bureau of Standards has made available SRM 1654 (α-quartz for HF solution calorimetry). The preparation of this material and its heat of solution in HF(aq) have been described in a comprehensive report by Kilday and Prosen (1973). Our results for reaction 1 (table 3) correspond to the heat of solution of 0.015 mol of α-quartz in 920.0g of 20.1 wt percent HF(aq) at 333.15 and 348.15 K.

The certificate accompanying SRM 1654 (α-quartz) (see also Kilday and Prosen, 1973) lists the results of several previous investigations of the heat of solution of α-quartz in HF(aq), which show a spread of 1.5 percent and include the NBS recommended values for $d\Delta H_{soln}/dT$ between 298 and 358 K and for the variation of the heat of solution in HF(aq) of 18 to 30 wt percent. The certified value for SRM 1654 is for the heat of solution of 5 g of α-quartz in 1000 cm^3 of 24.4 wt percent HF(aq) at 353.15 K, whereas our measurements and those of King (1951, 1952) refer to concentrations of 1.06 and 0.85 g in 1000 cm^3 of 20.1 wt percent HF(aq), respectively. The certificate does not include any possible heat of dilution correction for differences in the molality of SiO_2(aq) in the final solution. On the basis of the heat of dilution data for HF of Parker (1965), and of Johnson, Smith, and Hubbard (1973), this correction should be negligible.

The results of our studies and those of some earlier investigations are shown in figure 1.

Our results for ΔH_{soln} of SRM 1654 at 348 K are in excellent agreement with the values reported by Kilday and Prosen (1973) after their values have been adjusted to the HF(aq) concentration 20.1 wt percent using their equation. The results also agree well with the data of Kracek, Neuvonen, and Burley (1951) after their sample temperature has been corrected to that of the final solution. At 333 K, our values are significantly lower than those of Kilday and Prosen (1973).

One possible explanation for the difference between our values and those of Kilday and Prosen (1973) for temperatures below 343 K is the use of their equation relating the heat of solution of α-quartz to the weight percent of HF in the solvent. Their equation, based on measurements at 353 K for HF concentrations of between 17.5 and 30 wt percent HF, gives —80 J mol^{-1} (wt percent HF)$^{-1}$. Hummel and Schwiete (1959), however, obtained —350 J mol^{-1} (wt percent HF)$^{-1}$

TABLE 3.—*Heats of solution of* $NaAlO_2$, $Al(OH)_3$, H_2O, α-quartz *and* $NaAlSi_3O_8$ (*low albite*) *in 20.1 percent* HF(*aq*)

Sample mass (g)	Temperature change corrected for heat exchange (°C)	Mean solution temperature (°C)	Heat capacities (J deg^{-1}) Initial	Heat capacities (J deg^{-1}) Final	Heat of solution at mean T (J g^{-1})
$NaAlO_2$ (reaction 2)					
0.4099	0.356 93	60.04	3958	3961	−3447.7
.4100	.357 35	60.03	3955	3956	−3447.7
.4102	.358 47	60.09	3956	3956	−3457.0
.4103	.357 83	60.10	3959	3957	−3451.5
.4102	.357 48	60.10	3964	3957	−3451.4
$Al(OH)_3$ (reaction 15)					
0.3902	0.197 09	59.94	3951	3954	−1996.3
.3899	.197 33	59.95	3955	3961	−2003.2
.3900	.197 38	59.95	3956	3948	−2000.0
.3999	.205 90	50.22	3904	3910	−2011.4
.4003	.205 46	50.32	3906	3905	−2004.5
.3899	.200 60	50.21	3896	3899	−2005.4
.3900	.201 14	50.18	3893	3909	−2011.9
.3905	.201 19	50.25	3912	3927	−2019.4
H_2O (reaction 9)					
1.0578	0.002 79	50.07	3914	3910	−10.33
1.0575	.002 59	50.09	3911	3919	− 9.578
1.0581	.001 48	60.05	3947	3951	− 5.521
1.0574	.001 66	60.07	3953	3949	− 6.201
1.0574	.001 70	60.05	3951	3951	− 6.347
1.0596	.000 29	73.61	4009	3993	*− .500
α-quartz (reaction 1)					
0.9017	0.521 14	60.06	3956	3958	−2287.5
.9014	.523 05	59.95	3956	3957	−2296.0
.9015	.522 00	59.96	3960	3958	−2292.6
.9013	.524 18	59.99	3959	3952	−2300.5
.9015	.522 21	59.98	3958	3959	−2293.2
.9016	.522 38	59.94	3954	3950	−2289.8
.9017	.526 72	74.96	4004	4001	−2338.3
.9015	.526 36	74.95	4007	4002	−2338.5
.9019	.527 61	74.95	4003	4002	−2341.5
.9013	.521 50	74.93	4005	4006	−2317.7
.9015	.541 86	75.06	3889	3887	−2337.1
.9019	.538 22	75.06	3902	3897	−2327.7
.9019	.539 42	60.02	3836	3832	−2293.2
.9021	.537 95	60.08	3834	3832	−2285.8
Low albite, $NaAlSi_3O_8$ (reaction 3)					
1.3114[a]	0.795 40	59.99	3959	3961	−2401.9
1.3114[a]	.794 10	59.98	3960	3958	−2397.5
1.3115[a]	.793 54	59.91	3956	3954	−2393.3
1.3116[a]	.799 44	50.23	3927	3923	−2392.3
1.3115[b]	.793 83	60.04	3963	3959	−2397.5
1.3115[c]	.802 31	49.79	3920	3922	−2398.6
1.3115[d]	.794 57	60.03	3969	3959	−2401.6
1.3115[d]	.792 61	60.02	3962	3967	−2391.1
1.3115[a]	.792 22	66.04	3979	3974	−2402.1
1.3114[b]	.797 13	60.07	3951	3945	−2400.0
1.3113[b]	.802 56	50.24	3911	3909	−2393.0
1.3112[c]	.797 17	60.03	3950	3956	−2403.3
1.2295[c]	.745 95	60.01	3951	3949	−2396.6
1.3116[b]	.795 55	60.03	3957	3957	−2400.1
1.3115[c]	.803 16	49.81	3918	3924	−2401.4
1.3115[a]	.788 13	66.07	3981	3976	−2390.7

* No Al^{3+} in solution.
[a] Floras Creek, Oreg. (49–69).
[b] Floras Creek, Oreg. (57–69).
[c] Amelia, Va. (6306).
[d] Amelia, Va. (C–801).

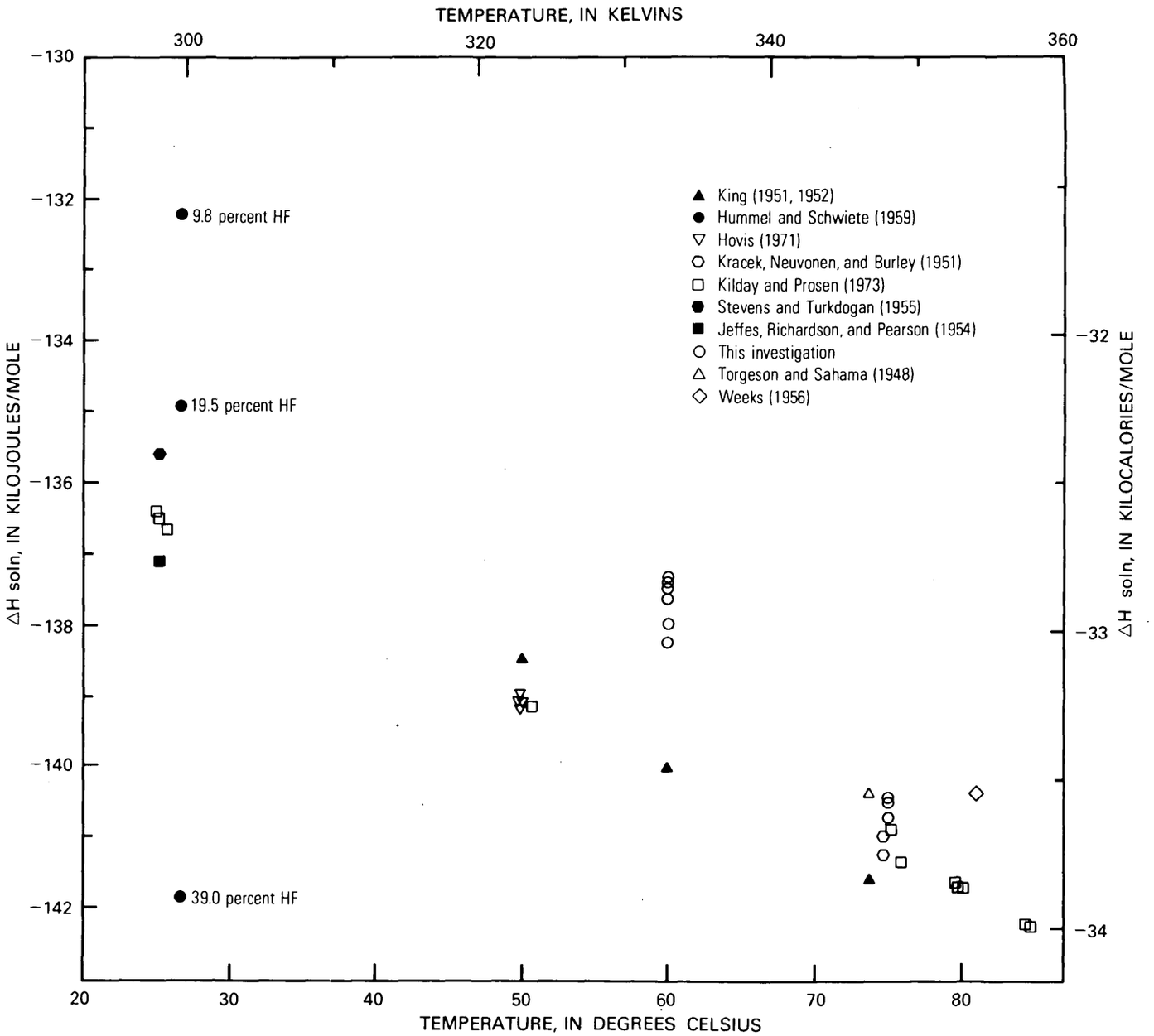

FIGURE 1.—Enthalpy of solution of α quartz in 20.1 wt percent HF(aq), except as indicated, and between 298 and 358 K. The data of Stevens and Turkdogan (1955), Hummel and Schweite (1959), Jeffes, Richardson, and Pearson (1954), and King (1951, 1952) are for material with mean particle diameters of less than 5 μm.

from measurements in HF(aq) of 9.8 to 39.0 wt percent of >2.5- to <5-μm α-quartz particles at 299.6 K.

Our results are approximately 1255 J mol^{-1} less negative than the values obtained by King (1951, 1952) between 323 K and 348 K. The quartz used by King was prepared by grinding to pass a 325-mesh sieve and was then suspended in water. The material remaining in suspension after 3 hours was recovered and dried at 453 K and was used for the heat of solution measurements. This material has a much smaller particle size than that of SRM 1654.

In order to check the effect of particle size upon the heat of solution, we prepared samples that remained in suspension in water for periods of 3 to 24 hours. Electron micrographs of this material show that the maximum particle diameter for the 3-hour suspension is about 5 μm and that the bulk of the material is less than 2 μm in diameter. The results of these studies, although incomplete at present, indicate that this material has a heat of solution greater than that of SRM 1654 (37 to 74 μm) by 1200 to 1400 J mol^{-1} at 348 K, and completely dissolves in less than one quarter of the time required for the solution of SRM 1654 at the same temperature and HF concentration.

Two further points are relevant to this problem. The temperature coefficient of the heat of solution of α-quartz in 20.1 wt percent HF(aq) obtained from the values of King (1951, 1952) at 323, 333, and 348 K is —130 J K^{-1}, whereas that from our own measurements in 20.1 wt percent HF(aq) is —190 J K^{-1}. The temperature coefficient obtained by Kilday and Prosen (1973) is 24.4 wt percent HF(aq) is —94 J K^{-1}.

Secondly, the values of Kilday and Prosen (1973) at 298.15 K for SRM 1654, which required more than 10 hours to dissolve, agree well with the measurements of Hummel and Schwiete (1959) for material of 2.5 to 5 μm particle diameter, which dissolved in less than 25 minutes at 298.15 K. This appears to us to be contrary to the results of earlier studies of the heat of solution of MgO, CaO, NaCl, and so forth, of the variation of the enthalpy of solution as a function of particle size, and is also at variance with our observed difference in the heat of solution of SRM 1654 and the very finely divided quartz (5 μm or less) obtained by suspension, as mentioned above, and with similar observations by Paul and Savin (S. Savin, written commun., 1974). If we assume that the Hummel and Schwiete (1959) data for ΔH_{soln} of α-quartz as a function of HF concentration at 298 K is correct rather than the relation given by Kilday and Prosen (1973), and if we correct Kilday and Prosen's data at 298 K and 24.4 wt percent HF to 20.1 wt percent HF, using Hummel and Schwiete's value for the dependence of ΔH_{soln} upon acid concentration, the values of Kilday and Prosen (1973) would be in much more reasonable agreement with our results.

We are presently investigating the variation of the heat of solution of α-quartz as a function of HF concentration at 333 K in the hope of resolving this point. For the present studies, we shall accept our value of —137 737 ± 209 J mol^{-1} at 333 K.

$NaAlO_2$

Reaction 2 represents the heat of solution of 0.005 mol of $NaAlO_2$ in the final solution resulting from reaction 1. Five measurements of the heat of solution of $NaAlO_2$ in 20.1 percent HF(aq) were made at 333.2 K,

TABLE 4.—*Heats of solution of aluminum,* $H_2O(l)$, $Al(OH)_3$, $NaAlO_2$, NaCl, *and* 4 N HCl(l) *in 920.0 g of 20.1 wt percent* HF

Sample mass (g)	Temperature change corrected for heat exchange (°C)	Mean solution temperature (°C)	Heat capacities (J deg^{-1}) Initial	Heat capacities (J deg^{-1}) Final	Heat of solution at mean T (J g^{-1})
Aluminum (Fisher A–557) (reaction 6)					
0.1344	0.763 61	30.28	3841	3845	−21 827
.1350	.774 20	30.23	3841	3843	−22 018
.1352	.779 58	30.20	3842	3842	−22 146
.1351	.781 70	30.26	3833	3827	−22 154
.1348	.769 78	30.24	3842	3843	−21 938
.1346	.763 78	30.30	3846	3846	−21 817
.1347	.772 20	30.59	3827	3830	−21 943
.1349	.773 03	30.58	3835	3834	−21 967
H_2O (reaction 7)					
1.0569	0.003 18	30.25	3855	3852	−11.59
1.0575	.003 02	30.25	3851	3851	−10.98
1.0573	.003 28	30.26	3853	3851	−11.95
$Al(OH)_3$(reaction 8)					
0.3899	0.207 62	30.23	3850	3844	−2048.3
.3902	.208 20	30.22	3837	3836	−2047.0
.3898	.207 00	30.23	3843	3846	−2041.5
.3896	.207 33	30.22	3849	3840	−2045.9
$NaAlO_2$ (reaction 11)					
0.4099	0.375 08	30.26	3846	3845	−3518.7
.4099	.374 06	30.27	3849	3840	−3508.2
.4095	.374 53	30.32	3833	3831	−3504.6
.4098	.374 48	30.35	3831	3831	−3500.4
.4097	.373 98	30.34	3834	3829	−3497.1
NaCl (reaction 10)					
0.2925	0.004 59	30.31	3850	3852	−60.39
.2918	.004 71	30.32	3850	3850	−62.18
.2925	.004 62	30.33	3852	3852	−60.79
.2920	.003 70	60.00	3962	3955	−50.14
.2927	.003 90	59.98	3951	3949	−52.64
4 *N* HCl (reaction 12)					
1.3559	0.002 79	30.28	3874	3875	7.97
1.3300	.002 77	30.29	3877	3860	8.05
1.3305	.002 75	30.24	3871	3879	8.00
1.3306	.004 54	73.70	4000	3999	13.65
2.4669	.005 56	29.62	3843	3839	*8.66
1.2635	.004 35	74.35	4000	4000	*13.77

* Dissolved in pure 20.1 wt percent HF.

(see table 3). The mean value for the heat of this reaction at 333.2 K is —282 884±280 J mol^{-1}.

We also made five measurements of the heat of solution of $NaAlO_2$ in 20.1 percent HF(aq), with no SiO_2 in solution at 303.5 K, that is, for reaction 11. The data are listed in table 4.

During our initial measurements on $NaAlO_2$, the sample holder occasionally had a minute leak from the surrounding acid. The reaction of a few drops of HF(aq) with excess $NaAlO_2$, within the sample holder prior to the initiation of the solution reaction leads to the formation of chiolite, $Na_5Al_3F_{14}$, and cryolite, Na_3AlF_6, which are effectively insoluble in HF(aq). Those runs that showed a precipitate when the calorimeter was dismantled were discarded. Kracek and Neuvonen (1952) also found occasional precipitates of $Na_5Al_3F_{14}$ and Al_2SiF_6 in their heat of solution studies on the plagioclase feldspars.

The mean value for the heat of reaction 11 is $-287\,378\pm610$ J mol^{-1} at 303.15 K. The temperature coefficient for the heat of reactions 2 and 11 is $+150$ J $mol^{-1}K^{-1}$.

Low albite ($NaAlSi_3O_8$)

Reaction 3 is the heat of solution of low albite in 20.1 percent HF. Ten measurements were made on four different samples of low albite at temperatures between 323 and 343 K (table 3). The heat of solution of low albite from Amelia, Va., has also been measured by Kracek and Neuvonen (1952) and by Waldbaum and Robie (1971).

In order to compare the results of Kracek and Neuvonen (1952) with the data presented in table 3 and with those of Waldbaum and Robie (1971), we must correct the data of Kracek and Neuvonen (1952) for the difference in temperature between the sample and the acid; that is, we must add the enthalpy change for the process

$$NaAlSi_3O_8(298\text{ K}) \rightarrow NaAlSi_3O_8(347.9\text{ K}) \quad (13)$$

The enthalpy change $H^\circ_{347.9} - H^\circ_{298}$ is 10 586 J mol^{-1} and was obtained from the heat capacity measurements on low albite of Openshaw, Hemingway, Robie, Waldbaum, and Krupa (1976). For the isothermal, constant pressure (10^5 pascals) process at 347.9 K

$$NaAlSi_3O_8(347.9\text{ K}) + \text{acid}(347.9\text{ K}) \rightarrow \text{solution}(347.9\text{ K}) \quad (14)$$

$\Delta H^\circ_{347.9} = -637\,307\pm460$ J mol^{-1} and $-630\,320\pm880$ J mol^{-1} from the measurements of Kracek and Neuvonen (1952) for low-albite samples from Amelia, Va. (USNM 930), and Varuträsk, Sweden, respectively. Because the HF concentration of the solvent used by Kracek and Neuvonen was very nearly the same as in the measurements of Waldbaum and Robie and the present work, and also because the ratio of sample weight to solvent weight differs only by 42 percent, the corrections for the heat of dilution of HF may be neglected.

The present results (table 3) together with those of Waldbaum and Robie (1971) and the corrected values of Kracek and Neuvonen (1952) are shown in figure 2. With the exception of Kracek and Neuvonen's value for the Amelia, Va., albite, the results from the three investigations are in excellent agreement. The temperature coefficient for the heat of solution derived from these data is -67 ± 8 J $mol^{-1}K^{-1}$, in good agreement with the tentative value, -57 ± 13 J $mol^{-1}K^{-1}$, of Waldbaum and Robie (1971).

We can offer no explanation (neither could Kracek and Neuvonen), for the apparently aberrant results for their Amelia albite sample. D. B. Stewart (oral commun., 1972) pointed out to us the presence of about 2 percent of muscovite in the sample of Amelia albite, which we believe is a part of the material used by Kracek and Neuvonen (1952). The heats of solution of muscovite and low albite in 20 percent HF are -2348 and -2397 J g^{-1} (that is, within 2 percent of each other). Thus, the presence of 2 percent muscovite in the low-albite sample studied by Kracek could account for only a small part of the observed difference. This is borne out by our measurements (fig. 2) on this sample.

On the basis of figure 2, we conclude that there is no significant difference in the heat of solution of the four different low-albite samples. Using the results from table 3, we obtain a ΔH°_{333} of $-628\,980\pm1000$ J for reaction 3.

Gibbsite ($Al(OH)_3$)

Eight measurements were made of the heat of solution of $Al(OH)_3$ (Baker's aluminum hydroxide) between 323 and 333 K in HF(aq) containing the stoichiometric amount of SiO_2 in solution, corresponding to the reaction

$$Al(OH)_3(c) + [3H_2SiF_6 + 1831HF + 8169H_2O](aq) = [AlF_3 + 3H_2SiF_6 + 1828HF + 8172H_2O](aq) \quad (15)$$

Our results are listed in table 3. The heat of this reaction was previously studied by Barany and Kelley (1961) and Koehler, Barany, and Kelley (1961). Their data, which correspond to the process

$$Al(OH)_3(298.15\text{ K}) + HF(aq)346.85\text{ K}) = \text{solution}(346.85\text{ K}) \quad (16)$$

were corrected to the isothermal reaction at 346.85 K, using the heat capacity data of Shomate and Cook

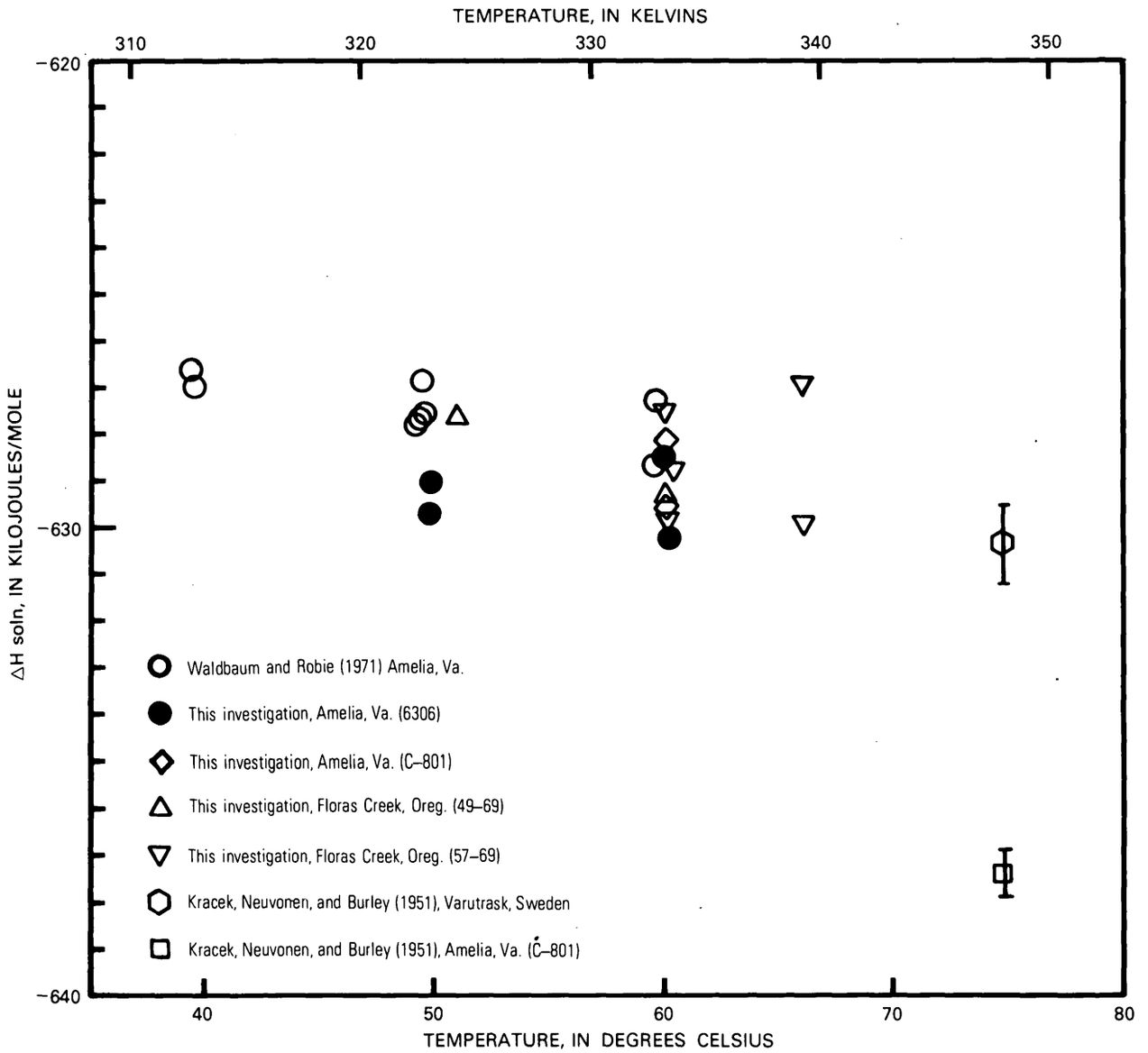

FIGURE 2.—Enthalpy of solution of low albite in 20.1 wt percent HF(aq) between 313 and 348 K. The data of Kracek, Neuvonen, and Burley (1951) are their mean values, and the bars indicate two standard errors.

(1946) and Hemingway, Robie, Fisher, and Wilson (unpub. data, 1976). Barany and Kelley's (1961) value thus corrected is $-154\ 377 \pm 250$ J mol^{-1} at 346.85 K. Four measurements of the heat of solution of $Al(OH)_3$ (Fisher reagent $Al_2O_3 \cdot 3H_2O$) in HF(aq) which contained no SiO_2 in solution, reaction 8, were also made at 303.4 K and are listed in table 4 and are also shown in figure 3.

Figure 3 suggests that the dissolved SiO_2 has very little effect upon the heat of solution of $Al(OH)_3$ in 20.1 percent HF(aq), and thus we adopt, as the heat of reaction 15, $-155\ 938 \pm 125$ J, and for reaction 8, $-159\ 578 \pm 105$ J, at 333.15 K and 303.15 K, respectively, and $d\Delta H/dT = 121$ J mol^{-1}K^{-1}. Hemingway, Robie, and Kittrick (unpub. data, 1976) have shown that the two samples have the same heat of solution at 333.15 and at 303.15 K.

H_2O(l)

The heat of solution of H_2O in 20.1 percent HF(aq) containing aluminum in solution was measured using the final solutions resulting from reactions 6 and 8. A single measurement of the heat of solution was made with no Al^{3+} in the acid to confirm our suspicion that the presence of Al^{3+} in the acid had no effect on the heat of solution of H_2O. The mean values of the data

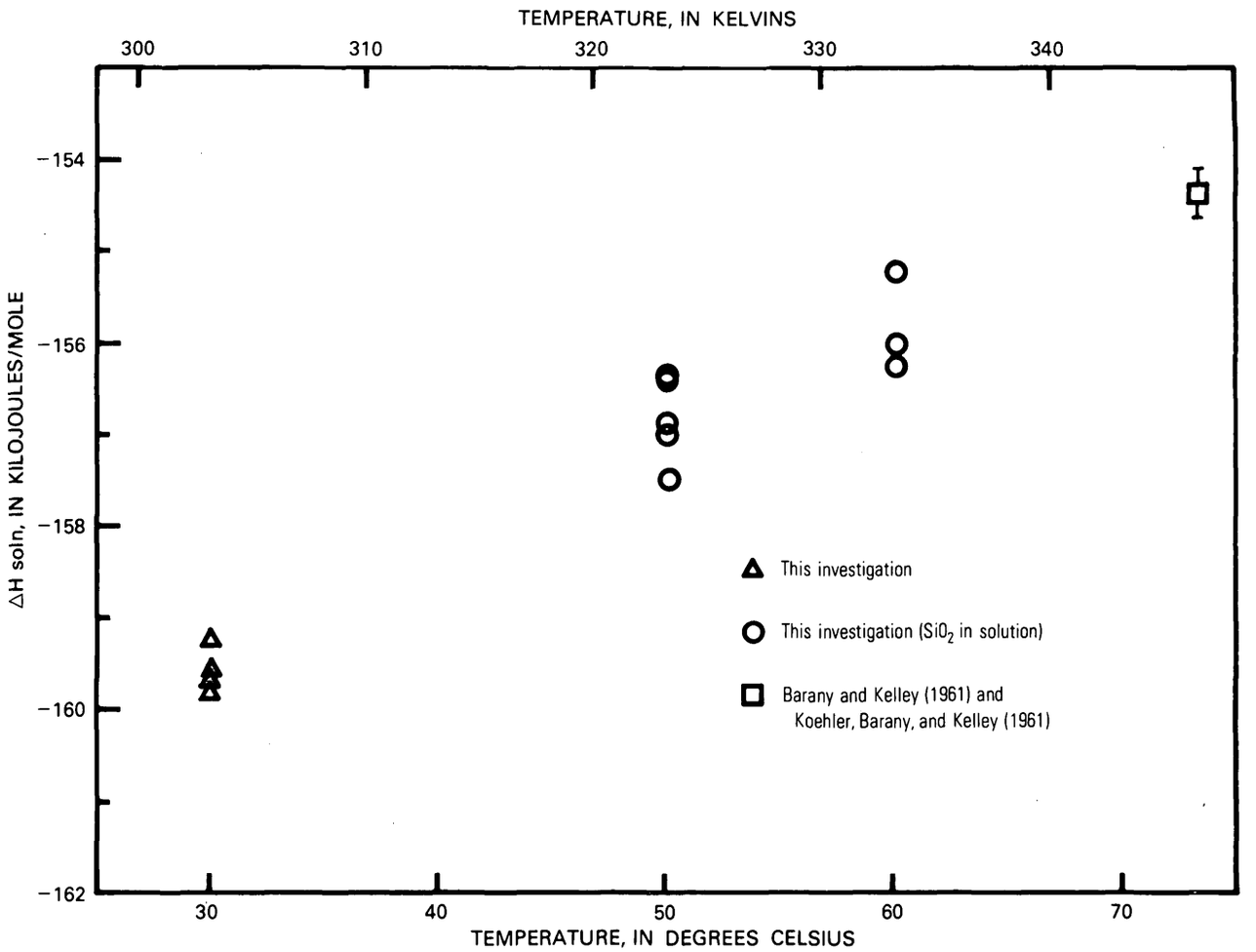

FIGURE 3.—Enthalpy of solution of gibbsite, $Al(OH)_3$, in 20.1 wt percent HF(aq) between 303 and 348 K. The results of this investigation at 303 K are for dissolution in pure 20.1 wt percent HF(aq). The measurements at 323 and 333 K had silica dissolved in the acid. The point at 346.7 K is the mean of 15 measurements by Barany and Kelley (1961) with silica in solution, and of Koehler, Barany, and Kelley (1961) with CaO in solution. The error bars are two standard errors.

listed in tables 3 and 4 were -6.01 ± 0.25 and -11.5 ± 0.3 J g^{-1} at 333 and 303 K, respectively. Only the single concentration, 1.06 g H_2O/920 g of 20.1 percent HF, was studied because of the small size of the heat effect and because the difference in the molality of the final solutions of reactions 7 and 9 is only 0.1 molal.

$HCl\cdot12.731H_2O$(4 *N* HCl)

The heat of solution of $HCl\cdot12.731H_2O$ in the final solution resulting from reaction 11 was measured at approximately 303 and 347 K. From the data listed in table 4, the mean value for the heat of solution at 303.15 K is $+8.01\pm0.04$ J g^{-1} or 2130 ± 13 J mol^{-1} per $HCl\cdot12.731H_2O$, that is ΔH_{303} for reaction 12. Two additional measurements of the heat of solution of $HCl\cdot12.731H_2O$ were made in pure 20.1 wt percent HF(aq) at 303 and 347 K (see table 3).

NaCl

The heat of solution of NaCl in the final solution resulting from reaction 9 was measured at 303 K. The mean value from the data (table 4) is -61.2 ± 3.2 J g^{-1} for the heat of solution at 303.5 K, reaction 10.

Aluminum metal

The use of metallic aluminum as a reactant in heat of solution measurements in HF(aq) at high temperatures is normally avoided because of the following consideration: When a mole of aluminum dissolves in HF (aq), ³⁄₂ mol of H_2 gas are produced. The H_2 gas escapes from the open calorimeter, carrying with it

H_2O and HF vapor, and causes a cooling of the solvent. The observed heat of solution of aluminum must therefore be corrected for the cooling caused by the vaporization of the H_2O and HF from the solvent in order to obtain the true ΔH°_{soln} for reaction 6. The correction, at 10^5 pascals external pressure, assuming that the H_2 gas escaping from the acid is saturated with H_2O and HF at the temperature of the reaction, is $\{P_{H_2O}/[750-(P_{H_2O}+P_{HF})]\}\ \Delta H^\circ_{v,H_2O} + \{P_{HF}/[750-(P_{H_2O}+P_{HF})]\}\Delta H^\circ_{v,HF}$ per mole of H_2 evolved, where P_{H_2O} and P_{HF} are the vapor pressures of H_2O and HF, in millimeters, over HF(aq) and $\Delta H^\circ_{v,H_2O}$ and $\Delta H^\circ_{v,HF}$ are enthalpies of vaporization of H_2O and HF from 20.1 percent HF(aq) (see, for example, Backstrom, 1925).

The vapor pressures of H_2O and HF over 20.1 percent HF(aq) at 303.15 K are 23.8 and 1.14 mm, respectively, according to Brosheer, Lenfesty, and Elmore (1947). Using these authors' enthalpies of vaporization for H_2O and HF over 20.1 percent HF(aq), (43 932 and 46 024 J mol^{-1}), the correction for $\frac{3}{2}$ H_2 gas is +2238 J. At 348 K, the vapor pressure of H_2O over 20.1 percent HF(aq) is approximately 210 mm, and accordingly the correction approaches 27 200 J mol^{-1} of aluminum dissolved. This, of course, is the reason why aluminum metal is rarely used as a reactant in HF solution calorimetric studies of alumino-silicates, which are normally carried out at about 348 K. (348 was adopted for silicate calorimetry because of the slow rate of solution of SiO_2 at lower temperatures.) It was for the above reason that most of the modern HF(aq) calorimetric determinations of ΔH°_f for alumino-silicate minerals measured by the Berkeley, Calif., laboratory of the U.S. Bureau of Mines used $AlCl_3 \cdot 6H_2O$ or $Al(OH)_3$ as the soluble aluminum phase instead of aluminum metal.

Although both aluminum samples, powder and foil, gave consistent results, the mean values for the two materials differed by almost 4180 J. To find the cause of this difference, we studied the mixing of the sample with acid by replacing the calorimeter with a pyrex beaker, turning on the stirrer, and then releasing the sample to the acid. The experiment showed conclusively that the aluminum foil, after a short time in contact with the acid near the bottom of the beaker, was buoyed up by the H_2 gas and thenceforth floated on the surface of the acid, whereas the powdered aluminum was uniformly dispersed throughout the acid during the solution period. We believe that for the foil sample, the escaping H_2 gas did not become saturated with H_2O or thermally equilibrated with the acid before leaving the calorimeter, and accordingly the vaporization corrections are indeterminate. We therefore discarded the measurements, that were made on the aluminum foil.

We made eight measurements of the heat of solution of the powdered aluminum in 20.1 percent HF(aq) at 303.5 K, reaction 6. The data are listed in table 4. The mean value is $-592\,952 \pm 1192$ J mol^{-1}. Correcting for the vaporization of H_2O and HF leads to $-595\,195 \pm 1192$ J mol^{-1} as the enthalpy change for reaction 6.

Kracek, Neuvonen, Burley, and Gordon (1953) measured the heat of solution of aluminum metal in 20.0 percent HF(aq) at 347.8 K and obtained $-602\,893 \pm 830$ J mol^{-1} which included a correction of nearly 29 290 J for the cooling caused by the H_2O vapor and HF gas carried away by the escaping H_2 gas.

Inasmuch as the vaporization correction increases approximately exponentially with temperature, we would not recommend the use of aluminum metal as a reactant for HF calorimetry for temperatures much above 303 K.

ENTHALPIES OF FORMATION OF GIBBSITE AND $NaAlO_2$

Gibbsite ($Al(OH)_3$)

The enthalpy change for the reaction

$$Al(c) + 3H_2O(l) = Al(OH)_3(c) + \tfrac{3}{2}H_2(g) \qquad (17)$$

was obtained from the measured heats of reactions 6, 7, and 8 (table 4), using Hess's law, that is, $\Delta H(17) = \Delta H(6) + \Delta H(7) - \Delta H(8) = -436\,240 \pm 1192$ J. The enthalpy change for reaction 17 at 303.5 K was corrected to 298.15 K using the heat-capacity data of Hemingway, Robie, J. R. Fisher, and W. H. Wilson (unpub. data, 1976) for $Al(OH)_3$ and the heat capacities of Al(c), H_2O(l), and H_2(g) listed in Wagman, Evans, Parker, Halow, Bailey, and Schumm (1968). The correction is 615 J, from which ΔH°_{298} of reaction 17 is $-435\,638 \pm 1192$ J.

Combining this result with the enthalpy of formation of $3H_2O$(l), $-857\,490 \pm 75$ J mol^{-1}, from the values listed in Robie and Waldbaum (1968), that is for the reaction

$$3H_2(g) + \tfrac{3}{2}O_2(g) = 3H_2O(l), \qquad (18)$$

we obtain $\Delta H^\circ_{f,298} = -1\,293\,130 \pm 1190$ J mol^{-1} for the formation of gibbsite, according to the reaction

$$Al(c) + \tfrac{3}{2}H_2(g) + \tfrac{3}{2}O_2(g) = Al(OH)_3(c). \qquad (19)$$

Our value for the enthalpy of formation of $Al(OH)_3$ is more negative than the value $-1\,281\,894 \pm 1255$ J mol^{-1}, obtained by Barany and Kelley (1961), by 11 236 J. Barany and Kelley measured the heat of solution of $AlCl_3 \cdot 6H_2O$, $Al(OH)_3$, H_2O, and 4 *N* HCl in 20.1 wt percent HF(aq) at 346.85 K and utilized the enthalpy of formation of $AlCl_3 \cdot 6H_2O$ obtained by Coughlin (1957), who used a different type of calorimeter and HCl as the solvent in his studies.

Gross, Christie, and Hayman (1970) measured the heat of the reaction

$$2AlCl_3(c) + 21.70H_2O(l) = Al_2O_3 \cdot 3H_2O(c) + 6(HCl \cdot 3.617H_2O)(aq) \quad (20)$$

by HF solution calorimetry (40 percent HF at 348 K). They obtained $\Delta H = -369\,447 \pm 2510$ J at 298.15 K. Combining this result with $\Delta H^\circ_{f,298}$ of $H_2O(l)$ and $HCl \cdot 3.617H_2O(aq)$ (Wagman and others 1968) and using the mean of the values of Gross and Hayman (1970) and of Coughlin (1958), $-705\,840 \pm 670$ J mol^{-1}, for $\Delta H^\circ_{f,298}$ of $AlCl_3(c)$, we obtain $-1\,294\,237 \pm 2930$ J mol^{-1} for $\Delta H^\circ_{f,298}$ of $Al(OH)_3$ (gibbsite), in excellent agreement with our value.

Parks (1972) on the basis of a systematic study of the solubility of aluminum hydroxide and oxide hydroxides adopted $-1\,151\,900$ J mol^{-1} as $\Delta G^\circ_{f,298}$ of gibbsite. The calorimetric value of the Gibbs free energy of formation of gibbsite on the basis of our enthalpy of formation is $-1\,154\,890 \pm 1200$ J mol^{-1}.

Our result for $\Delta H^\circ_{f,298}$ of gibbsite confirms the result of Gross, Christie, and Hayman (1970) and indicates that the accepted value of $\Delta H^\circ_{f,298}$ for $Al(OH)_3$ (Barany and Kelley, 1961), is in error. Because many of the accepted values of $\Delta H^\circ_{f,298}$ for the alkali and alkaline earth aluminosilicates that were obtained at the Berkeley Thermodynamics Laboratory of the U.S. Bureau of Mines used either $AlCl_3 \cdot 6H_2O$ or $Al(OH)_3$, as the soluble aluminum species, it is of some concern to pinpoint the exact source of the error in the gibbsite result.

Our value of $\Delta H^\circ_{f,298}$ of $NaAlO_2$ is in good agreement with that of Coughlin (1957) (see below), which was obtained by HCl calorimetry, and with the value obtained by Gross, Christie, and Hayman (1970) for gibbsite. Furthermore, Gross and Hayman's (1970) direct measurement of the heat of combustion of anhydrous aluminum in chlorine gas gave a $\Delta H^\circ_{f,298}$ of $AlCl_3$, in excellent agreement with Coughlin's (1958) measurement by HCl solution calorimetry. We therefore suspect that the probable source of error in the value of $\Delta H^\circ_{f,298}$ for gibbsite obtained by Barany and Kelley (1961) was in their use of $AlCl \cdot 6H_2O$ as a reactant (see below). We see no reason to suspect Coughlin's (1958) value of $\Delta H^\circ_{f,298}$ for $AlCl_3 \cdot 6H_2O$.

In Coughlin's studies, $AlCl_3 \cdot 6H_2O$ was contained in sealed glass ampules, whereas in the measurements of Barany and Kelley (1961), the sample was presumably enclosed in a gelatin capsule prior to solution. $AlCl_3 \cdot 6H_2O$ is highly hydroscopic; water from the sample may have reacted with the gelatin capsule after the capsule was loaded and before it was dropped into the calorimeter.

Much more serious objections are that the use of $AlCl_3 \cdot 6H_2O$ required two additional measurements, the heat of solution of H_2O and of HCl(aq), and that the stoichiometric coefficient for H_2O in their reaction is 70.39 mol. For the heat of solution of H_2O in HF(aq) at 346.7 K, Barany and Kelley (1961) obtained 3507 J mol^{-1} H_2O. However, all subsequent work from the Berkeley Thermodynamics Laboratory has used the value 3598 J mol^{-1} H_2O. Furthermore, a subsequent report by Barany (1962) has indicated that for more than 3 mol of H_2O, the value to be used for the dilution reaction be 3598 J mol^{-1}. Our own measurements for the heat of solution of water (tables 3 and 4) leads to 3657 J mol^{-1} for the process H_2O (liq, 298 K) +20.1 wt percent HF (aq, 346.7 K)→soln (346.7 K). For $70.39H_2O$, the difference between the two U.S. Bureau of Mines values corresponds to a possible error in the ΔH°_f of $Al(OH)_3$ of Barany and Kelly (1961) of 5858 J. A similar situation exists in the measurements reported by Barany (1962, 1964), Barany and Kelley (1961), and Kelley, Barany, King, and Christensen (1959) of the heat of solution of 4 *N* HCl in HF(aq). We suspect that this is a principal cause of the discrepancy between the values of $\Delta H^\circ_{f,298}$ for $Al(OH)_3$ of Barany and Kelley (1961) and our results.

$NaAlO_2$

Using the data listed in table 4 for the heats of solution of Al, $NaAlO_2$, NaCl, H_2O, and $HCl \cdot 12.731H_2O$, we obtain $-316\,500 \pm 1225$ J at 303.5 K for the heat of the reaction

$$Al(c) + NaCl(c) + 14.73H_2O = NaAlO_2(c) + HCl \cdot 12.731H_2O(l) + \tfrac{3}{2}H_2(g) \quad (21)$$

For this reaction, Coughlin (1957) obtained $\Delta H^\circ_{303} = -314\,220 \pm 545$ J using 4.36 *m* HCl as the solvent. Correcting our value from 303.5 to 298.15 K, using the heat capacities for Al, NaCl, and H_2O listed in Wagman and others (1968), the value adopted by Parker (1965) for the apparent molal heat capacities of aqueous HCl, and the data of King (1955) and the JANAF tables (Stull and Prophet, 1971) for C_p of $NaAlO_2$ we get $\Delta H^\circ_{298} = -315\,507 \pm 1255$ J. Combining this result with the enthalpies of formation of NaCl, $HCl \cdot 12.731H_2O$, and H_2O adopted by Wagman and others (1968 and 1976), we obtain $-1\,135\,990 \pm 1255$ J mol^{-1} for ΔH°_{298} for the reaction

$$Na(c) + Al(c) + O_2(g) = NaAlO_2. \quad (22)$$

This value is 2795 J more negative than Coughlin's (1957) result, $-1\,133\,195 \pm 753$ J mol^{-1}. We suspect that much of the discrepancy is due to the fact that our sample was prepared at 1583 K, whereas Coughlin's was prepared at 1323 K and thus was composed of much smaller particles.

ENTHALPIES OF FORMATION OF LOW ALBITE, ANALBITE, AND $NaAlSi_3O_8$ GLASS

Low albite ($NaAlSi_3O_8$)

The enthalpy change for reaction 4 from the data cited above is —67 115 ± 1045 J at 333.15 K. The enthalpy change at 333.15 K was corrected to the reference temperature 298.15 K, using the heat capacities of 44.60 J/(mol·K) for α-quartz (E. F. Westrum, Jr., written commun., 1957), that of 73.68 J/(mol·K) for $NaAlO_2$ (King, 1955; Stull and Prophet, 1971), and that of 205.1 J/(mol·K) for low albite (Openshaw, Hemingway, Robie, Waldbaum, and Krupka, 1976). Thus, ΔC_P is −2.4 J/(mol·K), and the correction to the reference temperature is only 83 J. ΔH°_{298} for reaction 4 is thus —67 032 ± 1046 J.

Combining this result with the enthalpy of formation of quartz, —910 700 ± 1000 J mol^{-1} adopted by the CODATA Task Group (1976), and the enthalpy of formation of $NaAlO_2$, —1 135 990 ± 1255 J mol^{-1}, from this investigation, we obtain as the standard enthalpy of formation from the elements for low albite, —3 935 115 ± 3415 J mol^{-1}.

Analbite ($NaAlSi_3O_8$)

Kracek and Neuvonen (1952), Holm and Kleppa (1968), and Waldbaum and Robie (1971) have reported measurements of the heats of solution of low albite and analbite, which lead to $\Delta H^\circ_{298} = -10\,880 \pm 1255$ J mol^{-1} for the transition of analbite to low albite. Combining this value with the above result for the enthalpy of formation of low albite, we obtain $-3\,924\,235 \pm 3640$ J mol^{-1} for $\Delta H^\circ_{f,298}$ of analbite.

$NaAlSi_3O_8$ (glass)

Similarly, the enthalpy of formation of $NaAlSi_3O_8$ glass at 298.15 K can be calculated from our value for $\Delta H^\circ_{f,298}$ for low albite and the result of Waldbaum and Robie (1971), $\Delta H^\circ_{298} = -59\,660 \pm 840$ J mol^{-1} for the phase change $NaAlSi_3O_8$ (glass) to $NaAlSi_3O_8$ (low albite). The resultant value for $\Delta H^\circ_{f,298}$ for $NaAlSi_3O_8$ (glass) is $-3\,875\,455 \pm 3700$ J mol^{-1}.

The results for the enthalpies of formation of low albite, analbite, and $NaAlSi_3O_8$ glass obtained in this investigation are approximately 14 100 J mol^{-1} more negative than the values calculated by Waldbaum (1968).

ENTHALPIES OF FORMATION OF PYROPHYLLITE AND KAOLINITE

Zen (1969) attempted to derive the enthalpy of formation of pyrophyllite, $Al_2Si_4O_{10}(OH)_2$, by consideration of equilibrium data for the reactions

kaolinite + 2 quartz = pyrophyllite + steam,
pyrophyllite = andalusite + 3 quartz + steam,
pyrophyllite + 3 corundum = 4 kyanite + steam,

and the solubility of pyrophyllite in water, using the available thermodynamic data and an estimated entropy of pyrophyllite, 264.8 J/(mol·K). He concluded that a significant error existed in the thermodynamic data for one or more of the aluminum silicates. Zen (1969) used the value $-3\,777\,610 \pm 4020$ J mol^{-1} for $\Delta G^\circ_{f,298}$ of kaolinite which was adopted by Robie and Waldbaum (1968) who had corrected the measurements of Barany and Kelly (1961) for the new value for $\Delta H^\circ_{f,298}$ of α-quartz. Barany and Kelley's value for $\Delta H^\circ_{f,298}$ of kaolinite involved the use of $AlCl_3 \cdot 6H_2O$(c) in their reaction scheme. We have indicated above that we believe that the data for this reaction scheme are incorrect and are the cause of the discrepancy noted by Zen (1969).

From Barany and Kelley's (1961) values for the enthalpies of solution of gibbsite, water, kaolinite, and α-quartz, and after correcting the α-quartz for the effect of small particle size, we calculate +1715 ± 840 J for ΔH°_{298} of the reaction

$$2SiO_2(\alpha\text{-quartz}) + 2Al(OH)_3\ (\text{gibbsite}) = Al_2Si_2O_5(OH)_4\ (\text{kaolinite}) + H_2O(l). \quad (23)$$

Combining this value with the enthalpies of formation of α-quartz (CODATA Task Group, 1976), and water (Robie and Waldbaum, (1968), and $\Delta H^\circ_{f,298}$ of $Al(OH)_3$ (obtained in the present investigation), we obtain $\Delta H^\circ_{f,298} = -4\,120\,115 \pm 3645$ J mol^{-1} for kaolinite and, using the entropies listed in Robie and Waldbaum (1968), $\Delta G^\circ_{f,298} = -3\,799\,350 \pm 2675$ J mol^{-1}. These values are 21 740 J more negative than the values used by Zen (1969). This value for $\Delta G^\circ_{f,298}$ brings the calculated value for the upper stability of kaolinite into much better agreement with the observed thermal breakdown data.

For his calculations, Zen (1969) used an estimated value, 264.8 J/(mol K) for S°_{298} for pyrophyllite. More recently, King and Weller (1970) obtained 236.3 ± 2.1 J/(mol K) for S°_{298} on the basis of heat capacity measurements between 52 and 296 K.

Robie, Hemingway, and Wilson (1976) measured the heat capacity of pyrophyllite from Staley, N.C., from 13 to 385 K and obtained 239.4 ± 0.4 J/(mol K) for S°_{298}. *K.* M. Krupka (unpub. data. 1974) has extended the heat capacity data for this same pyrophyllite sample to 700 K. Using the values for $\Delta G^\circ_{f,298}$ for kaolinite, obtained by the present authors, the entropy of pyrophyllite determined by Robie, Hem-

ingway, and Wilson (1976), and Krupka's high temperature heat capacity data, together with the ancillary data from Robie and Waldbaum (1968), recalculation of the equilibrium data utilized by Zen (1968) leads to ΔG°_f for pyrophyllite of $-52\,769\,400 \pm 4420$ J mol^{-1}. This is in agreement with Zen's (1972) revised calculations and with those of Thompson (1974).

SUMMARY AND CONCLUSIONS

From the calorimetric measurements of this investigation, enthalpies of formation of low albite, analbite, $NaAlSi_3O_8$ glass, and gibbsite have been determined that are approximately 11–14 kJ more negative than the previously accepted values.

We have shown that the enthalpy of formation of gibbsite ($Al(OH)_3$) obtained by Barany and Kelley (1961) is incorrect and that the heat of solution value for α-quartz in 20.1 wt percent HF(aq) used in several investigations of the enthalpies of formation of aluminosilicate minerals at the Berkeley Thermodynamics Laboratory of the U.S. Bureau of Mines refers to very small particles of α-quartz that have a heat of solution approximately 1255 J mol^{-1} greater than macroscopic quartz particles that are >10 μm.

On the basis of these considerations, we have recalculated the values of $\Delta H^\circ_{f,298}$ for several aluminosilicates originally determined by Barany (1962, 1964, 1966), Barany and Kelley (1961), and Barany and Adami (1966) and for several silicates originally determined by Barany (1959), Barany, King, and Todd (1957), and King, Barany, Weller, and Pankratz (1967). In table 5 we list these corrected values.

Chatterjee and Johannes (1974) have recently reinvestigated the thermal stability of muscovite, with the

TABLE 5.—*Thermodynamic properties at 298.15 K of gibbsite, several alkali and alkaline earth aluminosilicates, and selected silicates*

Name and formula	Formula weight (g)	S°_{298} in J/(mol·K)	$\Delta H^\circ_{f,298}$		$\Delta G^\circ_{f,298}$	
			From elements	From oxides	From elements	From oxides
			J/mol			
Gibbsite	78.003 7	68.44	−1 293 130	−26 535	−1 154 890	−7 960
$Al(OH_3)$		±0.14	±1190	±1360	±1200	±1370
Kaolinite	278.161	203.0	−4 120 115	−51 360	−3 799 350	−30 005
$Al_2Si_2O_5(OH)_4$		±1.3	±2645	±3125	±2675	±3155
Halloysite	258.161	203.3	−4 101 475	−32 720	−3 780 795	−11 460
$Al_2Si_2O_5(OH)_4$		±1.3	±2650	±3130	±2680	±3160
Dickite	258.161	197.1	−4 118 835	−50 075	−3 796 310	−26 975
$Al_2Si_2O_5(OH)_4$		±1.3	±2650	±3130	±2680	±3160
Chrysotile	277.134	221.3	−4 361 665	−164 140	−4 034 030	−39 330
$Mg_3Si_2O_5(OH)_4$		±1.7	±2840	±1330	±2880	±1425
Anorthite	278.210	199.3	−4 243 035	−110 845	−4 017 260	−118 755
$CaAl_2Si_2O_8$		±0.3	±3125	±3430	±3145	±3450
Hexagonal anorthite	278.210	*214.8	−4 222 575	−90 385	−4 001 420	−102 920
$CaAl_2Si_2O_8$		±1.3	±3250	±3545	±3275	±3570
$CaAl_2Si_2O_8$ (glass)	278.210	237.3	−4 171 280	−39 090	−3 956 835	−58 545
		±2.5	±3300	±3600	±3320	±3620
Talc	379.267	260.8	−5 915 900	−182 800	−5 536 320	−116 150
$Mg_3Si_4O_{10}(OH)_2$		±0.6	±4330	±1420	±4350	±1450
Lawsonite	314.214	237.6	−4 879 065	−175 220	−4 525 620	−152 755
$CaAl_2Si_2O_7(OH)_2 \cdot H_2O$		±2.1	±3690	±2970	±3900	±3180
Gehlenite (disordered)	274.205	209.8	−4 007 570	−150 995	−3 808 705	−163 000
$Ca_2Al(Si_{0.5}Al_{0.5})_2O_7$		±1.6	±2820	±3090	±2900	±3170
Leonhardite	922.867	922.2	−14 246 460	−338 470	−13 197 115	−314 535
$Ca_2Al_4Si_8O_{24} \cdot 7H_2O$		±10.9	±9635	±6950	±10 170	±7485
Low albite	262.224	207.4	−3 935 115	−157 755	−3 711 715	−163 590
$NaAlSi_3O_8$		±0.4	±3415	±2105	±3435	±2125
Analbite	262.224	*226.4	−3 924 235	−146 875	−3 706 500	−158 375
$NaAlSi_3O_8$		±0.4	±3640	±2450	±3660	±2470
$NaAlSi_3O_8$ (glass)	262.224	251.9	−3 875 455	−98 095	−3 665 325	−117 200
		±1.8	±3700	±2510	±3720	±2530
Nepheline	142.055	124.3	−2 110 290	−154 330	−1 995 665	−160 195
$NaAlSiO_4$		±1.3	±2040	±2220	±2075	±2255
Analcime	220.155	234.4	−3 309 845	−157 335	−3 091 725	−162 745
$NaAlSi_2O_6 \cdot H_2O$		±2.5	±2330	±1370	±2450	±1490
Microcline	278.337	214.2	−3 967 690	−216 155	−3 742 330	−221 160
$KAlSi_3O_8$		±0.4	±3370	±1970	±3400	±2000
High sanidine	278.337	*232.9	−3 959 530	−207 995	−3 739 745	−218 575
$KAlSi_3O_8$		±0.5	±3370	±1970	±3400	±2000
$KAlSi_3O_8$ (glass)	278.337	261.6	−3 914 740	−163 205	−3 703 515	−182 345
		±2.8	±3370	±1970	±3500	±2100
Kaliophilite	158.163	133.3	−2 121 920	−191 785	−2 005 985	−197 470
$KAlSiO_4$		±1.3	±1435	±1605	±1450	±1620
Muscovite	398.313	*306.4	−5 976 740	−263 675	−5 600 670	−260 000
$KAl_2[AlSi_3O_{10}](OH)_2$		±0.6	±3235	±2525	±3290	±2550

TABLE 5.—*Thermodynamic properties at 298.15 K of gibbsite, several alkali and alkaline earth aluminosilicates, and selected silicates*—Continued

Name and formula	Formula weight (g)	$S°_{298}$ in J/(mol·K)	$\Delta H°_{f,298}$		$\Delta G°_{f,298}$	
			From elements	From oxides	From elements	From oxides
			J/mol			
Leucite $KAlSi_2O_6$	218.252	*200.2 ±1.7	−3 038 650 ±2755	−197 815 ±2255	−2 875 890 ±2850	−211 045 ±2350
Eucryptite $LiAlSiO_4$	126.004	103.8 ±0.8	−2 123 300 ±1980	−75 385 ±2105	−2 009 175 ±1990	−80 630 ±2115
α-Spodumene $LiAlSi_2O_6$	186.090	129.3 ±0.8	−3 053 505 ±2790	−94 890 ±2300	−2 880 205 ±2800	−95 335 ±2315
β-Spodumene $LiAlSi_2O_6$	186.090	154.4 ±1.2	−3 025 305 ±2790	−66 690 ±2300	−2 859 490 ±2805	−74 620 ±2320
Wollastonite $CaSiO_3$	116.164	82.0 ±0.8	−1 635 220 ±1435	−89 430 ±540	−1 549 900 ±1455	−90 045 ±860
Rhodonite $MnSiO_3$	131.022	102.5 ±2.1	−1 319 350 ±1310	−23 515 ±710	−1 243 010 ±1440	−23 850 ±960
Tephroite Mn_2SiO_4	201.960	163.2 ±4.2	−1 728 070 ±3180	−47 100 ±2000	−1 629 700 ±3200	−47 790 ±2020
Fayalite Fe_2SiO_4	203.778	148.3 ±1.7	−1 479 360 ±2410	−24 575 ±4930	−1 379 370 ±2470	−20 120 ±5000
Clinoenstatite $MgSiO_3$	100.396	67.9 ±0.4	−1 547 750 ±1215	−35 560 ±630	−1 460 890 ±1225	−35 335 ±650
Forsterite Mg_2SiO_4	140.708	95.2 ±0.8	−2 170 370 ±1325	−56 690 ±610	−2 051 325 ±1345	−56 540 ±660
Larnite Ca_2SiO_4	172.244	127.6 ±0.8	−2 305 980 ±3220	−127 105 ±960	−2 191 260 ±3225	−128 000 ±970
Calcium olivine Ca_2SiO_4	172.244	120.5 ±0.8	−2 316 615 ±3920	−135 740 ±1000	−2 199 780 ±3950	−136 520 ±1020
Fluorphlogopite $KMg_3AlSi_3O_{10}F_2$	421.268	*336.3 ±2.1	−6 392 885 ±3660	-------	−6 053 070 ±3800	--------
$CdSiO_3$	188.484	97.5 ±0.8	−1 185 500 ±1385	−18 740 ±420	−1 101 770 ±1465	−19 045 ±450
$PbSiO_3$	283.274	109.6 ±1.3	−1 145 375 ±1405	−15 270 ±470	−1 061 300 ±1460	−15 675 ±500
$SrSiO_3$	163.704	-----	−1 627 840 ±3560	−125 105 ±670	----------	--------
Sr_2SiO_4	267.323	-----	−2 302 885 ±6845	−208 115 ±1000	----------	--------
$BaSiO_3$	213.424	-----	−1 616 665 ±2430	−157 865 ±710	----------	--------
Ba_2SiO_4	366.763	-----	−2 275 425 ±4460	−268 525 ±1170	----------	--------
$Ba_2Si_3O_8$	486.933	-----	−4 169 275 ±4650	−340 975 ±1470	----------	--------
$BaSi_2O_5$	273.509	-----	−2 539 710 ±3075	−170 210 ±1050	----------	--------

* Entropy for total Al/Si disorder.

intention of deriving the thermodynamic properties of muscovite from their equilibrium data. Unfortunately, in their discussion of the errors contained in the earlier thermodynamic data, they make corrections to the entropy and enthalpy of formation of sanidine adopted by Waldbaum (1968), which are incorrect and which we feel compelled to comment upon.

With respect to their corrected values for the entropy of sanidine, we point out that the heat capacity measurements by Openshaw, Hemingway, Robie, Waldbaum, and Krupka (1976) on microcline, sanidine, low albite, and analbite between 15 and 375 K show that ΔC_p° for the polymorphic pairs differs by less than 0.4 percent below 300 K and that $S°_{298} - S°_0$ for microcline and sanidine differs by less than only 0.1 percent. The "corrected entropies" of sanidine calculated by Chatterjee and Johannes (1974) are based on the incorrect assumption that the entropy data for adularia of Kelley and others (1953) gives $S°_{298}$. It does not! From the heat capacity measurements of Kelley and others (1953), and of Openshaw, Hemingway, Robie, Waldbaum, and Krupka (1976), one can only determine $S°_{298} - S°_0$. The Al/Si distribution in a disordered feldspar is frozen in at all temperatures below 400 K, and therefore $S°_0$ is not identically equal to zero.

Chatterjee and Johannes (1974) also made corrections to the enthalpy of formation of sanidine adopted by Waldbaum (1968) to take into account the newer data of Gross, Christie, and Hayman (1970) and Hemingway and Robie for $\Delta H°_{f,298}$ of gibbsite and for a supposed systematic error in the enthalpy of solution measurements of Waldbaum and Robie (1971). We agree with their correction for the new value of $\Delta H°_{f,298}$ of $Al(OH)_3$ but object strongly to their "correction" to the enthalpy of solution of sanidine of Waldbaum and Robie (1971), and Waldbaum (1968). Their contention that the 7100 J difference in values obtained by Hovis (1974) and those obtained by Waldbaum

and Robie (1971) in the heats of solution of the alkali feldspars is due to a systematic error in the work of Waldbaum and Robie (1971) is, however, not supported by any evidence known to us. On the contrary, the calorimeter and the data acquisition system used by Waldbaum and Robie (1971) were those described by Robie (1965). Measurements of the enthalpy of solution of KCl in water with this system gave a result that agreed to 0.1 percent with the value selected by Parker (1965).

The calorimeter and the data acquisition system used in the present investigation were described by Robie and Hemingway (1972). Their performance was checked by measuring the heat of solution of SRM 724, Tris, in 0.1 *N* HCl at 298, 303, and 308 K in both constant volume and constant pressure configurations and of SRM 1654, α-quartz, at 348 K in 20.1 percent HF. Furthermore, our present measurements on low albite agree with those of Waldbaum and Robie (1971), on part of the same sample, to ± 0.1 percent.

The calorimeter used by Hovis (1974) was the instrument described by Robie (1965) and used by Waldbaum and Robie (1971), but Hovis used a different data acquisition system constructed by Waldbaum. Hovis (1971) also measured the enthalpy of solution of α-quartz (-325 mesh, elutriated) in 20.1 percent HF(aq) at 323 K. His result is approximately 630 J more negative than the values obtained by King (1952), who worked on material that has been shown, in this paper, to have an enthalpy of solution greater than that of macroscopic α-quartz (SRM 1654).

The correction made by Chatterjee and Johannes (1974), on the assumtpion that the data of Waldbaum (1968) are systematically wrong by 7100 J mol^{-1} of $KAlSi_3O_8$, is thus not supported by fact. From the above arguments, we conclude that their corrections to $\Delta H^\circ_{f,298}$ and S°_{298} of sanidine are incorrect, and as a result, their derived values for $\Delta H^\circ_{f,298}$ and $\Delta G^\circ_{f,298}$ are also wrong.

REFERENCES CITED

Backstrom, H. L. J., 1925, The heat of dissociation of calcium carbonate and the entropy of carbon dioxide: Am. Chem. Soc. Jour., v. 47, p. 2443–2449.

Barany, R., 1959, Heat and free energy of formation data for crystalline cadmium and lead meta silicates: U.S. Bur. Mines Rept. Inv. 5466, 7 p.

——— 1962, Heats and free energies of formation of some hydrated and anhydrous sodium- and calcium-aluminum silicates: U.S. Bur. Mines Rept. Inv. 5900, 17 p.

——— 1963, Heats of formation of gehlenite and talc: U.S. Bur. Mines Rept. Inv. 6251, 9 p.

——— 1964, Heat and free energy of formation of muscovite: U.S. Bur. Mines Rept. Inv. 6356, 6 p.

——— 1966, Glass-crystal transformation of nepheline and wollastonite and heat of formation of nepheline: U.S. Bur. Mines Rept. Inv. 6784, 8 p.

Barany, R., and Adami, L. H., 1966, Heats of formation of lithium sulfate and five potassium- and lithium-aluminum silicates: U.S. Bur. Mines Rept. Inv. 6873, 18 p.

Barany, R., and Kelley, K. K., 1961, Heats and free energies of formation of gibbsite, kaolinite, halloysite, and dickite: U.S. Bur. Mines Rept. Inv. 5825, 13 p.

Barany, R., King, E. G., and Todd, S. S., 1957, Heats of formation of crystalline silicates of strontium and barium: Am. Chem. Soc. Jour., v. 79, p. 3639–3641.

Brosheer, J. C., Lenfesty, F. A., and Elmore, K. L., 1947, Vapor pressure of hydrofluoric acid solutions: Indus. and Eng. Chemistry, v. 39, p. 423–427.

Chase, M. W., Curnutt, J. L., Hu, A. T., Prophet, H., Syverud, A. N., and Walker, L. C., 1974, JANAF thermochemical tables, 1974 supplement: Jour. Phys. and Chem. Ref. Data, v. 3, p. 311–480.

Chatterjee, N. D., and Johannes, W., 1974, Thermal stability and standard thermodynamic properties of synthetic $2M_1$ muscovite, $KAl_2[AlSi_3O_{10}(OH)_2]$ Contr. Mineralogy and Petrology, v. 48, no. 2, p. 89–114.

CODATA Task Group, 1976, CODATA recommended key values for thermodynamics, 1975: Jour. Chem. Thermodynamics, v. 8, p. 603–605.

Coleman, R. G., and Lanphere, M. A., 1971, Distribution and age of high-grade blueschists, associated eclogites, and amphibolites from Oregon and California: Geol. Soc. America Bull., v. 82, no. 9, p. 2397–2412.

Commission on Atomic Weights, 1972, Atomic weights [for 1971]: Pure and Applied Chemistry, v. 30, p. 637–649.

Coughlin, J. P., 1957, Heats of formation of crystalline aluminates of sodium and lithium: Am. Chem. Soc. Jour., v. 79, p. 2397–2399.

——— 1958, Heats of formation and hydration of anhydrous aluminum chloride: Jour. Phys. Chem., v. 62, p. 419–421.

Gmelin, E., 1969, Thermal properties of alkaline-earth-oxides: I, Specific heat measurements: Zeitschr. Naturforschung, v. 24a, p. 1794–1800.

Gross, P., and Hayman, C., 1970, Enthalpy of formation of aluminum chloride: Faraday Soc. Trans., v. 66, p. 30–32.

Gross, P., Christie, J., and Hayman, C., 1970, Heats of formation of gibbsite and light element double oxides: Fulmer Research Inst. Rept. 6, PG/JMN/R, 24 p.

Holm, J. L., and Kleppa, O. J., 1968, Thermodynamics of the disordering process in albite: Am. Mineralogist, v. 53, nos. 1–2, p. 123–133.

Hovis, G. L., 1971, Thermodynamic properties of monoclinic potassium feldspars: Cambridge, Mass., Harvard Univ., Ph. D. thesis, 133 p.

——— 1974, A solution calorimetric and X-ray investigation of Al-Si distribution in monoclinic potassium feldspars, *in* MacKenzie. W. S., and Zussman, J., eds., The feldspars: Manchester, England, Manchester Univ. Press, p. 114–144.

Hummel, C., and Schwiete, H. E., 1959, Thermochemische Untersuchungen im System Na_2O–SiO_2. Teil 1: Losungskalorimetrische Untersuchungen von Bildung und Reaktions warmen: Glastech. Ber., v. 32, p. 327–335.

Jeffes, J. H. E., Richardson, F. D., and Pearson, J., 1954, The heats of formation of manganous orthosilicate and manganous sulfide: Faraday Soc. Trans., v. 50, p. 364–370.

Johnson, G. K., Smith, P. N., and Hubbard, W. N., 1973, The enthalpies of solution and neutralization of HF(l); enthalpies of dilution and derived thermodynamic properties of HF(aq): Jour. Chem. Thermodynamics, v. 5, p. 793–809.

Kelley, K. K., Todd, S. S., Orr, R. L., King, E. G., and Bonnickson, K. R., 1953, Thermodynamic properties of sodium-aluminum and potassium-aluminum silicates: U.S. Bur. Mines Rept. Inv. 4955, 21 p.

Kelley, K. K., Barany, R., King, E. G., and Christensen, A. U., 1959, Some thermodynamic properties of fluorphlogopite mica: U.S. Bur. Mines Rept. Inv. 5436, 16 p.

Kilday, M. V., and Prosen, E. J., 1973, The enthalpy of solution of low quartz (α-quartz) in aqueous hydrofluoric acid: U.S. Natl. Bur. Standards Jour. Research, v. 77A, p. 205–215.

King, E. G., 1951, Heats of formation of crystalline calcium orthosilicate, tri-calcium silicate, and zinc orthosilicate: Am. Chem. Soc. Jour., v. 73, p. 656–658.

——— 1952, Heats of formation of manganous metasilicate (rhodonite) and ferrous orthosilicate (fayalite): Am. Chem. Soc. Jour., v. 74, p. 4446–4448.

——— 1955, Heat capacities at low temperatures and entropies at 298.15°K of aluminates and ferrites of lithium and sodium: Am. Chem. Soc. Jour., v. 77, p. 3189–3190.

King, E. G., Barany, R., Weller, W. W., and Pankratz, L. B., 1967, Thermodynamic properties of forsterite and serpentine: U.S. Bur. Mines Rept. Inv. 6962, 19 p.

King, E. G., and Weller, W. W., 1970, Low-temperature heat capacities and entropies at 298.15°K of goethite and pyrophyllite: U.S. Natl. Tech. Inf. Service PB1–90976, 10 p.

Koehler, M. F., Barany, R., and Kelley, K. K., 1961, Heats and free energies of formation of ferrites and aluminates of calcium, magnesium, sodium, and lithium: U.S. Bur. Mines Rept. Inv. 5711, 14 p.

Kracek, F. C., Neuvonen, K. J., and Burley, Gordon, 1951, Thermochemistry of mineral substances. Part 1. A thermodynamic study of the stability of jadeite: Washington Acad. Sci. Jour., v. 41, no. 12, p. 373–383.

Kracek, F. C., and Neuvonen, K. J., 1952, Thermochemistry of plagioclase and alkali feldspars: Am. Jour. Sci., Bowen Vol., pt. 1, p. 293–318.

Kracek, F. C., Neuvonen, K. J., Burley, G., and Gordon, R. J., 1953, Contributions of thermochemical and X-ray data to the problem of mineral stability: Carnegie Inst. Washington, Geophys. Lab., Ann. Rept. Director, 1952–1953, p. 69–73.

O'Hare, P. A. G., 1972, Thermochemical and theoretical investigations of the sodium-oxygen system. Part I. The standard enthalpy of formation of sodium oxide (Na_2O): Jour. Chem. Phys., v. 56, p. 4513–4516.

Openshaw, R. E., Hemingway, B. S., Robie, R. A., Waldbaum, D. R., and Krupka, K. M., 1976, The heat capacities at low temperatures and entropies at 298.15 K of low albite, analbite, microcline, and high sanidine: U.S. Geol. Survey Jour. Research, v. 4, no. 2, p. 195–204.

Parker, V. B., 1965, Thermal properties of aqueous uni-univalent electrolytes: U.S. Natl. Bur. Standards, Natl. Standard Ref. Data Ser. 2, 66 p.

Parks, G. A., 1972, Free energies of formation and aqueous solubilities of aluminum hydroxides and oxide hydroxides at 25°C: Am. Mineralogist v. 57, nos. 7–8, p. 1163–1189.

Robie, R. A., 1965, A vacuum-jacketed hydrofluoric acid solution calorimeter: Rev. Sci. Instruments, v. 36, p. 484–486.

Robie, R. A., and Hemingway, B. S., 1972, Calorimeters for heat of solution and low-temperature heat capacity measurements: U.S. Geol. Survey Prof. Paper 755, 32 p.

Robie, R. A., Hemingway, B. S., and Wilson, W. H., 1976, The heat capacities of Calorimetry Conference copper and of muscovite $KAl_2(AlSi)_3O_{10}(OH)_2$, pyrophyllite $Al_2Si_4O_{10}(OH)_2$, and illite $K_3(Al_7Mg)(Si_{14}Al_2)O_{40}(OH)_8$ between 15 and 375 K and their standard entropies at 298.15 K: U.S. Geol. Survey Jour. Research, v. 4, no. 6, p. 631–644.

Robie, R. A., and Waldbaum, D. R., 1968, Thermodynamic properties of minerals and related substances at 298.15°K (25.0°C) and one atmosphere (1.013 bars) pressure and at higher temperatures: U.S. Geol. Survey Bull. 1259, 256 p.

Saalfeld, Horst, 1960, Strukturen des Hydrargillits und der Zwischenstufen beim Entwassen: Neues Jahrbuch Mineralogie, v. 95, p. 1–87.

Sahama, Th. G., and Neuvonen, K. J., 1951, A solution calorimeter for silicates: Finland Comm. Geol. Bull. 154, p. 177–180.

Shomate, C. H., and Cook, O. A., 1946, Low-temperature heat capacities and high temperature heat contents of $Al_2O_3 \cdot 3H_2O$ and $Al_2O_3 \cdot H_2O$: Am. Chem. Soc. Jour., v. 68, p. 2140–2142.

Stevens, C. G., and Turkdogan, E. T., 1955, Heat of formation of sodium di-silicate: Faraday Soc. Trans., v. 51, p. 356–360.

Stewart, D. B., and von Limbach, Dora, 1967, Thermal expansion of low and high albite: Am. Mineralogist, v. 52, no. 3–4, p. 389–413.

Stull, D. R., and Prophet, H., 1971, JANAF thermochemical tables [2d ed.]: U.S. Natl. Bur. Standards, Natl. Standard Ref. Data Ser. 37, 1141 p.

Thompson, A. B., 1974, Gibbs energy of aluminous minerals: Contr. Mineralogy and Petrology, v. 48, no. 2, p. 123–136.

Torgeson, D. R., and Sahama, Th. G., 1948, A hydrofluoric acid solution calorimeter and the determination of the heats of formation of Mg_2SiO_4, $MgSiO_3$, and $CaSiO_3$: Am. Chem. Soc. Jour. v. 70, p. 2156–2160.

Wagman, D. D., Evans, W. H., Parker, V. B., Halow, I., Bailey, S. M., and Schumm, R. H., 1968, Selected values of chemical thermodynamic properties. Tables of the first thirty-four elements in the standard order of arrangement: U.S. Natl. Bur. Standards Tech. Note 270–3, 264 p.

Wagman, D. D., Evans, W. H., Parker, V. B., and Schumm, R. H., 1976, Chemical thermodynamic properties of compounds of sodium, potassium, and rubidium: An interim tabulation of selected values: U.S. Natl. Bur. Standards NBSIR 76–1034, 73 p.

Waldbaum, D. R., 1968, High-temperature thermodynamic properties of alkali feldspars: Contr. Mineralogy and Petrology, v. 17, no. 1, p. 71–77.

Waldbaum, D. R., and Robie, R. A., 1971, Calorimetric investigation of Na-K mixing and polymorphism in the alkali feldspars: Zeitschr. Kristallographie, v. 134, p. 381–420.

Weeks, W. F., 1956, Heats of formation of metamorphic minerals in the system $CaO–MgO–SiO_2–H_2O$ and their petrological significance: Jour. Geology, v. 64, no. 5, p. 456–472.

Zen, E-an, 1969, Free energy of formation of pyrophyllite from hydrothermal data—values, discrepancies, and implications: Am. Mineralogist, v. 54, nos. 11–12, p. 1592–1606.

——— 1972, Gibbs free energy, enthalpy, and entropy of ten rock-forming minerals; calculations, discrepancies, implications: Am. Mineralogist, v. 57, nos. 3–4, p. 524–553.

Jour. Research U.S. Geol. Survey
Vol. 5, No. 4, July–Aug. 1977, p. 431–435

MICROWAVE RADIOMETRIC SURVEY OF THE SAN JOAQUIN NUCLEAR PROJECT SITE, KERN COUNTY, CALIF.

By G. R. JOHNSON and A. W. ENGLAND, Denver, Colo.

Abstract.—An airborne microwave survey was made in the region of the San Joaquin nuclear project site near Bakersfield, Calif. The purpose of the study was to determine if the variability of soil emissivity due to moisture content is a valid near-surface expression of buried fault systems. The results showed the existence of linear-emissivity anomalies paralleling, and to some extent, overlying the Greeley and Pond-Poso Creek faults. The anomalies seem to be direct expressions of silt-filled, northwesterly trending channels of the Pond-Poso Creek–Tulare Lake distributary system. The location, orientation, and linearity of the distributary channels suggest an association with buried faults, but no relationship has yet been determined.

During November, 1975, an airborne microwave survey was conducted over the site of the San Joaquin nuclear project. This site is located 53 km northwest of Bakersfield, Calif. (fig. 1). The survey was conducted to determine if microwave remote sensing could detect surface expressions of buried faults known to be in the vicinity. There is no stratigraphic or geophysical evidence of "capable" faults at or near the surface within a 7-km radius of the site (San Joaquin Project Early Site Review Report, Amendment 17, Nov. 18, 1975).

The Greeley and Pond-Poso Creek fault systems were the subjects of our effort to use microwave radiometry as a fault detection technique. Seismic-reflection profiles reveal a 45-km segment of the northwest-trending Greeley fault (fig. 2), which disrupts the acoustic basement 5 km beneath the northeast portion of the site. The Pond-Poso Creek fault, which also trends northwesterly, affects the surface or near-surface sediments 18 km east of the site (fig. 2). Both faults parallel the San Andreas fault which is 50 km to the west.

Recent studies by Poe and Edgerton, 1971, by Schmugge and others, 1974, and by England and Johnson, 1975, show that microwave radiometry can be used to infer the moisture content of soil. The principle is that moisture affects emissivity and emissivity affects radiobrightness, T_a, through the relationship

$$T_a = \epsilon T_o + (1-\epsilon)\ T_s, \qquad (1)$$

where ϵ is the effective microwave emissivity of the soil, T_o is the thermal temperature of the soil, and T_s is the effective microwave skybrightness. The monotonic reduction in radiobrightness with increasing moisture content reported by Poe and Edgerton and by Schmugge and others, occurs because the skybrightness, T_s, is relatively invariant at wavelengths longer than the 1.5-cm water-vapor absorption band, and be-

FIGURE 1.—Location of San Joaquin nuclear site, Kern County, Calif.

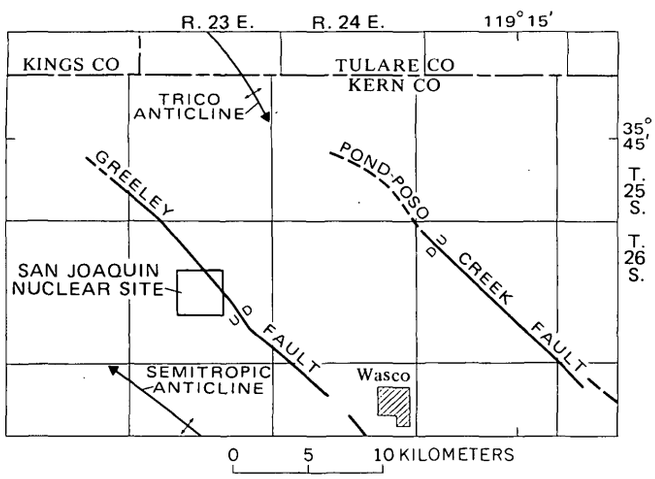

FIGURE 2.—Major faults and anticlines in the vicinity of the San Joaquin nuclear site. From San Joaquin nuclear project early site review report, amendment 17, 1975. U, upthrown side, D, downthrown side of fault; dashed where uncertain of extent.

cause the variability of emissivity far exceeds the variability of thermal temperature. The uncertainty caused by varying thermal temperature can be reduced. England and Johnson used infrared radiometry to estimate soil temperature, T_o, and arrived at a fairly precise value for the microwave emissivity.

Although moisture has a major influence on the microwave emissivity of soil, the effects of geometry and soil composition cannot be ignored. For example, surface roughness increases emissivity (Schmugge and others, 1974) and layering decreases emissivity (England and Johnson, 1977). Clay soil has a greater adsorbing surface area than does sandy soil, and therefore there is more surface-bound water in clay soil than in sand. Because it is predominately free water that contributes to the dielectric constant, moist sands have a higher dielectric constant than do equally moist clays. At 3 GHz and 25°C, the dielectric constant of a moist sandy soil (16.8 weight percent of water) is 20 while that of a moist clay soil (20.9 weight percent of water) is only 11.3 (Von Hippel, 1954). For emission normal to specular surfaces, these dielectric constants correspond to emissivities of 0.60 for sandy soil and 0.71 for clay soil. That is, clay soil can be approximately 30° warmer in radiobrightness than sandy soil of a similar wetness. This ambiguity between moisture content and soil type is not easily resolved.

An operational system for monitoring temporal variations in soil moisture would probably require an independent determination of soil type before radiobrightness could provide an absolute measure of soil moisture. In this microwave study, however, we explored the feasibility of using the aerial pattern of radiobrightness as an indicator of subtle geologic structure. Whether that structure was manifest in a moisture or a compositional pattern was immaterial if, in fact, an emissivity anomaly was produced. Therefore, we did not resolve the ambiguity in the relative contributions of moisture and of composition.

GEOLOGY ON THE SITE

[Condensed from the San Joaquin Nuclear Project Early Site Review Report, volume 1, 1974, and Amendment 17, 1975]

The San Joaquin nuclear site is located in the San Joaquin Valley, Calif. The valley is approximately 400 km long and averages 56 km wide; it is bounded on the east and southeast by the Sierra Nevada and on the south, southwest, and west by the Coast Ranges. The California Trough Section of the Pacific Border Province, in which the valley is located, trends north-northwesterly for about 725 km.

The San Joaquin Valley is a deep depositional basin whose shape and boundaries have changed little since Miocene time. Steeply sloping fans on the west, gentler eastside fans, and west-of-center valley trough result in an asymmetrical valley cross section. Alluvial fans in the vicinity of the site are nearly flat with slopes of 1 to 3 m/km. The site itself occupies a low alluvial plain with an average northwest slope of 1.3 m/km. Drainage is northwest toward Tulare Lake bed, but agricultural development has modified the natural drainage pattern to the extent that there are almost no well-defined stream courses through the area except during and after heavy rainfalls.

The site is directly underlain by Holocene deposits and by the Pliocene and Pleistocene Kern River or Tulare Formation, all of which are of lacustrine origin. These deposits, primarily derived from the Sierra Nevada, consist of alternating beds of sand, silt, and clay. The main lithologic units vary in thickness laterally but are continuous beneath the site.

Below 158 m, a thick sequence of marine and nonmarine sedimentary rocks of Eocene and younger age is present. The depth to crystalline basement at the site is about 7000 m. The upper 158 m of sediments are divided into three zones: (1) the upper oxidized zone, which extends from the surface to a depth of about 73 m; (2) the middle reduced zone, between 73 and 88 m; and (3) the lower oxidized zone, from 88 to about 158 m. The upper zone is oxidized throughout and consists mainly of brown to yellow-brown sand, silty sand, and sandy silt. Local pockets and streaks of more

highly oxidized material are abundant. The middle zone is characterized by grayish-blue, grayish-green, and dark brown, poorly sorted sand, silt, and clay. The lower oxidized zone is, in general, similar in color and lithology to the upper zone.

The site is in a structural depression with the Trico anticline on the north and the Semitropic anticline on the south (fig. 2). The Semitropic anticline forms a low topographic ridge, while the Trico anticline has no surface expression. Drill-hole and seismic data obtained at the site indicate a slight downwarping of strata to a depth of about 2200 m.

Several short faults and three relatively long faults occur in the vicinity of the site, but, except for the Pond-Poso Creek fault, no Quaternary faults lie within 24 km of the site. The surface or near-surface trace of the northwest-trending Pond-Poso Creek fault passes 18 km east of the northeast corner of the site. Seismic profiles show that the fault zone is 60 km long, 1 km wide, and comprises subparallel normal breaks, downthrown to the southwest, and dipping 50° to 70° to the southwest. The apparent vertical displacement varies from 76 m at a depth of 1100 m to 23 cm near the surface.

The Greeley fault trends northwesterly and passes at depth below the reactor site. The fault extends 51 km from the Greeley oil field, south of the site, through and beyond the site. The fault is reported to have an apparent vertical displacement of 53 to 76 m in lower Miocene strata (Sullivan and Weddle, 1960), but results of geophysical logging indicate that correlatable, 600 000- to 700 000-year-old sediment beds extend unfaulted over the Greeley fault. Furthermore, exploratory trenches adjacent to the site exposed unfaulted soil horizons.

THE MICROWAVE SURVEY

The microwave survey comprised 18 east-west aerial traverses, flown 0.85 km apart. The 32-km traverses were centered on quarter-section fields to minimize the effects of section-line roads. The traverse area extended from 4.5 km south to 9.5 km north and from 8.5 km west to 25 km east of the center of the nuclear site (fig. 3). The survey was conducted during a 10-h period the day following a 2-mm evening rainfall. There was a 10-percent cover of thin cirrus clouds during the survey.

The traverses were made with a deHavilland Beaver aircraft equipped with a nadir-viewing, L-band (21 cm) radiometer, an infrared radiometer, and a flight-line recovery camera. The flight altitude and speed were 122 m and 40 m/s, respectively. The L-band radiometer had a 0.1-s integration time and a 65-m-diameter footprint, and the IR radiometer had a 0.5-s integration time and a 7-m-diameter footprint. The microwave data were corrected for antenna and transmission-line losses and the resultant microwave radiometric temperatures, along with the thermal infrared temperatures, were continuously recorded on a strip chart.

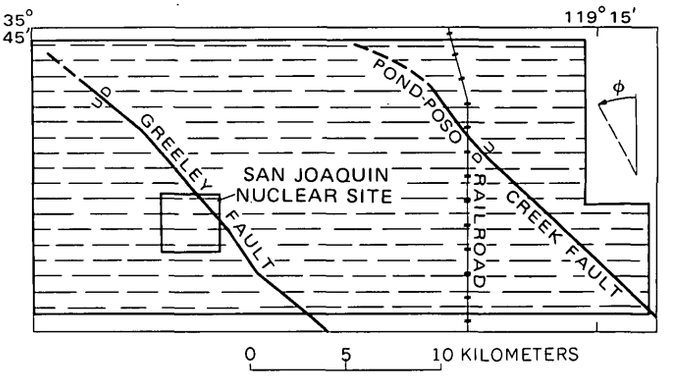

FIGURE 3.—Coverage of airborne microwave survey at San Joaquin nuclear site. Flight lines (dashed lines) are consecutively numbered 1 through 18 from south. Φ is correlation angle of figure 5. U, upthrown side, D, downthrown side of fault; dashed where uncertain of extent.

The land surrounding the site is both improved and unimproved farmland. At the time of the study, numerous fields were being irrigated, and drainage water was standing in marshes on some of the unimproved land. These randomly distributed wet areas caused abnormally low brightness temperatures that masked subtle linear patterns that might be associated with fault traces. The confusing effect of these random anomalies is greatly reduced by employing a multiple cross-correlation between the 18 traverse profiles. The cross-correlation enhances features that extend across most or all of the traverse lines whereas random features are suppressed. Therefore, the microwave- and infrared-temperature profiles were digitized at intervals corresponding to 45 m on the ground.

The microwave and soil temperature profiles were converted to microwave emissivity using a recast form of equation 1,

$$\epsilon = \frac{T_a - T_s}{T_o - T_s} \qquad (2)$$

where 6 K was taken to be the 21-cm skybrightness. The 8–14-μm infrared emissivity of soil is about 0.94 so that an approximation of the soil temperature, T_o, was obtained by dividing the thermal infrared temperatures by 0.94. These emissivity profiles are shown in figure 4. The individual profiles in the figure correspond to the 18 traverses and are spaced 0.2 emissivity

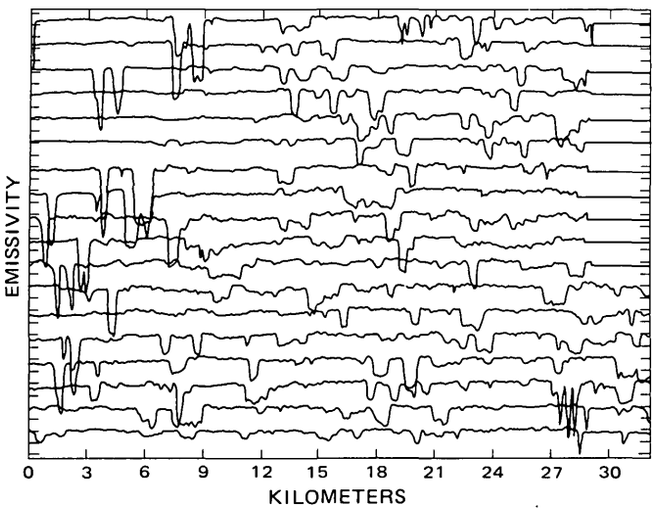

FIGURE 4.—Emissivity profiles of 18 east-west microwave traverses, San Joaquin nuclear site, Calif. One unit on vertical scale equals 10 percent change in emissivity. Emissivity varies between 0 and 1.

units apart to represent the 0.85-km spacing between flight lines. The flat sections on the right-hand portions of the upper eleven profiles correspond to the area near the town of Delano where data could not be taken. The emissivity in this portion of each line is the average emissivity for that particular line. The numerous, strong, negative peaks seen on the profiles are associated with standing water. The amplitude, width, and slope of each peak in figure 4 depends upon the proportion of standing water and of moist soil detected in the area swept by the 65-m footprint per unit integration time (0.1 s).

The emissivities in figure 4 can be thought of as having a relatively uniform value except for local, anomalous lows. Because these lows are the features of interest, the correlation among lines was computed between the complements of the emissivity, $\alpha = 1 - \epsilon$, or the absorptivity. That is, an anomalously high free-moisture content corresponds to a high absorptivity. If x is the distance from the left hand margin of a point on traverse line n in figure 3, the absorptivity at that point is $\alpha_n(x)$. The 18-point correlation based upon traverse line 8 is

$$\Psi(\phi) = \int_0^{34\text{km}} dx \left\{ \prod_{n=1}^{18} \alpha_n(0.85(n-8)\tan\phi) \right\} \quad (3)$$

where ϕ is the correlation angle, with respect to north, between traverse lines (figure 3). Where $x = [0.85(n-8)\tan\phi]$ in equation 3 falls outside of $0 \leqq x \leqq 34\text{km}$, $\alpha_n(x)$ is taken to be the average absorptivity for line n. The 18-point correlation for $-60° \leqq \phi \leqq 0°$ is shown in figure 5. The strong feature

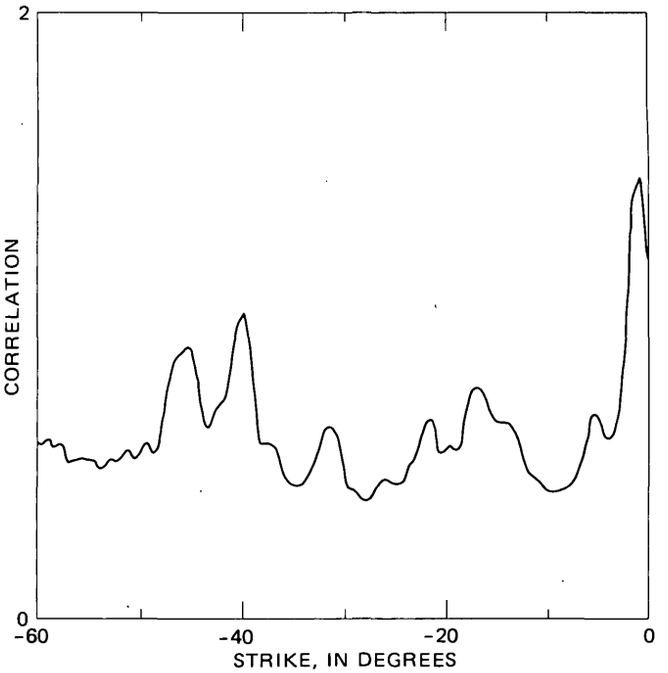

FIGURE 5.—Correlation of anomalies from emissivity profiles of figure 4. Strike measured counterclockwise from north.

at $\phi = 0$ corresponds to irrigation ditches, which tend to run parallel to field boundaries.

The peak at $-40°$ was explored because the major structural trend in the region is N 40°W ($-40°$). A sweeping 18-point correlation of the form

$$\Omega(x) = \prod_{n=1}^{18} \int_{x-0.4}^{x+0.4} \{\alpha_n(0.85(n-8)\tan(-38))\} dx \quad (4)$$

provides the striking pattern shown in figure 6. Correlation angles that are either greater than or less than

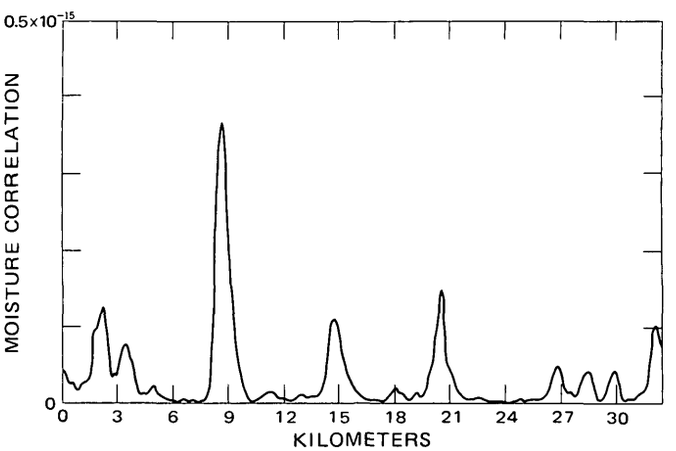

FIGURE 6.—A sweeping moisture correlation across emissivity profiles of figure 4. Correlation angle is $-38°$ (measured counterclockwise from north). Distance referenced to line 8, fig. 3.

−38° broaden the peaks and generally raise the background. Figure 6 shows that strong linear features, each having orientation N 38°W, cross traverse line 8 (which passes through the north edge of the reactor site) at about 2 km, 8.5 km, 14.8 km, 20.5 km, and about 32 km from the west boundary. The strongest peak, that at 8.5 km, lies above the Greeley fault and passes through the northeast corner of the reactor site. The set of features near 32 km lies above the Pond-Poso Creek fault. The other features do not correlate with any obvious structure revealed in vibroseis records.

INTERPRETATION

Some of the correlation peaks in figure 6 are nearly coincident with lineaments that are defined by vegetation seen in aerial photographs taken during the growing season (San Joaquin Nuclear Project, Early Site Review Report, Amendment 17, 1975). These lineaments, although numerous in the site vicinity, appear to be concentrated in a wide zone directly over the Greeley fault. According to the early site review report, the lineaments primarily represent fluvial and lacustrine features related to Poso Creek and Tulare Lake and have no relation to subsurface structures. During Holocene time, the Poso Creek distributary system locally incised channels in silty clay beds and these channels were, in turn filled with silty sands. Fine-grained material was deposited between distributaries resulting in plant-stress tonal differences seen in air photos.

While the ubiquitous clay soils are generally more moist than the sandy soils in the channels, the sandy soils are wetter after precipitation or after irrigation (Robert Morris, oral commun., 1976). Also, water in clay soils is partially bound resulting in higher microwave temperatures than in a similarly moist sandy soil. Because our microwave survey was conducted after a light rainfall, the emissivity of the sandy and (or) silt-filled channels was probably lower than normal, and the prominent zones of intertwining channels, represented as lineaments, resulted in the emissivity correlations shown in figure 6.

CONCLUSIONS

We have used 21-cm and infrared radiometers to produce an emissivity-profile map (fig. 4), showing the distribution of relative soil moisture and (or) soil type. In the extensively farmed region in and adjacent to the San Joaquin Nuclear Site, where the effects of irrigation make interpretation of natural soil moisture patterns difficult, an analysis that employs multiple correlation techniques enhances subtle linear features and suppresses random cultural effects.

The multipoint correlation showed northwest-trending emissivity alinements in the proximity of the Greeley or Pond-Poso Creek faults. Particularly strong correlation was found coincident with the location of the Greeley fault. It was determined, however, that this, and at least some of the other northwest-trending emissivity alinements, were probably caused by sandy, silt-filled channels of the Poso Creek distributary system. The location, orientation, and linearity of the distributary system suggests an imprint of the underlying fault system, but the relationship has not been established.

REFERENCES CITED

England, A. W., and Johnson, G. R., 1975, The thermal microwave detection of near surface thermal anomalies: United Nations Symposium on Development of Geothermal Resources, 2d, San Francisco, May 20–29, 1975, Proc., p. 971–977.

——— 1977, Microwave brightness spectra of layered media: Geophysics. (in press).

Los Angeles Department of Water and Power, 1974, San Joaquin nuclear project early site review report: Dept. of Water and Power, City of Los Angeles, project no. 499, v. 1, [146] p., 112 figs., 25 tables, Feb. 28.

Poe, G. A., and Edgerton, A. T., 1971, Determinations of soil moisture contents with airborne microwave radiometry: Azusa, Calif., Aerojet Electrosystems Co., Rept. 4006R–2, p. 1–43.

Schmugge, T., Gloersen, P., Wilheit, T., and Geiger, F., 1974, Remote sensing of soil moisture with microwave radiometers: Jour. Geophys. Research, 79, p. 317–323.

Sullivan, J. C., and Weddle, J. R., 1960, Rio Bravo Oil Field: Calif. Div. Oil and Gas, Summary of Operations, California Oil Fields, v. 46, no. 1, p. 27–40.

Von Hippel, A. R., ed., 1954, Dielectric Materials and Applications: Cambridge, Mass., M.I.T. Press, 438 p.

Jour. Research U.S. Geol. Survey
Vol. 5, No. 4, July–Aug. 1977, p. 437–443

MAGNITUDE, DISTANCE, AND INTENSITY DATA FOR C.I.T. STRONG MOTION RECORDS

By ROBIN K. McGUIRE and JAMES A. BARNHARD, Denver, Colo.

Abstract.—The site Modified Mercalli intensities and epicentral distances of strong motion records published by the California Institute of Technology are reported, as well as the magnitude, focal depth, and maximum Modified Mercalli intensity of the event associated with each record. These data were obtained from original sources. The use of the data to derive ground motion relations for design is discussed; possible biases in the data which might affect such relations are described.

The magnitude, distance, and epicentral intensity and site intensity data reported in table 1 have been compiled as part of a continuing research effort in the U.S. Geological Survey to define ground motion for seismic risk analysis and earthquake-resistant design of structures. These data were obtained independently of similar summaries because some other summaries have used only isoseismal maps to assign site intensities to strong motion records, have used inaccurate epicentral or station coordinates to calculate epicentral distances, or have used nonstandard methods to assign magnitudes. These data are reported here so that they might be available to others engaged in similar research.

Sources for the data are given in the list of references after the footnotes in table 1. Where possible, special studies of individual earthquakes were used as sources, rather than annual reports or summaries. The site intensity data represent intensities reported at the strong motion station or in the same city. Isoseismal maps were never the only source used to estimate site intensities. Epicentral distance, from the coordinates of the epicenter and the station, was calculated when no distances were reported in the references examined.

Missing data in table 1 indicate that no reports of those pieces of information could be found. Focal depths of larger events in California have generally been observed to be between 10 and 15 kilometers (Algermissen, 1969), so that focal depths not reported for California events can be assumed, with good accuracy, to be in this range.

Geological information and site classification have been reported by Trifunac and Brady (1975) for all sites described in table 1 except Carroll College, Helena, Mont. The user is referred to this work if distinction among records on the basis of site geology is desired.

Several earthquakes, primarily those in the northern California area, had epicentral locations offshore. These events are noted in table 1; for such cases, the maximum intensity is obviously that reported onshore.

The strong motion records obtained during the 1971 San Fernando earthquake (California Institute of Technology, 1969, 1971, 1972a, 1972b) have not been included in table 1 because these records have been studied at length by others. For example, epicentral distances and site geology for San Fernando records are reported by Maley and Cloud (1973) and an intensity map is available in Scott (1973).

A note of caution is appropriate to users of these data. In estimating future ground motion from past events, considerable bias may be introduced by only using available strong motion records. This follows because the records which are considered "outstanding" (in the terminology of "United States Earthquakes," table 1, ref. 18) following an event are those which exhibit strong motion; accelerograph stations which are located equivalent distances from the same event, but which experience less severe shaking, may not produce a record because the instrument did not trigger. If it did trigger, the record may not be digitized and published because the levels of acceleration were low. Thus, ground motion estimates based on published records are biased toward strong motions. This bias increases with increasing distance from the event.

The effect of this bias is to give a slower apparent attenuation of motion with distance than is real. For site intensities there is an obvious solution: One could use intensities reported at many locations (not only those with a strong motion station) to derive an attenuation function. For acceleration or other quantitative ground motion parameters, this option may not be readily available. What might be done for these parameters is to limit the data to those records which were obtained within distance X of the epicenter, with

X a function of magnitude. One could choose X to include only those stations which were almost certain to trigger, to produce an "outstanding" record, and to be digitized and published. This would likely have to be an iterative process, with the initial function X chosen based on attenuation equations using all available data, and later refined based on equations using data selected in the manner described above.

An additional bias comes from the fact that, for a given event, more records are generally available for sites which experience low intensities (at long distances) than high intensities (at short distances), due to the radial nature of attenuation of motion. Thus, low intensity records generally represent longer epicentral distances than do high intensity records. For example, the average epicentral distance of intensity V records in table 1 is about 110 km; for intensity VII it is about 55 km. The effect on ground motion prediction will, of course, depend on the parameter(s) being used and the particular seismic threat being studied.

Caution must be used in extrapolating predicted ground motions from the range of data available. One problem is the aforementioned bias. A second is that ground shaking at close distances to major earthquakes is undoubtedly governed by physical laws different from those which affect the shaking at close and medium distances to small and moderate events. The latter phenomenon is well documented by available records from the United States; the former is not. No strong motion records have been written in this country for an event larger than magnitude 7.7; no records have been written in the near-field region for an event at magnitude greater than 7.1. This dearth of data necessitates extreme caution in extrapolating the available data to large magnitudes and small distances.

Table 1 follows "References Cited."

REFERENCES CITED

Algermissen, S. T., 1969, Seismic risk studies in the United States: World Conf. on Earthquake Eng., 4th, Proc., v. 1, p. 14–27.

California Institute of Technology, 1969, Strong motion earthquake accelerograms—digitized and plotted data: Earthquake Eng. Research Lab. Rept. EERL 70–20, v. 1, pt. A and subsequent pts. B through Y.

———1971, Strong motion earthquake accelerograms—digitized and plotted data: Earthquake Eng. Research Lab. Rept. EERL 71–50, v. 2, pt. A and subsequent pts. B through Y.

———1972a, Analyses of strong motion earthquake accelerogram—response spectra: Earthquake Eng. Research Lab. Rept. EERL 72–80, v. 3, pt. A and subsequent pts. B through Y.

———1972b, Analyses of strong motion earthquake accelerograms—Fourier amplitude spectra: Earthquake Eng. Research Lab. Rept. EERL 72–100, v. 4, pt. A and subsequent pts. B through Y.

Maley, R. P., and Cloud, W. K., 1973, Strong motion accelerograph records, *in* Benfer, N. A., Coffman, J. L., and Bernick, J. R., eds., San Francisco, California, earthquake of February 9, 1971: U.S. Natl. Oceanic and Atmospheric Adm., v. 3, p. 325–348.

Scott, N. H., 1973, Felt area and intensity of San Fernando earthquake, *in* Benfer, N. A., Coffman, J. L. ,and Bernick, J. R., eds., San Fernando, California, earthquake of February 9, 1971: U.S. Natl. Oceanic and Atmospheric Adm., v. 3, p. 23–48.

Trifunac, M. D., and Brady, A. G., 1975, On the correlation of seismic intensity scales with the peaks of recorded strong ground motion: Seismol. Soc. America Bull., v. 65, no. 1, p. 139–162.

TABLE 1.—*Magnitude, distance, and intensity data for C.I.T. strong motion records*

[Numbers in parentheses are found in reference list following table. C.I.T., California Institute of Technology. M.M., Modified Mercalli. Leaders (---) indicate no data]

C.I.T. number	Date	Richter magnitude	Maximum reported M.M. intensity	Depth (km)	Instrument site	Site M.M. intensity	Distance to epicenter (km)
A001	5-18-40	7.1 (6)	X (18)	---	El Centro	VII-VIII (18)	11 (18)
A002	10-7-51	6.0 (6)	[1]VII (18)	---	Ferndale City Hall	V (18)	53 (18)
A003	7-21-52	7.7 (7)	XI (18)	---	Pasadena C.I.T. Athenaeum	VII (18)	[2]127
A004	7-21-52	7.7 (7)	XI (18)	---	Taft Lincoln School tunnel	VII (18)	[2]43
A005	7-21-52	7.7 (7)	XI (18)	---	Santa Barbara Court House	VII (18)	[2]89
A006	7-21-52	7.7 (7)	XI (18)	---	Hollywood Storage basement	VII (18)	119 (18)
A007	7-21-52	7.7 (7)	XI (18)	---	Hollywood Storage P. E. lot	VII (18)	119 (18)
A008	12-21-54	6.6 (18)	VII (18)	---	Eureka Federal Bldg.	VII (18)	24 (18)
A009	12-21-54	6.6 (18)	VII (18)	---	Ferndale City Hall	VII (18)	40 (18)
A010	9-4-55	5.8 (18)	VII (18)	---	San Jose Bank of America	VII (18)	10 (18)
A011	2-9-56	6.8 (7)	Epicenter in Mexico	---	El Centro	VI (18)	119 (18)
A012	Aftershock						
A013	3-22-57	5.3 (18)	VII (18)	7-11 (14)	San Francisco Southern Pacific Bldg.	VI (18)	16 (18)
A014	3-22-57	5.3 (18)	VII (18)	7-11 (14)	San Francisco Alexander Bldg.	VI (3)	[2]15
A015	3-22-57	5.3 (18)	VII (18)	7-11 (14)	San Francisco Golden Gate Park	VI (3)	[2]12
A016	3-22-57	5.3 (18)	VII (18)	7-11 (14)	San Francisco State Bldg.	VI (3)	[2]14
A017	3-22-57	5.3 (18)	VII (18)	7-11 (14)	Oakland City Hall	VI (18)	[2]24
A018	4-8-61	5.6 (18)	VII (18)	11 (13)	Hollister City Hall	VII (18)	21 (18)
A019	4-8-68	6.5 (18)	VII (18)	11 (2)	El Centro	VI (18)	64 (18)
A020	4-8-68	6.5 (18)	VII (18)	11 (2)	San Diego Power & Light Bldg.	VI (18)	96 (5)
B021	3-10-33	6.3 (6)	[1]VII-IX (18)	10 (18)	Vernon CMD Bldg.	VI (18)	53 (18)
B022	10-2-33	5.4 (6)	VI (18)	---	Hollywood Storage penthouse	V (18)	38 (18)
B023	10-2-33	5.4 (6)	VI (18)	---	Hollywood Storage basement	V (18)	38 (18)
B024	12-30-34	6.5 (6)	IX (18)	---	El Centro	VI (18)	64 (18)
B025	10-31-35	6.0 (6)	VIII (18)	7-30 (18)	Helena, Montana, Carroll College	---	[2]7
B026	9-11-38	5.5 (6)	[1]VI (18)	---	Ferndale City Hall	VI (18)	[2]55
B027	2-9-41	6.6 (6)	[1]VI (18)	---	Ferndale City Hall	VI (18)	104 (18)
B028	4-13-49	7.0 (6)	VIII (18)	70 (11)	Seattle, Wash., Army Base, Eng. Off.	VIII (18)	[2]58

TABLE 1.—*Magnitude, distance, and intensity data for C.I.T. strong motion records*—Continued

C.I.T. number	Date	Richter magnitude	Maximum reported M.M. intensity	Depth (km)	Instrument site	Site M.M. intensity	Distance to epicenter (km)
B029	4-13-49	7.0 (6)	VIII (18)	70 (11)	Olympia, Wash., Hiway Test Lab.	VIII (18)	16 (18)
B030	9-22-52	5.4 (6)	VII (18)	---------	Ferndale City Hall	VI (18)	43 (18)
B031	1-12-54	5.9 (18)	VII-VIII (18)	---------	Taft Lincoln School tunnel	VI (18)	43 (18)
B032	4-29-65	6.5 (18)	VIII (18)	59 (18)	Olympia, Wash., Hiway Test Lab.	VII (18)	[2]61
B033	6-27-66	5.3 (18)	VII (18)	10 (9)	Cholame-Shandon Array #2	VII (18)	[3].08(18)
B034	6-27-66	5.3 (18)	VII (18)	10 (9)	Cholame-Shandon Array #5	VI (8)	[3]5 (4)
B035	6-27-66	5.3 (18)	VII (18)	10 (9)	Cholame-Shandon Array #8	VI (8)	[3]9 (4)
B036	6-27-66	5.3 (18)	VII (18)	10 (9)	Cholame-Shandon Array #12	VI (8)	[3]38 (4)
B037	6-27-66	5.3 (18)	VII (18)	10 (9)	Temblor #2	VI (8)	[3]6 (4)
B038	6-27-66	5.3 (18)	VII (18)	10 (9)	San Luis Obispo	VI (18)	[3]77 (4)
B039	12-10-67	5.8 (18)	[1]VI (18)	---------	Eureka Federal Bldg.	V (18)	[2]51
B040	4-8-68	6.5 (18)	VII (18)	11 (2)	San Onofre SCE Power Plant	V (18)	[2]134
T274	4-12-38	--------	VI (18)	--------	El Centro	VI (18)	13 (18)
T275	6-5-38	--------	V (18)	--------	--do-----	---------	35 (18)
T276	6-6-38	--------	---------	--------	--do-----	---------	43 (18)
T277-T285	Aftershocks						
T286	10-21-42	6.5 (6)	VII (18)	--------	El Centro	VII (18)	48 (18)
T287	1-23-51	5.6 (6)	VII (18)	--------	--do-----	VI (18)	30 (18)
T288	6-13-53	5.5 (6)	VII (18)	--------	El Centro	VI (18)	11 (18)
T289	11-12-54	6.3 (18)	V (18)	--------	--do-----	IV (18)	150 (18)
T290-T291	Foreshocks						
T292	12-16-55	5.4 (18)	VII (18)	--------	El Centro	VI (18)	22 (18)
T293	8-7-66	6.3 (18)	VI (18)	--------	--do-----	VI (18)	[2]147
U294	7-6-34	Offshore	---------	--------	Ferndale City Hall	V (18)	128 (18)
U295	10-31-35	6.0 (6)	VIII (18)	7-30 (18)	Helena, Montana, Federal Bldg.	---------	3-8 (18)
U296	11-21-35	-------	VI (18)	7-30 (18)	--do----------	---------	3-8 (18)
U297	11-28-35	-------	VI (18)	7-30 (18)	--do----------	VI (18)	3-8 (18)
U298	2-6-37	5 3/4 (6)	[1]V (18)	---------	Ferndale City Hall	V (18)	80 (18)
U299	6-30-41	5.9 (6)	[1]VIII (18)	---------	Santa Barbara Court House	VIII (18)	16 (18)
U300	10-3-41	6.4 (6)	[1]VII (18)	---------	Ferndale City Hall	VI (18)	[2]50
U301	3-9-49	5.3 (6)	VII (18)	---------	Hollister Public Library	VII (18)	21 (18)
U302 U303 U304	Aftershocks						
U305	4-25-54	5.3 (18)	VII (18)	---------	Hollister Public Library	VI (18)	27 (18)
U306	9-4-55	5.8 (18)	VII (18)	---------	San Jose Bank of America, 13th floor	VII (18)	10 (18)

TABLE 1.—*Magnitude, distance, and intensity data for C.I.T. strong motion records*—Continued

C.I.T. number	Date	Richter magnitude	Maximum reported M.M. intensity	Depth (km)	Instrument site	Site M.M. intensity	Distance to epicenter (km)
U307	1-19-60	5.0 (18)	VI (18)	---------	Hollister Public Library	VI (18)	6 (18)
U308	6-5-60	5.7 (18)	VI (18)	---------	Ferndale City Hall	VI (18)	59 (18)
U309	4-8-61	5.5 (18)	VII (18)	---------	Hollister Public Library	VII (18)	21 (18)
U310	4-29-65	6.5 (18)	VIII (18)	59 (18)	Seattle, Wash., Federal Bldg.	VIII (18)	[2]22
U311	6-27-66	5.3 (18)	VII (18)	---------	Taft Lincoln School tunnel	IV (18)	[2]131
U312	12-10-67	5.8 (18)	[1]VI (18)	---------	Ferndale City Hall	VI (18)	32 (18)
U313	12-18-67	5.2 (18)	VI (18)	---------	Hollister Public Library	V (18)	[2]39
V314	3-10-33	6.3 (18)	[1]VIII-IX (18)	10 (18)	Los Angeles Subway Terminal Bldg.	VII (18)	59 (18)
V315	3-10-33	6.3 (18)	[1]VIII-IX (18)	---------	Long Beach Public Util. Bldg.	VII-IX(18)	27 (18)
V316	11-14-41	5.4 (6)	VII-VIII (18)	---------	--do----------	VI (18)	6 (18)
V317	11-14-41	5.4 (6)	VII-VIII (18)	---------	Los Angeles C. of C. Bldg.	VI (18)	27 (18)
V318	7-21-52	7.7 (7)	XI (18)	---------	Hollywood Storage penthouse	VII (18)	119 (18)
V319	11-21-52	6± (6)	VII (18)	---------	San Luis Obispo City Rec. Bldg.	VI (18)	77 (18)
V320-V328	Aftershocks						
V329	3-18-57	5.0 (18)	VI (18)	14 (7)	Port Hueneme Navy Res. Lab.	VI (18)	6 (18)
V330	9-4-62	5.0 (18)	VI (18)	---------	Eureka Federal Bldg.	VI (18)	[2]19
V331	7-15-65	4.5 (18)	VI (18)	---------	Castaic, Old Ridge Route	V (18)	[2]18
V332	9-12-66	6¼-6½ (18)	VII (18)	13 (7)	Sacramento Pacific T & T Bldg.	VI (18)	[2]151
V333	9-12-66	6¼-6½ (18)	VII (18)	13 (7)	Sacramento Pacific T & T Bldg., 12th floor	VI (18)	[2]151
W334	9-12-70	5.4 (18)	VII (18)	8 (18)	Wrightwood, 6074 Park Dr.	VI (17)	[2]13
W335	9-12-70	5.4 (18)	VII (18)	8 (18)	Cedar Spgs., Allen Ranch	V-VI (18)	[2]19
W336	9-12-70	5.4 (18)	VII (18)	8 (18)	Cedar Spgs, CWR Site	V-VI (18)	[2]22
W337	9-12-70	5.4 (18)	VII (18)	8 (18)	San Bernadino, Devil's Canyon	VI (17)	18 (18)
W338	9-12-70	5.4 (18)	VII (18)	8 (18)	San Bernadino Hall of Records	VI (17)	[2]18
W339	9-12-70	5.4 (18)	VII (18)	8 (18)	Colton, So. Calif. Edison Co.	VI (17)	[2]31
W340-W341	Records not published						
W342	9-12-70	5.4 (18)	VII (18)	8 (18)	Pasadena C.I.T. Library	V (17)	[2]56

TABLE 1.—*Magnitude, distance, and intensity data for C.I.T. strong motion records*—Continued

C.I.T. number	Date	Richter magnitude	Maximum reported M.M. intensity	Depth (km)	Instrument site	Site M.M. intensity	Distance to epicenter (km)
W343	9-12-70	5.4 (18)	VII (18)	8 (18)	Pasadena C.I.T. Library, 10th floor	V (17)	[2]56
W344	9-12-70	5.4 (18)	VII (18)	8 (18)	Pasadena J.P.L. C.I.T.	V (17)	[2]59
W345	9-12-70	5.4 (18)	VII (18)	8 (18)	Pasadena J.P.L. C.I.T., 9th floor	V (17)	[2]59
W346-W369	Records not published						
Y370	4-8-68	6.5 (18)	VII (18)	11 (2)	Colton, So. Calif. Edison Co.	VI (18)	144 (5)
Y371	4-8-68	6.5 (18)	VII (18)	11 (2)	Santa Ana Orange Cty. Eng. Bldg.	V (16)	[2]174
Y372	4-8-68	6.5 (18)	VII (18)	11 (2)	Long Beach, So. Calif., Edison Co. Terminal Island	VI (18)	[2]205
Y373	4-8-68	6.5 (18)	VII (18)	11 (2)	Pasadena, J.P.L. C.I.T.	---	[2]219
Y374	4-8-68	6.5 (18)	VII (18)	11 (2)	Pasadena, J.P.L. C.I.T., 9th floor	---	[2]214
Y375	4-8-68	6.5 (18)	VII (18)	11 (2)	Pasadena, C.I.T. Library	---	[2]214
Y376	4-8-68	6.5 (18)	VII (18)	11 (2)	Pasadena, Athenaeum C.I.T.	---	[2]214
Y377	4-8-68	6.5 (18)	VII (18)	11 (2)	Los Angeles SCE, 601 W. 5th St.	V (16)	[2]218
Y378	4-8-68	6.5 (18)	VII (18)	11 (2)	Los Angeles Subway Terminal Bldg.	V (16)	214 (5)
Y379	4-8-68	6.5 (18)	VII (18)	11 (2)	Vernon, CMD Bldg.	V (16)	[2]214
Y380	4-8-68	6.5 (18)	VII (18)	11 (2)	Hollywood Storage PE lot	V (16)	[2]223
Y381	4-8-68	6.5 (18)	VII (18)	11 (2)	Hollywood Storage penthouse	V (16)	[2]223

[1]Offshore epicenter.
[2]Distance calculated from coordinates of epicenter and station.
[3]Closest distance to fault.

References found in table

1. Algermissen, S. T., 1969, Seismic risk studies in the United States: World Conf. on Earthquake Engineering, 4th, Proc., v. 1, p. 14-27.
2. Allen, C. R., and Nordquist, J. M., 1972, Foreshock, mainshock, and larger aftershocks of the Borrego Mountain earthquake, in the Borrego Mountain earthquake of April 9, 1968: U.S. Geol. Survey Prof. Paper 787, p. 16-23 [1973].
3. Cloud, W. K., 1957, Intensity and ground motion of the San Francisco earthquake of March 22, 1957, in San Francisco earthquakes of March 1957: California Div. Mines Spec. Rept. 57, p. 49-58.
4. Cloud, W. K., and Perez, V., 1967, Accelerograms-Parkfield earthquake: Seismol. Soc. America Bull., v. 57, p. 1179-1192.
5. Cloud, W. K., and Scott, N. H., 1968, The Borrego Mountain, California, earthquake of April 9, 1968, a preliminary engineering seismology report: Seismol. Soc. America Bull., v. 58, no. 3, p. 1187-1191.
6. Coffman, J. L., and von Hake, C. A., eds., 1973, Earthquake history of the United States: U.S. Dept. Commerce Pub. 41-1, 208 p.

TABLE 1.—*Magnitude, distance, and intensity data for C.I.T. strong motion records*—Continued

7. Harding, S. T., and Rinehart, W., 1966, Preliminary seismological report, in Coffman, J. L., ed., The Parkfield, California, earthquake of June 27, 1966: U.S. Environmental Sci. Services Adm., p. 1-16.
8. Hileman, J. A., Allen, C. R., and Nordquist, J. M., 1973, Seismicity of the southern California region 1 January 1932 to 31 December 1972: Geol. Planetary Sci. Div., Contrib. 2385, Pasadena, Calif. Inst. Technology, 83 p.
9. Lander, J. F., 1966, Seismological notes, May and June, 1966: Seismol. Soc. America Bull., v. 56, no. 6, p. 1429-1432.
10. Maley, R. P., and Cloud, W. K., 1973, Strong motion accelerograph records, in Benfer, N. A., Coffman, J. L., and Bernick, J. R., eds., volume 3 of San Fernando, California, Earthquake of February 9, 1971: U.S. National Oceanic and Atmospheric Admin., p. 325-348.
11. Nuttli, O. W., 1952, The western Washington earthquake of April 13, 1949: Seismol. Soc. America Bull., v. 42, no. 1, p. 21-28.
12. Scott, N. H., 1973, Felt area and intensity of San Fernando earthquake, in Benfer, N. A., Coffman, J. L., and Bernick, J. R., eds., volume 3 of San Fernando, California, Earthquake of February 9, 1971: U.S. National Oceanic and Atmospheric Administration, p. 23-48.
13. Seismological Society of America, 1956, Seismological notes: Seismol. Soc. America Bull., v. 46, no. 2, p. 160-163.
14. Tocher, D., 1959, Seismographic results from the San Francisco earthquakes, in San Francisco earthquakes of March 1957: California Div. Mines and Geology, Spec. Rept. 57, p. 59-71.
15. Trifunac, M. D., and Brady, A. G., 1975, On the correlation of seismic intensity scales with the peaks of recorded strong ground motion: Seismol. Soc. America Bull., v. 65, no. 1, p. 139-162.
16. U.S. Coast and Geodetic Survey, 1968, Abstracts of earthquake reports for the U.S., April-June 1968: Boulder, Colo., U.S. Environmental Data Service, p. 5-56.
17. _____ 1970, Abstracts of earthquake reports for the U.S., July-September 1970: Boulder, Colo., U.S. Environmental Data Service, p. 35.
18. U.S. Department of Commerce, 1933-1970, United States earthquakes: U.S. Dept. Commerce, ann. repts.

Jour. Research U.S. Geol. Survey
Vol. 5, No. 4, July–Aug. 1977, p. 445–451

SPHERULITIC RHYOLITE DIKE FROM GOAT ISLAND, SOUTHEASTERN ALASKA

By WALTER R. VENNUM [1] and G. DONALD EBERLEIN,
Rohnert Park, Calif., Menlo Park, Calif.

Abstract.—Spherulites, as much as 4 mm in diameter, locally constitute almost 50 percent by volume of a dark-red rhyolite dike that intrudes porphyritic pyroxene gabbro along the northeast coast of Goat Island, 3.2 km northwest of Hydaburg, southeastern Alaska. The largest spherulites are composed mainly of α-quartz, whereas the smallest consist of a microcrystalline intergrowth of tridymite and alkali feldspar. Textural relations indicate that the radial and concentrically zoned structures are the products of devitrification of glassy lava. The mineralogy of the dike is similar to that of other spherulitic rhyolites except that quartz occurs to the exclusion of cristobalite. The posteruptive formation of the spherulites has also resulted in alkali transfer, the groundmass of the dike being enriched in both sodium and potassium relative to the spherulites.

A spherulitic rhyolite dike crops out along the northeast coast of Goat Island, 3.2 km northwest of the village of Hydaburg in southeastern Alaska (fig. 1). The dike intrudes a porphyritic pyroxene metagabbro, which, in turn, intrudes poorly sorted polymictic sedimentary breccia of Ordovician age that probably is correlative with the lower part of the Descon Formation (Eberlein and Churkin, 1970). Petrographically similar gabbro crops out along the east shore of Natzuhini Bay, 1.9 km north of Hydaburg. Berg (1974) described spherulite-bearing rhyolites in the middle Paleozoic Puppets Formation, which crops out on Gravina Island 75 km to the east, and Sainsbury (1961) reported nonspherulitic Devonian rhyolite of similar composition on Kasaan Island 40 km to the northeast. The complex structure of intervening Prince of Wales Island, however, precludes a positive correlation.

Acknowledgment.—Scott Strathouse, a student at California State College, Sonoma, helped considerably with the X-ray work.

PETROGRAPHY OF THE GABBRO

The gabbro (tables 1 and 2) is dark green and contains 10 to 15 percent blocky clinopyroxene phenocrysts (4–12 mm) in an aphanitic groundmass. In thin section, none of the pyroxene is fresh, and at least two-thirds of each crystal has been replaced by colorless chlorite. Tremolite is localized along cleavage planes or fractures and in places rims the pyroxene. Unaltered pyroxene relics have the following optical properties: $Z \wedge c = 37°$, $\delta = 0.27$, and $2V_\gamma = 60°$. Rare plagioclase phenocrysts (4–5 mm) are so completely saussuritized that compositional determination is impossible. Rather broad albite twin lamellae suggest at least a moderate original calcium content.

The groundmass is largely fibrous tremolite ($Z \wedge c = 18°$ and $\delta = 0.022$) with subordinate colorless chlorite and rare granular epidote, but relic lath-like plagioclase microlites can be recognized. Opaque octahedral grains have been completely converted to leucoxene. This mineral assemblage indicates either the quartz-albite-muscovite-chlorite or quartz-albite-epidote-biotite subfacies of the greenschist facies (Winkler, 1967).

PETROGRAPHY OF THE DIKE

The dike is a rhyolite (tables 1 and 2) that has a dark-red aphanitic groundmass, is about 30 cm wide,

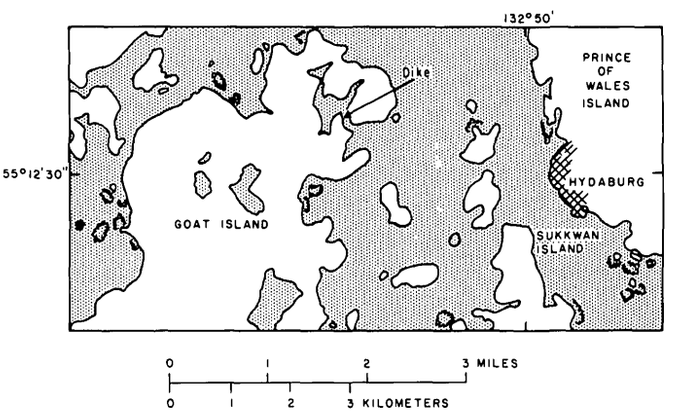

FIGURE 1.—Location of spherulitic rhyolite dike on Goat Island, southeastern Alaska.

[1] California State College, Sonoma, Calif.

TABLE 1.—*Chemical analyses, in weight percent, of pyroxene gabbro and spherulitic dike from Goat Island, Alaska*

[Rapid-rock analysis according to the method of Shapiro and Brannock (1962), supplemented by atomic absorption. Analyst: Sam Botts]

Oxides	Pyroxene gabbro 71AV135a	Spherulitic dike 71AV135b
SiO_2	46.2	74.8
Al_2O_3	13.0	11.0
Fe_2O_3	1.7	2.0
FeO	8.2	.8
MgO	13.7	.3
CaO	6.6	1.4
Na_2O	2.4	4.5
K_2O	.5	2.2
H_2O+	5.0	.6
H_2O-	.2	.2
TiO_2	.6	.1
P_2O_5	.2	.0
MnO	.3	.1
CO_2	1.3	1.4
Total	99.9	99.4
Powder density ---- g/cm³ ---	2.90	2.64
Bulk density ------ g/cm³ ---	2.87	2.51

TABLE 2.—*Trace-element concentrations, in parts per million, of samples from Goat Island, Alaska*

[Semiquantitative six-step spectrographic analysis. Analyst: Chris Heropoulos. Looked for but not detected: Ag, As, Au, B, Bi, Cd, Ge, In, Li, Mo, Pd, Pt, Re, Sc, Ta, Te, Th, Tl, U, W, Zn.]

Element	Pyroxene gabbro 71AV135a	Spherulitic dike 71AV135b
Ba	300	70
Be	----	3
Ce	----	100
Co	50	----
Cr	1000	----
Cu	100	5
Ga	10	50
Hf	----	50
La	----	70
Nb	----	50
Ni	500	----
Pb	----	10
Sc	70	----
Sn	----	7
Sr	150	70
V	200	----
Y	15	200
Yb	3	20
Zr	50	1500

and can be traced along strike for approximately 12 m. Spherulites (2–4 mm) that exhibit both a radial structure and a concentric zonation (fig. 2*A–C*) constitute about 30 percent of the dike interior but are rare and poorly developed within a 12.5-mm-wide, fine-grained, chilled marginal zone. Flow layering parallel to the dike walls (figs. 2*D* and 3*A*) persists inward for 7.5 cm and is defined by alternating lenses of minute hematite and titanomagnetite grains.

X-ray data indicate that the spherulites are composed mainly of α-quartz. The concentric zonation is defined by hematite-free cores and outer hematite-rich zones. Outermost hematite-free rims occur on a few of the spherulites, and a few spherulites display several concentric zones alternately rich and poor in hematite. The spherulites commonly contain nuclei of dolomite(?) rhombs (some of which are marginally replaced by hematite), titanomagnetite octahedra, hematite grains or rarely muscovite (fig. 2*A–B*).

Within the fine-grained marginal zone the groundmass is a variable-grain-size mosaic (50–150 micrometers) of α-quartz and oligoclase. The feldspar occurs mainly in coarser grained, irregularly shaped patches in which many of the grains are fan shaped (fig. 3*B*). Some of these grains show slight zoning, and most are discontinuously twinned. Many of the patches are localized near the borders of the spherulites, and the matrix quartz occurs mainly in the groundmass farthest from the spherulite margins (fig. 3*C*). Many of the larger spherulites have thin rims (50 μm) of radial untwinned feldspar, and a few are veined by similar material. Twinned grains yield a composition of An_{16} (Michel-Lévy).

Inward from the chilled margin, twinning in the feldspar disappears, and the amount of quartz increases. Small spherulites (150 μm) with well-developed radial structure (figs. 3*D* and 4*A*) begin to appear within the groundmass near the inner margin of the chilled zone and increase inward in abundance until they locally make up nearly 50 percent of the matrix. Accessory minerals include rounded zircons, slightly pleochroic green hornblende, muscovite, and titanomagnetite. Very fine grained disseminated hematite is abundant throughout the dike.

X-ray diffraction studies (table 3) show the groundmass of the dike interior to be composed of α-quartz, alkali feldspar, and tridymite. Feldspar and tridymite are concentrated in the small spherulites, and quartz constitutes the remaining granoblastic matrix. Although the feldspar peaks are generally sharp, the mineral cannot be unambiguously identified. Comparison with powder data published by Donnay and Donnay (1952) indicates only that the feldspar composition lies in the albite-anorthoclase range. The diffraction peaks closely match low-temperature oligoclase with 81.6 percent albite, 16.5 percent anorthite and 1.9 percent or-

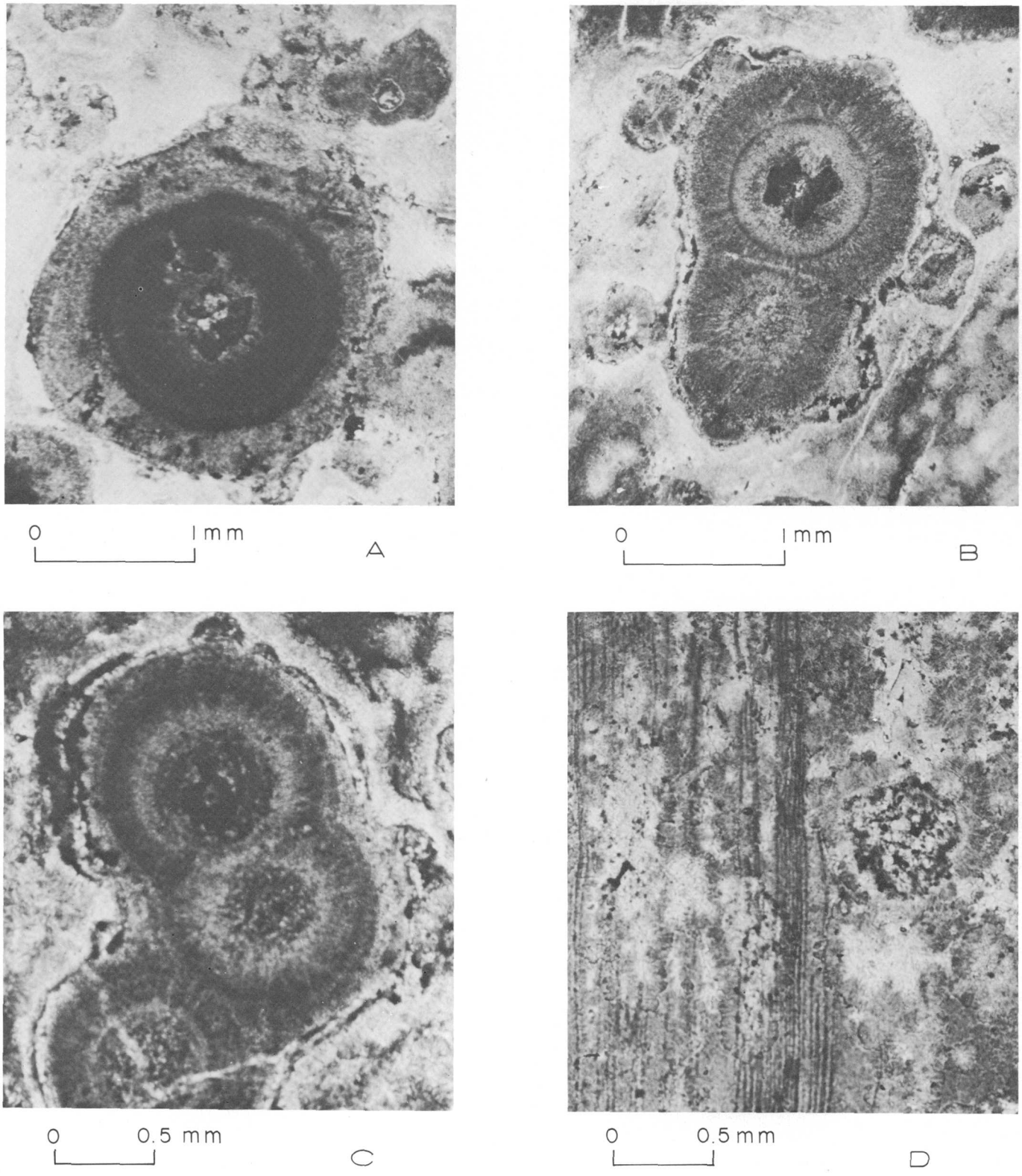

FIGURE 2.—Photomicrographs of spherulitic rhyolite. *A*, Large, concentrically zoned spherulite nucleated about a dolomite(?) rhomb. Plane-polarized light. *B*, Large, coalesced spherulites with concentric zonation and radial structure, nucleated about several dolomite(?) rhombs. Plane-polarized light. *C*, Three large, coalesced spherulites with concentric zonation and radial structure, nucleated about hematite grains. Plane-polarized light. *D*, Layering of minute magnetite grains parallel to dike margins. Plane-polarized light.

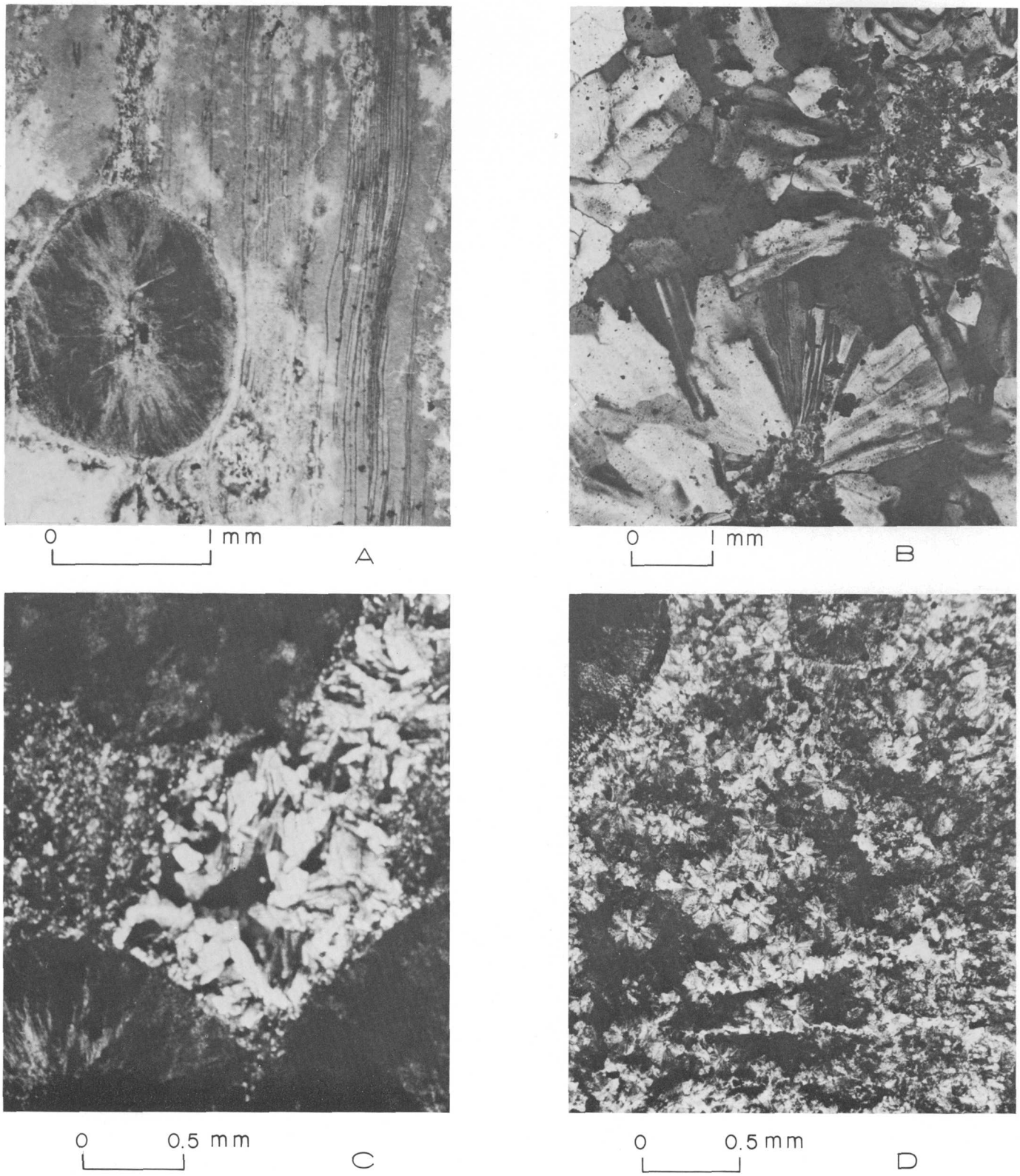

FIGURE 3.—Photomicrographs of spherulitic rhyolite. *A*, Layering of minute magnetite grains parallel to dike margins. Plane-polarized light. *B*, Fan-shaped oligoclase grains in dike matrix. Crossed nicols. *C*, Coarse-grained patch of untwinned feldspar adjacent to spherulite margins. Crossed nicols. *D*, Small spherulites in groundmass of dike interior. Crossed nicols.

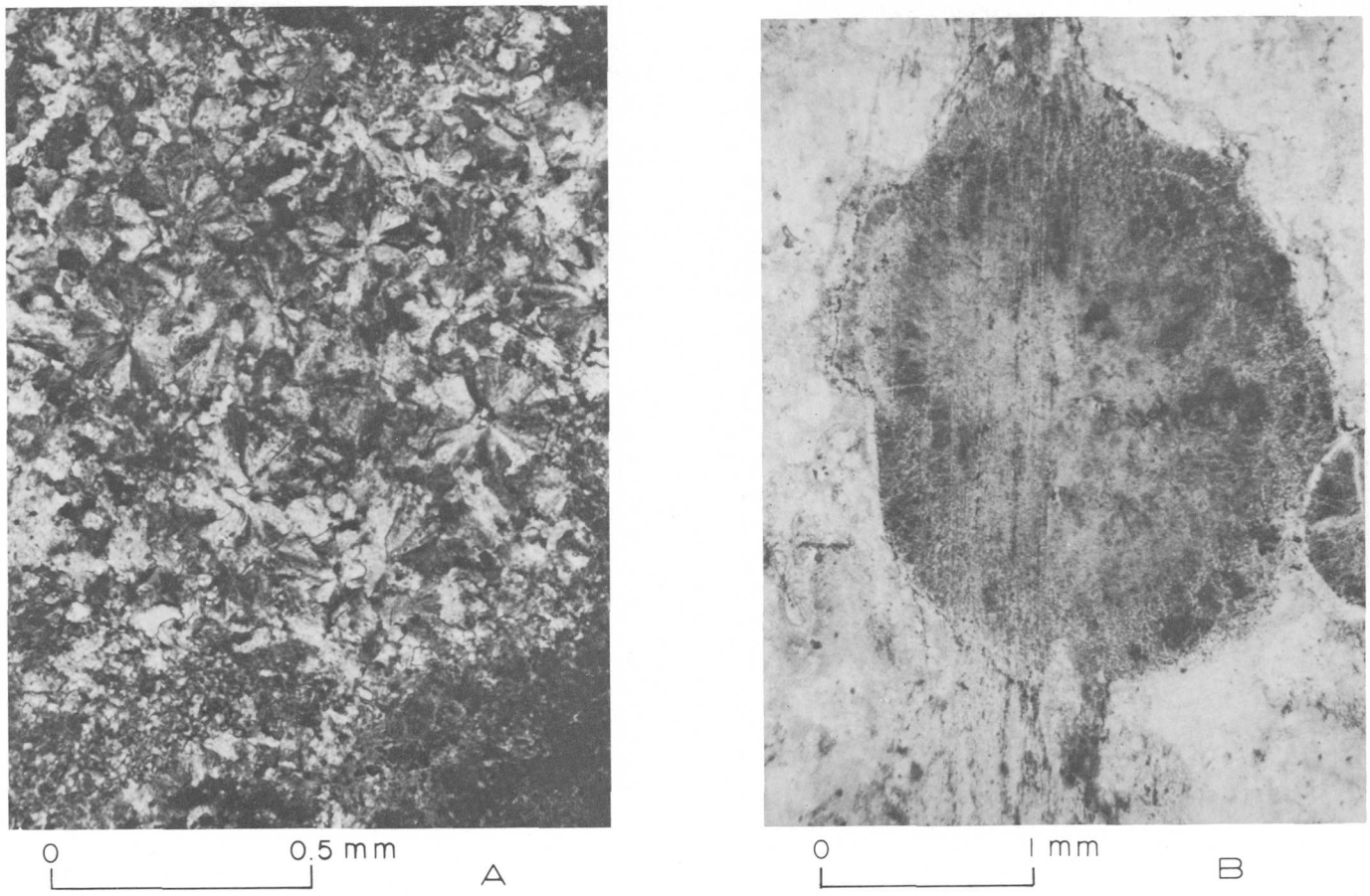

FIGURE 4.—Photomicrographs of spherulitic rhyolite. *A*, Small spherulites in groundmass of dike interior. Crossed nicols. *B*, Layers of small magnetite grains pass undeflected through spherulite in dike margin. Plane-polarized light.

TABLE 3.—*X-ray powder data from dike matrix*

[Cu-Kα radiation, Ni-filtered, 35KV, 18mA; Scanning range 20°2θ-44°2θ; Scanning speed 2° 2θ/minute. A, anorthoclase; Ab, albite; S, sanidine; Q, quartz; T, tridymite.]

d (Å)	I	
4.25	12.0	Q
4.005	10.5	T
3.83	1.0	A, Ab, T
3.75	10.0	A, Ab, T
3.65	11.5	Ab, T
3.50	1.0	Ab
3.46	1.5	S, A, T
3.34	81.5	Q, T
3.23	4.5	A, Ab, S, T
3.16	39.0	Ab, T
3.02	1.0	Ab, T
2.93	3.0	A, Ab, S
2.84	1.0	Ab
2.44	6.0	Q
2.115	3.5	Q

thoclase (Goodyear and Duffin, 1954). Three of the peaks fit sanidine as well as albite-anorthoclase, and sanidine may be present. Salic constituents compose 94.5 percent of the norm (table 4). Normative feldspar

TABLE 4.—*CIPW norms of spherulitic dike*

[A, original analysis; B, original analysis calculated volatile free.]

	71AV135b	
	A	B
Quartz	36.59	38.46
Orthoclase	12.80	13.36
Albite	38.29	39.33
Anorthite	3.34	3.34
Wollastonite	.58	.70
Diopside (Fe free)	1.73	1.73
Magnetite	2.55	2.55
Hematite	.32	.32
Total	96.20	99.79

recalculated on the basis of 100 percent (70.2 percent albite, 23.8 percent orthoclase, 6.0 percent anorthite) plots near the anorthoclase-anorthoclase cryptoperthite boundary in Tuttle's (1952) classification of alkali feldspars. This agrees well with the X-ray results. Tridymite was identified from the X-ray pattern and typical wedge-shaped crystal form and was confirmed optically with oil immersion techniques.

Similar mineralogy has been reported from other spherulitic rhyolites. Ewart (1971) found spherulites in the Aratiatia Rhyolite of New Zealand to be composed of cryptocrystalline intergrowths of α-cristobalite and an alkali feldspar in the albite-anorthoclase range. Tanida (1961) reported cristobalite, tridymite, albite-anorthoclase, and sanidine in spherulites collected from welded dacite tuffs and rhyolite lava flows in Japan, but he observed sanidine only in rocks with greater than 16 percent normative orthoclase.

ORIGIN OF THE SPHERULITES

The mineralogy and texture of the dike indicate that it is a devitrified glassy rhyolite. Ewart (1971) has described rhyolite flows and domes from New Zealand that grade from outer vesicular glassy zones through partly devitrified spherulitic rock to completely devitrified spherulitic lava containing no trace of residual volcanic glass. In the completely devitrified New Zealand rocks, interstitial glassy areas remaining after initial spherulite formation have been transformed into a nonspherulitic microcrystalline mosaic similar to the nonspherulitic granoblastic part of the Goat Island dike matrix. The latter dike appears to have been completely devitrified. Devitrification began with the formation of the large quartz spherulites and was followed by transformation of the remaining interstitial glassy areas into a microcrystalline aggregate of granoblastic quartz and small spherulites of intergrown tridymite and alkali feldspar.

Lofgren (1971) has produced spherulites in experimentally devitrified natural rhyolitic glass, and spherulitic crystallization is usually attributed to high-temperature partial devitrification. Spherulites can, however, also form as primary features in other types of igneous rocks. Variolitic texture, for example, is often reported in petrographic descriptions of deep-sea basalts (Erlank and Reid, 1974; Paster, 1971; Yeats and others, 1973) and presumably originated by partial devitrification. Flow layering in the margin of the Goat Island dike passes through the spherulites without deflection (fig. 4*B*) thus indicating a postconsolidation age for the spherulites. Hooper (1962, p. 41) has described "* * * long thin albite crystals which form a vague radiating pattern surrounded by a quartz-potash feldspar intergrowth * * *" in a metasomatic alkali granite from Anvers Island off the northwest coast of the Antarctic Peninsula. This description appears similar to that of the fan-shaped oligoclase grains found in the groundmass of the Goat Island dike (fig. 3*B*). Although alkali transfer appears to have taken place (see below), the dike itself is not metasomatic in origin.

CHEMISTRY OF THE DIKE

The dike is characterized by abundant rare-earth elements, low barium and strontium contents, and a zirconium-hafnium ratio of 30:1 (table 2). Fleischer (1955) has estimated the zirconium-hafnium ratio in the Earth's crust to be close to 50:1. Some of Fleischer's samples with low zirconium-hafnium ratios also had high concentrations of uranium and thorium but do not show a consistent correlation between radioactivity and hafnium content. Zircon grains in the dike are minute and do not exhibit the lowered birefringence and refractive indices characteristic of metamict varieties. Gottfried and Waring (1964) found that the zirconium-halfnium ratio in the southern California batholith decreased from mafic to more silicic rocks. Although the average ratio for the entire batholith approximated Fleischer's value, the zirconium-hafnium ratio in some of the granites is as low as 25:1.

Chemical data (tables 1 and 2) do not conclusively substantiate or negate a genetic relation between the dike and gabbro. Fractional crystallization could account for differences in major- and trace-element amounts, but several features suggest that the dike is not a late-stage differentiate of the gabbro: a striking difference in silica and zirconium contents; complete absence of cobalt, chromium, nickel, scandium, and vanadium from the dike; and the much lower barium content of the dike. Barium has been shown to concentrate in residual liquids until the crystallization of potassium feldspar begins (Taylor, 1965). The fact, that the dike contains 75 percent less barium than the gabbro strongly suggests a different magmatic source for the two rocks. Nockolds and Allen (1953, 1954, 1956) have shown that the ratio gallium/aluminum remains constant in most rock series except for occasional slight enrichment of gallium in the final stages of differentiation. The gallium-aluminum ratio in the dike is 6.5 times that in the gabbro.

Several authors (Lipman, 1965; Lipman and others, 1968; Noble, 1967) have shown that rhyolitic volcanic rocks are especially prone to posteruptive chemical modification; the original composition of the Goat Island dike thus can only be approximated. Contrasting mineralogy of the spherulites and the matrix strongly

suggests that alkali transfer has taken place, the matrix being enriched in both sodium and potassium in relation to the large spherulites. This process has been documented in rhyolitic rocks from New Zealand (Ewart, 1971), Arizona (Simons, 1962) and Washington (Coombs, 1952) and appears to have taken place in the Japanese specimens examined by Tanida (1961). Lipman (1965, p. D5) has attributed a higher Fe_2O_3–FeO ratio in reddish crystallized glass relative to coexisting black rhyolitic vitrophyre from Nevada to the postextrusive conversion of magnetite crystallites to hematite; this process may readily account for the oxidized state of the iron and the red color of the Goat Island dike.

REFERENCES CITED

Berg, H. C., 1974, Geology of Gravina Island, Alaska: U.S. Geol. Survey Bull. 1373, 41 p.

Coombs, H. A., 1952, Spherulitic breccias in a dome near Wenatchee, Washington: Am. Mineralogist, v. 37, nos. 3–4, p. 197–206.

Donnay, G. H., and Donnay, J. D. H., 1952, The symmetry change in the high temperature alkali-feldspar series: Am. Jour. Sci., Bowen vol., p. 115–132.

Eberlein, G. D., and Churkin, Michael, Jr., 1970, Paleozoic stratigraphy in the northwest coastal area of Prince of Wales Island, southeastern Alaska: U.S. Geol. Survey Bull. 1284, 67 p.

Erlank, A. J., and Reind, D. L., 1974, Geochemistry, mineralogy and petrology of basalts, Leg 25, Deep Sea Drilling Project, *in* Simpson, E. S. W., Schlich, R., and others, Initial reports of the Deep Sea Drilling Project, v. 25, Washigtnon, D.C., U.S. Govt. Printing Office, p. 543–551.

Ewart, A., 1971, Chemical changes accompanying spherulitic crystallization in rhyolitic lavas, central volcanic region, New Zealand: Mineralog. Mag., v. 38, p. 424–434.

Fleischer, Michael, 1955, Hafnium content and hafnium-zirconium ratio in minerals and rocks: U.S. Geol. Survey Bull. 1021–A, 13 p.

Goodyear, Jeffrey, and Duffin, W. J., 1954, The identification and determination of plagioclase feldspars by the X-ray powder method: Mineralog. Mag., v. 30, p. 306–326.

Gottfried, David, and Waring, C. L., 1964, Hafnium content and Hf/Zr ratio in zircon from the southern California batholith: U.S. Geol. Survey Prof. Paper 501–B, p. B88–B91.

Hooper, P. R., 1962, The petrology of Anvers Island and adjacent islands: Falkland Islands Dependencies Survey Sci. Rept., no. 34, 69 p.

Lipman, P. W., 1965, Chemical comparison of glassy and crystalline volcanic rocks: U.S. Geol. Survey Bull. 1201–D, 24 p.

Lipman, P. W., Christiansen, R. L., and van Alstine, R. E., 1968, Retention of alkalis by calc-alkaline rhyolites during crystallization and hydration: Am. Mineralogist, v. 54, p. 286–291.

Lofgren, G. E., 1971, Experimentally produced devitrification textures in natural rhyolitic glass: Geol. Soc. America Bull., v. 82, p. 111–124.

Noble, D. C., 1967, Sodium, potassium, and ferrous iron contents of some secondarily hydrated natural silicic glasses: Am. Mineralogist, v. 52, p. 280–286.

Nockolds, S. R., and Allen, R., 1953, The geochemistry of some igneous rock series, 1: Geochim. et Cosmochim. Acta, v. 4, p. 105–142.

——— 1954, The geochemistry of some igneous rock series, 2: Geochim. et Cosmochim. Acta, v. 5, p. 245–285.

——— 1956, The geochemistry of some igneous rock series, 3: Geochim. et Cosmochim. Acta, v. 9, p. 34–77.

Paster, T. P., 1971, Petrologic variations within submarine basalt pillows of the south Pacific Ocean, *in* Reid, J. L., ed., Antarctic oceanology I: Am. Geophys. Union, p. 283–308.

Sainsbury, C. L., 1961, Geology of part of the Craig C–2 quadrangle and adjoining areas, Prince of Wales Island, southeastern Alaska: U.S. Geol. Survey Bull. 1058–H, p. 299–362.

Shapiro, Leonard, and Brannock, W. W., 1962, Rapid analysis of silicate, carbonate, and phosphate rocks: U.S. Geol. Survey Bull. 1144–A, p. A1–A56.

Simons, F. S., 1962, Devitrification dikes and giant spherulites from Klondyke, Arizona: Am. Mineralogist, v. 47, p. 871–885.

Tanida, Katsutoshi, 1961, A study on salic effusive rocks: Tohoku Univ. Sci. Repts., Ser. 3, v. 7, no. 1, p. 47–100.

Taylor, S. R., 1965, The application of trace element data to problems in petrology: Phys. Chem. Earth 6, p. 133–213.

Tuttle, O. F., 1952, Optical studies on alkali feldspars: Am. Jour. Sci., Bowen vol., p. 553–567.

Winkler, H. G. F., 1967, Petrogenesis of metamorphic rocks (2nd ed.): New York, Springer-Verlag, 220 p.

Yeats, R. S., Forbes, W. C., Heath, G. R., and Scheidegger, E. F., 1973, Petrology and geochemistry of Deep Sea Drilling Project Leg 16 basalts, eastern equatorial Pacific, *in* van Andel, T. H., Heath, G. R., and others, Initial reports of the Deep Sea Drilling Project, v. 16, Washington, D.C., U.S. Govt. Printing Office, p. 617–645.

Jour. Research U.S. Geol. Survey
Vol. 5, No. 4, July–Aug. 1977, p. 453–455

LECTOTYPE FOR THE MIOCENE PLANKTONIC FORAMINIFER *GLOBIGERINOIDES PSEUDORUBER* TODD, 1957

By R. Z. POORE, Menlo Park, Calif.

Abstract.—A lectotype is designated and illustrated for the Miocene planktonic foraminifer *Globigerinoides pseudoruber* Todd, 1957. Planktonic foraminifers in the type sample are indicative of foraminiferal Zone N–8.

The holotype of *Globigerinoides pseudoruber* Todd, a Miocene planktonic foraminifer, was lost during handling in 1974. Thus a lectotype has been chosen from a suite of unfigured paratypes of *G. pseudoruber* located in the U.S. National Museum.

***Globigerinoides pseudoruber* Todd, 1957**

Figures 1–5

Globigerinoides pseudorubra Todd, 1957, p. 303, pl. 74, fig. 10.

Globigerinoides subquadratus subelongatus Brönnimann and Resig, 1971, p. 1274, pl. 13, figs. 1–2, 4–5.

Description of lectotype.—The fairly large test consists of three whorls of subglobular chambers arranged in a very high trochospire. Three chambers are present in the ultimate whorl, three and one-half in the penultimate whorl, and four in the antepenultimate whorl. Sutures are distinctly incised. Maximum diameter of the test is approximately 0.55 mm. The umbilical, highly arched, subcircular primary aperture of the ultimate chamber is situated over the suture between the penultimate and antepenultimate chambers of the outer whorl. Two smaller supplementary apertures, also situated at suture junctions, are present on the spiral side. Supplementary apertures are present in each chamber of the ultimate whorl, but, as matrix obscures parts of the test, it could not be determined if two supplementary apertures are present in every chamber.

Examination of the suite of paratypes indicates that apertures are commonly bordered by a narrow rim. The test surface is coarsely pitted.

The lectotype (USNM 689869) has been separated from the other paratypes and is housed in the U.S. National Museum. The type locality of *G. pseudoruber* is the Fina-sisu Formation, 2.6 kilometers northeast of the seaward tip of the southwest point of Saipan, USGS sample f21133 (C–85) of Todd (1957). The sample was collected by P. E. Cloud, Jr., R. G. Schmidt, and H. W. Burke.

Discussion.—Todd (1957) noted that the prominent spire of *Globigerinoides pseudoruber* serves to distinguish it from *G. subquadratus* Brönnimann (figs. 6–8), a form described from the same locality with an indistinct or low spire (Brönnimann, in Todd and others, 1954). The present author has noted that when populations of the two taxa are viewed, the two taxa also differ in the following respects:

1. The primary aperture of *G. pseudoruber* tends to be slightly asymmetrical with respect to a line projected along the suture between the other two chambers of the final whorl. Thus in many individuals referable to *G. pseudoruber*, this imaginary line would not precisely bisect the aperture, whereas it would in most individuals referable to *G. subquadratus*.
2. Significantly reduced (kummerform) ultimate chambers occur more often in *G. pseudoruber* than in *G. subquadratus*.

These differences are relatively minor, however, and the presence of transitional forms between the two taxa in C–85 suggsts that they are closely related.

Planktonic foraminifers, including *Globorotalia grata* (Todd) (figs. 9, 12, 13), detected in sample C–85 are listed in table 1. Differences between the planktonic assemblage listed here and that given by Todd (1957, table 2) are, in general, minor and due primarily to taxonomic changes and studies completed since 1957. The occurrence of *Globigerinoides sicanus*, *Globigerinatella insueta*, and *Praeorbulina* spp.(figs. 10, 11) in C–85 without *Orbulina sensu* Blow (1956) is indicative of foraminiferal Zone N–8 of Blow (1969). Following present calibrations of Blow's zonation to the Cenozoic time scale, this zone is just below (Berggren, 1972) or at (Ryan and others, 1975) the early Miocene–middle Miocene boundary of international usage.

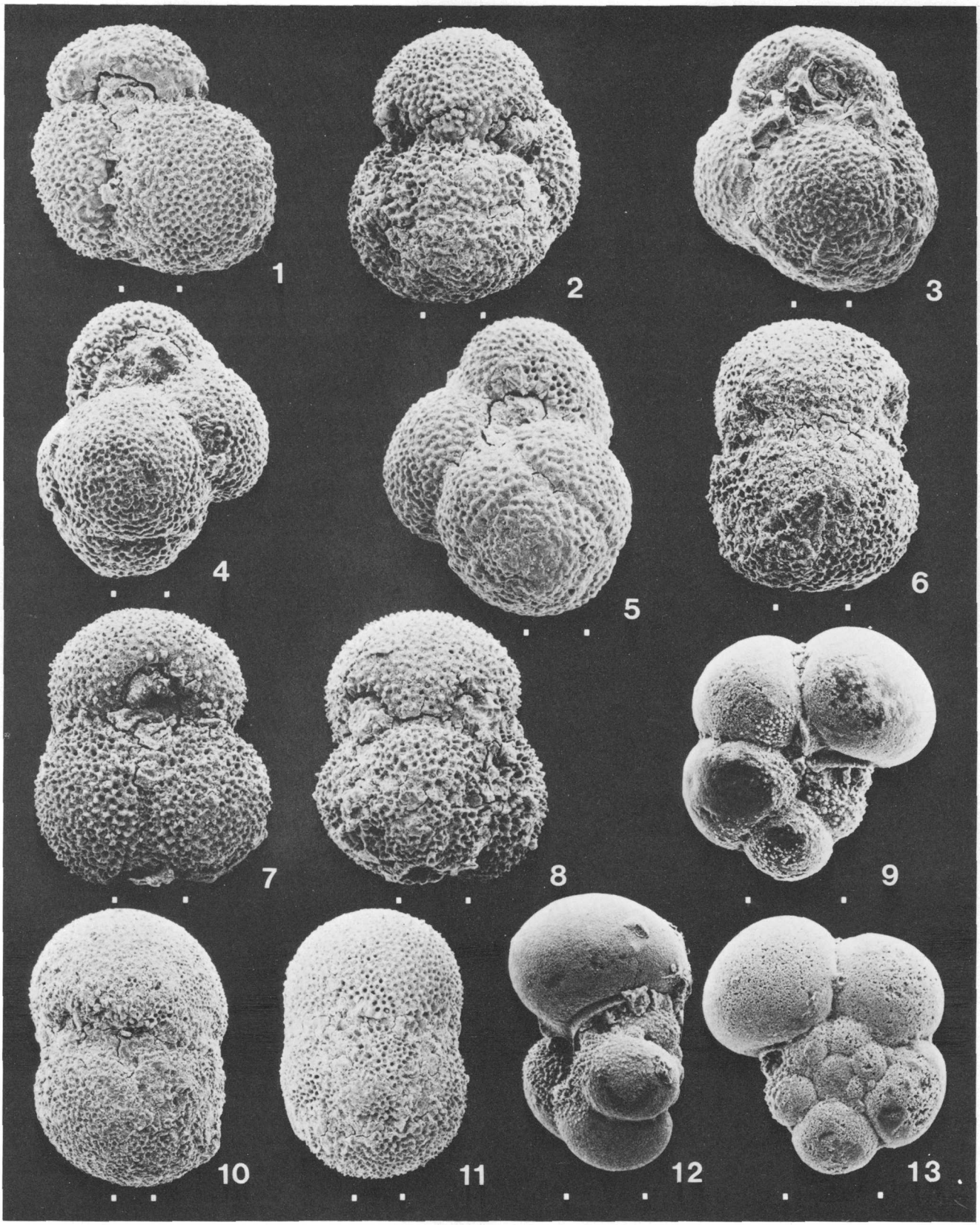

FIGURES 1–13.—All specimens from locality C–85 of Todd, 1957. Scale bar, delineated by white dots, equals 100 μm for all figures.

Globigerinoides pseudoruber has been recorded from the equatorial west Pacific (DSDP site 64) as *G. subquadratus subelongatus* (Brönnimann and Resig, 1971). A reconnaissance examination of material on hand of appropriate age revealed the presence of good examples of *G. pseudoruber* at DSDP site 289 (core 51, section 2, 62–64 cm; Zone N–9) near DSDP site 64. In addition rare, poorly preserved specimens of *G. pseudoruber* were found in a sample from the type Langhian in Italy (locality E of Cita, 1967; approx. Zone N–8). Thus it appears that *G. pseudoruber* has a fairly wide geographic distribution and may prove useful in early and middle Miocene biostratigraphic studies once its range is more fully documented.

Acknowledgments.—Ruth Todd and Beverly Tate greatly assisted locating material from C–85 stored in the U.S. National Museum.

TABLE 1.—*Planktonic foraminifers found in C–85*

Globigerinoides subquadratus Brönnimann
G. trilobus (Reuss)
G. quadrilobatus (d'Orbigny)
G. sicanus (de Stefani)
G. pseudoruber Todd
G. diminutus Bolli
Globigerinatella insueta Cushman and Stainforth
Globorotalia archeomenardii Bolli
G. grata (Todd)
Globorotaloides suteri Bolli
Globoquadrina altispira (Cushman and Jarvis)
G. dehiscens (Chapman, Parr, and Collins)
Praeorbulina transitoria (Blow)
P. glomerosa curva (Blow)
Globigerina praebulloides Blow
G. spp.

REFERENCES CITED

Berggren, W. A., 1972, A Cenozoic time-scale—Some implications for regional geology and paleobiogeography: Lethaia, v. 5, p. 195–215.

Blow, W. H., 1956, Origin and evolution of the foraminiferal genus *Orbulina* d'Orbigny: Micropaleontology, v. 2, no. 1, p. 57–70.

———1969, Late Middle Eocene to Recent planktonic foraminiferal biostratigraphy, *in* Internat. Conf. Planktonic Microfossils, 1st, Geneva 1967; Leiden, Netherlands, E. J. Brill, Proc., v. 1, p. 199–422.

Brönnimann, Paul, and Resig, Johanna, 1971, A Neogene globigerinacean biochronologic time-scale of the southwestern Pacific: Deep Sea Drilling Proj. Initial Repts., v. 7, p. 1235–1470.

Cita, M. B., 1967, Remarks on the type-Langhian, *in* Selli, Raimondo, ed., Excursion Guidebook 1: Internat. Union Geol. Sci., Mediterranean Neogene Comm., 4th Cong., Bologna, Italy, 1967, p. 65–72.

Ryan, W. B. F., Cita, M. B., Rawson, M. D., Burckle, L. H., and Saito, Tsunemasa, 1975, A paleomagnetic assignment of Neogene stage boundaries and the development of isochronous datum planes between the Mediterranean, the Pacific and Indian Oceans in order to investigate the response of the world ocean to the Mediterranean "Salinity Crisis": Riv. Italiana Paleontologia e Stratigrafia, v. 80, no. 4, p. 631–688.

Todd, Ruth, 1957, Smaller Foraminifera, *in* Geology of Saipan, Mariana Islands: U.S. Geol. Survey Prof. Paper 280–H, p. 265–320.

Todd, Ruth, Cloud, P. E., Jr., Low, Doris, and Schmidt, R. G., 1954, Probable occurrence of Oligocene on Saipan: Am. Jour. Science, v. 252, p. 673–682.

FIGURES 1–5. *Globigerinoides pseudoruber* Todd.
1. Umbilical view of lectotype. USNM 689869.
2. Spiral view of lectotype.
3. Umbilical view of topotype; note slightly asymmetric position of aperture with respect to suture between first two chambers of final whorl. USNM 689870.
4. Oblique umbilical view of paratype. Part of ultimate chamber near aperture is broken off. USNM 689871.
5. Spiral view of figure 4. Note prominent spire.

6–8. *Globigerinoides subquadratus* Brönnimann.
6. Side view of topotype, note flat spiral side. USNM 689872.
7. Umbilical view of topotype. USNM 689873.
8. Spiral view of figure 7.

9, 12–13. *Globorotalia grata* (Todd).
9. Umbilical view of topotype. USNM 689874.
12. Side view of topotype. USNM 689875.
13. Spiral view of figure 9.

10–11. *Praeorbulina transitoria* (Blow).
10. Side view. USNM 689876.
11. Spiral view. USNM 689877.

Jour. Research U.S. Geol. Survey
Vol. 5, No. 4, July–Aug. 1977, p. 457–462

A NEW CURVED BACULITE FROM THE UPPER CRETACEOUS OF WYOMING

By W. A. COBBAN, Denver, Colo.

Abstract.—*Baculites reduncus*, n. sp., is a moderately large ammonite that has a curved shell, a large angle of taper, and a stout ovate cross section. Conspicuous broad, arcuate ribs cross the upper two-thirds of the flank. The suture, which is fairly complex, has a distinctive lateral lobe. All the types are from the lower part of the Rock River Formation near Rock River, Wyo. The species is of late Campanian age and marks a zone between the Zones of *Baculites gregoryensis* Cobban and *B. scotti* Cobban.

A baculite, herein named *Baculites reduncus*, is characterized by its curvature and high degree of taper. The species is common in the lower part of the upper Campanian Rock River Formation near Rock River, Wyo., where the form was first recorded as *Baculites ovatus* Say (Stanton and Knowlton, 1897, p. 139; Darton and Siebenthal, 1909, p. 39, 42) and later as *Baculites* n. sp. (Hyden, 1965; McAndrews, 1965; Gill and others, 1970, p. 23). Outside the Rock River area, *B. reduncus* is represented by a few baculites from the Pierre Shale at Horse Creek (northwest of Cheyenne, Wyo.), in the North Park area of Colorado, and just east of the Front Range in the Boulder-Denver area of Colorado.

The occurrences of *B. reduncus* near Rock River are in an outcrop belt that begins 2 miles (3.2 km) southeast of Rock River and extends eastward for 7 miles (11.3 km) across the Rock River and Cooper Lake North 7.5-minute quadrangles (Hyden, 1965; McAndrews, 1965). U.S. Geological Survey Mesozoic localities shown on these quadrangles that have *B. reduncus* are D1400 and D3386–88 on the Rock River quadrangle and D3384 and D3908 on the Cooper Lake North quadrangle. The baculites occur in large brown-weathering sandstone concretions and smaller brownish-gray-weathering sandstone concretions in soft, massive sandstone beds 616–671 ft (188–205 m) above the base of the Rock River Formation (Gill and others, 1970, p. 23). Fossils in these concretions represent a large and varied fauna including bryozoans (Toots and Cutler, 1962a); many species of bivalves and gastropods, some having Gulf and Atlantic coast affinities (Toots and Cutler, 1962b); species of the ammonite genera *Didymoceras*, *Oxybeloceras*, *Anapachydiscus*, *Menuites*, and *Placenticeras;* fish bones, scales, and teeth; and reptilian bones.

In the Rock River area, *Baculites reduncus* forms a distinct zone between those of *B. gregoryensis* and *B. scotti*. *B. scotti* Cobban (Cobban, 1958, p. 660, pl. 90, figs. 1–9; text fig. 1*a–e*, *h* was not found in the type section of the Rock River Formation (Gill and others, 1970, p. 21–24), but specimens of it were found 2 miles (3.2 km) east of the type section at locality D3389, in the SE¼NE¼ sec. 10, T. 20 N., R. 76 W. (Hyden, 1965) in rocks stratigraphically above those containing *B. reduncus*. *B. gregoryensis*, likewise, was not

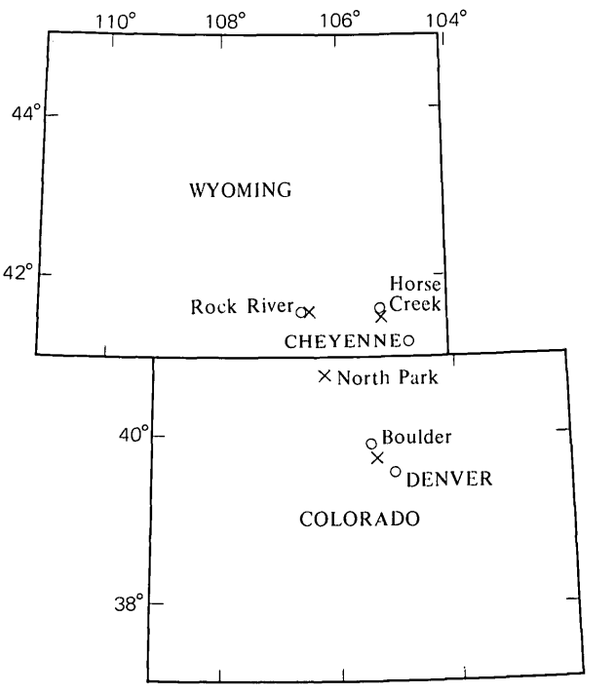

FIGURE 1.—Index map of Wyoming and Colorado showing occurrences of *Baculites reduncus*, shown as ×'s.

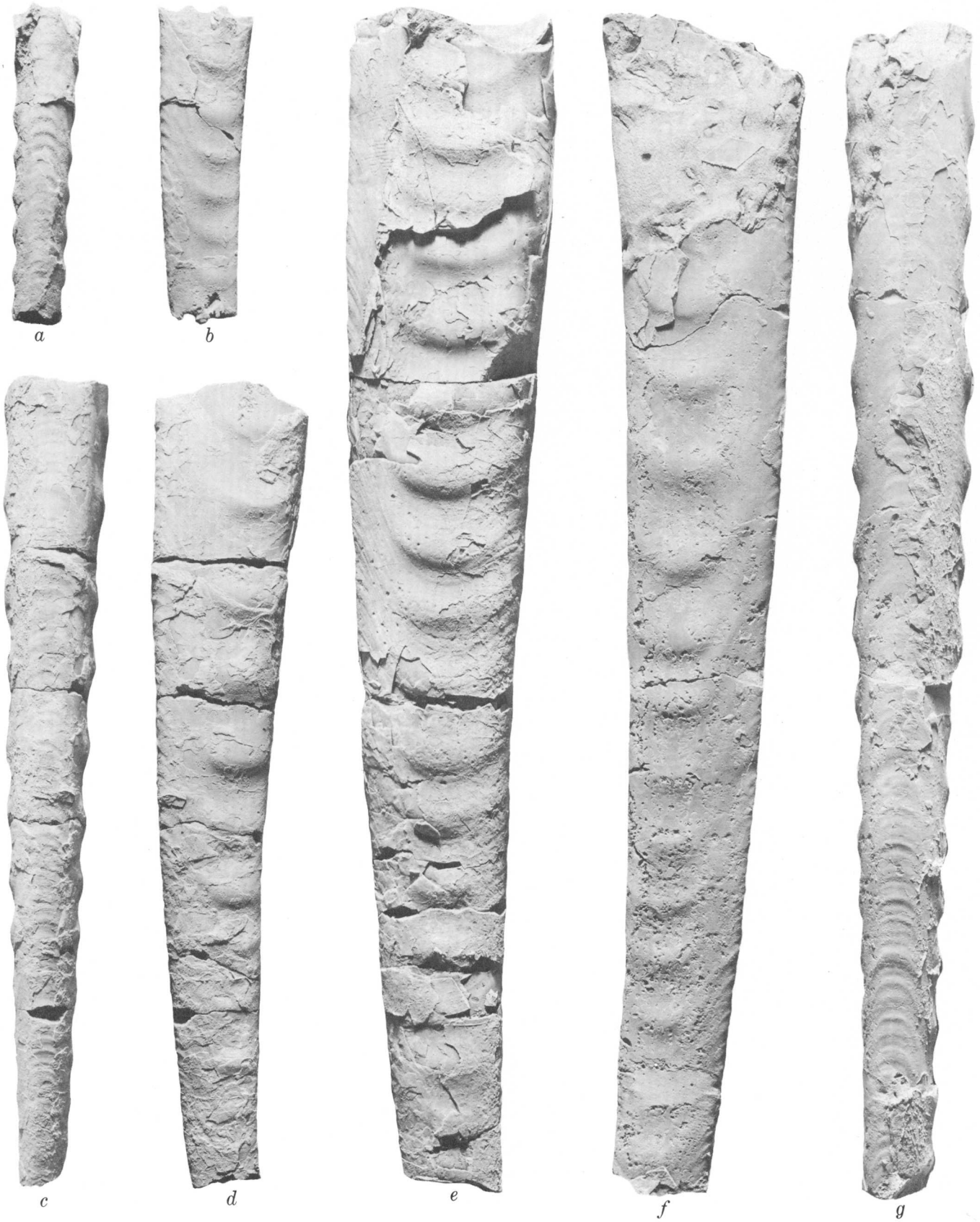
a
b
c
d
e
f
g

found in the type section of the Rock River Formation, but this species was collected 2 miles (3.2 km) east of the type section at locality D3385, in the SW¼SE¼ sec. 3, T. 20 N., R. 76 W. (Hyden, 1965) in rocks stratigraphically below those containing *B. reduncus*.

Several very good specimens were collected in the Rock River area by Mr. Edward Shibata, Laramie, Wyo. These specimens were acquired by the late Mr. J. P. Conlin, Ft. Worth, Tex., who kindly donated them to the U.S. Geological Survey. Some of the specimens collected by Mr. Shibata are shown in figures 2 and 3.

Baculites reduncus Cobban, n. sp.

Figures 2–6

This moderately large species is characterized by its curved shell that has a large angle of taper. The stoutly ovate cross section has a narrowly rounded venter. Broad, arcuate ribs cross the upper two-thirds of the flank. The suture is like that of *B. gregoryensis* Cobban (Cobban, 1951, figs. 10, 12) in that the lateral lobe is pinched just above the upper of the two lower major branches (also see Gill and Cobban, 1973, figs. 3*B* and 4*B*).

The largest collection is from locality D1400, on the west slope of a hill, in the SE¼SE¼NE¼ and NE¼NE¼SE¼ sec. 8, T. 20 N., R. 76 W., at the type section of the Rock River Formation (Gill and others, 1970, p. 23). This collection has 105 specimens suitable for measurement of angle of taper and, where present, determination of spacing of flank ribs. Taper angles range from 3° to 9°, but most are 6° or 7° (fig. 4*B*.) There is no noticeable change in the angle of taper as the shell enlarges. Flank ribs first appear at some diameter between 10 and 19 mm. The ribs are arcuate, moderately broad, nodelike on some individuals, and extend over much of the flank. The number of ribs per shell diameter (diameter of shell divided by distance between crests of two adjacent ribs) ranges from 0.9 to 2.7 with most in the 1.5–2.3 range (fig. 4*A*). The spacing decreases slightly as the shell enlarges. Ventral ribbing is present but inconspicuous. The ribs tend to be weak, closely spaced, and irregular in strength.

Axial curvature of the baculites from the Rock River area varies considerably, but it is most conspicuous on juveniles and young adults. Older adults have little or no curvature. Where curvature occurs, the venter is always convex.

Shells having diameters of less than 5 mm are not present in the collections. The largest specimen, a nearly complete body chamber 230 mm long (paratype, USNM 240427), has a diameter of 60.8 mm at its larger end. Although many specimens are parts of body chamber, none has the complete aperture preserved.

The suture closely resembles that of *B. gregoryensis* Cobban (Cobban, 1951, text figs. 10, 12). The two sutures illustrated in figure 5 are typical of the degree of complexity and the form of the diagnostic lateral lobe.

The holotype (figs. 2 *f*, *g*) and some of the paratypes (fig. 3 *a*, *c–e*, and *n*) are from U.S. Geological Survey Mesozoic locality 22935, 2.2 miles (3.5 km) southeast of Rock River, in the S½NE¼NW¼ sec. 9, T. 20 N., R. 76 W. The holotype is a moderately curved shell 227 mm long that has end diameters of 18.2 and 35.0 mm. Most of the specimen has 5° of taper. About 60 percent of the shell is phragmocone; the larger end of the phragmocone has a diameter of 28.2 mm. The ovate cross section is typical for most specimens (fig. 6). Broad flank ribs, spaced 1.6–2.0 per shell diameter, are present on the entire specimen.

Baculites reduncus differs from *B. gregoryensis* Cobban (Cobban, 1951, p. 820, pl. 118, figs. 1–5; text figs. 8–13) in having greater curvature and in possessing flank ribs. *B. reduncus* resembles *B. rex* Anderson (Anderson, 1958, p. 191, pl. 49, fig. 2), as figured by Matsumoto (1959, p. 136, pl. 31, fig. 5 a–d; pl. 34, fig. 5; pls. 39, 40; text figs. 45–52), in its size, taper, and curvature, and in some suture patterns, but *B. rex* lacks flank ribs. *B. palestinensis* Picard (Picard, 1929, p. 438, pl. 10, figs. 1–7; text figs. 1, 2) closely resembles *B. reduncus* in its curvature and ornamentation, but the Palestine species has a broader venter and a much simpler suture.

FIGURE 2.—*Baculites reduncus*, n. sp., from the Rock River area, Wyoming, all natural size except *e*.

a, b. Ventral and lateral views of part of a juvenile phragmocone collected by Edward Shibata. Paratype, USNM 240418.

c, d. Ventral and lateral views of a specimen from U.S. Geological Survey Mesozoic locality D1400. Paratype, USNM 240422.

e. Laterial view, × 0.8, of an adult 260 mm long collected by Edward Shibata. Paratype, USNM 240419.

f, g. Lateral and ventral views of the holotype from U.S. Geological Survey Mesozoic locality 22935. USNM 108909.

REFERENCES CITED

Anderson, F. M., 1958, Upper Cretaceous of the Pacific coast: Geol. Soc. America Mem. 71, 378 p.

Cobban, W. A., 1951, New species of *Baculites* from the Upper Cretaceous of Montana and South Dakota: Jour. Paleontology, v. 25, no. 6, p. 817–821.

——— 1958, Two new species of *Baculites* from the western interior region: Jour. Paleontology, v. 32, no. 4, p. 660–665.


a
b
c
d
e
f
g
h
i
j
k
l
m
n

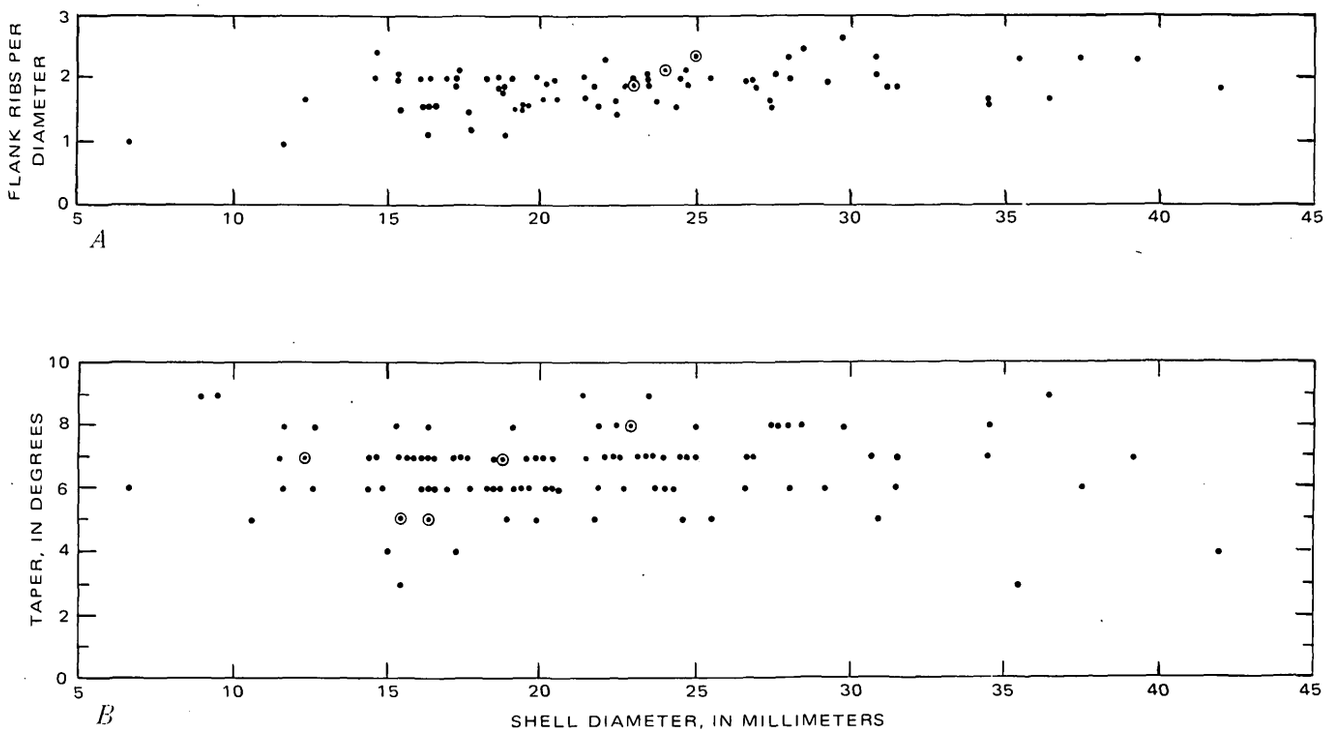

FIGURE 4.—Scatter diagrams showing *A* number of flank ribs per shell diameter and *B* degrees of taper of 105 specimens of *Baculites reduncus*, n. sp., from a 27-foot (8.2-m) sandstone unit 616–643 feet (188–196 m) above the base of the Rock River Formation at U.S. Geological Survey Mesozoic locality D1400, 2 miles (3.2 km) southeast of Rock River, Wyo. Circles around dots indicate two specimens that have the same measurements.

FIGURE 3.—*Baculites reduncus*, n. sp., natural size, from the Rock River area, Wyoming.

a. End view of a small phragmocone from U.S. Geological Survey Mesozoic locality 22935. Paratype, USNM 240423.

b. Smaller end of the specimen shown in figure 2*a*, *b*. Paratype, USNM 240418.

c. End view of a phragmocone from U.S. Geological Survey Mesozoic locality 22935. Paratype, USNM 240424.

d. End view of a small body chamber from U.S. Geological Survey Mesozoic locality 22935. Paratype, USNM 240425.

e. End view of a phragmocone from the same locality. Paratype, USNM 240426.

f–h. End, ventral, and lateral views of a septate specimen from U.S. Geological Survey Mesozoic locality D1400. Paratype, USNM 240423.

i, j. Ventral and lateral views of an adult collected by Edward Shibata. Paratype, USNM 240420.

k. Lateral view of a well-curved young adult collected by Edward Shibata. Paratype, USNM 240421.

l, m. End and lateral views of a small specimen showing beginning of lateral ribs, from U.S. Geological Survey Mesozoic locality D1400. Paratype USNM 240428.

n. Lateral view of a specimen from U.S. Geological Survey Mesozoic locality 22935. Paratype, USNM 108910.

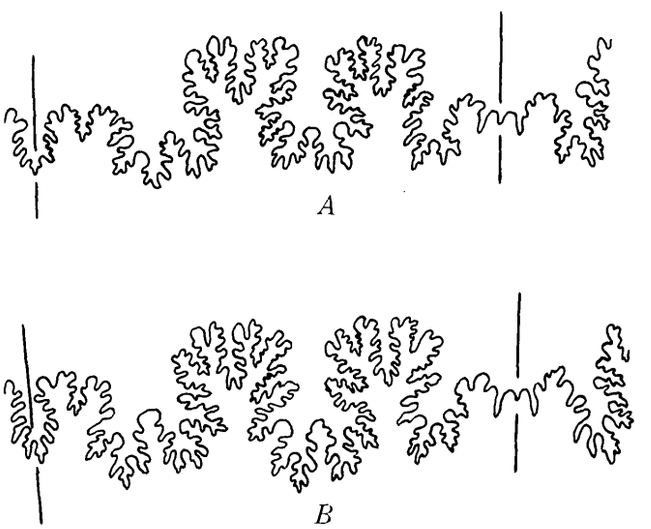

FIGURE 5.—Sutures, × 2, of *Baculites reduncus*, n. sp. *A*, Holotype, USNM 108909, at a diameter of 23.8 mm, *B*, Paratype, USNM 240426, at a diameter of 24.7 mm.

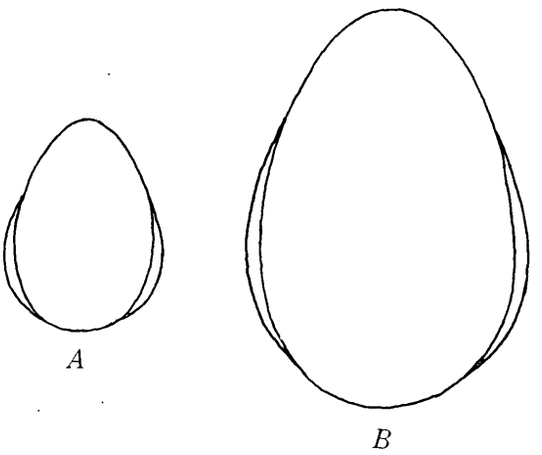

FIGURE 6.—Cross sections of *Baculites reduncus*, n. sp. *A*, Holotype, USNM 108909, at a diameter of 28.5 mm. *B*, Paratype, USNM 240427, at a diameter of 53.5 mm.

Darton, N. H., and Siebenthal, C. E., 1909, Geology and mineral resources of the Laramie Basin, Wyoming: U.S. Geol. Survey Bull. 364, 81 p.

Gill, J. R., and Cobban, W. A., 1973, Stratigraphy and geologic history of the Montana Group and equivalent rocks, Montana, Wyoming, and North and South Dakota: U.S. Geol. Survey Prof. Paper 776, 37 p.

Gill, J. R., Merewether, E. A., and Cobban, W. A., 1970, Stratigraphy and nomenclature of some Upper Cretaceous and lower Tertiary rocks in south-central Wyoming: U.S. Geol. Survey Prof. Paper 667, 50 p.

Hyden, H. J., 1965, Geologic map of the Rock River quadrangle, Albany County, Wyoming: U.S. Geol. Survey Geol. Quad. Map GQ–472, scale 1:24,000.

McAndrews, Harry, 1965, Geologic map of the Cooper Lake North quadrangle, Albany County, Wyoming: U.S. Geol. Survey Quad. Map GQ–430, scale 1:24,000.

Matsumoto, Tatsuro, 1959, Upper Cretaceous ammonites of California, Pt. 1: Kyushu Univ. Fac. Sci. Mem., Ser. D, Geology, v. 8, no. 4, p. 91–171.

Picard, Leo, 1929, On Upper Cretaceous (chiefly Maestrichtian) Ammonoidea from Palestine: Annals and Mag. Nat. History, ser. 10, v. 3, p. 433–456.

Stanton, T. W., and Knowlton, F. H., 1897, Stratigraphy and paleontology of the Laramie and related formations in Wyoming: Geol. Soc. America Bull., v. 8, p. 127–156.

Toots, Heinrich, and Cutler, J. F., 1962a, Bryozoa from the "Mesaverde" Formation (Upper Cretaceous) of southeastern Wyoming: Jour. Paleontology, v. 36, no. 1, p. 81–86.

——— 1962b, Gulf and Atlantic coast mollusks in the Late Cretaceous Mesaverde Formation of Wyoming: Wyoming Univ. Contr. Geology, v. 1, no. 1, p. 7–12.

Jour. Research U.S. Geol. Survey
Vol. 5, No. 4, July–Aug. 1977, p. 463–472

MIOSPORE DIVERSITY AND ITS RELATIONSHIP TO LITHOLOGY IN THE COKER FORMATION (UPPER CRETACEOUS) OF WESTERN ALABAMA

By RAYMOND A. CHRISTOPHER, Reston, Va.

Abstract.—A multiple-regression procedure was applied to samples from two cores of the Coker Formation (Upper Cretaceous) of western Alabama in an attempt to characterize the relationship between the diversity of miospore species and selected lithologic factors. The resulting prediction equations suggest that the number of miospore species in these samples is inversely related to changes in median grain size and to other as yet undefined factors not reflected by lithology. In addition, it appears that the degree of sorting of the sediment has no effect on species diversity.

A plot of these prediction equations shows that changes in the number of miospore species are negligible in samples of clay and silt size but that the number of species decreases rapidly in sediments of fine sand size or coarser.

The results presented here agree with those presented by other workers for the relationship between grain size and the absolute abundance of miospores.

Transportation of the vast majority of spores and pollen grains that eventually become incorporated in sediments is almost certainly initiated by the wind. Studies by Muller (1959), Koreneva (1964, 1966), Stanley (1965), Cross and Shaeffer (1965), and others, however, have shown that generally the final stages of miospore transportation and deposition are carried out in an aqueous medium. As a result, the composition of an assemblage and the number of grains per unit volume of sediment are related to such factors as distance from shore, proximity to river mouths, water depth, water movements, water-density patterns, and turbulence; wind transportation plays a minor role in the final pollen sedimentation. The conclusions reached by several workers in the field of miospore sedimentation (Traverse and Ginsburg, 1966; Cross and others, 1966) are that spores and pollen grains, once delivered to water, are transported and deposited in the same way as are inorganic particles of the same size range and specific gravity and that the composition of an assemblage and the absolute frequency of a given species often reflect the lithologic makeup of the sample from which they were recovered.

Studies conducted to date on miospore sedimentation have dealt primarily with the relationship between either the abundance of a given species or the total number of miospores per unit volume of sediment and rock. It is the purpose of this report to expand our knowledge of the effect of lithology on miospore assemblages by examining the relationship between species diversity and lithology in samples from two cores of the Coker Formation (Upper Cretaceous) in western Alabama. This relationship is quantitatively expressed by means of a multiple-regression model which includes two lithologic factors (median grain size and sorting coefficient) as well as depth in the cores, so that the results presented here can be applied to future studies of species diversity.

Acknowledgments.—The writer extends his appreciation to Dr. K. L. Koonce, Department of Experimental Statistics, Louisiana State University, Baton Rouge, for his help in analyzing the data and for critically reviewing the original draft of the manuscript.

PREVIOUS STUDIES AND THEIR BEARING ON THE PRESENT INVESTIGATION

Many studies have been made that demonstrate the effectiveness of aerial dispersion of spores and pollen in altering the abundance, selectively removing, or selectively adding species to the total spore-pollen spectra. Conclusions are that the ultimate composition of a palynological assemblage in a rock does not reflect the assemblage initially produced by plants (Tauber, 1967; Raynor and others, 1972, 1973; Rowley and Walch, 1972).

Other studies have shown that, at least in the marine environment, the spore-pollen fraction of an assemblage is more closely related to the hydrodynamics and bathymetry of the depositional basin than to the aerodynamics of the surrounding area.

Muller (1959), in an investigation of the spores and pollen in sediments from the Orinoco Delta and Shelf, reasoned that because the prevailing wind direction

for this region is onshore during the time of pollination of most plants, airborne transportation of miospores to offshore areas is negligible. Rather, he found a close similarity between miospore abundance and proximity to river mouths, indicating the effectiveness of water transport of spores and pollen to the marine environment. Similar results were presented by Stanley (1965) for miospore sedimentation off the eastern coast of the United States.

Traverse and Ginsburg (1966) made an extensive investigation of the palynology of surface sediments of Great Bahama Bank as it relates to water movements and patterns of sedimentation. Especially significant are their studies on the distribution of pine pollen; these studies indicate that the abundance of pine pollen in surface sediments is more indicative of water turbulence than it is of time of pollination or distance from the source. High concentrations of pollen were regularly found in sediments from the leeward sides of the larger islands, where water turbulence is minimal and the sediment is prevailingly fine grained. In fact, Traverse and Ginsburg's data suggest a direct relationship between the number of pine pollen grains per gram of sediment and the grain size of that sediment; pine pollen being more abundant in finer grained mud regardless of distance from shore, prevailing wind direction, or water depth.

A similar relationship between miospore abundance and sediment grain size was observed by Koreneva (1964, 1966) in samples from the Pacific Ocean, where she found the highest concentrations of spores and pollen associated with argillaceous silt. In addition, Koreneva (1964) noted a sharp decrease in miospore abundance in samples having high content of amorphous silica; the silica probably reflected a high rate of diatom accumulation.

Cross and others (1966) also noted the relationship between spore-pollen concentration and grain size in surface samples from the Gulf of California, but in their samples, this relationship is apparently complicated by other factors, such as proximity to river mouths, winnowing of sediment, and distance from shore.

The results of these and other studies indicate that a strong relationship exists between miospore concentration and certain hydrodynamic and bathymetric factors of the depositional basin. It follows, then, that in a sediment, changes in lithology that are the result of some of these factors should be reflected in the palynological composition of an assemblage. For the purposes of the present investigation, I hypothesize that changes in lithology would also be reflected by changes in the number of species in a sample. In this study, a particular rock type is characterized by its median grain size and sorting coefficient, as these factors provide a measure of its central tendency and dispersion. Changes in either or both of these factors can be readily used to differentiate rocks.

When assemblages of fossil miospores from a vertical stratigraphic sequence rather than from Holocene surficial samples are being studied, time must be taken into account. Changes in species diversity through time could reflect such factors as variations in distance from shore, ecologic or climatic changes, changes in the position of contributing streams, and (or) postdepositional alteration or destruction of palynomorphs by oxidation or biologic degradation—changes that are not necessarily reflected in the lithology of a sample. For this reason, depth of samples below the surface in each core was considered in the present study in order to evaluate the effect of lithology on species diversity independently of nonlithologically related changes through time.

Multiple regression was selected as the method of relating species diversity to certain lithologic factors, for two reasons. First, this method is well suited for evaluating the effect of several variables (median grain size, sorting coefficient, and depth) on a single dependent variable (species diversity); second, it is applicable to measurements made on a continuous scale, making it more efficient than methods in which observations are recorded as discrete classes or categories.

METHODS

Sample selection and preparation

Samples used in the present study were obtained from two cores of the Coker Formation which were drilled near the type locality of the formation in west-central Alabama (fig. 1). Drilling of both cores began at the base of the overlying Gordo Formation, penetrated the entire Coker Formation, and bottomed in Paleozoic sedimentary rock.

The Coker Formation is the basal unit of the outcropping Gulf Coastal Plain deposits in Alabama, and together with the overlying Gordo Formation, constitutes the Tuscaloosa Group of the eastern Gulf Coast. Studies of plant megafossils by Berry (1919), scarce and poorly preserved invertebrate fossils by Sohl (1964), and selected palynomorphs by Leopold and Pakiser (1964) and by Christopher (1976) suggest that the Coker Formation of western Alabama is middle to possibly late Cenomanian in age and that it can be correlated with the Woodbine Formation of Texas and the Woodbridge Clay Member of the Raritan Formation of New Jersey.

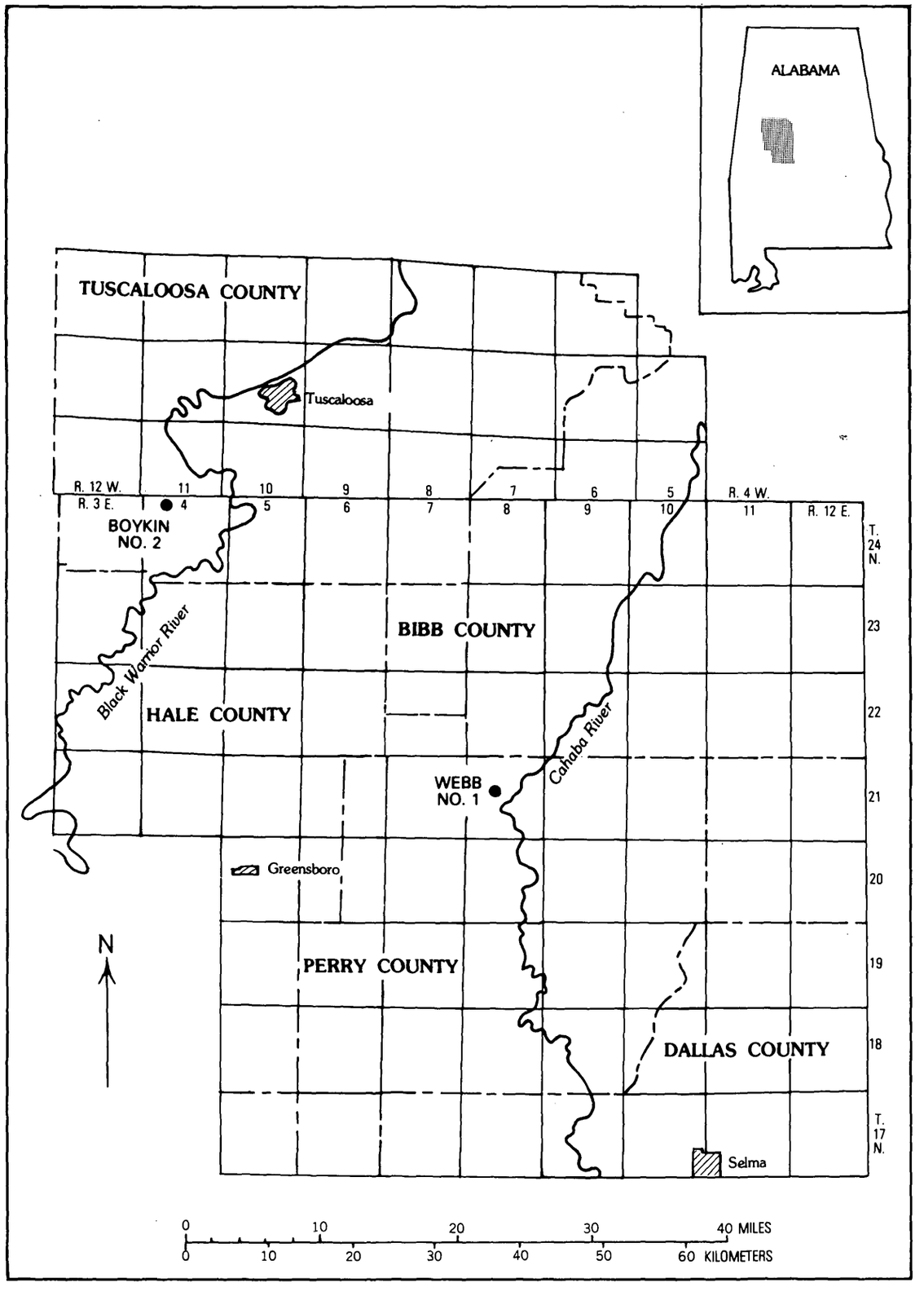

FIGURE 1.—Parts of Tuscaloosa, Bibb, Hale, Perry, and Dallas Counties, Ala., showing the location of the Webb No. 1 and Boykin No. 2 boreholes. Inset shows location of area.

Bergenback (1964) reported on grain-size analyses, X-ray identification of clay minerals, and the mineralogy of detrital grains and matrix from quarter cuts of the same cores upon which the present study is based; the values presented by him for median grain size and sorting coefficient of the samples, as well as his sampling intervals, are used here. Fifty-two lithologic units were recognized by Bergenback in each core; in the material made available for this investigation, samples from all 52 units were represented in the Boykin core, but samples 14, 43, and 44 of Bergenback were not available for the Webb core.

Two samples were taken from each lithologic unit as part of a separate study designed to evaluate the variation shown by taxa within lithologic units. Samples of 100 grams were taken at one-third and two-thirds of the stratigraphic thickness of each unit. The stratigraphic position of both samples was recorded as the midpoint of the lithologic unit being sampled, as both samples from a given lithologic unit would then have identical values for their median grain size, sorting coefficient, and depth below the surface.

Samples were prepared for palynological examination by standard chemical maceration procedures. In order to minimize variation, all samples were treated in an identical manner, although the amount of each sample initially subjected to maceration ranged from 10 to 50 g, and the length of time that samples were allowed to remain in acid ranged from 8 to 48 hours, depending on the sediment type.

Two complete cover slips (22×22 mm) were scanned for each sample, and the number of palynomorphs found on each slide was recorded. For this study, the results obtained from the two slides of a sample were both used, so that two estimates of the number of species in a given lithologic unit were obtained, one from each of the two samples representing that unit.

When no palynomorphs were observed on either slide examined for a given sample, that sample was assumed to be barren. In the Boykin core, samples from lithologic units 1 to 22 inclusive were barren, and in the Webb core, samples 1 to 9 inclusive, 11 to 21 inclusive, 34, and 47 to 52 inclusive were barren. These samples were not used in the study, as it could not conclusively be demonstrated that the absence of palynormorphs in them is directly affected by their median grain size, sorting coefficient, or depth.

Several indices of species diversity have been introduced in the literature (Simpson, 1949; Kornicker and Odum, 1958; Straaten, 1960), but, for the most part, these indices are based on the frequencies of individual species as well as on the number of species in an assemblage. Although species-diversity indices of this sort are well suited to paleoecologic or paleoclimatic studies, they would tend to bias the results of the present study by overemphasizing the importance of dominant species and neglecting the presence of rare species. As a result, the data analyzed in this study consisted of the total number of species present in each of two samples taken from lithologic units in two cores.

The slides used in this investigation have been deposited in the palynology laboratory of the Geology Department, Louisiana State University, Baton Rouge.

The sample numbers assigned to each lithologic unit by Bergenback (1964) are presented in tables 1 and 2 for the Webb and Boykin cores, respectively, along with the values for median grain size, sorting coefficient, stratigraphic range, depth of the midpoint of the unit, and the two estimates of the number of palynomorph species contained in that lithologic unit.

Regression model and procedures

Species diversity was related to changes in lithology and depth in each core and over both cores through a combined multiple and curvilinear regression model, which included the linear, quadratic, and cubic effects of median grain size, sorting coefficient, and depth. (The reader is referred to Snedecor and Cochran, 1967, chaps. 6, 13, and 15; Steel and Torrie, 1960, chaps. 9, 14, and 16; and Li, 1964, for a complete discussion of the rationale and procedures used in multiple and curvilinear regression.)

The initial regression model applied to the data is expressed as

$$Y_{ij}=\alpha+\beta_1 m_i+\beta_2 m_i^2+\beta_3 m_i^3+\beta_4 s_i+\beta_5 s_i^2+\beta_6 s_i^3+\beta_7 d_i+\beta_8 d_i^2+\beta_9 d_i^3+\varepsilon_{ij} \quad (1)$$

where

Y_{ij} = the number of species in the jth sample of the ith lithologic unit $j=1, 2$; $i=1, 2, \ldots, 23$ for the Webb core, $i=1, 2, \ldots, 30$ for the Boykin core),

α = the Y-intercept (the value of the dependent variable when median grain size, sorting coefficient, and depth are all equal to zero),

β_1 = the partial regression coefficient that measures the change in the number of species with a unit change in the linear trend of median grain size, holding the quadratic and cubic effects of median grain size and the linear, quadratic, and cubic effects of sorting coefficient and depth constant,

β_2 = the partial regression coefficient that measures the change in the number of species with a unit change in the quadratic trend of median grain size, holding all other independent variables constant,

TABLE 1.—*Webb core: Dependent and independent variables upon which the regression procedures discussed in this report are based*

Bergenback's (1964) sample No.	Median grain size (mm)	Sorting coefficient[1] ($\sqrt{Q_{75}/Q_{25}}$)	Stratigraphic range		Depth of midpoint		Number of palynomorph species	
			Feet	Meters	Feet	Meters	Sample 1	Sample 2
10	0.045	9.9*	128.8-135.5	39.3- 41.3	132.1	40.3	54	43
22	.042	9.4*	238.8-248.0	72.8- 75.6	243.4	74.2	24	30
23	.060	2.4	248.0-261.0	75.6- 79.6	254.5	77.6	33	33
24	.100	1.5	261.0-265.0	79.6- 80.8	263.0	80.2	29	31
25	.120	1.9	267.0-277.2	81.4- 84.5	272.1	82.9	28	34
26	.165	1.4	277.2-282.0	84.5-86.0	279.6	85.2	35	28
27	.075	5.1	282.0-286.0	86.0- 87.2	284.0	86.6	34	31
28	.067	3.9	292.7-296.1	89.2- 90.3	294.4	89.7	39	38
29	.063	4.7	299.6-311.0	91.3- 94.8	306.3	93.4	41	36
30	.077	1.3	330.0-336.0	100.6-102.4	333.0	101.5	31	29
31	.203	1.3	336.0-338.8	102.4-103.3	337.4	102.8	24	29
32	.115	1.5	350.0-354.0	106.7-107.9	352.0	107.3	24	29
33	.078	1.6	364.0-366.0	110.9-111.6	365.0	111.3	38	33
35	.063	5.7	366.8-369.8	111.8-112.7	368.2	112.2	29	31
36	.145	1.4	369.8-372.8	112.7-113.6	371.3	113.2	37	29
37	.155	1.7	374.3-375.8	114.1-114.5	375.0	114.2	31	36
38	.190	1.3	422.0-427.0	128.6-130.1	424.5	129.4	20	34
39	.098	2.6	435.5-439.5	132.7-134.0	437.5	133.4	34	28
40	.041	3.0	442.3-445.5	134.8-135.8	443.9	135.3	29	35
41	.174	1.4	452.7-454.8	138.0-138.6	453.8	138.3	33	33
42	.180	1.2	455.0-456.2	138.7-139.0	455.6	138.9	40	32
45	.075	3.2	506.0-509.0	154.2-155.1	507.5	154.7	44	37
46	.257	1.3	509.0-515.5	155.1-157.1	512.2	156.1	24	27

[1]Trask (1932). *Data supplied from analyses made by the writer.

TABLE 2.—*Bokyin core: Dependent and independent variables upon which the regression procedures discussed in this report are based*

Bergenback's (1964) sample No.	Median grain size (mm)	Sorting coefficient[1] ($\sqrt{Q_{75}/Q_{25}}$)	Stratigraphic range		Depth of midpoint		Number of palynomorph species	
			Feet	Meters	Feet	Meters	Sample 1	Sample 2
23	0.045	2.3	235.8-242.7	71.9- 74.0	239.3	72.9	28	24
24	.044	3.0	245.4-246.0	74.8- 75.0	245.7	74.9	32	31
25	.056	9.9*	246.0-246.4	75.0- 75.1	246.2	75.0	33	35
26	.032	8.6*	249.2-259.2	76.0- 79.0	254.2	77.5	23	32
27	.047	9.3*	259.2-264.0	79.0- 80.5	261.6	79.7	29	22
28	.131	1.4	271.4-276.0	82.7- 84.1	273.7	83.4	33	29
29	.073	9.9*	281.0-286.6	85.6- 87.4	284.0	86.6	40	35
30	.073	9.9*	286.6-289.0	87.4- 88.1	287.8	87.7	33	29
31	.064	7.7	290.0-292.5	88.4- 89.2	291.2	88.8	22	23
32	.105	1.7	292.5-302.0	89.2- 92.0	297.2	90.6	29	29
33	.165	1.2	307.0-310.5	93.7- 94.6	308.7	94.1	33	24
34	.041	9.2*	310.5-314.2	94.6- 95.8	312.3	95.2	39	35
35	.060	7.3	314.2-320.0	95.8- 97.5	317.1	96.7	36	29
36	.085	5.5	320.0-331.0	97.5-100.9	325.5	99.2	36	39
37	.079	2.4	343.1-345.1	104.6-105.2	344.1	104.9	30	36
38	.060	5.2	345.1-348.5	105.2-106.2	346.8	105.7	36	39
39	.031	8.3*	366.0-367.7	111.6-112.1	366.9	111.8	44	34
40	.042	7.2	367.7-369.0	112.1-112.5	368.4	112.3	36	38
41	.036	9.4*	369.0-378.1	112.5-115.2	373.6	113.9	36	36
42	.001	2.8*	378.1-385.1	115.2-117.4	381.6	116.3	37	37
43	.056	2.6	386.8-388.1	117.9-118.3	387.4	118.1	42	45
44	.165	1.2	390.0-392.0	118.9-119.5	391.0	119.2	40	35
45	.068	1.9	393.3-398.0	119.9-121.3	395.6	120.6	40	46
46	.029	8.6*	435.5-436.7	132.7-133.1	436.1	132.9	33	52
47	.051	9.7*	436.7-444.0	133.1-135.3	441.3	134.5	51	45

TABLE 2.—*Boykin core: Dependent and independent variables upon which the regression procedures discussed in this report are based*—Continued

Bergenback's (1964) sample No.	Median grain size (mm)	Sorting coefficient[1] ($\sqrt{Q_{75}/Q_{25}}$)	Stratigraphic range		Depth of midpoint		Number of palynomorph species	
			Feet	Meters	Feet	Meters	Sample 1	Sample 2
48	.061	4.8	445.3-447.6	135.7-136.4	446.5	136.1	45	39
49	.155	1.2	457.0-459.0	139.3-139.9	458.0	139.6	44	35
50	.068	2.1	459.4-466.2	140.0-142.1	462.8	141.1	38	42
51	.100	1.3	477.0-480.0	145.4-146.3	478.5	145.8	43	46
52	.300	1.3	500.0-510.0	152.4-155.4	505.0	153.9	34	33

[1]Trask (1932). *Data supplied from analyses made by the writer.

β_3 = the partial regression coefficient that measures the change in the number of species with a unit change in the cubic trend of median grain size, holding all other independent variables constant,

β_4 = the partial regression coefficient that measures the change in the number of species with a unit change in the linear trend of sorting coefficient, holding all other independent variables constant,

β_5 = the partial regression coefficient that measures the change in the number of species with a unit change in the quadratic trend of sorting coefficient, holding all other independent variables constant,

β_6 = the partial regression coefficient that measures the change in the number of species with a unit change in the cubic trend of sorting coefficient, holding all other independent variables constant,

β_7 = the partial regression coefficient that measures the change in the number of species with a unit change in the linear trend of depth, holding all other independent variables constant,

β_8 = the partial regression coefficient that measures the change in the number of species with a unit change in the quadratic trend of depth, holding all other independent variables constant,

β_9 = the partial regression coefficient that measures the change in the number of species with a unit change in the cubic trend of depth, holding all other independent variables constant,

m_i = the median grain size of the ith lithologic unit,

s_i = the sorting coefficient of the ith lithologic unit,

d_i = the depth of the ith lithologic unit,

ε_{ij} = random error, assumed to be normally and independently distributed about a mean of zero and with a variance equal to σ^2.

Because changes in species diversity do not necessarily follow a linear trend with unit changes in median grain size, sorting coefficient, and (or) depth, I decided to include the quadratic and cubic as well as the linear effects of these factors to insure a greater efficiency in relating the number of species in a sample to its lithologic factors.

In order to arrive at a regression equation that meaningfully relates species diversity to lithologic factors, a backwards elimination procedure was conducted on the initial regression equations generated from the model in equation 1. According to this procedure, tests of significance were performed on each of the nine partial regression coefficients included in the initial regression equation; when one or more was determined nonsignificant at the 0.05 level of probability, the term that had the least effect on changes

in species diversity was deleted, and a new regression equation was derived based on the eight remaining variables. This deletion process was repeated until the resulting regression or prediction equation contained only those independent variables that significantly affected changes in species diversity.

Three prediction equations were generated in this manner, one for each of the two cores used in the study and a third based on data combined from both cores. These three equations allow for the comparison of results within and between cores.

RESULTS AND CONCLUSIONS

One hundred and thirty-one palynomorph species were recovered from samples of the Webb and Boykin cores, and, with the exception of five reworked Paleozoic miospores, all miospore species were included in the data analyzed. Facies controls and biostratigraphic considerations relating to these palynomorphs are under further investigation.

Although evidence is strong that parts of both the Webb and Boykin cores represent nonmarine environments (for example, the presence of lignites), most of the samples used in this study contain dinoflagellate cysts and (or) acritarchs and are interpreted as being marine sediments. Dinoflagellate cysts and (or) acritarchs were not recorded from lithologic units 10, 42, or 46 in the Webb core, or from units 27, 44, or 51 in the Boykin core.

All three regression analyses performed on species diversity in the Coker Formation of western Alabama provide strikingly similar results. Specifically, species diversity is controlled by the combined effects of depth and median grain size and is apparently independent of sorting of the sediment. The prediction equations relating median grain size and depth to species diversity for each core and for the data from the combined cores are as follows:

Webb core:

$$R^2 = 0.4107$$
$$\hat{Y} = 67.5142 - 740.0\, m^3 - 0.2045\, d + 0.000296\, d^2,$$

Boykin core:

$$R^2 = 0.5472$$
$$\hat{Y} = 24.1563 - 173.3\, m^2 + 0.00010\, d^2,$$

Combined cores:

$$R^2 = 0.3797$$
$$\hat{Y} = 113.2036 - 152.65\, m^2 - 0.7629\, d + 0.002261\, d^2 - 0.0000012\, d^3.$$

Two facts are apparent upon inspection of these equations. First, the number of species in a series of samples decreases as the median grain size of the samples increases (indicated by the sign of the partial regression coefficient associated with m), and second, this inverse relationship does not follow a linear trend (indicated by the significant quadratic and cubic effects of median grain size).

Unfortunately, the effect of median grain size on species diversity is confounded with depth for each equation, prohibiting any generalizations concerning the number of species that could be expected in a sample of known median grain size, or the characterization of those palynomorphs most affected by changes in median grain size. However, because each partial regression coefficient is a measure of the change in species diversity while all other independent variables are held constant, we can explore the relationship between the number of species in a sample and median grain size if we assume a given depth and if we express diversity as a percent of the number of species in a sample having a given median grain size.

Figure 2 is a graphic representation of the change in the number of species as a function of median grain size in the Webb core, in the Boykin core, and in the combined cores. All three curves reflect similar changes in species diversity. There is no appreciable decrease in the number of species throughout the clay and silt size range, and even in sediments of very fine sand size, the number of species decreases by 12 percent or less. In samples of fine sand size or coarser, however, the number of species decreases drastically. For example, in a sample having a median grain size in the medium sand size range, one would expect to find approximately half the number of species (or fewer) that would be recovered if that sample were in the clay or silt size range, regardless of its depth in the core.

Cross and others (1966) examined the relationship between the number of miospores per gram of sediment and grain size of surface samples from the Gulf of California and found that the relationship between these variables is similar to the results presented here for the relationship between species diversity and grain size. The highest concentrations of miospores in the Gulf of California are in silty sediments; in coarser sediments, numbers of miospores are extremely low. Samples from the Gulf of California that contain more than 75 percent sand also contain only a few tens to a few hundreds of miospores per gram of sediment (as opposed to more than 80,000 grains per gram in some finer grained samples).

The results of the study by Cross and others (1966) combined with those presented here show that an increase in median grain size results in a decrease in both the number of species and the total number of miospores per gram of sediment. These changes are negligi-

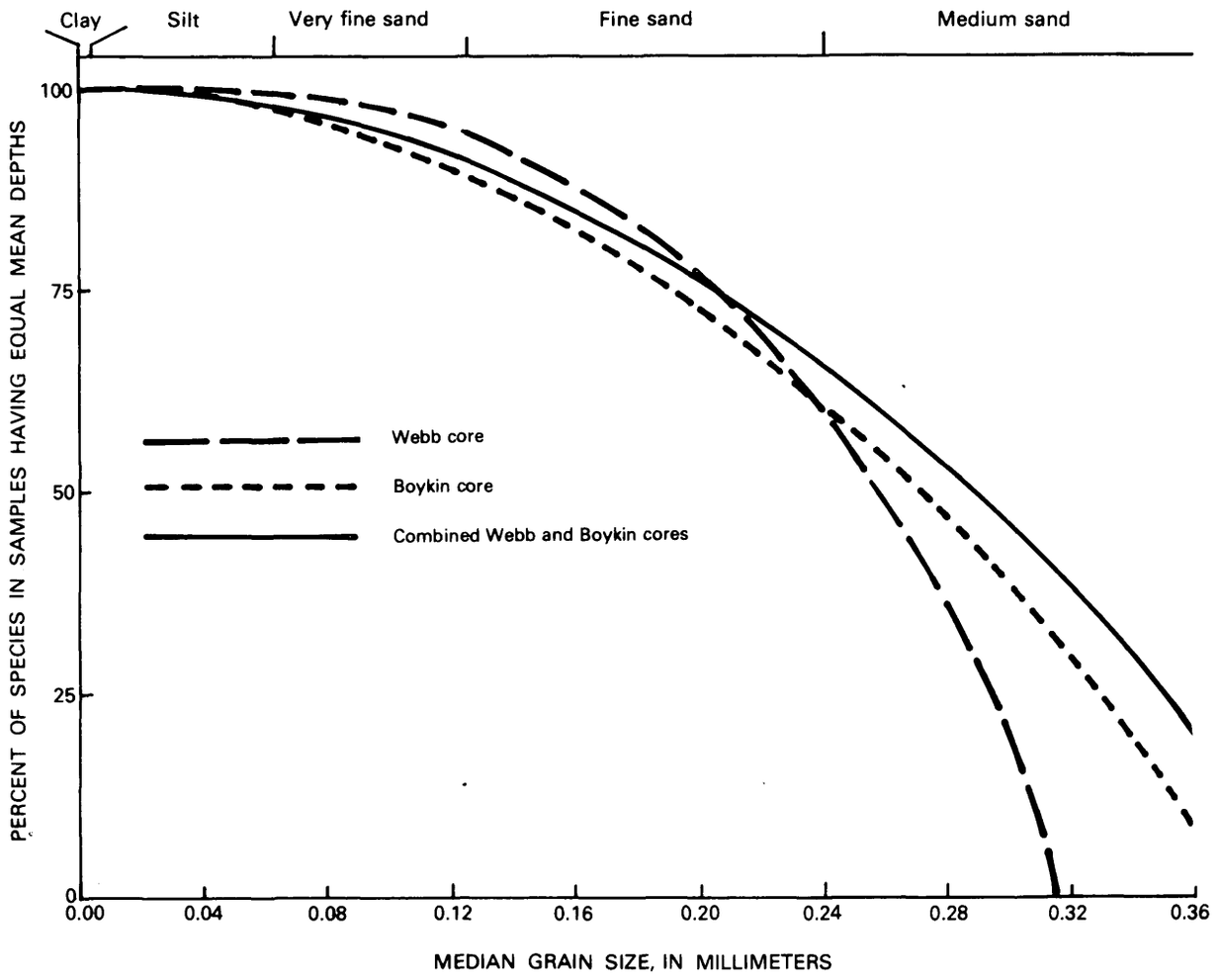

FIGURE 2.—Graphic representation of the prediction equations relating median grain size to species diversity in the Webb and Boykin cores and in the combined cores. Each curve was constructed by holding the effect of depth constant (equal mean depth of all samples) and by assuming a species diversity of 100 percent in an extremely fine grained clay (theoretically having a median grain size squal to zero).

ble within the clay and silt size range, but as grain size increases into the sand size range, its effect is increasingly noticeable.

The results of this and similar studies are of significance to those palynologists concerned with paleoecologic reconstructions. Although factors such as distance from shore, water depth, proximity to source area, and others have been shown to affect species diversity and abundance (which, in the present study, are probably represented by changes in depth), the results presented here suggest that these factors are confounded with changes in median grain size. It is advisable, therefore, to be cautious when palynomorph diversity is used for paleoecologic reconstruction. If the curves presented in figure 2 showing the relationship between species diversity and median grain size can be extended to other geographic localities and geologic horizons, then I recommend that paleoecologic studies that incorporate species diversity be based on samples consisting of clay and silt size sediments, and that samples of fine sand or coarser be avoided.

DISCUSSION

A backward elimination regression procedure was applied to samples from the Coker Formation (Upper Cretaceous) of western Alabama in order to relate species diversity to selected lithologic factors. The results of this study indicate that species diversity is inversely proportional to changes in median grain size, confounded with other factors not reflected by lithology. The study also indicates that species diversity appears to be independent of the degree of sorting of the sediment.

The results presented here help to support the hypothesis previously investigated by Neves (1958), Chaloner and Muir (1968) and others that fossil spores

and pollen, because of their size, are subject to the same sedimentological processes as are inorganic particles of similar size and specific gravity. In addition, the study has demonstrated the usefulness of multiple regression in isolating and evaluating those effects that are the result of changes related to lithologic factors as opposed to those related to other factors. As a result, the effect of median grain size on species diversity can be characterized independently of such factors as distance from shore, proximity to source area, water depth, and water-density differences.

A great deal of work has yet to be done before all the factors that affect species diversity are fully understood; investigations so far have only begun to pinpoint them. Additional studies are needed in the laboratory and in the field and on Holocene and on ancient sediment samples.

REFERENCES CITED

Bergenback, R. E., 1964. Petrology of pre-Selma strata from core holes in western Alabama *in* Monroe, W. H., and others, Studies of pre-Selma Cretaceous core samples from the outcrop area in western Alabama: U.S. Geol. Survey Bull. 1160, p. 9–53.

Berry, E. W., 1919, Upper Cretaceous floras of the eastern Gulf region in Tennessee, Mississippi, Alabama, and Georgia: U.S. Geol. Survey Prof. Paper 112, 177 p.

Chaloner, W. G., and Muir, M., 1968, Spores and floras, *in* Murchison, D., and Westoll, T. S., eds., Coal and coal-bearing strata: Edinburgh, Oliver and Boyd, p. 137–146.

Christopher, R. A., 1976, Palynologic correlation of Cenomanian-aged deposits from New Jersey, South Carolina and Alabama: Geol. Soc. America. Abs. with Programs, v. 8, no. 2, p. 151–152.

Cross, A. T., and Shaeffer, B. L., 1965, Palynology of modern sediments, Gulf of California and environs [abs.]: Am. Assoc. Petroleum Geologists Bull., v. 49, no. 3, p. 337.

Cross, A. T., Thomson, G. G., and Zaitzeff, J. B., 1966, Source and distribution of palynomorphs in bottom sediments, southern part of Gulf of California: Marine Geology, v. 4, no. 6, p. 467–524.

Koreneva, E. V., 1964, Distribution of spores and pollen of terrestrial plants in bottom sediments of the Pacific Ocean, *in* Cranwell, L. M., ed., Ancient Pacific floras: Honolulu, Univ. Hawaii Press, p. 31.

——— 1966, Marine palynological researches in the U.S.S.R.: Marine Geology, v. 4, no. 6, p. 565–574.

Kornicker, L. S., and Odum, H. T., 1958, Characterization of modern and ancient environments by species diversity [abs.]: Geol. Soc. America Bull., v. 69, no. 12, pt. 2, p. 1599.

Leopold, E. B., and Pakiser, H. M., 1964, A preliminary report on the pollen and spores of the pre-Selma Upper Cretaceous strata of western Alabama *in* Monroe, W. H., and others, Studies of pre-Selma Cretaceous core samples from the outcrop area in western Alabama: U.S. Geol. Survey Bull. 1160, p. 71–96.

Li, J. C. R., 1964, Statistical inference II: Ann Arbor, Mich., Edwards Brothers, 575 p.

Muller, Jan, 1959, Palynology of Recent Orinoco delta and shelf sediments; Reports of the Orinoco Shelf Expedition, V. 5: Micropalenotology, v. 5, no. 1, p. 1–32.

Neves, R., 1958, Upper Carboniferous plant spore assemblages from the *Gastrioceras subcrenatum* horizon, north Staffordshire: Geol. Mag., v. 95, no. 1, p. 1–18.

Raynor, G. S., Ogden, E. C., and Hayes, J. V, 1972, Dispersion and deposition of Timothy pollen from experimental sources: Agr. Meteorology, v. 9, p. 347–366.

——— 1973, Dispersion of pollens from low-level, crosswind line sources: Agr. Meteorology, v. 11, p. 177–195.

Rowley, J. R., and Walch, K. M., 1972, Recovery of introduced pollen from a mountain glacier stream: Grana, v. 12, p. 146–152.

Simpson, E. H., 1949, Measurement of diversity: Nature, v. 163, p. 688.

Snedecor, G. W., and Cochran, W. G., 1967, Statistical methods: Ames, Iowa, Iowa State Univ. Press, 593 p.

Sohl, N. F., 1964, Pre-Selma larger invertebrate fossils from well core samples in western Alabama *in* Monroe, W. H., and others, Studies of pre-Selma Cretaceous core samples from the outcrop area in western Alabama: U.S. Geol. Survey Bull. 1160, p. 55–64.

Stanley, E. A., 1965, Abundance of pollen and spores in marine sediments off the eastern coast of the United States: Southeastern Geology, v. 7, no. 1, p. 25–33.

Steel, R. G. D., and Torrie, J. H., 1960, Principles and procedures of statistics: New York, McGraw-Hill Book Co., 481 p.

Straaten, L. M. J. U. van, 1960, Marine mollusc shell assemblages of the Rhône Delta: Geologie Mijnbouw, n.s., v. 39, p. 105–129.

Tauber, Henrick, 1967, Investigations of the mode of pollen transfer in forested areas: Rev. Palaeobotany and Palynology, v. 3, p. 277–286.

Trask, P. D., 1932, Origin and environment of source sediments of petroleum: Houston, Tex., Gulf Publishing Co., 323 p.

Traverse, Alfred, and Ginsburg, R. N., 1966, Palynology of the surface sediments of Great Bahama Bank, as related to water movement and sedimentation: Marine Geology, v. 4, no. 6, p. 417–459.

Jour. Research U.S. Geol. Survey
Vol. 5, No. 4, July–Aug. 1977, p. 473–485

HYDROLOGIC CHARACTERISTICS OF THE MADISON LIMESTONE, THE MINNELUSA FORMATION, AND EQUIVALENT ROCKS AS DETERMINED BY WELL-LOGGING FORMATION EVALUATION, WYOMING, MONTANA, SOUTH DAKOTA, AND NORTH DAKOTA

By WILLIAM J. HEAD and RICHARD H. MERKEL,[1]
Cheyenne, Wyo., Denver, Colo.

Work done in cooperation with the Old West Regional Commission

Abstract.—Geophysical logs from wells distributed throughout the Powder River Basin were digitized, processed, and interpreted to get a regional understanding of the lithologic and ground-water characteristics of aquifers in the Madison Limestone and Minnelusa Formation. The percentage of sand, porosity, and apparent ground-water resistivity of the Minnelusa closely follow structural trends in the basin. Values increase from the structural axis of the basin toward the flanks. Close correlations between the water resistivities in the Madison and the Minnelusa indicate possible hydrologic connection between the two units. The low primary porosity from geophysical logs in the Madison indicates that secondary porosity is necessary to develop water supplies of economic importance from the Madison. Because of increased porosity and better water quality, the flanks of the basin appear to be the most favorable places for water production from either the Madison or the Minnelusa.

The development of large deposits of coal, uranium, oil, and gas in the Powder River structural basin depends on adequate water-supply sources. Exploration for water has markedly increased over the past few years. The water will be used for secondary oil and gas recovery, mineral transportation, and electric power generation. Most surface water has been appropriated for other uses and is not available for energy development. Therefore, supplies of ground water not already committed are needed.

Regional studies of the deep aquifers in the Powder River Basin have been limited by the scarcity of water-well information; however, other information exists on the aquifers. Oil and gas industry borehole logs available commercially were utilized in this study to obtain a better regional understanding of the physical nature of the deep aquifers. The thickness and extent of two major Paleozoic aquifers, along with the mineralogy, porosity, and pore-fluid properties were calculated by the use of computerized geophysical log-analysis techniques. This paper describes the log-analysis routine applied to the hydrologic evaluation of the formations and discusses the results on a regional basis.

The Minnelusa Formation of Pennsylvanian and Permian age and the Madison Limestone of Mississippian age were the major geologic units investigated for their aquifer properties. The Minnelusa Formation and its equivalent, the Tensleep Sandstone, are an agglomeration of beds of sandstone, dolomite, shale, and anhydrite. The Madison Limestone and its equivalents, the Pahasapa Limestone and underlying Englewood Formation and the Guernsey Formation, are mainly massive limestone and dolomite deposits with thin beds of sandstone, shale, and anhydrite. At many locations some limestone is argillaceous or siliceous. In the northeastern section of the basin the Madison is a group and is divided into (decending) the Charles Formation, Mission Canyon Limestone, and the Lodgepole Limestone. These formations are highly variable in composition, but carbonate rocks dominate (Foster, 1958; Roberts, 1966).

METHODS

Well data, including wildcat test data and geophysical well logs, for the Minnelusa and the Madison were assembled from U.S. Geological Survey and oil and gas industry records. Standard well logging units were used in this study. However, many of these units

[1] Exploration Data Consultants, Inc., Denver, Colo.

have since been converted to the metric system for this report to comply with current U.S. Geological Survey policy. Information on depths to the Minnelusa was compiled from approximately 2,400 wildcat oil tests, and a structure-contour map for the top of the Minnelusa was machine drawn at 500-ft contour in-

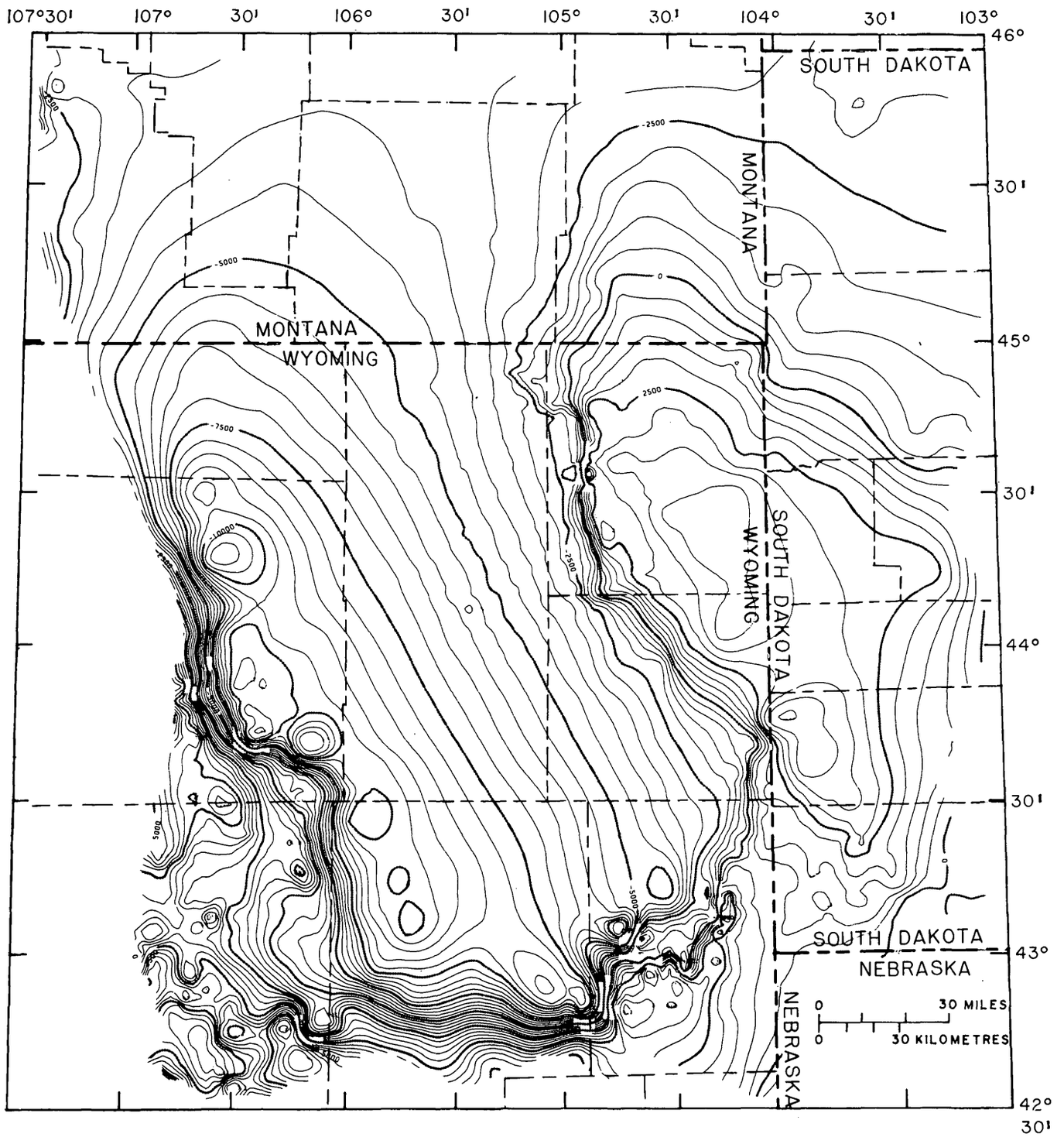

FIGURE 1.—Structure-contour map of the top of the Minnelusa Formation in the Powder River Basin. The machine contour interval shown is 500 ft. The metric conversion would be about 152.4 meters per interval. Datum is mean sea level. Well data compiled by Petroleum Information Corp., Denver, Colo.

tervals (fig. 1). Each interval is also equal to 152.4 meters. Locations where the Minnelusa does not exist, because of intrusions and locations of faults and outcrops, were not specifically noted in the contouring.

The types of geophysical logs sought were combinations of gamma-gamma density, neutron porosity, sonic, natural gamma, and laterolog or deep induction log. Log suites were chosen from the assembled well and test data on the basis of geographic distribution and preferred log types available. The suites had to include at least one of the three porosity logs (density, neutron porosity, and sonic). All the logs were inspected for calibration and log quality. Usable geophysical logs from seventy wells were then digitized at 0.61-m intervals. The logs used were recorded between 1955 and 1974. Areas on the logs where major borehole diameter changes occurred were corrected as well as possible prior to digitizing.

The digitized data for each well were analyzed using computer-generated frequency cross plots for different log-type responses, for example, gamma-gamma versus neutron (fig. 2). The printed values in this cross plot represent the number of recurrences of a particular combination of log responses over a chosen interval. The porosity and density distributions from the logs over the interval are given horizontally and vertically on the graph. In this example, the interval includes the lower part of the Minnekahta Limestone Member and the Opeche Shale Member of the Goose Egg Formation of Permian age, and the underlying upper part of the Minnelusa Formation. The lines on the figure indicate the response of the logs for distinct rock types with varying porosities (after Schlumberger, 1972). The porosity is calculated as if the rock matrix had similar properties to a water-saturated limestone matrix and, therefore, it is shown as ap-

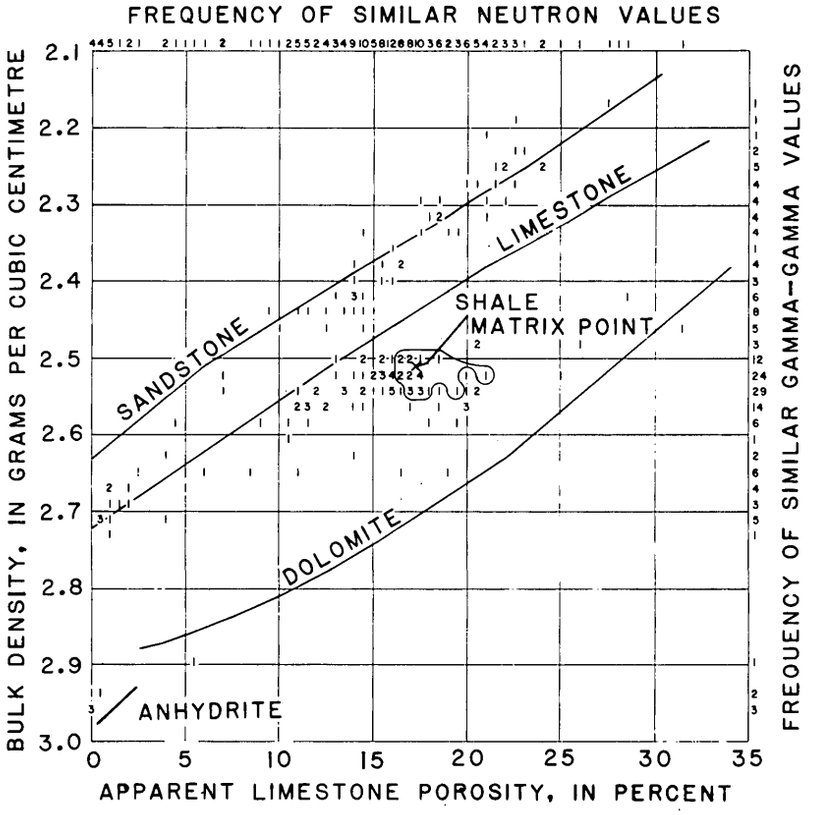

FIGURE 2.—Typical frequency cross plot of the gamma-gamma density response versus the sidewall neutron response for a section of the upper part of the Minnelusa Formation, Opeche Shale Member and lower part of the Minnekahta Limestone Member of the Goose Egg Formation. The integers inside the grid represent the number of density and porosity log responses simultaneously occurring at this value at any given depth. The shale-matrix point was determined from the third variable (gamma) values in figure 3. The ideal response curves (solid lines) represent log values of distinct rock types for varying porosities (Schumberger, 1972, p. 34).

parent limestone porosity. Initial identifications of the lithology were made from these cross plots. The presence of shale in the formations may cause a shift in the cross-plotted points in the direction of the shale-matrix point.

The natural-gamma response was added to the frequency cross plot in the form of a z-axis third variable (fig. 3) to determine the presence of shale. The numbers on the third-variable plot represent a scaled average (from 1 to 10) of the natural-gamma response. The z numbers occur at the same locations as the frequency values of the standard cross plot. Concentrations of high natural-gamma values (>8) indicate the matrix response for shale. Third-variable plots were made for each chosen interval where natural-gamma logs of good quality were available.

Computer-generated cross plots and third-variable plots furnished information regarding the rock-matrix responses of various rock types. Extrapolating the data to the zero-porosity point on the lithology lines provides the basic lithologic matrix responses with the exception of shale. The shale-matrix point was chosen by examining trends in the third-variable plot as shown in figure 3. In addition to determining the matrix response, the cross plots and third-variable plots were used to adjust logs that were inadequately calibrated.

It was initially assumed that characteristic responses would hold over a few townships. However, because of the variations in log quality, each interval to be analyzed in each well had to be cross plotted. It could not be assumed that the rock-matrix points for limestone from one well to another were 0.0-percent porosity, 2.71 g/cm^3 bulk density, and a transit time of 147.5 μs/m. If this were not done, the automated lithologic computations would become erratic.

Corrected rock-matrix responses were used as input to the computer program that calculated the percentage of the total volume of the rock type and the pore volume at a chosen interval. Algorithms to do this type of computations were first proposed by Burke, Curtis, and Cox (1967). However, their solutions were

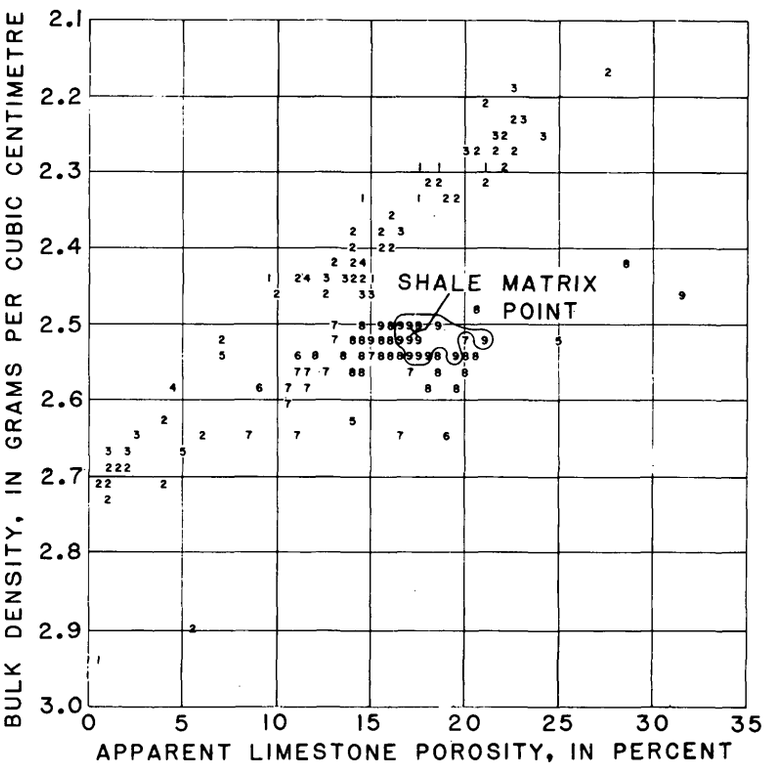

FIGURE 3.—Typical third-variable plot (weighted third variable) for a section of the upper part of the Minnelusa Formation, the Opeche Shale Member and lower part of the Minnekahta Limestone Member of the Goose Egg Formation (same as fig. 2). The third variable is a weighted function, 1–10, of the natural-gamma response and is plotted on the z axis. The shaliness of this section is demonstrated showing a bias in the responses towards the shale-matrix point.

limited to the same number of matrix constituents as logs. The algorithm used in this study incorporated a linear programing technique (Simplex) that will find the best solution for an underspecified problem (more unknowns than input equations). Therefore, the percent volume of one to three constituents more than input logs could be reasonably solved. This technique operates with the assumption that a particular log response can be controlled by more than one geologic variable. Too many unknowns will lead to erroneous interpretations.

A simplified formulation of the linear programing technique (Merkel and others, 1976) can be stated as follows:

We define an objective function (Z) as:

$$Z=\sum_{i=1}^{N} P_i C_i. \tag{1}$$

The mineral fractions (C_i) are subject to the following constraints:

$$\sum_{i=1}^{N} M_{ji} C_i = L_j \pm \epsilon_j, \tag{2}$$

$$\sum_{i=1}^{N} C_i = 1.0, \tag{3}$$

and

$$C_i(\min) \leq C_i \leq C_i(\max), \tag{4}$$

where

C_i = mineral fraction of the ith mineral constituent,
N = number of mineral constituents to be solved for (including porous water),
P_i = predetermined probability of occurrence of the ith constituent,
M_{ji} = the jth tool matrix response for the ith constituent,
L_j = jth tool log value,
ϵ_j = the probable error of the jth tool,
$C_i(\min)$ = the lower allowable bound of the ith constituent, and
$C_i(\max)$ = upper allowable bound of the ith constituent.

The linear programing technique also has the advantage that it is possible to constrain any given component (C_i) between a range [$C_i(\min) \leq C_i \leq C_i(\max)$] predetermined by the cross plots and third-variable plots. Input variations may be controlled by imposing probable tool and recording errors (ϵ_j) on each log. If it is determined from the cross plots that a given tool was not functioning properly, or is poorly calibrated, a large tool error could be used in association with the given tool input values to weight these values less than the other log inputs.

The input parameters P_i, M_{ji}, ϵ_j, $C_i(\min)$, and $C_i(\max)$ are all determined from cross plots and third-variable plots and do not vary during an analysis over a specific interval. As previously discussed, small inaccuracies in the M_{ji} values will lead to erroneous results. C_i is initially given the value P_i. The terms in equations 1–4, when properly positioned in an algebraic matrix, are in a linear programing format. This large matrix solved the four equations simultaneously using the Simplex method (Hillier and Lieberman, 1967). C_i will then iterate between $C_i(\min)$ and $C_i(\max)$ until a maximum value of Z is obtained. The calculation is repeated for each L_j within the chosen interval. The result is a solution for C_i (the volumetric percentages of each constituent), which is graphically displayed. The total mineral and porosity percentages always equal 100. For example, in figure 4 at 3383 m, there is about 10 percent porosity, 79 percent sandstone, and 11 percent shale. Errors are likely in areas where the lithology changes rapidly (for example stringers) since the various geophysical tool responses are measured averages over different vertical distances in the borehole.

The apparent resistivity of the pore fluid (R_{wa}) contained in the Minnelusa Formation and the Madison Limestone was computed using Archie's equation:

$$R_{wa} = (R_T \phi^m)/a.$$

The resistivity of the formation, R_T, was determined from deeply penetrating electric logs. The porosity (ϕ) was determined from the calculated, lithology-corrected porosity. The cementation factor, m, varies from less than 2 for poorly sorted, poorly cemented rocks to greater than 2 for well-sorted, well-cemented rocks. The average value of $m=2$ was used in all calculations. The parameter, a, varies with porosity type; it is less than 1 for intergranular porosity and more than 1 for secondary porosity. A value of $a=1$ was used for the calculations. The apparent resistivity is an approximation of the true fluid resistivity. True fluid resistivity is not directly measured owing to the affects of the mud column in the borehole, the invaded zone, and the influence of adjacent geologic beds.

MINNELUSA FORMATION RESULTS

Computed lithology analyses were made of the entire thickness of the Minnelusa Formation available on the logs. Figure 4 illustrates a typical analysis of the upper part of the formation. Sandstone is the dominant rock type. Carbonate rocks are also present in an appreciable quantity. Both are slightly argillaceous. Shale stringers and beds occur in many Minnelusa sequences. Anhydrite is not readily distinguishable from carbonates without proper log combinations

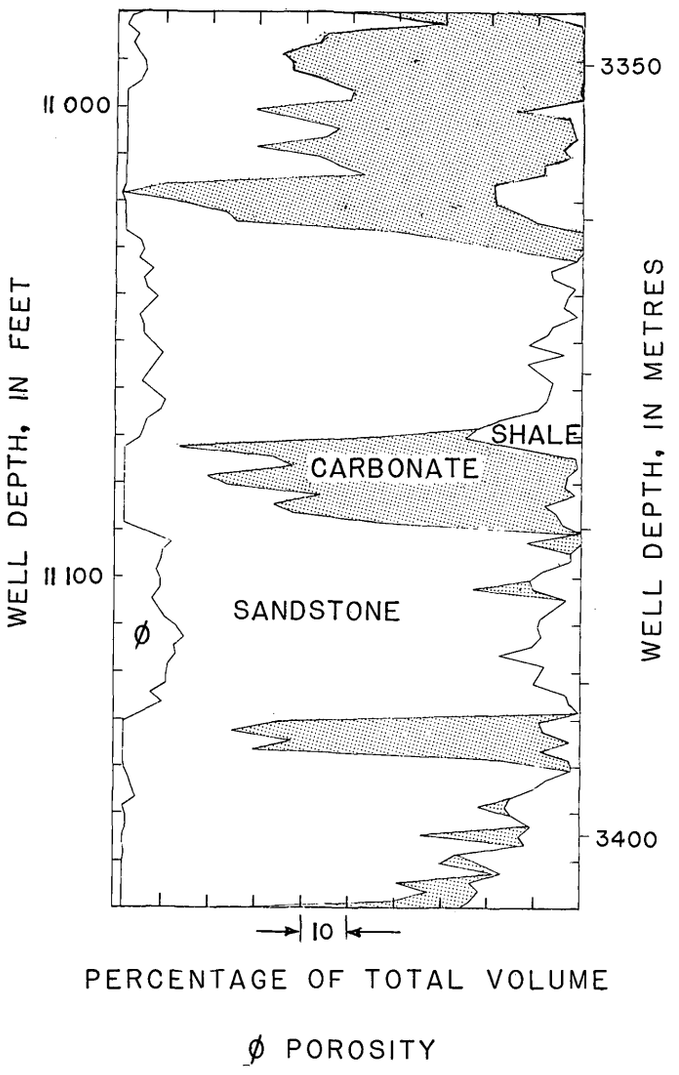

FIGURE 4.—A typical computed lithologic log of the upper part of the Minnelusa Formation. At 3383 meters, the analysis would read 10 percent porosity, 79 percent sandstone, and 11 percent shale.

(sonic and density). Therefore, the first indicated carbonate occurrence at or near the top of the formation actually may be an anhydrite layer that is known to be present at this interval. Where the sonic and density logs were available, anhydrite was separated from the carbonates.

Computed porosity values were variable within the units of the Minnelusa. Zones of high porosity were in the sandstone units having a low shale content, while low porosities were in the carbonates and very shaly sands.

The first major sandstone-carbonate-sandstone sequence near the top of the formation was chosen for regional mapping. This interval in figure 4 is from 3360–3392 m. The mapped unit was chosen near the top of the Minnelusa because of its continuity across the basin and the fact that some wells only penetrate the upper part of the formation. The unit is also below any major occurrences of anhydrite.

A lithology map was compiled showing average percent volume of sandstone and the average percent volume of shale for the selected unit in the upper part of the Minnelusa. A contour map of the percent sandstone is shown in figure 5. The general area of lowest sandstone content corresponds to an imaginary line east of and approximately parallel to the structural axis of the basin. The highest percentage of sandstone per unit volume is in the flank areas of the basin. Most of the areas of high sandstone content occur where the Minnelusa is closest to the surface. No trends in shale content were apparent. Changes in the percentage of sandstone are due mainly to the changes in stratigraphic relationships between sandstone and carbonate rocks. The total thickness of the mapped interval remained about the same. Log quality was acceptable and borehole-diameter effects tended to average. The largest difficulty in comparing lithologic analysis for mapping is the variance caused by using different log types. Cross plots were made for every well penetrating the selected interval to minimize mineralogic input error.

Average porosity values of the mapped interval were compiled for the basin. The porosities that were obtained represent good data resolution and were on a basis of ±1.0 percent (fig. 6). If there are fractures or vugs present, the porosity values from sonic logs would represent a lower boundary of the total rock porosity. Therefore, since sonic porosities were often used and compared with neutron and density porosities, the values in this report should generally be considered representative of the primary rock porosity.

The zones of low porosity are along an imaginary line approximately parallel to and near the structural axis of the basin. Zones of high porosity are along the flanks of the basin and near the center of Campbell County, Wyo. The zones of high porosity correspond to the higher percentage sand zones. The carbonates evidently have low porosity. The area of Campbell and Crook Counties has the most variation in porosity, corresponding to similar variations in lithology. The porosity contours correlate approximately with the structural trends. This would imply some type of structural control for the porosity. Low porosities (2 percent) in the center of the basin could be attributed to compaction resulting from the depth of burial of the rocks.

The average value of apparent water resistivity (R_{wa}) was calculated for the selected interval of the

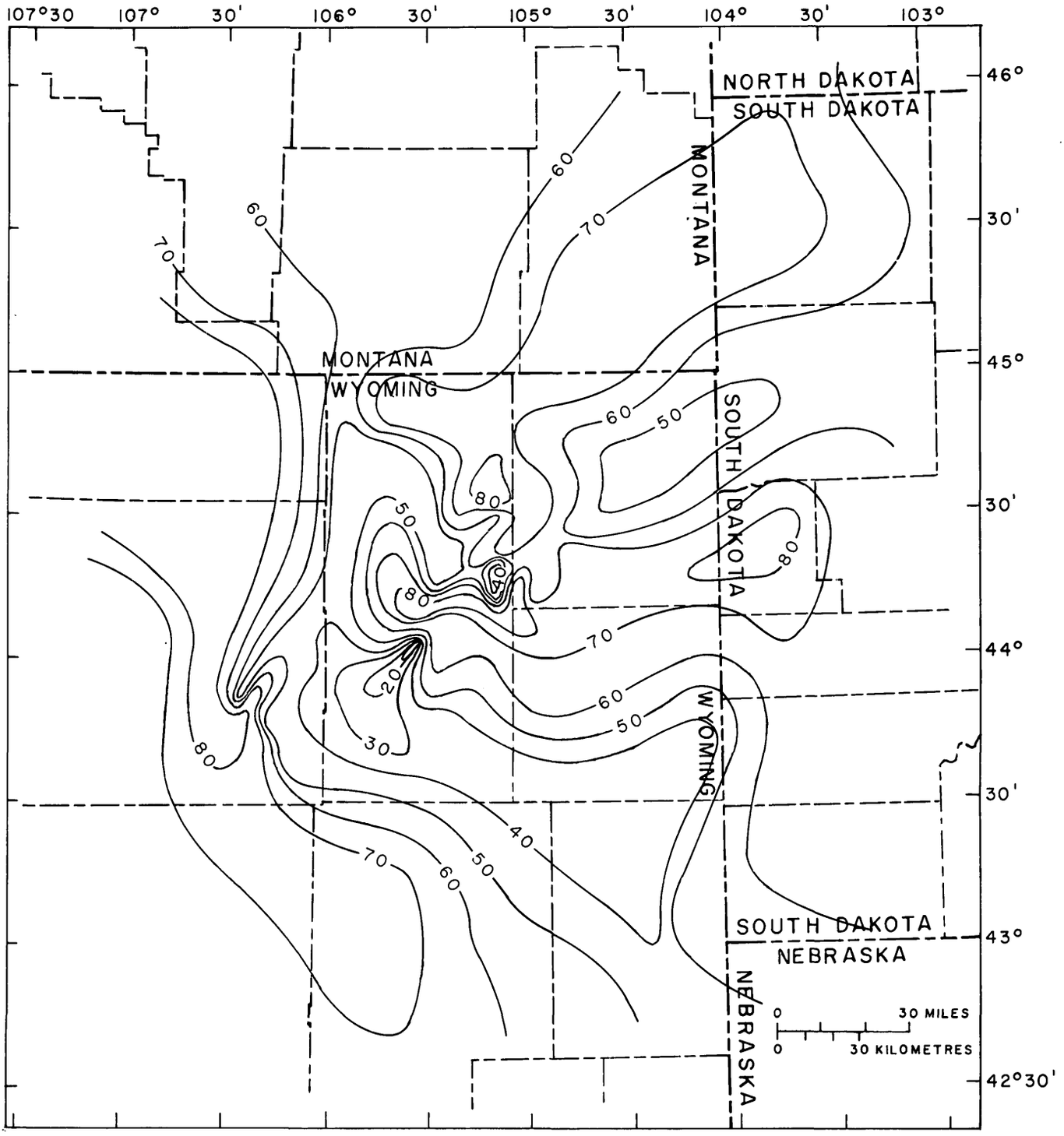

FIGURE 5.—Computed average percent sand in the top major sand-carbonate-sand sequence of the upper part of the Minnelusa Formation. Contours are in 10-percent intervals.

upper part of the Minnelusa. A contour map of the apparent water resistivity for the region is shown in figure 7. Temperature corrections were not made. A constant temperature effect was assumed for the basin, however, such an assumption may not always apply to all data points. Anomalous values may be partially due to extreme temperature variations.

The low-resistivity areas in figure 7 trend approximately parallel to the structural axis of the basin. A low-resistivity area also trends southwestward about

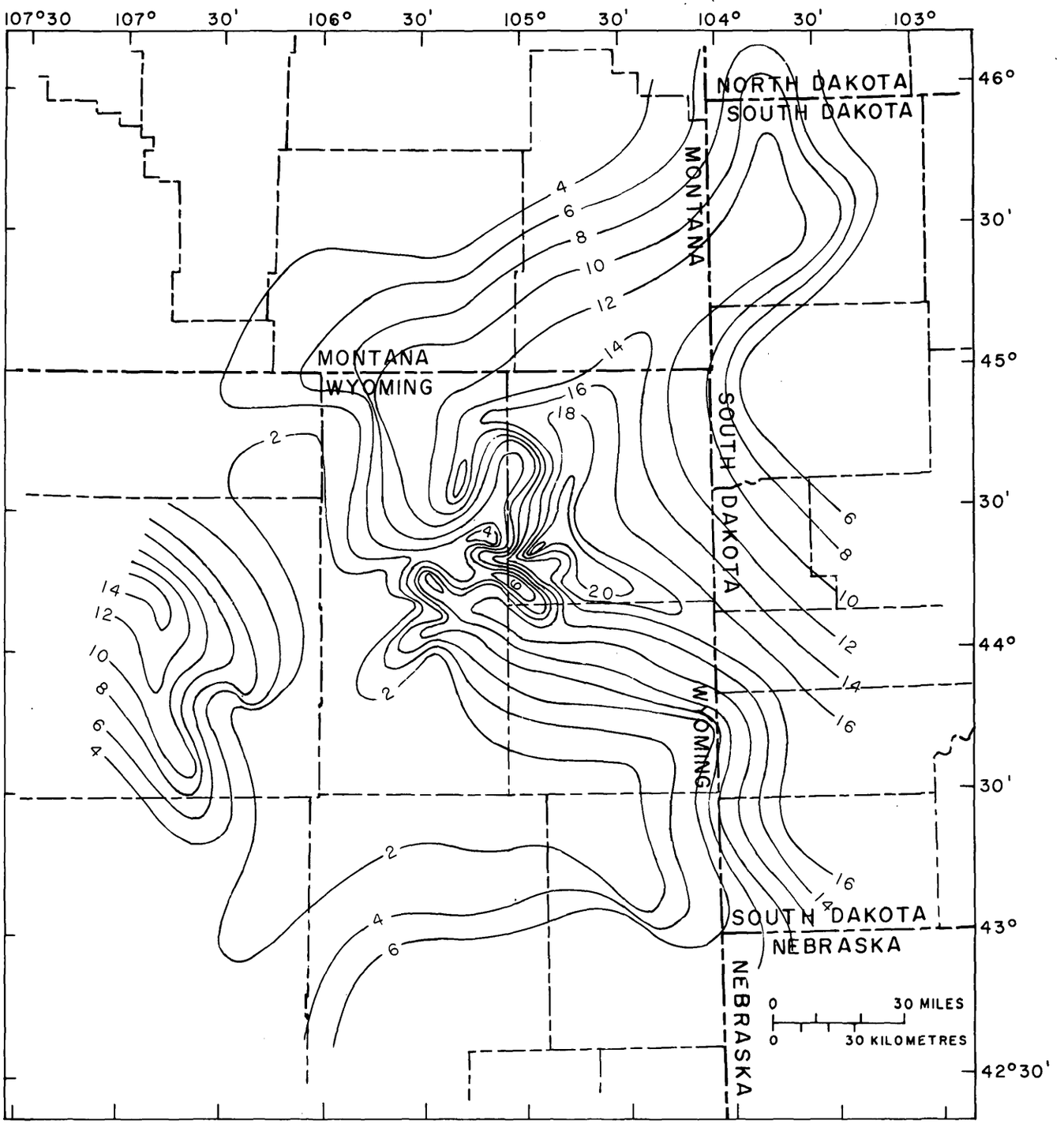

FIGURE 6.—Computed average porosity for the top major sand-carbonate-sand sequence of the upper part of the Minnelusa Formation. Contours are in 2-percent intervals.

normal to this axis. High-resistivity areas are generally along the flanks of the basin. These high-resistivity areas correspond to areas of high porosity and high percentage of sandstone.

In a study of formation waters, Evers and Iyer (1975) found that the dominant cations in the Minnelusa Formation and the Madison Limestone of the Powder River Basin were calcium and magnesium.

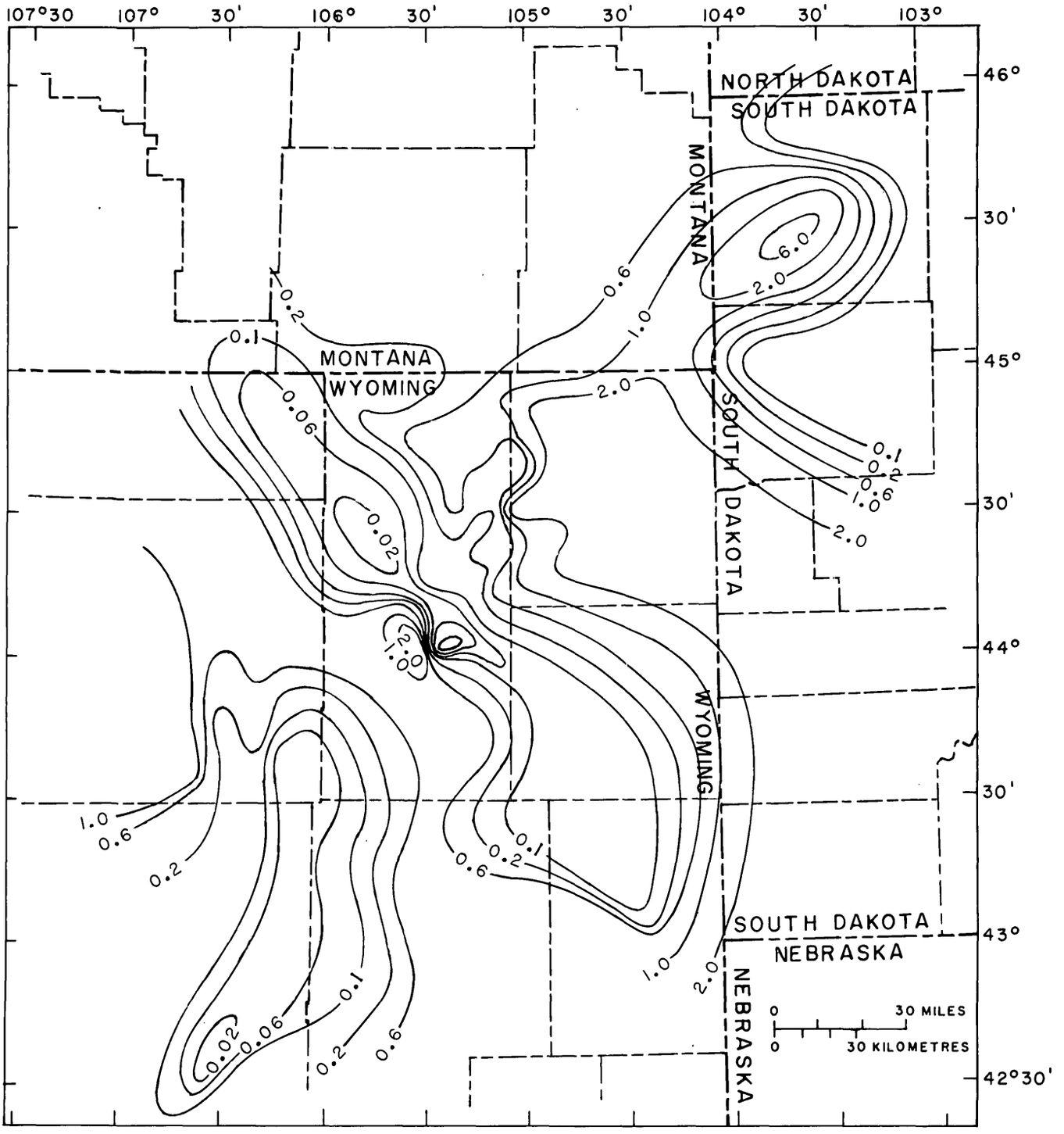

FIGURE 7.—Computed average apparent water resistivity in ohm meters for the top major sand-carbonate-sand sequence of the upper part of the Minnelusa Formatin. Intervals are in log format with a scale of three divisions per cycle.

They also found that bicarbonates and sulfates of sodium and calcium dominate in most of the fresher water. The sulfate concentration was less than the bicarbonate concentration in the fresher water. Hence, the primary source of dissolved solids in the fresher waters (>1 ohm meter resistivity) along the margins of the basin appears to be the dissolution of limestone and dolomite, with a secondary source being gypsum and anhydrite.

The high dissolved solids in the water towards the center of the basin (<1.0 ohm meter) are probably due to large concentrations of sulfates in the water. The many shale units in the Minnelusa also sorb and retain sulfate ions. This retention can significantly lower the resistivity values in shale zones.

MADISON LIMESTONE RESULTS

Interpretations from 18 wells show the Madison Limestone and equivalent rocks increase in thickness from about 60 m in Niobrara County, Wyo., to over 460 m in Bowman County, N. Dak. The interpreted logs of the Madison in the southern part of the basin demonstrate the dominant lithology to be carbonate rocks. Interpreted logs of the Madison Group in the northern part of the basin exhibited a greater variability of rock types. The Charles Formation is dominantly limestone with significant sequences of shale, anhydrite, and sandstone. The Mission Canyon Limestone is limestone and dolomite with small amounts of shale. The Lodgepole Limestone is predominantly a slightly argillaceous limestone with small amounts of sandstone.

Compilation of analyses of the Madison indicates some generalizations about the lithology: (1) The average dolomite occurrence in percentage of total volume for the Madison is about 29 percent, (2) the average total volume of limestone is approximately 50 percent, (3) where the average volume of limestone is greater than 70 percent, the average volume of dolomite is less than 20 percent, and (4) the shale content, including argillaceous units, generally increases to the north. This is mainly due to the lithology of the Charles Formation.

Porosity values in the Madison range from 2.3 percent to 13 percent. The average porosity is 5.5 percent. Where the limestone occurrence is greater than 50 percent, the primary porosity is less than 8 percent. This would suggest that any significant porosity for water development would have to be secondary porosity. The porosity of the Madison increases from the center of the basin to the flanks approximately the same as the porosity of the Minnelusa. The average density of the Madison section ranges from 2.48 g/cm^3 in the west to 2.76 g/cm^3 in the east, with an overall average density of 2.6g/cm^3.

A comparison of a geophysical log analysis of the Madison with a lithologic log constructed by R .T. Ryder (written communication, 1975) from chip samples is shown in figure 8. The results of the comparison demonstrate a good qualitative correlation. Quantitatively, the correlation is not as good since the computer analysis was affected by poorer than average

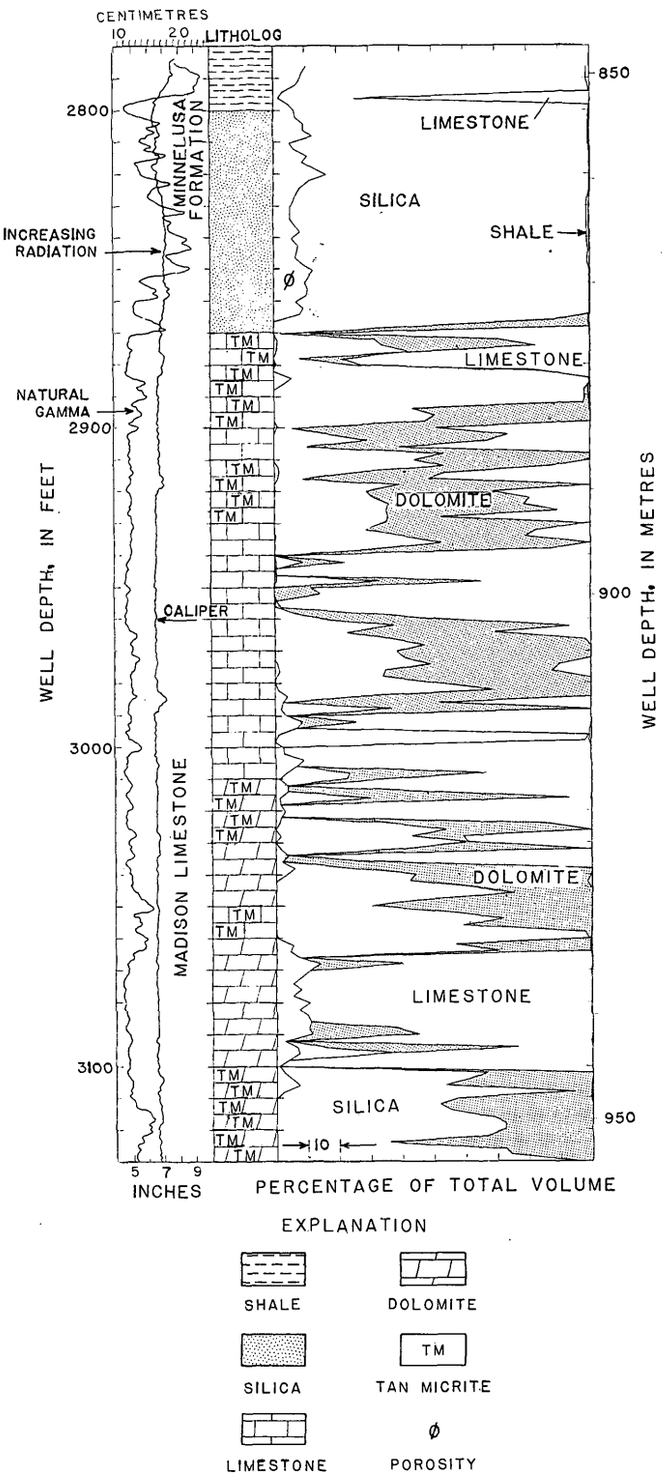

FIGURE 8.—Computed lithology log, natural gamma log, and caliper log compared to a lithology log prepared from chip samples (Ryder, R. T., 1975, written commun.) of a section of the Madison Limestone and the Minnelusa Formation in Niobrara County, Wyo. At 929.6 m, the computed log reads 31 percent sandstone (silica) and 69 percent dolomite.

geophysical log quality. Changes in the borehole diameter contribute to errors in the estimates of sandstone (silica content). Sandstone volumes (silica content) of greater than 50 percent, not represented on the lithologic log, may be due to failure of the computer program to recognize a definable log response from the geophysical logs.

The interpretation in this example shows the Madison to be a consistent siliceous carbonate rock. Most zones of higher silica content on the computed log are associated with the tan micrite zones on the lithologic log. All zones of high silica content on the computed log correspond to the higher radiation zones on the gamma log. The gamma response could also be caused by clay-filled, small vugs in the rock. Minute traces of shale may be present, as shown on the computed log, which would affect the silica analyses. The calculated limestone-to-dolomite relationships are similar to those determined from rock samples. The "Bell sandstone unit" (local usage) of the lower part of the Minnelusa Formation is correctly shown on the computed log.

Figure 8 demonstrates the usefulness of computerized analysis of geophysical logs in lieu of any other lithologic descriptions. It also provides supplemental information to verify or add to the lithologic log description. For instance, the lithologic log from rock chip samples did not present the possibility of the small vugs being clay filled. The vertical detail in the computed log is accurate to the nearest 0.61 m, whereas the lithologic log is accurate to the nearest 3.1 m. If the geophysical analysis could be done with good quality logs, digitized at 0.305-m intervals, and compensated for borehole changes, it would likely stand alone as the most accurate method of determining lithology.

Apparent resistivity of water values vary considerably with depth in many wells (fig. 9). The variations in resistivity are caused by inorganic salts, clay, and shale which contribute ions into solution. Some variations in calculated resistivity values are due to the digitizing technique used. Hydrocarbons in the water will also affect resistivity values. Large variations in restivity may indicate areas of water movement and possible head differences within a unit, much in the same way as borehole conductivity meters are used to detect inhole flow. Areas of high water resistivity are likely locations of hydrocarbons or very fresh water.

Part of a general trend of decreasing water resistivity with depth could be due to temperature effects. Temperature compensated resistivity values are shifted with increasing depth to slightly higher resistivities (fig. 9). The R_{wa} values for for the deepest penetrations of the Madison were changed no more than 25

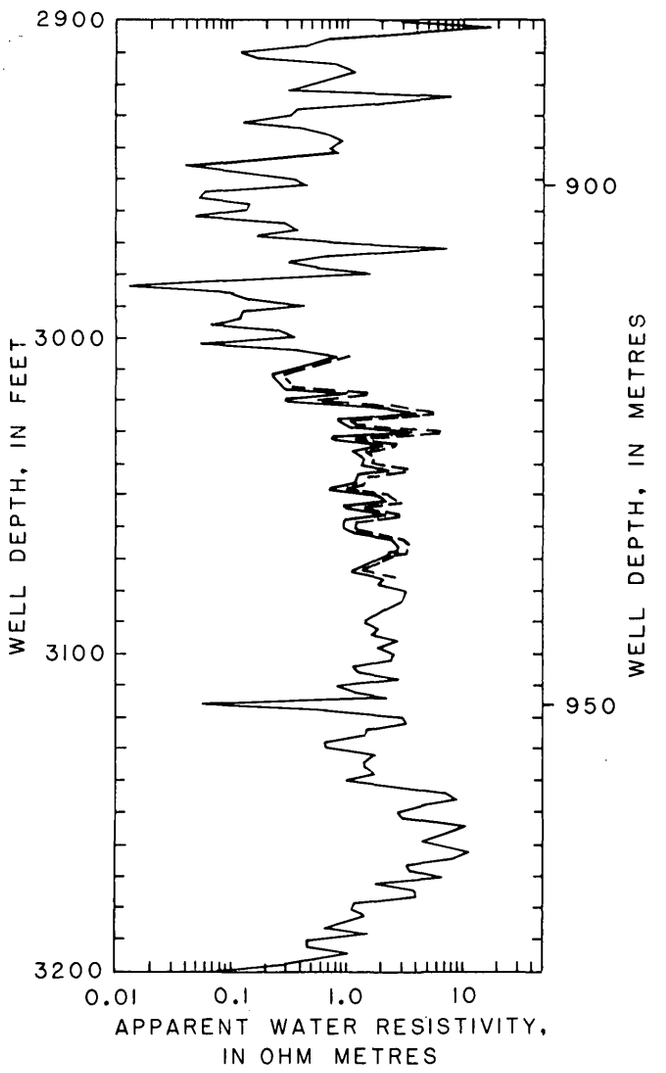

FIGURE 9.—Variation of the apparent water resistivity in a part of the Madison Limestone in Crook County, Wyo. Correction for temperature is shown by dashed line.

percent by the temperature correction using a standard gradient of 24°C/km. Anomalously high temperatures are known to exist in the Madison and could produce significant variations in resistivity. Accordingly, future work should involve establishing a regional temperature gradient to be used to correct water resistivity values for the Madison and the Minnelusa.

The concentrations of dissolved solids in water from the Madison Limestone shown in figure 10 (Hodson, 1973, written commun.) indicate variations from fresh to saline water in the Wyoming part of the basin that are similar to those in the Minnelusa Formation (fig. 7). This suggests possible hydraulic connection between the Madison and the Minnelusa and similar recharge areas for the units. The concentrations (dis-

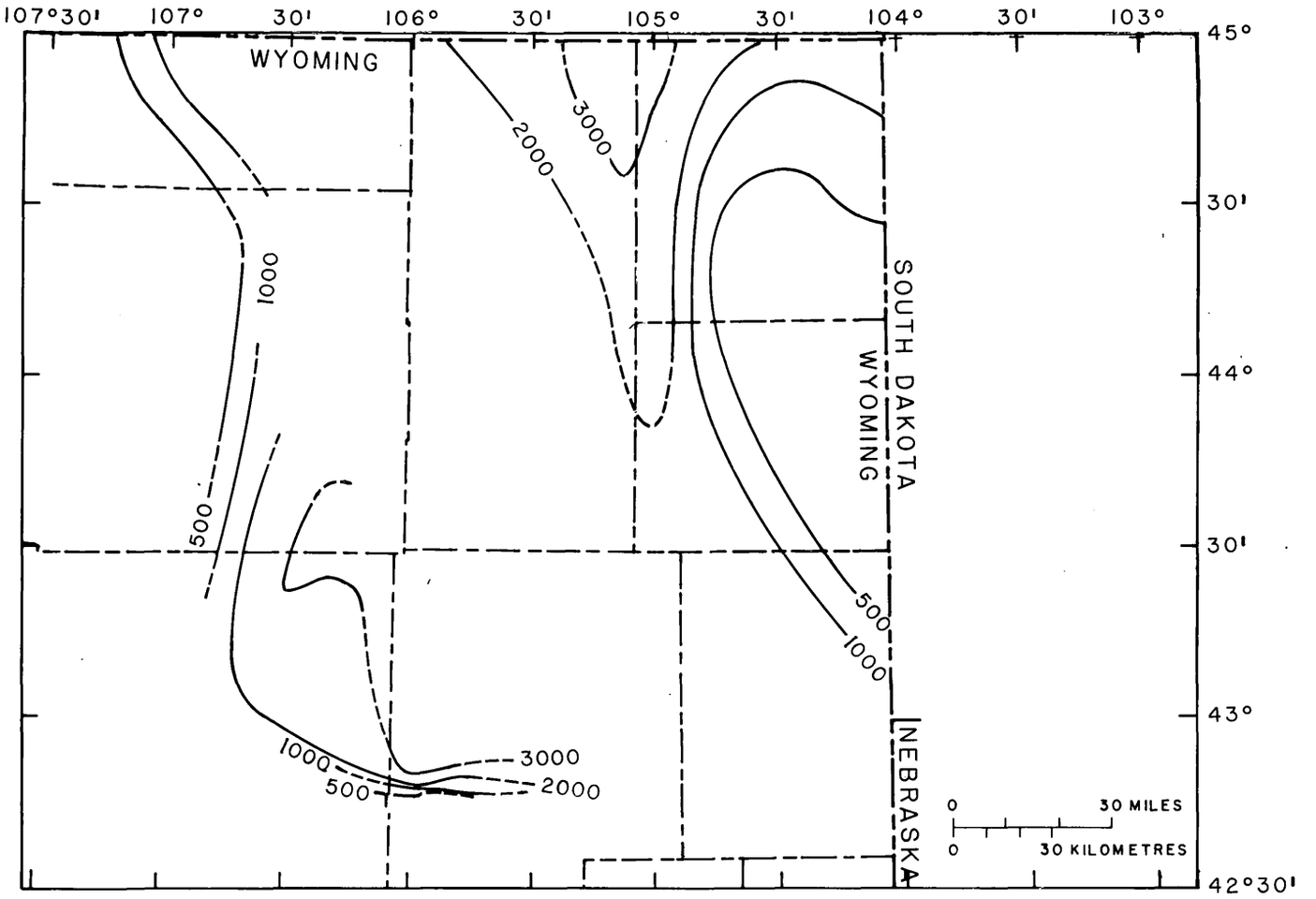

FIGURE 10.—Approximate dissolved-solids concentration of water in the Madison Limestone for the Wyoming part of the Powder River Basin (Hodson, W. G., 1973, written comm.) Contoured in 500- and 1,000-mg/L intervals.

solved solids) appear to be controlled by geochemical relationships based on the lithology and the structure of the formations.

The R_{wa} values for the Madison are higher than those for the Minnelusa. The Madison water resistivities are higher near the outcrops or recharge areas. The average R_{wa} is 1.2 ohm meters. This average resistivity of the Madison water indicates the dissolved solids are higher than is desirable for most uses. Most low R_{wa} values are associated with limestone or dolomite rock units that contain or are adjacent to gypsum, clay, or shale beds. It may be possible to compare resistivities of the Minnelusa and the Madison and find relationships to potentiometric head. Variations in the regional trends of either unit may indicate the presence of water from the other unit. For example, a noticeable anomaly (R_{wa}=2.7 ohm meters) in central Campbell County, Wyo., may indicate upward movement of water into the Minnelusa.

DISCUSSION

Confidence in the modified Simplex computer method depends mainly on log quality, input log combinations, and the rock parameters chosen from the cross plots. A calibrated logging device should give responses that accurately relate to borehole conditions and formation properties. Logs must be inspected for mechanical and electronic malfunctions. Abnormal borehole conditions, such as washouts, generate log responses incompatible with the theoretical formation limitations of the device. Large erroneous values must be corrected or eliminated before analysis. Use of several types of logs can present true formation characteristics. As shown by cross plots, a small variance in log response can be misinterpreted as to rock type. Care should be taken before calculations are made to correct for extreme changes in the borehole environment, such as temperature, salinity, and diameter changes. The computer method is intrinsically capable

of high precision because smaller tool errors can be accounted for in the computation.

Although computer techniques used in this report have limitations, the approach did prove legitimate for a regional survey where knowledge of the dominant rock types and distribution is needed. The study was useful in delineating areas where further intensified investigations should be made. It is important to note that the accuracy of the results increases with both log quality and number of input logs.

The porosity determinations were consistently accurate. The greatest difficulty occurred when only one of the three porosity logs was available. Therefore, secondary porosity was not determined in all analyses. Assumptions made about the matrix porosity being a lower bound of the total porosity are valid. Where secondary porosity is greater than 5 percent, the lithology determinations are less accurate. Compensations should be made in the linear programing technique in situations of known high secondary porosity.

Apparent water resistivity determinations are related to the accuracy of the porosity measurements, temperature, and electric log quality. The apparent water resistivity is underestimated in areas where the total porosity is underestimated. Except in highly anomalous areas, temperature corrections are minimal.

The water resistivities give a reasonable approximation of the dissolved solids in the formation water because the deep-penetrating electrical probes measure pore-fluid conductivity in situ more accurately than any other presently available system. The dissolved-solids distribution throughout the basin by geologic unit relates information on both the hydrology and geology. Possible leakage between aquifers and water movement from recharge areas to discharge areas can be studied. Changes in water quality with depth can also be measured from resistivity data.

CONCLUSIONS

The results of the analysis of the Minnelusa Formation in 70 wells show a high variability in rock type within the formation over the basin. Sandstone, shale, limestone, dolomite, and anhydrite are present as major units, intercalated occurrences, and as stringers. High values of primary porosity, sandstone content, and resistivity of water from a selected interval in the Minnelusa exist along the flanks of the basin and in the Black Hills; low values occur at or near the center of the basin parallel to the structural axis.

The analysis of the Madison Limestone in 18 wells shows the dominant presence of carbonate rocks throughout the basin. Sand, shale, and anhydrite beds are occasionally present in the Madison in the southern part of the basin. In the northern part of the basin the Charles Formation, Mission Canyon Limestone, and Lodgepole Limestone of the Madison Group have a much greater degree of variability with major units present of sandstone, shale, and anhydrite. The Madison has a low primary porosity with an average of less than 13 percent. Restivity of water values agree with the trends in the Minnelusa, although values from the Madison are generally higher than those from the Minnelusa for the same location.

The results of the study indicate that the best areas for development of freshwater are along the margins of the basin. The unfavorable areas are near the center of the basin where water quality and potential water volume decrease. Many of the sandstone units in the Minnelusa have high porosity and resistivity of water and could possibly be tapped for freshwater. Of the two formations, the Madison is the better aquifer for freshwater. Large production of water from the Madison will probably be limited to high secondary porosity areas. The results of the study infer the possibility of hydraulic connection between the Madison and the Minnelusa.

REFERENCES CITED

Burke, J. A., Curtis, M. R., and Cox, J. T., 1967, Computer processing of log data improves production in Chaveroo Field: Soc. Petroleum Eng. Trans., July, p. 889–895.

Evers, J. F., and Iyer, B. G., 1975, A statistical study of the SP log, in fresh water formations of Wyoming's Big Horn and Wind River basins: Calgary, Alberta, Canadian Well Logging Society Trans., Fifth Formation Evaluation Symposium, p. H1–H4.

Foster, D. I., 1958, Summary of the stratigraphy of the Minnelusa Formation, Powder River Basin, Wyoming, *in* Wyoming Geol. Assoc. Guidebook 13th Ann. Field Conf., Powder River Basin, p. 39–44.

Hillier, F. S., and Liberman, G. J., 1967, Introduction to Operation Research: San Francisco, Holden-Day, 639 p.

Merkel, R. H., MacCary, L. M., and Chico, R. S., 1976, Computer techniques applied to formation evaluation: The Log Analyst, v. 17, no. 3, p. 3–10.

Roberts, A. E., 1966, Stratigraphy of Madison Group near Livingston, Montana, and discussion of karst and solution-breccia features: U.S. Geol. Survey Prof. Paper 526–B, 23 p.

Schlumberger Limited, 1972, Schlumberger Log Interpretation charts: New York, Schlumberger Limited rept., p. 33.

Jour. Research U.S. Geol. Survey
Vol. 5, No. 4, July–Aug. 1977, p. 487–490

RELATION OF SURFICIAL EROSION ON HILLSLOPES TO PROFILE GEOMETRY

By R. F. HADLEY and T. J. TOY,[1] Denver, Colo.

Abstract.—Differences in erosion rates in relation to the geometry of hillslope profiles were hypothesized by R. E. Horton in 1945. Experimental testing of this hypothesis is described for natural hillslopes in western Colorado using a rainfall simulator to apply five "storms" each having an intensity of 1.85 inches per hour (47 millimeters per hour).

Erosion from straight hillslope segments was about twice the amount from convex and concave segments along nine hillslope transects. Standard deviations of erosion measurements for each segment show that the greatest variation occurs in concave slope segments. This is probably because the concave segment is the only place on the profile where deposition occurs. Analysis of variance indicates that the amount of erosion is significant at the 1-percent level of confidence between convex and straight slope segments and at the 5-percent level of confidence between straight and convex slope segments.

Although disagreement persists as to the number of geometric segments that constitute a natural hillslope (Carson and Kirby, 1972, p. 304), most hillslope profiles contain segments that are convex, straight, and concave in shape. White (1966, p. 592) found all segments in 70 percent of the hillslopes he analyzed in southwestern Ohio. He found that the three slope-form segments were typical of short slopes as well as long slopes, gentle slopes as well as steep slopes, and that all three segments are well developed on different types of parent material.

The relation of erosion to slope segments was suggested by Horton (1945). In his definitions, the convex segment is the "belt of no erosion"; the straight segment is the "zone of active erosion"; and the concave segment is the zone of "deposition of sediment." However, there has been little experimental verification of Horton's theoretical categories. Young and Mutchler (1969a, 1969b) provide some data on the relation of slope shape to erosion, but their findings are probably not applicable to natural hillslopes because of the experimental design. In their studies, the slopes were mechanically shaped and the profiles were all unisegmental, that is, either convex, straight, or concave. Also, runoff and erosion undoubtedly were influenced by plowing and cultivation parallel to the slope. In our experiments, simulated rainfall was applied to natural hillslopes with convex-concave profiles that were not altered in any way.

The purpose of the research was to test the validity of Horton's hypothesis that there are differences in the amount of surficial erosion on various segments of natural hillslopes. Application of the research results can be useful in studies of rehabilitation of disturbed land such as that resulting from surface mining. For example, the ability to predict which geometric segment of a hillslope is more subject to surficial erosion will be useful in the design of the topography of reshaped mine-spoils material. The relation of the hillslope profile to erosion will be especially important during the initial phase of rehabilitation before vegetation is established while the bare soil is exposed to raindrop impact.

In this report values are given in U.S. customary units of measurement. Following is a list of factors used to convert to SI (International System) units:

U.S. customary unit	Factor	SI unit
Inch	× 25.4	=millimeters
Foot	× 0.3048	=meter
Square foot	× 0.09290	=square meter
Mile	× 1.609	=kilometers

LOCATION

The field data were collected in the Badger Wash basin in western Colorado, about 7 mi northwest of Mack and 6 mi east of the Colorado-Utah boundary. Both experimental basins are underlain by Mancos Shale of Cretaceous age which is nearly flat-lying in this area. The climate of the region is arid with an average annual precipitation of 8.3 in, and vegetation is sparse consisting mainly of salt-desert shrubs.

[1] Present address: Department of Geography, University of Denver, Denver, Colo.

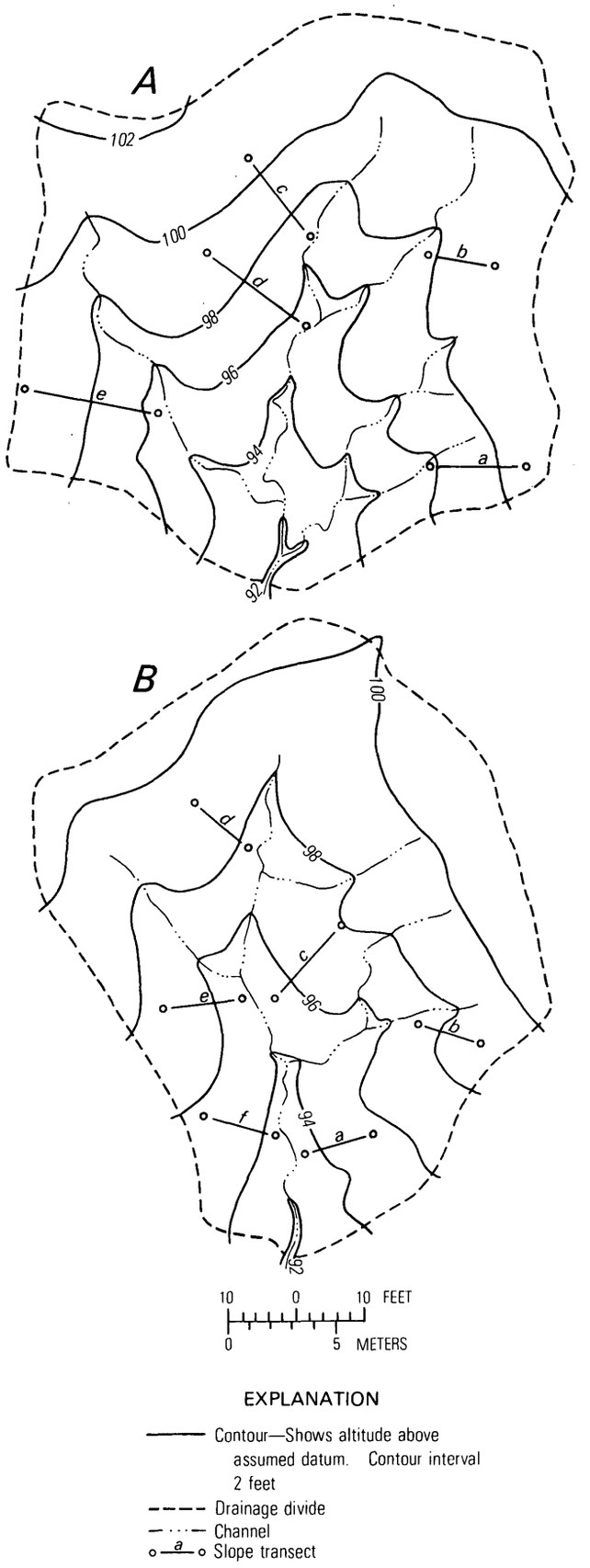

FIGURE 1.—Topography and hillslope transects used in analysis of erosion. *A*, Basin 1. *B*, Basin 2.

METHODS

In order to test Horton's theory of surface erosion by overland flow, a field experiment was designed using a rainfall simulator (Lusby, 1976) to produce precipitation and runoff on natural hillslopes. Rainfall was applied at an average rate of 1.85 in/hr for 42 min over two drainage basins of approximately 4 000 ft^2 each with natural boundaries. Hillslopes were surveyed in each of the basins before and after the simulated storms and these survey measurements provided the erosion data for a test of Horton's hypothesis. In all, erosion was measured on the hillslopes from five simulated rainfall periods of similar intensity and duration.

Topographic maps of the two basins used in the experiment are shown in figure 1 with the location of 11 hillslope transects. Nine hillslopes were chosen from those measured for use in the analysis. The basis for selecting the nine hillslopes was that each could be easily divided into convex, straight, and concave seg-

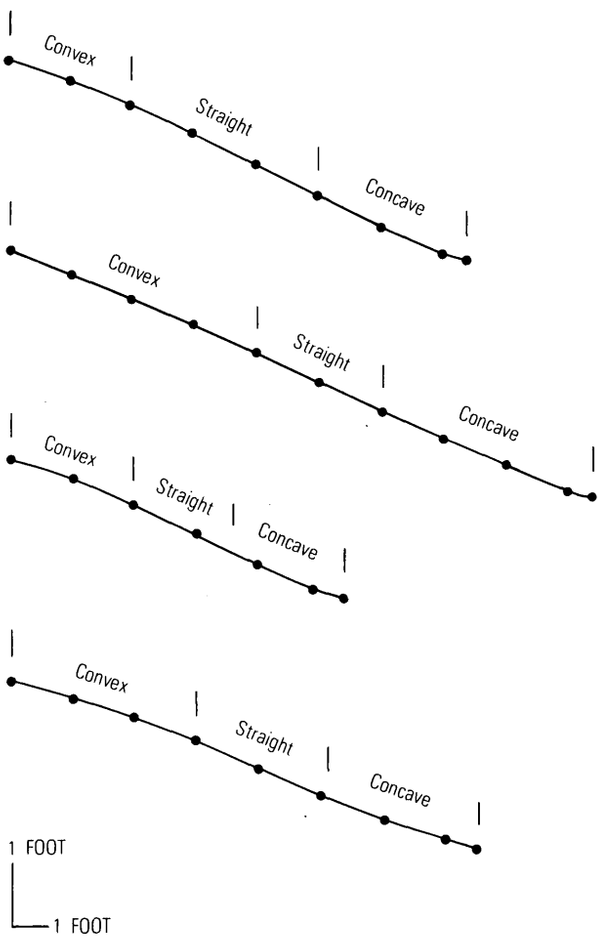

FIGURE 2.—Four typical hillslope transects showing geometric segments. Profile 1, transect *c*, basin 1. Profile 2, transect *d*, basin 1. Profile 3, transect *b*, basin 2. Profile 4, transect *c*, basin 2. See figure 1 for location of transects in basins.

ments. Figure 2 illustrates four typical hillslopes and their segments used in the analysis.

DATA ANALYSIS

Erosion along the nine hillslope transects for five storms is summarized in table 1. The mean erosion from the straight segments was approximately twice the amount from the convex and concave segments. This supports Horton's hypothesis that the straight segment is the zone of "active erosion." There was also net soil loss from the convex and concave segments. Therefore, the Horton definition of these segments as "belts of no erosion" and zones of "deposition of sediment" is not entirely correct. It would be impossible for the straight segment to erode without erosion occurring at least at the lower end of the convex segment and the upper end of the concave segment in order to provide continuity. Horton (1945, p. 316) undoubtedly was aware of this when he constructed his generalized illustration.

The standard deviations for each segment reflect the fact that there was more variation in the measurements on the concave segments than those in the convex or straight segments. The individual measurements in the concave segments ranged from 0.11 ft of erosion to 0.08 ft of deposition. It might be concluded that the designation of the concave segment as the zone of "deposition of sediment" is justified since this is the only element where substantial deposition occurred.

While the measurements in table 1 suggest differences in the erosional characteristics of the hillslope segments, the significance of these differences remains in question. Analyses of variance were used to compare statistically the erosion of the convex, straight, and concave segments of the nine analyzed hillslope transects. The null hypothesis states that there were no differences in the amount of erosion from the three slope segments. The results of the analysis of variance, are summarized in table 2.

The results comparing all slope segments indicate that the null hypothesis must be rejected; there are significant differences among the amounts of erosion from the three hillslope segments. This statistical test, however, does not identify the segment or segments which differ significantly.

It is necessary to compare pairs of segments in order to locate the source of variation. Table 2 also contains the results of the comparison between the convex and straight segments. These results indicate that the amount of erosion between the convex and straight segments along the nine hillslope transects is significantly different at the 1-percent level of confidence.

Next, the results of analysis for the comparison of straight and concave slope segments is shown in table 2. This analysis indicates that the difference between the amounts of erosion from the straight and concave segments is significant at the 5-percent level of confidence. The variance ratio (F) for these two segments was not as high as that for the convex and straight segments. This is a reflection of the variability in the measurements on the concave segments that showed deposition as well as erosion.

TABLE 1.—*Summary of erosion measurements resulting from five simulated rainstorms*

	Slope segments		
	Convex	Straight	Concave
Number of measurements	27	21	26
Mean erosion ——feet	0.0215	0.0538	0.0277
Standard deviation ——feet	0.0260	0.0282	0.0506

DISCUSSION

There are significant differences in the amount of erosion on the convex, straight, and concave segments of natural hillslopes in this study. These differences suggest morphogenetic reasons for slope geometry. In the strictest sense we cannot concur with Horton's theoretical erosion zones. There is, in fact, some ero-

TABLE 2.—*Analysis of variance of hillslope segments*
[D.f., degrees of freedom]

	Sum of squares	D.f.	Variance estimate	F ratio	Significance level of F ratio (percent)
All segments:					
Between groups	0.0134	1	0.0067	4.88	5
Within group	.0975	71	.0014	---	--
Convex and straight segments:					
Between groups	.0123	1	.0123	16.98	1
Within group	.0334	46	.0007	---	--
Straight and concave segments:					
Between groups	.0079	1	.0079	4.46	5
Within group	.0800	45	.0018	---	--
Concave and convex segments:					
Between groups	.0005	1	.0005	.32	[1]
Within group	.0816	51	.0016	---	[1]

[1] Not significant at 5 percent.

sion in both the convex and concave segments. However, in a general way, we can regard the convex segments as a belt of a minimum erosion, the straight segment as a belt of maximum erosion, and the concave segment as the only segment in which substantial deposition occurs.

The erosion characteristics of the concave segment are particularly interesting. Whether erosion or deposition takes place in the concave segment may well depend on the erosional environment as affected by slope exposure and described by Melton (1960). Schumm (1966) states that the removal of the hillslope sediment from the base of the slope appears to be a prerequisite for its parallel retreat. These findings suggest that both the parallel retreat and declining angle modes of development are occurring simultaneously in this study area.

Removal of sediment from the bases of hillslopes in arid areas is also favored by the characteristicly high-intensity thunderstorms. An example of these events and their impact on this study area was reported by Hadley and Lusby (1967). Low-intensity rainstorms may succeed in removing material from the convex and straight segments but may be unable to transport this material across the concave segment to the streams. The result would be deposition in the concave segment. On the other hand, high-intensity thunderstorms generate more runoff and are thereby more likely to transport the sediment to the larger streams.

The foregoing analysis shows significant differences in the erosion characteristics of hillslope segments. The soil loss from the straight segments is approximately twice that of either the convex or concave segments. Attempts to control erosion on hillslopes and thereby reduce the sediment load of streams, therefore, should be focused on the straight segments of the hillslopes from which the sediment is derived. In addition, control measures on straight segments may also trap soil moving from the convex segments. The utility of these findings in a model for predicting the sediment yield from an individual basin is constrained by such factors as soil type, vegetation cover, and climate. For example, a rate-of-erosion ratio of 2:1 may exist between straight to concave segments of a slope underlain by shale in an arid environment. However, this ratio may not be valid in a humid or arctic environment.

REFERENCES CITED

Carson, M. A., and Kirby, M. J., 1972, Hillslope form and process: Cambridge Univ. Press, London, 475 p.

Hadley, R. F., and Lusby, G. C., 1967, Runoff and hillslope erosion resulting from a high-intensity thunderstorm near Mack, western Colorado: Water Resources Research, v. 3, no 1, p. 139–143.

Horton, R. E., 1945, Erosional development of streams and their drainage basins: Geol. Soc. Am. Bull., v. 56, p. 275–370.

Lusby, G. C., 1976, Determination of runoff and sediment yield by rainfall simulation, *in* Research techniques, erodibility, and sediment delivery: Am. Assoc. Geographers Symposium on Erosion, Milwaukee, Wisc., ann. mtg., 1974, p. 19–30.

Melton, M. A., 1960, Intravalley variation in slope angles related to microclimate and erosional environment: Geol. Soc. Am. Bull., v. 71, p. 133–144.

Schumm, S. A., 1966, The development and evolution of hillslopes: Jour. Geol. Education, v. 14, no. 3, p. 31–51.

White, J. F., 1966, Convex-concave landslopes—A geometric study: Ohio Jour. Sci., v. 66, no. 6, p. 592–608.

Young, R. A., and Mutchler, C. K., 1969a, Effect of slope shape on erosion and runoff: Am. Soc. Agr. Engineers Trans., v. 12, no. 2, p. 231–239.

——— 1969b, Soil movement on irregular slopes: Water Resources Research, v. 5, no. 5, p. 1084–1089.

Jour. Research U.S. Geol. Survey
Vol. 5, No. 4, July–Aug. 1977, p. 491–496

COMBINED USE OF DIGITAL AQUIFER MODELS AND FIELD BASE-FLOW DATA TO IDENTIFY RECHARGE-LEAKAGE AREAS OF ARTESIAN AQUIFERS

By RICHARD H. JOHNSTON and P. PATRICK LEAHY,
Dover, Del.

Work done in cooperation with the city of Dover, Delaware Department of Natural Resources and Environmental Control, Delaware Geological Survey, and Kent County

Abstract.—As a result of continuous pumping since the 1890's, a regional cone of depression encompassing 363 km² has developed within the artesian Miocene Cheswold aquifer at Dover, Del. The aquifer is not being recharged significantly by leakage near the center of the cone, nor is major recharge induced in the updip subcrop area. The source of pumped water is apparently an area of about 65 km² northwest of Dover, where vertical leakage is substantial. This area was delineated by use of a digital aquifer model and streamflow data. A model of the unconfined aquifer was used to compute the unconfined aquifer's natural discharge to streams, assuming no leakage to underlying artesian aquifers. The area of substantial leakage to the underlying Cheswold was delineated as being coincident with that area where model-computed values of stream discharge were substantially larger than actual values of stream discharge determined in the field.

Accurate delineation of areas of intensive recharge or leakage to heavily pumped artesian aquifers is highly useful in understanding the hydraulics of the aquifer system and may aid in protecting aquifers from contamination.

Artesian aquifers may be recharged by infiltration in outcrop or subcrop areas or by vertical leakage through confining beds wherever pressure gradients are favorable. For heavily pumped artesian aquifers, the possible area of infiltration and leakage can be extremely large. Promulgating regulations to protect such an aquifer from contamination may be nearly impossible if its recharge-leakage area encompasses hundreds of square kilometers. On the other hand, if the area of effective recharge leakage is small and can be delineated accurately, workable regulations can be promulgated. This report describes a method used to pinpoint a relatively small area where the Cheswold (Miocene) artesian aquifer in central Delaware is receiving most of its recharge leakage.

HYDROGEOLOGIC SETTING

At Dover, Del., about three-quarters of the water used for public supply is provided by the Cheswold (Miocene) aquifer. Pumpage averaged about 25 000 m³/d (6.5 Mgal/d) during the late 1960's and early 1970's. The aquifer is composed of fine to coarse sand and is 15 to 23 m thick at Dover. Transmissivity ranges from 140 to 370 m²/d. A southward-thickening confining bed, somewhat heterogeneous but consisting mostly of silt, separates the Cheswold from an overlying unconfined aquifer at Dover. The northward featheredge of the confining bed is about 13 km north of Dover, as shown in the geologic section in figure 1. The Cheswold directly underlies the unconfined aquifer in a narrow subcrop belt (Sundstrom and Pickett, 1968).

The Cheswold aquifer has been continuously pumped at Dover since 1893, with a gradual increase to the present to 25 000 m³/d (6.5 Mgal/d). An extensive cone of depression has developed in the regional potentiometric surface, as shown in figure 2. The cone is centered around the supply wells of the city of Dover and Dover Air Force Base.

The overlying unconfined aquifer consists of fine to coarse sand and occurs as a southward-thickening blanket across central and southern Delaware (Johnston, 1973). The saturated thickness of this aquifer ranges from 8 to 15 m at Dover to more than 46 m in southern Delaware. Transmissivity (T) also increases southward, with values ranging from 190 to 460 m²/d

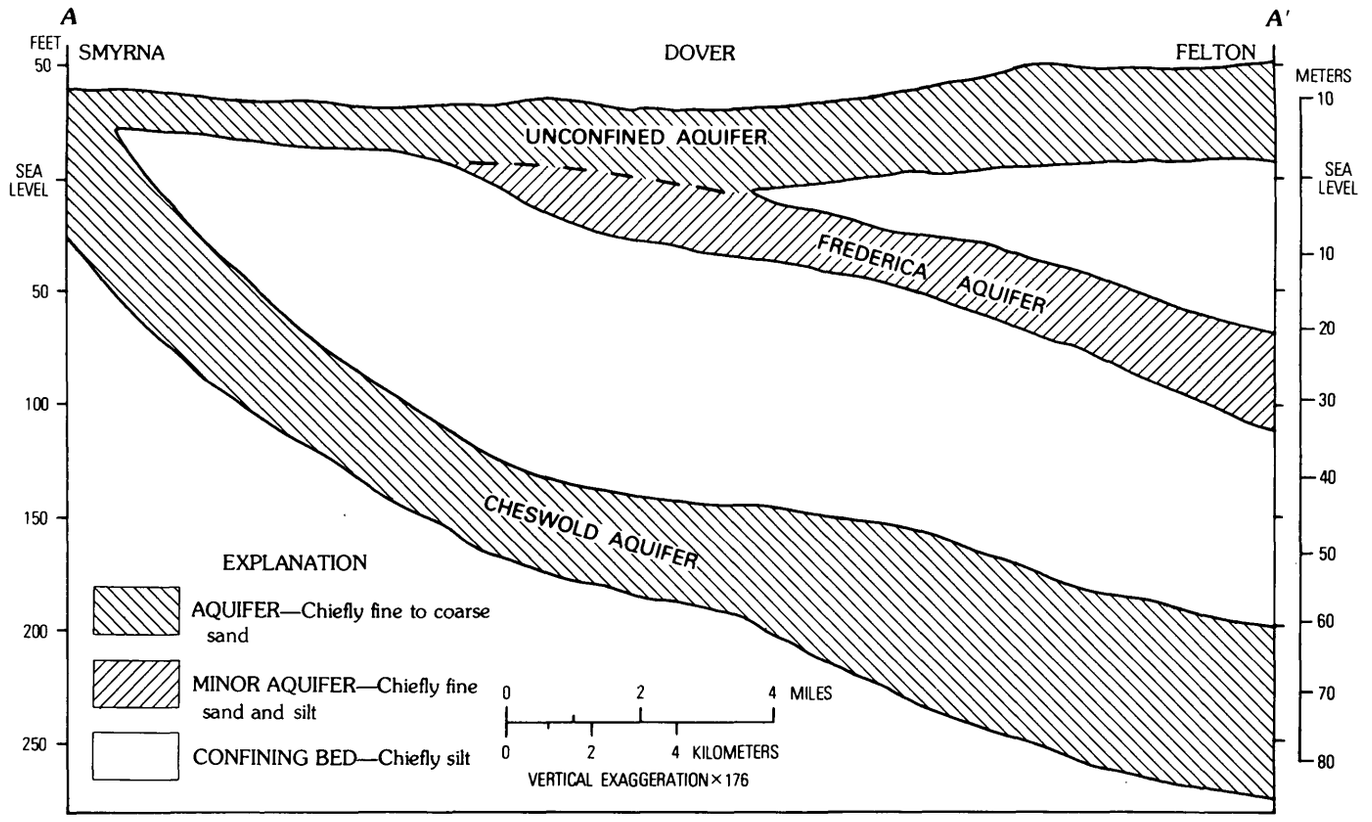

FIGURE 1.—Generalized geologic section from Smyrna, Del., to Felton, Del., showing relation of Cheswold and unconfined aquifers. Line of section shown in figure 2.

near Dover to more than 1900 m^2/d in parts of southern Delaware.

The small Coastal Plain streams derive about three-quarters of their flow from ground-water discharge. During base-flow conditions, the streams are virtually shallow drains from the unconfined aquifer. The unconfined aquifer is presently pumped only by a few widely spaced irrigation and public-supply wells and many domestic wells of low yield. Withdrawals are small, and no long-term decline in the water table has been observed. The unconfined aquifer is not used for public water supply at Dover because of its thinness and because the quality of its water is inferior to that of the Cheswold and the deeper Piney Point (Eocene) aquifers.

The hydraulics of the unconfined aquifer system, at least under natural (prepumping) conditions, involved recharge by precipitation, lateral water movement through the aquifer, and discharge to streams or to the sea. It discharged extremely small amounts of water to deeper aquifers by natural leakage in inland areas and was, in turn, recharged by an upward flow from deeper aquifers coastward. Within the unconfined aquifer this natural hydraulic equilibrium has been altered to the extent that light and primarily seasonal pumping now accounts for a small part of regional discharge, and downward leakage to the Cheswold is now appreciable. The fact that water levels are stable in the unconfined aquifer indicates that a new hydraulic equilibrium has been attained.

A digital-model analysis of the unconfined aquifer has been completed by the authors. Part of this analysis involved simulating the actual steady-state condition of the hydrologic system but ignoring both pumpage from the unconfined aquifer and leakage to or from deeper aquifers. In other words, only uniform recharge to the unconfined aquifer from precipitation and discharge from the aquifer to streams were considered. Winter conditions were simulated, so that ground-water evapotranspiration (relatively small) could be ignored.

RECHARGE TO THE CHESWOLD AQUIFER

Before pumping began, hydraulic equilibrium prevailed in the Cheswold aquifer system. The Cheswold was probably recharged in its subcrop area and to some extent by downward leakage from the unconfined aquifer through the semiconfining bed in inland areas.

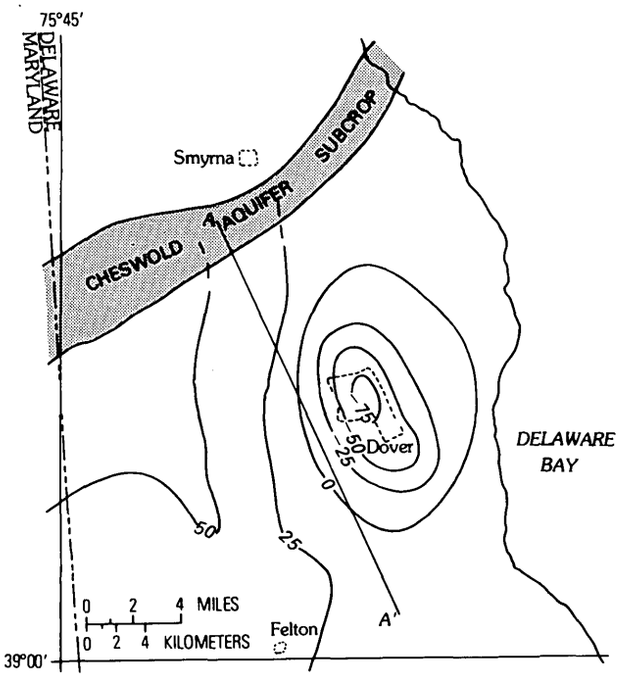

FIGURE 2.—Potentiometric surface of the Cheswold aquifer in the Dover, Del., area, August–September 1975.

It discharged coastward by upward leakage through the semiconfining bed to the unconfined aquifer, thence to streams or the Delaware Bay. It probably also received a very small amount of water by upward movement from deeper aquifers near the Bay and discharged a very small amount of water by downward leakage to deeper aquifers inland.

Initially, water pumped from wells in the Cheswold was withdrawn from aquifer storage. Such storage withdrawal over time decreases natural discharge and (or) increases natural recharge, until a new hydraulic equilibrium is reached. That such a new equilibrium under pumping conditions was reached in the Cheswold is indicated by the fact that water levels in the Cheswold have remained virtually unchanged since 1963. Adjustment of an aquifer to a new equilibrium under pumping is discussed by Theis (1940).

Changes caused by pumping probably include: (1) increased recharge from areas where recharge was formerly negligible and decreased natural discharge in the subcrop area; (2) increased downward or decreased upward leakage through the overlying confining bed; (3) changed flow to or from deeper aquifers through the underlying confining bed; and (4) any combination of the above. Changes in leakage through the overlying confining bed would, in turn, be balanced by increased recharge or decreased natural discharge in the overlying unconfined aquifer; any change in flow between the Cheswold and deeper aquifers would similarly increase recharge or reduce natural discharge somewhere in the system.

The Cheswold potentiometric surface (fig. 2) varies markedly away from the pumping center at Dover. Three factors might contribute to the variation. First, flow within the aquifer could be distributed irregularly by irregular vertical leakage. Second, pumping drawdown is superposed on an original coastward gradient; the resultant gradient is, thus, steeper inland from pumping centers and gentler coastward. Third, variations in transmissivity of the Cheswold affect gradient. The potentiometric surface alone does not indicate the relative importance of the three factors. It is, therefore, impossible to identify areas of significant leakage with only the potentiometric-surface map as a guide.

A possible approach to identifying areas of intense vertical leakage might be to consider the head differences between the aquifer and the source bed supplying the leakage—in this case, the overlying unconfined aquifer. Figure 3 shows a map of this head difference. The contour line indicating zero head difference defines the total area within which measurable downward leakage can occur, approximately 360 km^2. Determination of the distribution of downward leakage within this area is not possible, however, without detailed information on the thickness and vertical hydraulic conductivity of the semiconfining bed. Such information, particularly that pertaining to hydraulic conductivity, is lacking. Note, moreover, that the zero head-difference contour line encloses only the region of present downward flow from the unconfined aquifer to the Cheswold. Areas in which upward flow has been diminished are not identified, nor, for that matter, are those in which downward flow has been increased in response to pumping. This more complete breakdown of recharge into its components would require data on original head differences between the unconfined aquifer and the Cheswold, and these data are lacking.

An indirect method of identifying areas of intense vertical leakage, would concentrate on the source bed—the overlying unconfined aquifer—rather than on the aquifer receiving the recharge or on the semiconfining unit separating the two. If a careful hydraulic analysis of the unconfined aquifer indicated water losses from

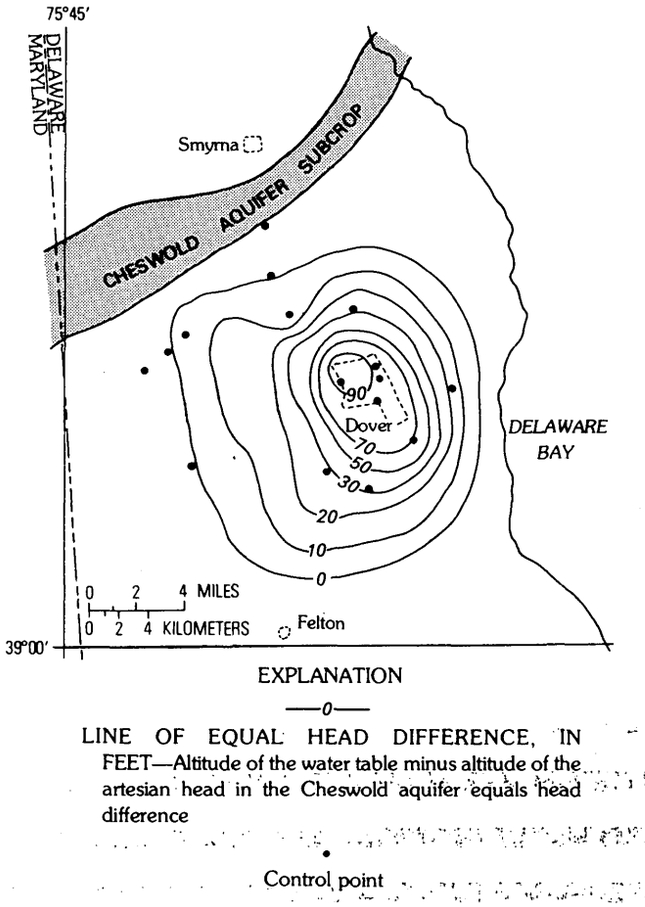

FIGURE 3.—Head difference between the unconfined aquifer and the Cheswold aquifer in the Dover, Del., area, August–September 1975.

the aquifer in a given area and if the losses cannot be accounted for otherwise, it is only reasonable to assume leakage to the underlying artesian aquifer. This is basically the method used in this study. The source aquifer was analyzed hydraulically by a digital model of the aquifer, together with detailed information on base flow of streams. No prepumping information on base flow is available, so it was not possible to identify areas of recharge simply by locating streams whose base flow had decreased with time during pumping. However, reliable information on present base flows is available, and, by comparing this information with model results, areas of intense leakage from the unconfined aquifer were identified.

Before pumping began, the unconfined aquifer was recharged almost wholly by precipitation and was discharged principally by seepage to streams, Delaware Bay, and the ocean and to a small extent by downward leakage to deeper aquifers. Under present conditions, a new equilibrium prevails, in which pumping from aquifers deeper than the Cheswold has increased downward leakage from the unconfined aquifer to the Cheswold. In addition, natural discharge from the unconfined aquifer may have been increased; natural discharge from the unconfined aquifer to streams has been reduced; and a very small discharge caused by pumping directly from the unconfined aquifer has been imposed.

The digital model of the unconfined aquifer was used to simulate present-day hydraulic equilibrium in an approximate sense, in that only recharge by precipitation and discharge to streams, to Delaware Bay, and to the ocean were represented. Leakage to and from deeper aquifers and pumpage from the unconfined aquifer were not simulated because they were negligible in comparison. The indirect method of identifying areas of intense vertical leakage from the unconfined aquifer involves a comparison of base flow of streams, as indicated by the model, with base flow as measured in the field. Neglecting the small pumpage from the unconfined aquifer, differences between model base flow and measured base flow should arise wherever downward leakage from the unconfined aquifer is significant. Where downward leakage is significant, model base flow should be higher than measured base flow.

The digital model of the unconfined aquifer is a two-dimensional representation of the flow system, utilizing a finite-difference approximation to the equations of ground-water flow. It employs a computer program developed by Pinder (1970) and later revised by Trescott (1973). The area modeled was approximately 1735 km² in central and southeastern Delaware. A total of 670 nodal points were utilized in the simulation, and the model was calibrated by steady-state analysis. Areal recharge was simulated uniformly, based on annual estimated infiltration of precipitation (356 mm). Points along streams and the coast were held at constant head, and hydraulic conductivity was adjusted throughout the model until observed water-level contours were duplicated. In some areas where conductivity values had been obtained by analysis of lengthy aquifer tests, no changes in input values of conductivity were required. In areas of no available aquifer-test data and where geologic and well data were scanty, however, conductivity values had to be changed as much as 100 percent. After calibration, approximately 70 percent of the computed heads differed from the measured water-table values by less than 0.8 m and so fell within the 1.5-m average annual fluctuation of the water table.

After calibration, the model was used to compute seepage into stream reaches throughout the study area. These computed seepage values were then summed along each stream to obtain computed base flow, which, in turn, was compared with field estimates of average winter base flow, wherever field data were available. Results of this comparison in the part of the modeled

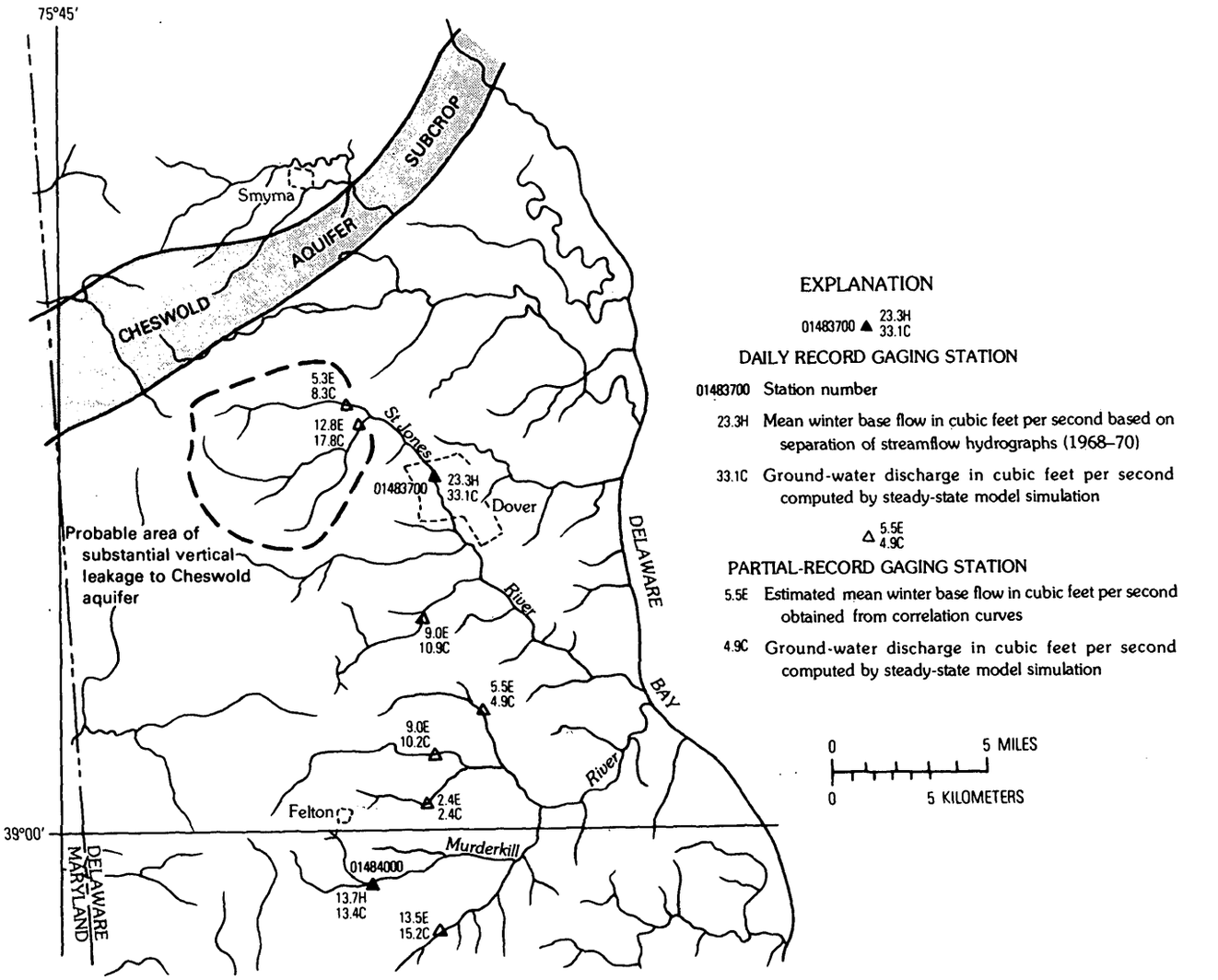

FIGURE 4.—Comparison of mean winter base flow at stream-gaging stations in central Delaware with ground-water discharge computed by steady-state model simulation. To convert ft^3/s to m^3/s, multiply by 0.028.

area near Dover are shown in figure 4. In interpreting this figure, keep in mind that results at each station constitute an integrated comparison of the modeled and the actual aquifer over the drainage area upstream from that station. Agreement between the computed and field base flows is excellent except in the area northwest of Dover. Note that the winter base flow of the St. Jones River at Dover (Station No. 01483700 in fig. 4) is about 0.3 m^3/s (10 ft^3/s) less than the model-computed value. The 0.3 m^3/s (10 ft^3/s or 6.5 Mgal/d) difference is equivalent to pumpage from the Cheswold aquifer at Dover and suggests that virtually all downward leakage from the unconfined aquifer to Cheswold aquifer is concentrated within the St. Jones basin (83 km^2). Furthermore, base-flow measurements on the two tributaries of the St. Jones River shown in figure 4 suggest that much of the leakage is concentrated within these two tributary basins (which together drain about 65 km^2).

Both the base flow estimates from streamflow and the computer-simulated values from the aquifer model contain errors of estimation. It is not possible to compute the accuracy of the base-flow values, however, the methods used to obtain these values are discussed briefly.

The estimated winter base flow for the St. Jones River at Dover and other continuous-record gaging stations were obtained by separation of the streamflow hydrographs into the overland-runoff and base-flow components using a method described by Riggs (1963). This method is based on the preparation of a master base-flow recession curve which is overlain on the hydrograph to make the separation. Preparation of the

base-flow recession curves and the assumptions upon which they are based are discussed in a separate report (Johnston, 1976 p. 7–12). The winter base-flow values shown in figure 4 are average values for December through February for the 3-year period 1968–70. This period was selected for determining average groundwater discharge because precipitation was near normal and streamflow was about average during the 3 years.

The winter base-flow estimates of the tributary streams are based on correlation curves relating base-flow measurements on the tributaries to concurrent flow at the St. Jones River gage. (See Cushing, Kantrowitz, and Taylor, 1973, p. 26–29 for a discussion of this method of transferring flows from continuous-record gaging stations to short-term record sites on the Delmarva Peninsula.) The errors involved in this method include the error in estimating the 0.66 m^3/s (23.3 ft^3/s) for the St. Jones River as well as errors in preparing the correlation curves. Although estimates of winter base flow obtained by correlation methods are less reliable than data from continuous gaging stations, figure 4 shows that agreement is generally good between the computer-generated values and base-flow estimates—except for the St. Jones River and its tributaries.

Other possible sources of the Dover pumpage, such as decreased upward discharge from the Cheswold to the unconfined aquifer in areas outside the zero contour of figure 3, are apparently negligible in comparison to downward leakage within the St. Jones basin. More generally, the fact that computed and field base flows agree closely elsewhere suggests that, except for downward leakage to the Cheswold northwest of Dover, the only significant terms in the water balance of the unconfined aquifer, at least in the winter, are recharge by precipitation and discharge to surface-water bodies. Pumpage from the unconfined aquifer, natural downward leakage to deeper aquifers, and upward flow from deeper aquifers all seem to be so small by comparison as to cause no measurable difference between model determinations, which neglect these terms, and field measurements.

Differences between computed and field base-flow values northwest of Dover might, of course, be caused by errors in estimating recharge. No climatologic or geologic reason is apparent, however, for recharge to be appreciably different northwest of Dover than elsewhere in the study area. Moreover, if recharge rates were lower, overland runoff rates would have to be higher to satisfy the water balance. Such is not the case in the St. Jones basin, which is deficient in total streamflow as well as base flow. During the 1968–70 period used for model simulation, average runoff from the St. Jones basin was (0.010 m^3/s)/km^2 or (0.99 ft^3/s)/mi^2 compared with an average of (0.014 m^3/s)km^2 or (1.25 ft^3/s)/mi^2 for five nearby basins.

CONCLUSIONS

In summary, major leakage to the heavily pumped Cheswold aquifer is concentrated within the 83 km^2 area of the St. Jones River basin northwest of Dover. Actually, nearly all the leakage is probably concentrated in two tributary basins, Fork Branch and Maidstone Branch, which together drain about 65 km^2. This area of significant vertical leakage is about midway between Dover and the Cheswold subcrop, as shown in figure 4. The regional cone of depression, produced by more than 80 years of pumping from the Cheswold, has developed a downward hydraulic gradient from the water table in an area of about 363 km^2 (fig. 3). The comparison of computer-generated ground-water-discharge values with field base-flow values, however, suggests that leakage is significant only in about 18 percent of that area. No significant recharge to the Cheswold is apparently induced from the subcrop area.

REFERENCES CITED

Cushing, E. M., Kantrowitz, I. H., and Taylor, K. R., 1973, Water Resources of the Delmarva Peninsula: U.S. Geol. Survey Prof. Paper 822, 58 p.

Johnston, R. H., 1973, Hydrology of the Columbia (Pleistocene) deposits of Delaware: Delaware Geol. Survey Bull. 14, 78 p.

——— 1976, Relation of ground water to surface water in four small basins of the Delaware Coastal Plain: Delaware Geol. Survey Rept. of Inv. No. 24, 55 p.

Pinder, G. F., 1970, A digital model for aquifer evaluation: U.S. Geol. Survey Tech. Water-Resources Inv., 7–C1, 18 p.

Riggs, H. C., 1963, The base-flow recession curve as an indicator of ground water: Internat. Assoc. Sci. Hydrology Pub. 52, p. 314–323.

Sundstrom, R. W., and Pickett, T. E., 1968, The availability of ground water in Kent County, Delaware, with special reference to the Dover area: Univ. of Delaware Water Resources Center rept., 123 p.

Theis, C. V., 1940, The source of water derived from wells: Civil Eng., v. 10, no. 5, p. 277–280.

Trescott, P. C., 1973, Iterative digital model for aquifer evaluation: U.S. Geol. Survey open-file rept., 63 p.

Jour. Research U.S. Geol. Survey
Vol. 5, No. 4, July–Aug. 1977, p. 497–508

A GALERKIN, FINITE-ELEMENT ANALYSIS OF STEADY-STATE FLOW AND HEAT TRANSPORT IN THE SHALLOW HYDROTHERMAL SYSTEM IN THE EAST MESA AREA, IMPERIAL VALLEY, CALIFORNIA

By R. E. MILLER, Laguna Niguel, Calif.

Abstract.—A steady-state simulation model was applied to the shallow hydrothermal system in the East Mesa area of Imperial Valley, Calif. The steady-state equations of flow and heat transport were solved by use of a Galerkin, finite-element method. A solution was obtained by iterating between the temperature and pressure equations, using updated densities and viscosities. Temperature and pressure were obtained for each node, and corresponding head values were calculated. The simulated temperature and pressure patterns correlated well with the observed patterns. Additional data, mainly from test drilling, would be required for construction of a similar model of the deep hydrothermal system.

The Imperial Valley is a major focal point for geothermal development in southern California. The geothermal resources of the valley are contained in an area of about 4400 km² (California Department of Water Resources, 1974). Plans for geothermal development call for pressure maintenance in the geothermal reservoirs by injection back into the system of return water from all geothermal power or desalting plants. The operation of an efficient withdrawal and injection system requires knowledge of the interrelationship of the aquifers in the hydrothermal system and of the methods of predicting the effects of general development on reservoir pressures.

A common approach to this problem involves the use of numerical models. Mercer, Pinder, and Donaldson (1975) developed a single-phase simulation model of the hot-water hydrothermal field at Wairakei, New Zealand, and the results of that investigation indicate that the response of hot-water hydrothermal systems to exploitation can be simulated by using a mathematical-reservoir model based on a Galerkin, finite-element approach. The objective of this study is to apply the same modeling technique to the Imperial Valley hydrothermal system.

The initial phase of this study, begun in July 1974, was a review of the hydrologic and heat-flow data available for Imperial Valley. The principal sources of hydrologic data were reports by Hutchins (1915), Brown (1923), Bradshaw and Donnan (1952), and Tischler (1964) and files of the U.S. Geological Survey. Most of these data have subsequently been summarized or tabulated in reports by Loeltz, Ireland, Robison, and Olmsted 1975) and Hardt and French (1976). The principal sources of heat-flow data are reports by Combs (1971, 1972), U.S. Bureau of Reclamation (1971a, 1971b, 1973, 1974), and Swanberg (1974).

The limited areal distribution of available data indicated that it would be feasible to model only the southeastern part of Imperial Valley (fig. 1). The focal point of the model would therefore be the East Mesa KGRA (Known Geothermal Resource Area). Further limitations of data with depth restricted the modeling effort to include only the shallow aquifer and steady-state conditions. The finite-element configuration used in this study and the boundaries of the East Mesa KGRA are shown in figure 2.

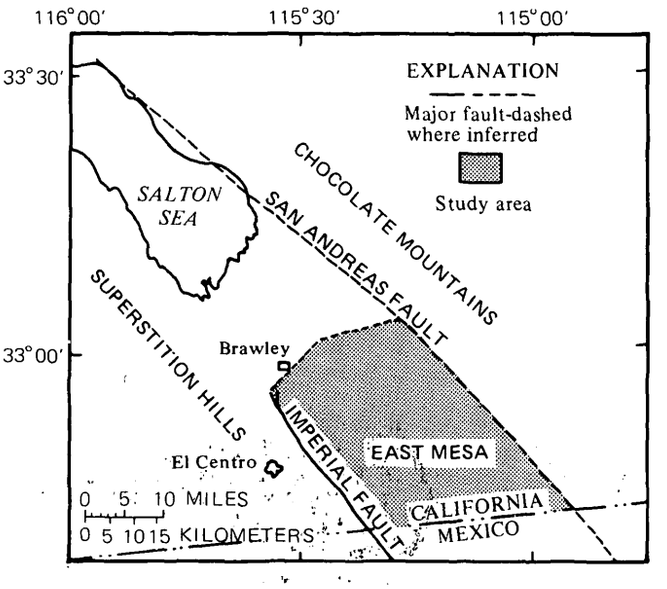

FIGURE 1.—Imperial Valley, Calif., showing location of study area and major faults.

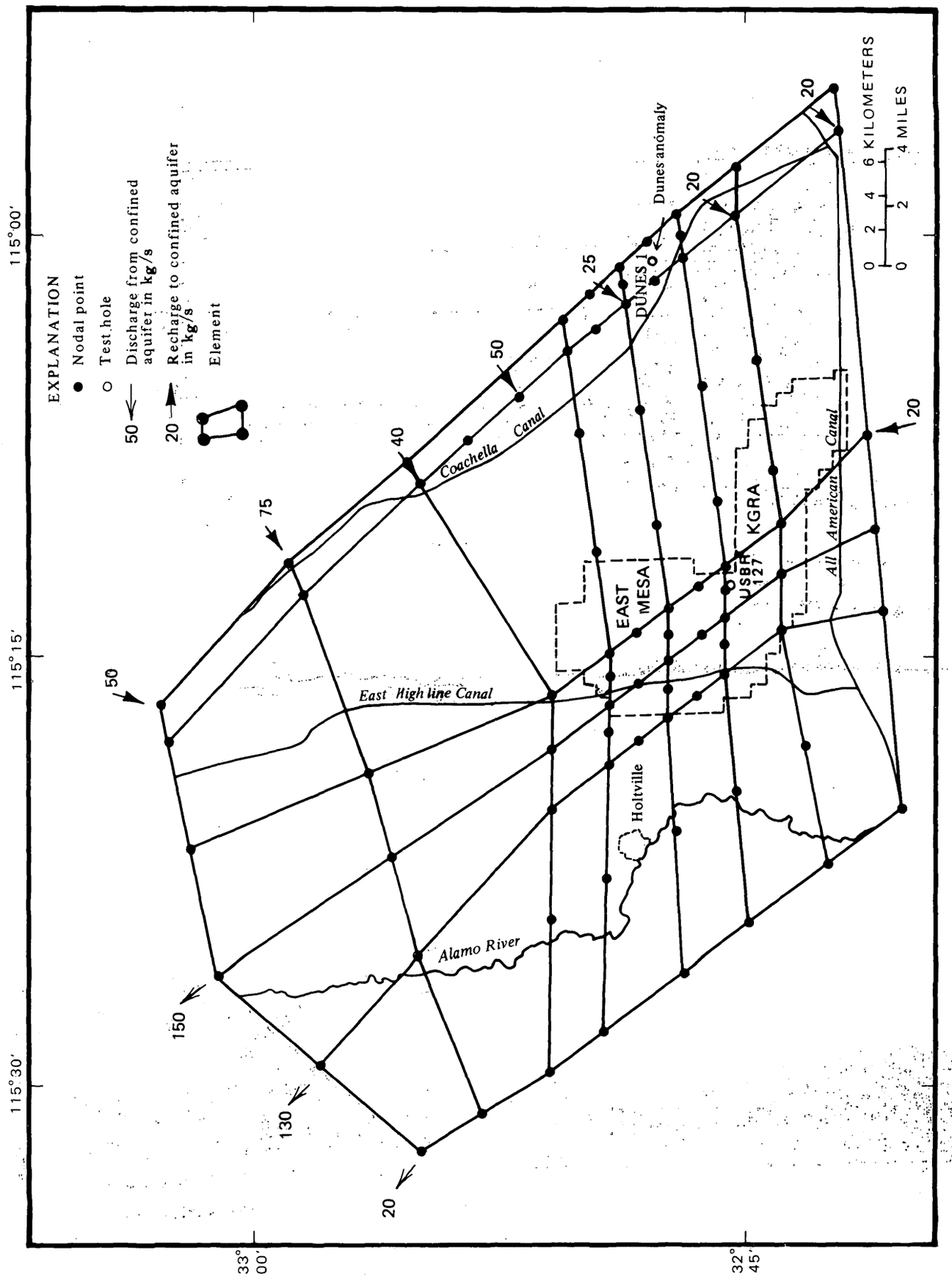

FIGURE 2.—East Mesa model area showing selected geographic features, configuration of nodal points and elements, distribution of recharge and discharge nodes, and location of East Mesa KGRA and selected test holes. U.S. Bureau of Reclamation; KGRA, Known Geothermal Resource Area.

EAST MESA MODEL AREA

The study area covers about 1490 km² in southeastern Imperial Valley (fig. 1). It encompasses most of East Mesa and part of the central valley and includes the East Mesa KGRA which has an area of 156 km².

Structure

East Mesa, on the east flank of the Salton trough, is a sloping surface that merges gradually with central Imperial Valley. The Salton trough was formed by rifting of the crust and sinking of the crustal blocks and consequent filling of the depression by riverborne sediments of the Colorado River and its ancestral streams. The deltaic sediments in the East Mesa KGRA are about 3.7 km thick, as indicated by seismic data (Biehler and others, 1964).

The Imperial fault, which forms the western boundary of the model area, was mapped from surface breaks that occurred as a result of an earthquake in 1940 (Ulrich, 1941). The fault at the eastern boundary of the model area is an approximate extension of the San Andreas fault which has been inferred on the basis of alinement of anomalously low gravity measurements that extend from the Salton Sea southeastward to the Colorado River (Biehler, 1964). This interpretation of gravity data is supported by seismic-refraction profiles (Kovach and others, 1962) and aeromagnetic profiles (Griscom and Muffller, 1971). One or more smaller faults are probably present in the East Mesa KGRA. Such faults have been postulated by Rex (1970), Babcock (1971), and Combs and Hadley (1973).

Geohydrology

East Mesa was formed by fluvial processes locally modified by lacustrine or marine processes. It is extensively mantled by irregular sheets of windblown sand. The Mesa merges gradually with the main valley which consists primarily of cultivated agricultural land and is entirely within the shorelines of prehistoric Lake Cahuilla. The soils developed on the lakebed contain a large proportion of clay and silt of low permeability, in contrast to the sandy soils of East Mesa (Dutcher and others, 1972).

The importation of Colorado River water has transformed the main valley area into one of the most productive agricultural areas in the world. Drainage ditches which empty into the Salton Sea by way of the New and Alamo Rivers have been installed to maintain the salt balance in the valley. The system of drainage ditches is more than 2245 km long and is fed by a network of over 27 400 km of tile drains buried to depths of 1.8 to 3.7 m.

Water-table aquifer

Underlying East Mesa and the drainage system in the main valley is a water-table aquifer that ranges from 5 to 120 m in thickness. Over most of the East Mesa area, which is unirrigated, the depth to water ranges from about 9 to 14 m. The temperature of the water in this aquifer averages about 29° to 30°C in the East Mesa area; sparse data indicate an average temperature of 1° or 2°C lower in the adjacent irrigated main valley area. These temperatures exceed the mean annual temperature at the land surface, which is probably not greater than 25°C. The cause of this difference is not known; it may be leakage of warm water through the confining bed beneath the water-table aquifer.

Confining zone

A poorly defined zone of low-permeability sediments, approximately 10 to 100 m thick, separates the water-table aquifer from an underlying confined-aquifer system. The sediments in this zone consist of alternating layers of clay, sandy clay, and silt with sand stringers. The confining zone is thicker in the northwestern part of the model area and thinner and less well defined in the southeastern part. In the East Mesa KGRA the confining zone averages about 60 m in thickness, and, as modeled, its intrinsic permeability ranges from 1×10^{-15} m² to 1×10^{-16} m².

Confined aquifer

The shallow aquifer underlying the confining zone (fig. 3) is about 0 to 350 m thick. It consists of layers of slightly to moderately permeable sand and sandy clay interspersed with silt and clay stringers. A Schlumberger Saraband log (a resistivity log that has been interpreted by computer) for a test hole in the East Mesa KGRA (USBR 127, fig. 2) suggests an average intrinsic permeability on the order of 1×10^{-12} m² for this aquifer. Mathias (1974, p. 11) compared permeability values inferred from Saraband logs with laboratory values determined from cores for nearby wells in the East Mesa and concluded that the Saraband and laboratory values are comparable. Data from water wells suggest that the transmissivity of the confined aquifer is higher in the East Mesa area than in the main valley area to the west (Loeltz and others, 1975).

Wells tapping this aquifer are used primarily for domestic and stock purposes. The water in the aquifer

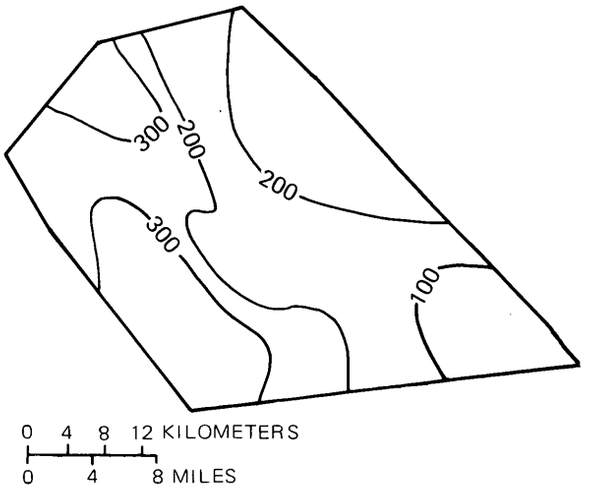

FIGURE 3.—Thickness of shallow confined aquifer of the study area; contour interval 100 meters.

is under sufficient head to raise the water level above land surface in most of the wells, which are generally 100 to 400 m deep.

The dissolved-solids content of the water commonly ranges from 700 to 5000 mg/L. Only the better quality water is used for domestic and stock purposes. Near Holtville a few of the wells that yield hot water (37°–43°C) have been used to heat homes.

Geothermal reservoir

The geothermal reservoir, which underlies the confined aquifer in the East Mesa KGRA, has abnormally high subsurface temperatures and can be used for comparison and evaluation of geothermal-exploration techniques. Five deep geothermal wells have been completed at the U.S. Bureau of Reclamation site at the East Mesa anomaly. The geothermal reservoir, as described by Swanberg (1975), is confined beneath a cap that is about 60 percent clay. The stratigraphic interval at a depth of about 600–700 m is a transition zone between the clay cap and the underlying geothermal reservoir. The reservoir itself is at least 1400 m thick, and its presence is shown by a high heat flow of more than 5 hfu (1 heat-flow unit=41.84 milliwatts per square meter) over an area of 40 km^2. The sediments within the reservoir are loosely consolidated continental deposits that have an average permeability of 1×10^{-13} m^2 and a mean porosity of about 20 percent. An active fault has been determined to be the conduit for the ascending geothermal fluids which are of a sodium chloride type with a dissolved-solids content of 2500 mg/L or less (Swanberg, 1975). The base temperature of the reservoir ranges approximately from 170° to 182°C.

As stated earlier, because of insufficient data, this reservoir is not included in the model described in this report.

Heat Flow

In the East Mesa area approximately 40 boreholes have been temperature logged, and cores were recovered from three holes for laboratory determination of thermal conductivity (Combs, 1972). The thermal conductivity measurements on the unconsolidated cores were made using a transient needle-probe technique (Von Herzen and Maxwell, 1959). An additional 24 test holes were drilled for heat-flow measurements by the U.S. Bureau of Reclamation (1974). Heat-flow contours based on measurements from the two programs are shown in figure 4.

A small area of high heat flow a short distance inside the southeastern margin of the model area, along the San Andreas fault, is known as the Dunes anomaly. A test hole (Dunes 1) was drilled to a depth of 612 m in the center of this area by the California Department of Water Resources (Coplen and others, 1973). Oxygen and hydrogen stable-isotope studies of water samples from the test hole indicate that the geothermal fluid is probably derived from a source deeper than 400 m (Elders and others, 1974).

DESCRIPTION OF NUMERICAL MODEL

A detailed development of the governing equations, assumptions, and application of the model can be found in Mercer, Pinder, and Donaldson (1975) and Mercer and Pinder (1975). Although their development includes transient and steady-state flow conditions, only the steady-state condition is considered in this analysis, and the equations are modified appropriately. A brief summary of the major assumptions and final equations is presented. Meter-kilogram-second units are used throughout the computer program; however, where possible, SI metric units are used in this report. The major symbols used are listed in table 1.

Assumptions

1. Density is assumed to be a function of temperature and pressure, according to J. W. Mercer (written commun., 1975), as follows:

$$\rho = 2.07473\times10^{3} + 5.56172\times10^{-9}\,p - 4.26895\times10^{5}\frac{1}{\gamma} - 2.35494\times10^{-3}\,\gamma^{2} + 4.95912\times10^{7}\frac{1}{\gamma^{2}} \quad (1)$$

where ρ is in kilograms per cubic meter, p is in newtons per square meter, and γ is in degrees absolute ($\gamma = T + 273.15$). Equation 1 was ob-

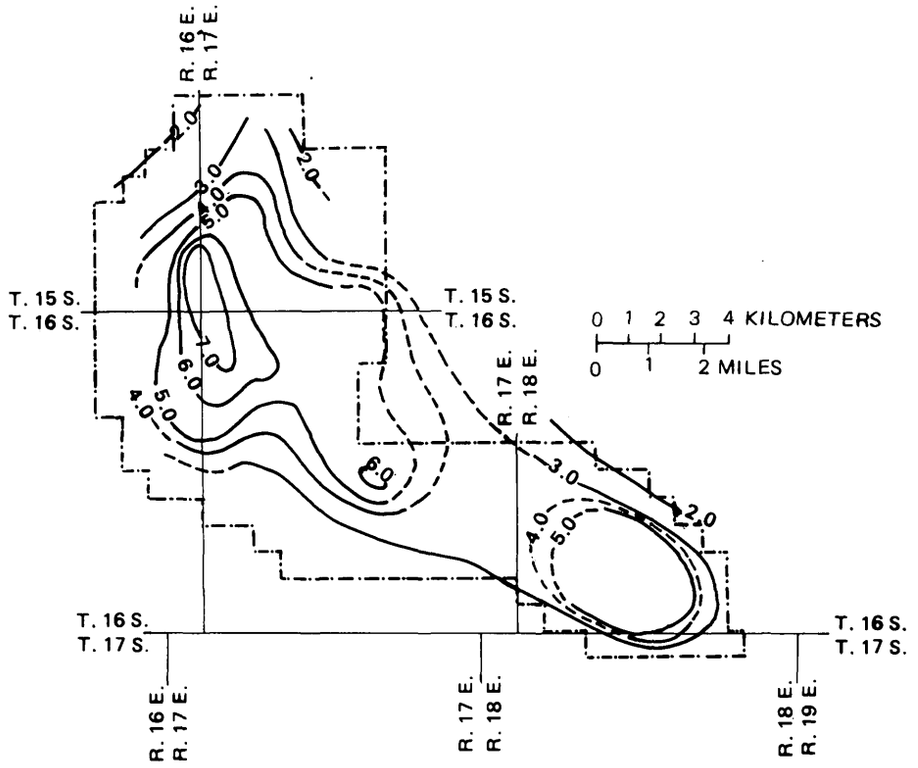

FIGURE 4.—Heat-flow anomaly at East Mesa KGRA in heat-flow units (1 hfu=41.84 mW/m²) ; contour interval, 1 hfu (U.S. Bureau of Reclamation, 1974).

TABLE 1.—*Major symbols*

[Dimension is given in brackets at end of definition of symbol: *M*, mass ; *L*, length ; *t*, time ; *T*, thermodynamic temperature]

b	saturated thickness of the aquifer $[L]$
b'	saturated thickness of the confining bed $[L]$
c_v	heat capacity at constant volume per unit mass $[L^2t^{-2}T^{-1}]$
g	gravitational acceleration $[Lt^{-2}]$
K^l_{ij}	hydrodynamic thermal dispersion tensor (K_{zz}, vertical component) $[MLt^{-3}T^{-1}]$
K^d	molecular thermal diffusion coefficient $[MLt^{-3}T^{-1}]$
K^s_{ij}	thermal diffusion tensor of the solid phase (K^s_{zz}, vertical component) $[MLt^{-3}T^{-1}]$
K^l	mechanical thermal dispersion coefficients $[MLt^{-3}T^{-1}]$
k_{ij}	local intrinsic permeability tensor (k_{zz}, vertical component) $[L^2]$
k'	permeability of the confining bed $[L^2]$
p	pressure $[ML^{-1}t^{-2}]$
p′	pressure distribution above the confining bed $[ML^{-1}t^{-2}]$
Q'	areally distributed heat source $[Mt^{-3}]$
q'	vertical mass flow term $[Lt^{-1}]$
T	temperature $[T]$
T'	temperature distribution at the top (or bottom) of the aquifer (in practice the temperature distribution above the confining bed is used) $[T]$
v_i	velocity (v_z, vertical component) $[Lt^{-1}]$
γ	mass density on a bulk volume basis where $\gamma=\rho\phi$ $[ML^{-3}]$
μ	viscosity $[ML^{-1}t^{-1}]$
ρ	average density $[ML^{-3}]$
ϕ	porosity (dimensionless)

Subscripts and superscripts

l	refers to liquid phase
s	refers to solid phase
z	refers to the z-direction (vertical)
′	indicates properties associated with confining beds
0	refers to a reference or initial quantity
ij	refer to rectangular coordinate system

tained using a least-squares regression and data from Meyer and others (1968). In comptuing equation 1, the temperatures ranged from 0° to 350°C, and the pressure ranged from 1.0×10^5 to 1.75×10^7 N/m².

2. Viscosity is assumed to be a function of temperature alone, according to Meyer and others (1968), as follows:

$$\mu=10^{-7}\{241.4\times10^{[247.8/(T+133.15)]}\} \qquad (2)$$

where T is in degrees Celsius and μ is in kilograms per meter per second (kg m^{-1} s^{-1}). Equation 2 is valid for liquid water along the saturation line from 0° to 300°C.

3. Heat transport is assumed to occur by convective flow and dispersion in water and by conduction in the solid matrix.
4. Heat capacity, c_v, and solid density, ρ_s, are treated as constants. The variation of these parameters with temperature is relatively small so that this assumption does not significantly reduce the accuracy of the model.
5. Flow within the confined aquifer is essentially horizontal, so that only two horizontal dimensions need be considered.
6. A chemically inert, single-phase (hot-water) system is assumed and is justified as a first approximation because of the relatively low dissolved chemical load.
7. Steady-state conditions are assumed.

Equations

Based on these assumptions, the liquid-flow equation and heat-transport equation (modified from Mercer and others, 1975) are as follows:

$$\frac{\partial}{\partial x_i} b\left(\frac{\rho k_{ii}}{\mu}\frac{\partial p}{\partial x_i}\right) = -\frac{\rho k_{zz}}{\mu}\left(\frac{\partial p}{\partial z}+\rho g\right)\Bigg|_{z_2} + \frac{\rho k_{zz}}{\mu}\left(\frac{\partial p}{\partial z}+\rho g\right)\Bigg|_{z_1} \tag{3}$$

and

$$b\gamma c_v v_i \frac{\partial T}{\partial x_i} = \frac{\partial}{\partial x_i} b[\phi K^l{}_{ij} + (1-\phi)K^s{}_{ij}]\frac{\partial T}{\partial x_j} + [\phi K^l{}_{zz} + (1-\phi)K^s{}_{zz}]\frac{\partial T}{\partial z}\Bigg|_{z_2} - [\phi K^l{}_{zz} + (1-\phi)K^s{}_{zz}]\frac{\partial T}{\partial z}\Bigg|_{z_1} + \gamma c_v v_z (T-T')\Big|_{z_2} - \gamma c_v v_z (T-T')\Big|_{z_1} \tag{4}$$

where the equation parameters have been vertically averaged between the top of the aquifer, z_2, and the bottom, z_1, and $b=b(x_i)$ is the saturated thickness of the aquifer. The vertical bars indicate terms which are evaluated at either the top or the base of the aquifer. In obtaining these terms it was assumed that the mass and heat flow moving through both the top and bottom of the aquifer are vertical and colinear with the z-axis. These terms depend on observed field conditions and will be evaluated later.

The system of equations 3 and 4 cannot, in general, be solved analytically, and a numerical approach is required. The numerical scheme used in this analysis is a combination of the finite-element concept and the Galerkin method of weighted residuals. Details of this approach are given in Mercer and Pinder (1975). General references on the application of the Galerkin, finite-element method to field equations include Zienkiewicz and Parekh (1970) and Pinder and Frind (1972).

Vertical Flow

Equations 3 and 4 were obtained by integrating the steady-state, three-dimensional flow equation and the heat-transport equation over the aquifer thickness. The resulting two-dimensional areal equations include terms which account for vertical flows of mass and heat at the top and base of the aquifer. (These are sometimes referred to as leakage terms.)

The conceptual model as related to the East Mesa area consists of a layered system as shown in figure 5. Mass (fluid) and heat flow vertically through the confining zone. The direction of flow is determined by the potential and thermal gradients across the confining beds and may vary spatially. To determine the direction and magnitude of these flows, the pressure and temperature distributions at the top of the confining zone are required. It is assumed that the water-table aquifer is in equilibrium with the confined aquifer and that the pressures at the top of the confining zone can be calculated by using the thickness of the water-table aquifer. The temperature distribution for the top of the confining zone was obtained from temperature logs.

Using these assumptions, the vertical-flow terms in equations 3 and 4 for the top of the aquifer may be evaluated. For the flow equation,

$$\frac{\rho k_{zz}}{\mu}\left(\frac{\partial \rho}{\partial z}+\rho g\right)\Bigg|_{z_2} = \rho q' \tag{5}$$

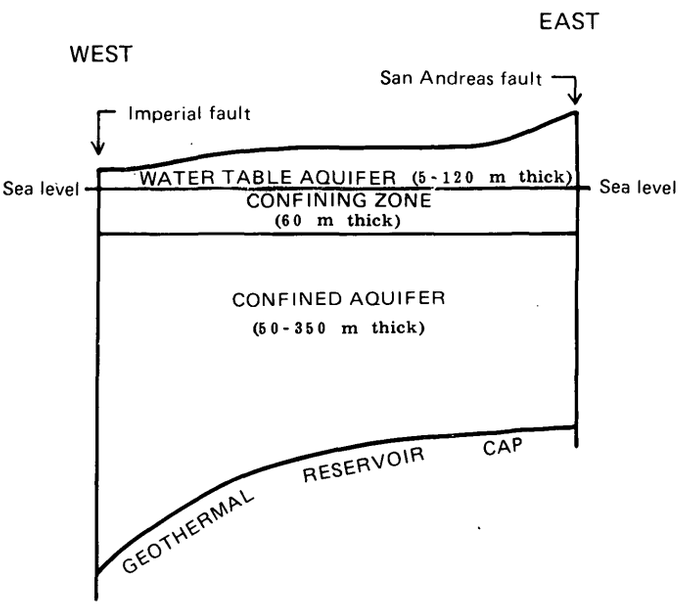

FIGURE 5.—Conceptual model of shallow hydrothermal system, southeastern Imperial Valley.

where q' represents vertical liquid flow through the confining zone. For steady state, q' becomes

$$q' = \frac{k'}{\mu b'}(p' - p + \rho g b') \tag{6}$$

where k' is the permeability and b' is the thickness of the confining zone, p' is the pressure distribution at the top of the confining zone, and p is the pressure in the confined aquifer.

For the heat-transport equation 4 there are two vertical-flow terms which must be evaluated at the top of the aquifer, one for conduction and one for convection. These terms are assumed to be of the following form:

$$[\phi K^{l}_{zz} + (1-\phi)K^{s}_{zz}]\frac{\partial T}{\partial z}\bigg|_{z_2} = [\phi' K'^{l}_{zz} + (1-\phi')K'^{s}_{zz}]\frac{T'-T}{b'+b/2} \tag{7}$$

and

$$\gamma c_v v_z (T - T')\Big|_{z_2} = \rho q' c_v (T - T') \tag{8}$$

where K'^{l} and K'^{s} are the vertical components of the liquid-thermal dispersion and solid-thermal diffusion coefficients for the confining zone, respectively, T' is the temperature distribution for the top of confining zone, and T is the temperature distribution in the confined aquifer. As can be seen from equation 8, convective heat flows depends on q' as defined earlier. For the conductive heat flow in equation 7, a Fourier-type equation is used. This equation is similar to that used by Mercer and Pinder (1975); however, it has been modified by adding $b/2$ to b' in the denominator. This modification was made to improve the approximation of the conduction-dominated heat flow which occurs in the shallow confined aquifer at East Mesa.

The vertical-flow terms in equations 3 and 4 for the bottom of the confined aquifer are

$$\frac{\rho k_{zz}}{\mu_l}\left(\frac{\partial p}{\partial z} + \rho g\right)\bigg|_{z_1} = 0 \tag{9}$$

$$[\phi K^{l}_{zz} + (1-\phi)K^{s}_{zz}]\frac{\partial T}{\partial z}\bigg|_{z_1} = -Q' \tag{10}$$

$$\gamma c_v v_z (T - T'\Big|_{z_1} = 0 \tag{11}$$

where Q' is an areally distributed (conductive) heat source. Equation 9 implies that the bottom of the aquifer is an impermeable boundary; that is, there is no mass flow across it, and hence, the convective heat flux (eq 11) is also zero. Since only the heat flow at the surface is known in the East Mesa KGRA, a spatially distributed (conductive) heat function, Q', is used in the steady-state model to reproduce the observed temperature distribution. As additional information becomes available, this treatment of the lower boundary may be relaxed.

EAST MESA STEADY-STATE MODEL

Steady-State Conditions

The hydrologic system in southeastern Imperial Valley is now near equilibrium. Recharge to the groundwater reservoir from precipitation is insignificant since average annual rainfall for the area is less than 76 mm. The water table including the ground-water mounds beneath the All-American and Coachella Canals is about stabilized with the bulk of the canal leakage being discharged through the unconfined aquifer into the drainage system underlying the irrigated main valley area. It is assumed that the source of recharge to the confined aquifer is primarily leakage from the unlined canals that traverse the sandy areas of East Mesa.

Pumpage from the confined aquifer is small: the average discharge from individual wells is approximately 0.6 L/s (Loeltz and others, 1975); and since there are no more than 100 active wells in the model area, total pumpage is probably less than 60 L/s. This relatively small discharge from the confined aquifer is assumed to be counterbalanced by recharge derived from canal leakage.

The potentiometric surface in 1965, contoured in meters (from Loeltz and others, 1975), is shown in figure 6. For modeling purposes, it is used to represent steady-state head distribution in the confined aquifer as related to mean sea level. The shaded area is where the potentiometric surface is above the water table and where there is upward vertical leakage of ground water through the confining zone.

Since there has been no significant production from the geothermal reservoir, the existing distribution of conductive heat transfer through the reservoir cap represents steady-state condition. Conductive and convective heat transfer within the overlying confined-aquifer system is assumed to have adjusted to the effects of canal leakage; therefore, the vertically averaged confined-aquifer temperatures contoured in figure 7 are considered to represent steady-state conditions. The average aquifer temperatures represent the temperature of the water in the aquifer at the midpoint horizon as calculated from temperature logs. Although temperatures do vary slightly with depth, vertically averaged temperature values are used because the problem is treated as two-dimensional in the areal plane.

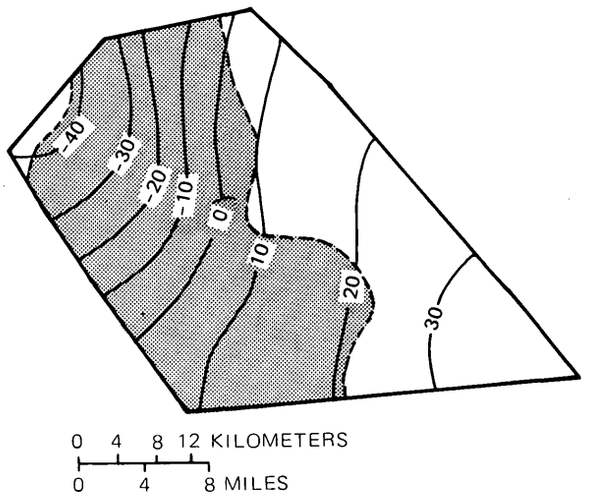

FIGURE 6.—Potentiometric surface of the study area in 1965, based on water levels measured in wells (from Loeltz and others, 1975). Surface contoured in meters above or below (—) mean sea level.

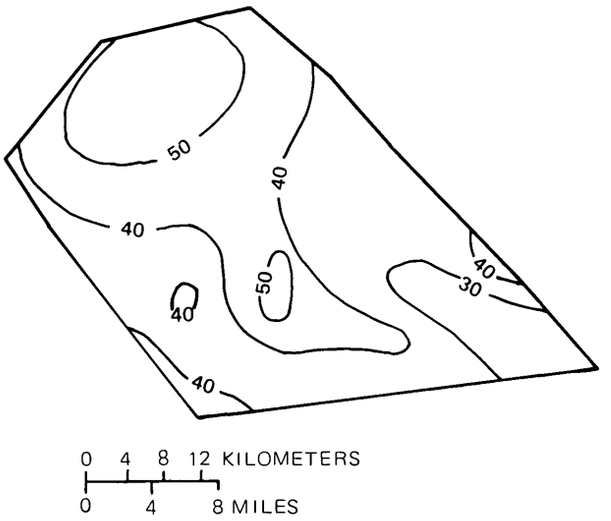

FIGURE 7.—Average temperature, in degrees Celsius, of water in confined aquifer of the study area; contour interval 10°C.

Boundary Conditions

The southwestern and northeastern boundaries of the model correspond approximately to the Imperial and San Andreas faults, respectively. Water-quality differences detected by a resistivity survey have shown the Imperial fault to be a hydrologic barrier south of El Centro (Meidav and Furgerson, 1971). Therefore, in the model the southwestern boundary and the northeastern boundary are considered to be impermeable (that is, no-flow boundaries). The southern boundary follows approximately the All-American Canal. This boundary corresponds to the ground-water divide caused in part by leakage from the All-American Canal. Initially, therefore, this boundary was treated as impermeable. However, in order to match the potentiometric surface in the southeastern part of the model, it was necessary to allow some flow through the eastern part of this boundary, as indicated in figure 2. The general direction of ground-water movement as implied by figure 6 is from southeast to northwest toward the Salton Sea. The northwestern boundary was therefore treated as a constant-flux boundary (directed outward); the fluxes were determined by adjusting the model to match the potentiometric surface in that area, and the final values used in the model are shown in figure 2.

A sensitivity test on thermal boundary conditions indicated that the solution varied only slightly when either constant-temperature or insulated boundary conditions were used. Since this model is relatively insensitive to the type of thermal boundary conditions, insulated boundary conditions were assumed for convenience.

Finally, vertical leakage may be considered a type of boundary condition and is treated as follows. Vertical mass leakage from below is assumed to be zero; that is, the confining bed separating the deeper geothermal reservoir and the shallow confined aquifer is assumed impermeable. As more hydrologic information is obtained for simulating transient changes caused by development, this assumption should be relaxed. Vertical mass leakage from above is determined using Darcy's equation, the permeability of the shallow confining bed, and the head difference between the shallow confined aquifer and the water-table aquifer. This flux is computed implicitly in the numerical model. In order for the model to match the potentiometric surface in the eastern part of the area, near the Coachella Canal, it was necessary to increase the leakage into the confined aquifer. The need to increase the leakage in this region is probably due to a higher confining-bed permeability under the Coachella Canal. Instead of increasing the confining bed permeability in this region however, for convenience, source terms were used to represent the increased leakage from the canal. These are indicated in figure 2.

Vertical heat flow from below is assumed to be by conduction only and was determined by trial and error. The vertical heat flow from above is determined by equations 7 and 8. The temperatures for the water-table aquifer used in these equations ranged only slightly, from 2° to 36°C, and a map of these data is not presented.

Model Assumptions

In modeling the East Mesa area the following assumptions were made:

1. Flow is essentially horizontal in the confined aquifer that overlies the low-permeability cap of the geothermal reservoir.
2. The clays that form the confining zone above the aquifer transmit significant quantities of fluid vertically and also transmit heat by both conduction and convection. Further, this zone is assumed to be horizontal and of constant thickness (60 m), the average thickness in the East Mesa KGRA.
3. The geothermal-reservoir cap is impermeable, and heat is transmitted vertically through the cap by conduction alone. This assumption is made because of the lack of data; it can be relaxed when more information becomes available.
4. The shallow system is in equilibrium; that is, net recharge equals net discharge, and these are approximated in the model by boundary conditions and vertical leakage terms.
5. The confined aquifer is in equilibrium, and groundwater outflow is equal to recharge (largely canal leakage).

Model Results

The finite-element configuration used in modeling the East Mesa area is illustrated in figure 2. It consists of 35 elements and 81 nodes. Higher order elements offering a higher order approximation (see Mercer and Pinder, 1975) were used in the area of the principal geothermal anomalies. Boundary nodes at which mass recharge was introduced into the model, or at which discharge (leakage from canals and groundwater outflow) was removed from it, are identified in figure 2.

The Fortran program used for this study required meter-kilogram-second units; hence, the hydrologic and thermal properties listed in table 2 are given in those units.

The computed steady-state potentiometric surface (datum, sea level) is shown in figure 8. Comparison of the computed potentiometric surface with the measured potentiometric surface (fig. 6) shows that both surfaces have a very similar flow pattern which is basically from southeast to northwest. The minor difference in contour configuration in the northwestern part of the model area occurs where the thickness of the confining layer probably deviates most from the assumed 60-m average thickness used in the model. The two surfaces, in general, however, show a good correlation.

The temperature distribution in the aquifer (fig. 7) was reproduced by the model to within ± 0.9°C at each nodal point with a total conductive heat flow at the base of the aquifer of 251 MW. Because the computed temperatures are so near to those shown in figure 7, no computed contours are presented. Using a reference temperature of 0°C, conductive heat flow

TABLE 2.—*Properties of the shallow hydrothermal system*

Property	Value	Reference
	Confined aquifer	
Porosity	$\phi=0.25$	Dutcher, Hardt, and Moyle (1972, p. 36).[1]
Heat capacity of solid phase	$c_{vs}=0.20\frac{\text{kcal}}{\text{kg °C}}$	Somerton (1958, p. 377).
Density of solid phase	$\rho_s=2670\frac{\text{kg}}{\text{m}^3}$	Morris and Johnson (1966, p. 49).[1]
	Confining zone	
Porosity	$\phi=0.40$	U.S. Bureau of Reclamation (1971a, p. 11).
Thermal conductivity of solid phase	$K_s=2.65\times10^{-4}\frac{\text{kcal}}{\text{m s °C}}$	Combs (1972, p. B5).
	Liquid	
Heat capacity	$c_v=1.0\frac{\text{kcal}}{\text{kg°C}}$	Weber, White, and Manning (1959, p. 206).
Thermal diffusion coefficient	$K^d=1.50\times10^{-4}\frac{\text{kcal}}{\text{m s °C}}$	Kappelmeyer and Haenel (1974, p. 223).[1]

[1] Value estimated from given reference.

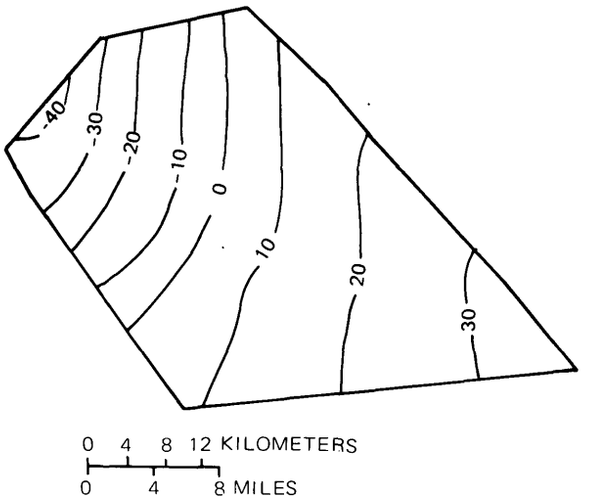

FIGURE 8.—Computed steady-state potentiometric surface of the study area, contoured in meters above or below (—) mean sea level.

through the confining layer was calculated in the model to be 203 MW, and net convective heat-flow loss in ground-water leakage through the confining layer was calculated to be 37 MW. The net heat leaving the model convectively in ground-water outflow through the aquifer (other than vertical leakage) was calculated to be 15 MW. This gave a heat-balance error of approximately 1 percent. As a further check, the average calculated conductive heat flow for the model area (1490 km^2) was 3.3 hfu (1 hfu=41.84 mW/m^2). A comparison of this value with heat-flow measurements made in the East Mesa KGRA (fig. 4) shows the compared value to be within the limits of those measurements which range from 1.5 to 7.9 hfu. A heat-flow range of 2.4 to approximately 25 hfu has been estimated for the Dunes anomaly (Combs, 1972). Combs and Rex (1971) have suggested that a typical regional value of heat flow in the Imperial Valley is 1.9 to 2.0 hfu which is in agreement with the regional value reported by Henyey and Sclater (1971) for the northern Gulf of California. Since the Dunes heat-flow anomaly and the East Mesa KGRA occupy only about 10 percent of the model area, an average calculated heat flow of 3.3 hfu may be slightly high. The error is very likely inherent in the assumption of an average thickness of 60 m for the confining zone which partially distorts the temperature gradient in the heat-flow calculation. A revision of the model, planned by J. W. Mercer (oral commun., 1976), will eliminate this source of error.

DATA REQUIREMENTS FOR A MODEL OF THE DEEP HYDROTHERMAL SYSTEM

Although modeling the deep hydrothermal system was beyond the scope of this report, experience with steady-state modeling of the shallow aquifer has given insight into the data necessary for such a model. Data collection for a future steady-state model of the deep hydrothermal system should include additional data from test-drilling programs. Test-hole data for the most sensitive model parameters should include the following:

1. Static reservoir pressures.
2. Logs for defining thickness, porosity, and permeability of the reservoir and reservoir cap.
3. Thermal and hydrologic conductivity measurements on representative cores of the reservoir cap.
4. Temperature data for determination of average reservoir temperature and the thermal gradient of the reservoir cap.

Prior to constructing a transient model, additional data defining the location and barrier effects of the local fault system are required. An accurate record of pressure and temperature changes caused by water or steam withdrawals from the reservoir should be maintained. Also a periodic releveling of surface and subsurface benchmarks, as described by Lofgren (1974), should be made in order to obtain data on the compaction characteristics of the hydrothermal system.

CONCLUSIONS

This modeling effort represents an initial step in understanding the hydrothermal system at East Mesa. Since the long-range development of the deep reservoir will certainly affect the shallow aquifer, a model of the deep reservoir must also include the shallow aquifer. Future work should include extending the model developed in this report to include the steady-state condition for the deep reservoir which may be used as initial conditions for a transient model that will incorporate the effects of exploitation. The two-dimensional (areal) model used for modeling the shallow aquifer at the East Mesa hydrothermal field shows promise for use in modeling the underlying geothermal reservoir when the required additional data become available.

Solving the flow and heat-transport equations using Galerkin, finite-element approximations for the space derivations is a flexible and efficient approach to modeling hot-water geothermal systems. The present model is restricted to use only on liquid systems; however, work is underway (Mercer and Faust, 1975) on developing a three-dimensional model incorporating the behavior of the steam-water interactions of vapor-dominated systems.

REFERENCES CITED

Babcock, E. A., 1971, Detection of active faulting using oblique infrared aerial photography in the Imperial Valley, California: Geol. Soc. Amer. Bull., v. 82, p. 3189–3196.

Biehler, Shawn, 1964, Geophysical study of the Salton Trough of Southern California: California Inst. Technology, Ph. D. dissert., 139 p.

Biehler, Shawn, Kovach, R. L., and Allen, C. R., 1964, Geophysical framework of northern end of Gulf of California structural province, *in* Van Andel, T. H., and Shor, G. G., Jr., eds., Marine geology of the Gulf of California—a symposium: Am. Assoc. Petroleum Geologists Mem. 3, p. 126–143.

Bradshaw, G. B., and Donnan, W. W., 1952, Ground-water investigations of Imperial County, California: U.S. Dept. Agriculture Soil Conserv. Service Research rept., 61 p.

Brown, J. S., 1923, The Salton Sea region, California, a geographic, geologic, and hydrologic reconnaissance, with a guide to desert watering places: U.S. Geol. Survey Water-Supply Paper 497, 292 p.

California Department of Water Resources, 1974, Water and power from geothermal resources in California, an overview: California Dept. Water Resources Bull. 190, 52 p.

Combs, Jim, 1971, Heat flow and geothermal resource estimates for the Imperial Valley, *in* Cooperative geological-geophysical-geochemical investigations of geothermal resources in the Imperial Valley area of California: U.S. Bur. Reclamation, Final rept. (FY 1971), Contr. No. 14–06–300–2194, p. 5–28.

——— 1972, Thermal studies, *in* Cooperative investigation of geothermal resources in the Imperial Valley area and their potential value for desalting of water and other purposes: Riverside, Caifornia Univ., no. 72–33 p. B1–B23.

Combs, Jim, and Hadley, D. M., 1973, Microearthquake investigations of the Mesa geothermal anomaly, Imperial Valley, California: EOS (Am. Geophys. Union Trans.), v. 54, p. 1213–1214.

Combs, Jim, and Rex, R. W., 1971, Geothermal investigations in the Imperial Valley of California: Geol. Soc. America Abs. with Programs, p. 101–102.

Coplen, T. B., Combs, Jim, Elders, W. A., Rex, R. W., Burckhalter, George, and Laird, Robert, 1973, Preliminary findings of an investigation of the Dunes thermal anomaly, Imperial Valley, California: California Dept. Water Resources and California [Riverside] Univ., Inst. Geophysics and Planetary Physics, no. 73–7, 48 p.

Dutcher, L. C., Hardt, W. F., and Moyle, W. R., Jr., 1972, Preliminary appraisal of ground water in storage with reference to geothermal resources in the Imperial Valley area, California: U.S. Geol. Survey Circ. 649, 57 p.

Elders, W. A., Combs, Jim, Coplen, T. B., Kolesar, P., and Bird, D. K., 1974, Geophysical, geochemical, and geological investigations of the Dunes geothermal system, Imperial Valley, California: Conf. on Research for Devel. of Geothermal Energy Resources, Pasadena, Calif., Sept. 23–25, 1974, Proc., p. 45–72.

Griscom, Andrew, and Muffler, L. J. P., 1971, Aeromagnetic map and interpretation of the Salton Sea geothermal area, California: U.S. Geol. Survey Geophys. Inv. Map GP–754.

Hardt, W. F., and French, J. J., 1976, Selected data on water wells, geothermal wells, and oil tests in the Imperial Valley, California: U.S. Geol. Survey open-file rept.

Henyey, T. L., and Sclater, J. G., 1971, Heat flow in the northern Gulf of California: Geol. Soc. America Abs. with Programs, p. 135–136.

Hutchins, W. A., 1915, Report on investigation of wells in Imperial Valley, 1914: California Dept. Eng. Bull. 1, p. 59–74.

Kappelmeyer, O., and Haenel, R., 1974, Geothermics with special reference to application: Geoexploration mon., ser. 4, no. 4, 238 p., Berlin, Gebrüder Borntraeger.

Kovach, R. L., Allen, C. A., and Press, Frank, 1962, Geophysical investigation in the Colorado delta region: Jour. Geophys. Research, v. 67, no. 7, p. 2845–2871.

Loeltz, O. J., Irelan, Burdge, Robison, J. H., and Olmsted, F. H., 1975, Geohydrologic reconnaissance of the Imperial Valley, California: U.S. Geol. Survey Prof. Paper 486–K, 54 p.

Lofgren, B. E., 1974, Measuring ground movement in geothermal areas of Imperial Valley, California: Conf. on Research for Devel. of Geothermal Energy Resources, Pasadena, Calif., Sept. 23–25, 1974, Proc., p. 128–138.

Mathias, K. E., 1974, Preliminary results of geothermal wells Mesa 6–1 and Mesa 6–2, East Mesa KGRA, Imperial Valley, California: Geothermal Energy, v. 2, no. 6, p. 8–22.

Meidav, Tsvi, and Furgerson, R. B., 1971, Electrical resistivity for geothermal exploration in the Imperial Valley, California: Geothermics, v. 1, p. 47–62.

Mercer, J. W., and Faust, C. R., 1975, Simulation of water- and vapor-dominated hydrothermal reservoirs: Soc. Petroleum Engineers, 50th Ann. Fall Mtg., Dallas, Tex., Sept. 28–Oct. 1, 1975, Paper SPE 5520, 12 p.

Mercer, J. W., and Pinder, G. F., 1975, A finite-element model of a two-dimensional, single-phase heat transport in a porous medium: U.S. Geol. Survey Open-File Rept. 75–574, 115 p.

Mercer, J. W., Pinder, G. F., and Donaldson, I. G., 1975, A Galerkin-finite element analysis of the hydrothermal system at Wairakei, New Zealand: Jour. Geophys. Research, v. 80, no. 17, p. 2608–2621.

Meyer, C. A., McClintock, R. B., Silvestri, G. J., and Spencer, R. C., 1968, 1967 ASME steam tables [2d ed.]: New York, Am. Soc. Mech. Engineers, 328 p.

Morris, D. A., and Johnson, A. I., 1966, Summary of hydrologic and physical properties of rock and soil materials, as analyzed by the hydrologic laboratory of the U.S. Geological Survey, 1948–60: U.S. Geol. Survey open-file rept., 60 p.

Pinder, G. F., and Frind, E. O., 1972, Application of Galerkin's procedure to aquifer analysis: Water Resources Research, v. 8, no. 1, p. 108–120.

Rex, R. W., 1970, Investigations of geothermal resources in the Imperial Valley and their potential value for desalination of water and electricity production: Riverside, California Univ., Inst. Geophysics and Planetary Physics Rept. 92502, 14 p.

Somerton, W. H., 1958, Some thermal characteristics of porous rocks: Am. Inst. Mining Engineers Trans., no. 213, p. 375–378.

Swanberg, C. A., 1974, Heat flow and geothermal potential of the East Mesa KGRA, Imperial Valley, California: Conf. on Research for Devel. of Geothermal Energy Resources, Pasadena, Calif., Sept. 23–25, 1974, Proc., p. 85–97.

——— 1975, The Mesa geothermal anomaly, Imperial Valley, California: A comparison and evaluation of results obtained from surface geophysics and deep drilling [abs.]: Devel. and Use of Geothermal Resources, 2d, San Francisco, Calif., May 20–29, 1975, no. III–85.

Tischler, M. S., 1964, Water resources, *in* Minerals for industry, southern California, summary of Geological Survey 1955–1961: Southern Pacific Co., v. 3, p. 199–237.

Ulrich, F. P., 1941, The Imperial Valley earthquakes of 1940: Seismol. Soc. America Bull. 31, p. 13–31.

U.S. Bureau of Reclamation, 1971a, Geothermal resource investigations, deep geothermal test well, Imperial Valley, California: U.S. Bur. Reclamation site location rept., October 1971, 12 p.

——— 1971b, Geothermal resource investigations, Imperial Valley, California: U.S. Bur. Reclamation status rept., April 1971, 47 p.

——— 1973, Geothermal resource investigations, test well Mesa G–1, Imperial Valley, California: U.S. Bur. Reclamation special rept., February 1973, 44 p.

——— 1974, Geothermal resource investigations, East Mesa site, Imperial Valley, California: U.S. Bur. Reclamation status rept., November 1974, 64 p.

Von Herzen, R. P., and Maxwell, A. E., 1959, The measurement of thermal conductivity of deep-sea sediments by a needle-probe method: Jour. Geophys. Research, v. 64, p. 1557–1563.

Weber, R. L., White, N. W., and Manning, K. V., 1959, Physics for science and engineering: New York, McGraw-Hill, 640 p.

Zienkiewicz, O. C., and Parekh, C. J., 1970, Transient field problems: Two dimensional and three dimensional analysis by isoparametric finite elements: Internat. Jour. Numerical Methods Eng., v. 2, p. 61–71.

Jour. Research U.S. Geol. Survey
Vol. 5, No. 4, July–Aug. 1977, p. 509–517

SOLUBILITY OF NATURAL FLUORITE AT 25°C

By D. W. BROWN and C. E. ROBERSON, Menlo Park, Calif.

Abstract.—The solubility products of two samples of natural fluorite from Rosiclare, Ill., and from Madoc, Ontario, were determined at 25°C by analyses of calcium and fluoride in sodium perchlorate solutions of varying ionic strength over a period of 3 years. Calcium concentrations were analyzed by atomic absorption spectrophotometry, fluoride concentrations were measured colorimetrically, and fluoride activities were measured using a specific ion electrode. The solubility products at the end of 3 years were determined by extrapolation to zero ionic strength. The final solubility product was found to be $10^{-10.58\pm0.17}$.

Fluoride concentrations in natural waters are of interest from both geochemical and environmental standpoints. Many geothermal waters have high concentrations of fluoride relative to most waters used for domestic supply, and development of geothermal power involves potential sources of contamination of potable waters. Contamination of potable waters may also result from certain industrial processes, including the manufacturing of phosphate fertilizer from phosphate rock.

Fluoride, being an anion, is more likely to be controlled by solubility factors than by adsorption processes in the hydrologic environment. The solubility of fluorite determined by different workers, however, varies by up to three orders of magnitude, as shown in table 1.

The pK_{s0} (negative logarithm of solubility product) value of 8.27 (Lingane, 1967) appears to be much too small (K_{s0} too large). The largest pK_{s0} (smallest K_{s0}) from Strübel's (1965) data was obtained from weight loss of CaF_2. The values for K_{s0}, with the possible exception of Lingane's value, have been calculated for zero ionic strength. Solubility product values calculated by us from solubility data from references 1–4, 6, and 11 (table 1) were obtained from the relations

$$K_{s0} = (m_{\pm}\gamma_{\pm})^3 \text{ and } m_{\pm} = (4)^{1/3}m, \qquad (1)$$

where $m_{\pm}$, $\gamma_{\pm}$, and m are the mean molality, mean activity coefficient, and the molality of the CaF_2 dissolved, respectively. (For derivation of analogous relations see Klotz, 1964, p. 392). Values for $\gamma_{\pm}$ were obtained from Hamer (1968) for the appropriate ionic strength, μ, where $\mu = 3m$ for CaF_2. For studies involving precipitation, the precipitated phase controlling solubility may have been, in at least one study (Roberson and Schoen, 1973), a metastable structure having greater solubility than natural fluorite, even though the precipitate gave the X-ray pattern for fluorite.

The large spread in solubilities reported may be related to kinetic effects. For studies in which equilibrium was approached from undersaturation, especially at low temperature, equilibrium may sometimes not have been attained. The present study therefore attempts to help to resolve the many differences in reported values for the solubility product. This study differs from most previous work in that 3 years were allowed for the CaF_2–H_2O system to come to equilibrium from undersaturation. It also differs from previous studies in that calcium was determined by

TABLE 1.—*Solubility of crystalline* CaF_2 *at 1 atmosphere pressure (101.3 kilopascals)*
[25°C uness otherwise indicated]

Reference No.	Solubility of CaF_2 (g/L)	pK_{s0}	Reference	Remarks
1	0.016	10.46	Kohlrausch (1908)[1]	Fluorspar.
2	.018	10.39	Aumeras (1927)[1]	
3	.040	9.39	Carter (1928)[1]	pH 6.4.
4	.0308	9.76	Stephen and Stephen (1964).	18°C.
5	------	10.57	Smyshlyaev and Edeleva (1962).	
6	.00876	11.26	Strubel (1965)	23°C.
7	------	8.27	Lingane (1967)	
8	------	9.75	Roberson and Schoen (1973)	Synthetic fluorite.
9	------	9.77	Latimer (1952)	From free-energy data.
10	------	10.96	D. K. Nordstrom and E. A. Jenne (written commun., 1975).	See text.
11	.0151	10.54	Mougnaud (1931)	18°C.
12	------	10.58	This report	Ontario fluorite.

[1] Compiled by Linke (1958).

atomic absorption, while fluoride was determined both colorimetrically and by specific ion electrode.

Acknowledgments.—During this investigation the many discussions held with D. Kirk Nordstrom of the U.S. Geological Survey aided in forming the conclusions expressed here. Reviews of this paper by Nordstrom and by Prof. Alexis N. Moiseyev, California State University (Hayward), were helpful in developing the presentation and are acknowledged with thanks.

THEORETICAL ASPECTS

The equilibrium constant for the solution of fluorite, represented by the reaction $CaF_{2c} \rightleftharpoons Ca^{2+} + 2F^-$, is given at equilibrium by $K_{s0} = a_{Ca^{2+}} a_{F^-}{}^2$, where $a_{Ca^{2+}}$ and a_{F^-} are the aqueous activities of calcium and fluoride, respectively. For a system not at equilibrium, we refer to the activity product Q, where $Q = a_{Ca^{2+}} a_{F^-}{}^2$. The activity a_i of a particular ionic species i is given by $a_i = m_i \gamma_i$, where m_i is its molality and γ_i is its ion activity coefficient. The activity coefficient γ_i in this study is calculated for ionic strength less than 0.1 using the extended Debye-Hückel relation

$$\log_{10}\gamma_i = \frac{-Az_i^2\sqrt{\mu}}{1 + \mathring{a}_i B\sqrt{\mu}} \qquad (2)$$

where A and B are the Debye-Hückel coefficients, respectively equal to 0.5085 and 0.3286×10^8 cm^{-1} at 25°C, z_i is the charge on the ion, $\mathring{a}_i$ is the effective diameter for the hydrated aqueous ion in centimeters, and μ is the ionic strength of the solution, given by $\mu = \Sigma[(m_i z_i^2)/2]$. The values obtained from equation 2 for activity coefficients at ionic strengths less than 0.1 agree to within ±1 percent with those obtained using the more complicated expression given by Helgeson (1969). The semiempirical Davies equation gives activity coefficients which result in wider spread of activity products than does use of the extended Debye-Hückel relation. According to Butler (1964), this equation was designed to fit experimental data for the mean activity coefficient of a uni-univalent salt rather than di-univalent salt such as fluorite. For these reasons, the Davies equation is not used to calculate activity coefficients. The common features of the various expressions for ion activity coefficients is that $\log_{10}\gamma_i$ is approximately proportional to the square of the ionic charge and to the square root of the ionic strength. This fact has been used in determining solubility products of minerals at different ionic strengths by extrapolating to zero strength a plot of the logarithm of a solubility product containing one or more concentration terms versus $\sqrt{\mu}$.

In this study, fluoride activities were first determined using an Orion solid-state fluoride electrode, and calcium concentrations were determined by atomic absorption spectrophotometry. The activity data for fluoride and the concentration data for calcium give rise to what we call a "hybrid" product $Q' = m_{Ca^{2+}} a_{F^-}{}^2$ containing both concentration and activity terms. The dependence of this hybrid product on ionic strength is as follows:

$$Q' = m_{Ca^{2+}} a_{F^-}{}^2 = \frac{a_{Ca^{2+}} a_{F^-}{}^2}{\gamma_{Ca^{2+}}} = \frac{Q}{\gamma_{Ca^{2+}}}, \qquad (3)$$

so that $\log_{10}Q' = \log_{10}Q - \log\gamma_{Ca^{2+}}$. Therefore $\log_{10}Q' = \log_{10}Q + (4A\sqrt{\mu})/(1 + \mathring{a}_{Ca^{2+}} B\sqrt{\mu})$, which would be expressed at equilibrium as $\log_{10}K'_{s0} = \log_{10}K_{s0} + (4\sqrt{\mu})/(1 + \mathring{a}_{Ca^{2+}} B\sqrt{\mu})$. The effective diameter $\mathring{a}_{Ca^{2+}}$ of the hydrated Ca^{2+} ion is 6×10^{-8} cm or 6 Å (angstroms) so that the denominator in the Debye-Hückel expression for $\log_{10}\gamma_{Ca^{2+}}$ is $1 + 1.97\sqrt{\mu}$. It is apparent from the above expressions that a plot of $\log_{10}Q'$ as a function of $\sqrt{\mu}$, or more precisely as a function of $\sqrt{\mu}/(1 + 1.97\sqrt{\mu})$ at 25°C, should give a straight line of intercept equal to the logarithm of the activity product. This is the hybrid product extrapolated to zero ionic strength, and at equilibrium this intercept is equal to the solubility product K_{s0}.

Where fluoride as well as calcium is measured in terms of concentration rather than activity, the function with which the logarithm of the concentration product $m_{Ca^{2+}} m_{F^-}{}^2$ varies linearly is more complicated than $\sqrt{\mu}$ or even than $\sqrt{\mu}/(1 + \mathring{a}_{Ca^{2+}} B\sqrt{\mu})$. The concentration product Q'' can be written in terms of the activity product Q as

$$Q'' = m_{Ca^{2+}} m_{F^-}{}^2 = \frac{a_{Ca^{2+}} a_{F^-}{}^2}{\gamma_{Ca^{2+}} \gamma_{F^-}{}^2} = \frac{Q}{\gamma_{Ca^{2+}} \gamma_{F^-}{}^2},$$

so that

$$\log_{10}Q'' = \log_{10}Q - \log_{10}\gamma_{Ca^{2+}} - 2\log_{10}\gamma_{F^-}. \qquad (4)$$

This may be expressed approximately as $\log_{10}Q'' = \log_{10}Q + 6A\sqrt{\mu}$, so that a plot of $\log_{10}Q''$ versus $\sqrt{\mu}$ should give $\log_{10}Q$ as intercept and 6A or 3.05 at 25°C as slope. For greater accuracy at higher ionic strength, however, use of the extended Debye-Hückel expression gives rise to the relation

$$\log_{10}Q'' = \log_{10}Q + A\left(\frac{4\sqrt{\mu}}{1 + 1.97\sqrt{\mu}} + \frac{2\sqrt{\mu}}{1 + 1.15\sqrt{\mu}}\right), \qquad (5)$$

where K is used in place of Q at equilibrium. A plot of $\log_{10}Q''$ as a function of the term in parentheses in equation 5 should give a straight line of slope equal to A (0.5085 at 25°C) and whose intercept is equal to the logarithm of the solubility product K_{s0} at equilibrium.

Calcium and fluoride ions form many complexes with other dissolved species in natural waters. In our laboratory solutions CaF^+, $CaOH^+$, and HF are the only important complexes. Calculations using $K_{CaF^+} = 10^{1.04}$, $K_{CaOH^+} = 10^{1.50}$ (Sillén and Martell, 1964), and the highest pH and fluoride and calcium concentrations show CaF^+ and $CaOH^+$ to account for less than 1 percent of the total calcium concentrations; they are therefore not considered in this study. At the lowest pH encountered in this study it was similarly found, using $10^{-3.17}$ (Sillén and Martell, 1964) for the dissociation constant of HF, that undissociated HF accounts for less than 2 percent of the total fluoride concentration.

EXPERIMENTAL RESULTS

Two samples of natural fluorite were obtained, one from Madoc, Ontario, Canada, and the other from Rosiclare, Ill. X-ray fluorescence studies showed traces of iron associated with both samples, and of yttrium with the Ontario variety. X-ray diffraction showed the iron present with the Ontario fluorite to be in the form of goethite, with which the fluorite crystals were closely associated and from which complete separation was difficult. X-ray diffraction also showed a small amount of calcite to be present with the Illinois variety. These samples were ground by using a mortar and pestle, and the particle-size fractions between 60 to 140 mesh were saved, washed with distilled deionized water, and centrifuged to constant conductivity of the rinse water. In addition, the particles were temporarily suspended in water, and that fraction containing the slowly settling fine particles was poured off. This rather coarse particle-size range was used in order to avoid obtaining metastably high solubilities of fluorite due to the particle-size effect. The wet, coarse crystals were dried over a water bath for several hours, then in a 110°C oven for several more hours.

Two sets of five 200-mL (milliliter) solutions of varying initial sodium perchlorate concentrations were made by successive dilutions of a 0.0957 *M* $NaClO_4$ solution for each of the fluorite minerals. The sodium perchlorate concentrations, equal to the initial ionic strengths of the solutions, were approximately 0, 10^{-4}, 10^{-3}, 10^{-2}, and 10^{-1} molar. Measurement of sodium by atomic absorption confirmed these values, and ionic strengths were computed from the analyses to be 0, 1.04×10^{-4}, 1.09×10^{-3}, 9.57×10^{-3}, and 0.0957 molar. Approximately 0.5 gram of the Ontario fluorite was placed in each of the first set of five sodium perchlorate solutions in 250-mL polypropylene bottles numbered 1 through 5, and the same amount of Illinois fluorite was placed in each of the second set of solutions in bottles numbered 6 through 10. These solutions were allowed to stand in a constant-temperature room at 25.0±0.5°C for 3 years. Measurements of fluoride activities and of calcium concentrations after filtration through 0.45-μm (micrometer) pore-diameter Millipore filters were taken 2, 14, 20, and 34 days after placement of the fluorites in the solutions. Analyses for these times are given in table 2. The activity products calculated using $\gamma_{Ca^{2+}}$ values obtained from the extended Debye- Hückel relation had not reached a constant value after 34 days aging, although the rates of increase in the activity products were leveling off. This implied that perhaps equilibrium would not be attained for at least several months, perhaps years. Consequently no further analyses were performed until the solutions had aged 1103 days, or approximately 3 years. These 3-year analyses (table 3) also included measurements of pH and concentrations of sodium and of possible potassium and magnesium impurities, which were found to be very small. Tabulated values for ionic strengths in tables 2 and 3 were calculated from available cation analyses to include the anionic contribution, assuming only univalent anions such as perchlorate, fluoride, and bicarbonate to be present in appreciable concentrations. These ionic strengths were used to calculate the $\gamma_{Ca^{2+}}$ values which were then used for calculating calcium activities. The values of pQ or $-\log_{10}(a_{Ca^{2+}}a_{F^-}{}^2)$ tabulated in these tables are calculated from these calcium activities, while values of pQ' or $-\log_{10}(m_{Ca^{2+}}a_{F^-}{}^2)$ are calculated directly from calcium molar concentrations. Figure 1 shows $\log_{10}Q'$ at 1103 days plotted as a function of $\sqrt{\mu}/(1+1.97\sqrt{\mu})$. Least-squares lines give zero intercepts of −10.51 for Ontario fluorite and −10.13 for the Illinois variety. The respective slopes are 2.96 and 0.935, and the correlation coefficients are 0.967 and 0.718. The very high scatter of the Illinois fluorite data points and the nontheoretical slope, probably related to the calcite impurity found to be present, are discussed later.

The pH's of the 10 solutions at 1103 days fell within the range in which analyses for fluoride are free from interferences attributable to pH. At pH less than 4, fluoride ion complexes to a considerable degree and forms the uncharged complex HF in solution; at pH greater than 8, hydroxide ion contributes a positive interference for fluoride as measured by the solid-state fluoride electrode.

Summaries of the negative logarithms of the hybrid and activity products for each set of analyses are shown in table 4 (Ontario fluorite solutions 1–5 and Illinois fluorite solutions 6–10). Means and standard deviations of the activity products and zero intercepts

TABLE 2.—*Calcium concentrations and fluoride activities in sodium perchlorate solutions in contact with fluorite at 25°C after aging for 2, 14, 20, and 34 days*

Solution	Ca (mg/L)	pF	Ionic strength (μ)	$\frac{\sqrt{\mu}}{1+1.97\sqrt{\mu}}$	Ca^{2+} activity coefficient ($\gamma_{Ca^{2+}}$)	pCa	pQ[1]	pQ'[2]
2 days								
Ontario fluorite:								
1	3.6	3.72	2.6×10^{-4}	0.0159	0.928	4.08	11.52	11.49
2	4.0	3.69	4.03×10^{-4}	.0193	.914	4.04	11.42	11.38
3	4.1	3.69	1.40×10^{-3}	.0348	.850	4.06	11.44	11.37
4	5.0	3.64	9.94×10^{-3}	.0833	.678	4.07	11.35	11.18
5	5.2	3.70	.0961	.192	.407	4.28	11.68	11.29
Illinois fluorite:								
6	6.1	3.69	4.57×10^{-4}	.0205	.909	3.86	11.24	11.20
7	7.0	3.62	6.28×10^{-4}	.0239	.894	3.81	11.05	11.00
8	8.0	3.58	1.69×10^{-3}	.0380	.837	3.78	10.94	10.86
9	8.0	3.62	.0102	.0841	.675	3.87	11.11	10.94
10	10.0	3.64	.0964	.193	.407	3.99	11.27	10.88
14 days								
Ontario fluorite:								
1	5.1	3.59	3.82×10^{-4}	0.0188	0.916	3.93	11.11	11.08
2	5.9	3.54	5.46×10^{-4}	.0223	.901	3.88	10.96	10.91
3	5.5	3.57	1.50×10^{-3}	.0360	.845	3.94	11.08	11.00
4	6.8	3.50	.0101	.0938	.676	3.94	10.94	10.77
5	7.1	3.57	.0962	.193	.407	4.14	11.28	10.89
Illinois fluorite:								
6	8.1	3.59	6.06×10^{-4}	.0235	.896	3.74	10.92	10.87
7	8.9	3.58	7.70×10^{-4}	.0263	.884	3.71	10.87	10.81
8	9.3	3.52	1.79×10^{-3}	.0390	.833	3.71	10.75	10.67
9	9.6	3.54	.0103	.0845	.674	3.79	10.87	10.70
10	12.5	3.58	.0966	.193	.406	3.90	11.06	10.67
20 days								
Ontario fluorite:								
1	5.4	3.55	4.04×10^{-4}	0.0193	0.914	3.91	11.01	10.97
2	6.1	3.50	5.61×10^{-4}	.0226	.900	3.86	10.86	10.82
3	6.0	3.54	1.54×10^{-3}	.0364	.844	3.90	10.98	10.90
4	7.3	3.47	.0101	.0839	.676	3.91	10.85	10.68
5	7.6	3.54	.0963	.192	.407	4.11	11.19	10.80
Illinois fluorite:								
6	8.6	3.51	6.44×10^{-4}	.0242	.893	3.72	10.74	10.69
7	10.0	3.50	8.53×10^{-4}	.0276	.879	3.66	10.66	10.60
8	10.1	3.52	1.85×10^{-3}	.0396	.831	3.68	10.72	10.64
9	10.2	3.53	.0103	.0847	.673	3.77	10.83	10.65
10	13.2	3.55	.0967	.193	.406	3.87	10.97	10.58
34 days								
Ontario fluorite:								
1	6.0	3.47	4.49×10^{-4}	0.0203	0.909	3.87	10.81	10.76
2	6.4	3.43	5.83×10^{-4}	.0230	.898	3.84	10.70	10.66
3	6.2	3.48	1.55×10^{-3}	.0366	.843	3.88	10.84	10.77
4	7.9	3.41	.0102	.0841	.675	3.88	10.70	10.53
5	8.4	3.47	.0963	.193	.406	4.07	11.01	10.62
Illinois fluorite:								
6	9.4	3.54	7.04×10^{-4}	.0252	.889	3.68	10.76	10.71
7	10.3	3.52	8.75×10^{-4}	.0280	.878	3.65	10.69	10.63
8	11.3	3.47	1.94×10^{-3}	.0405	.827	3.63	10.57	10.49
9	11.3	3.49	.0104	.0850	.672	3.72	10.70	10.53
10	14.1	3.49	.0968	.193	.406	3.84	10.82	10.43

[1] $pQ = -\log_{10}(a_{Ca^{2+}}a_{F^-}{}^2)$.
[2] $pQ' = -\log_{10}(m_{Ca^{2+}}a_{F^-}{}^2)$.

of the logarithms of hybrid products plotted as a function of $\sqrt{\mu}/(1 + 1.97\sqrt{\mu})$ are shown for each date. After 1118 days, final aliquots of 15 mL were taken from the solutions and filtered through Millipore 0.45-μm pore-diameter filters. The filtrates were analyzed for calcium by atomic absorption, and for fluoride using the Zirconium Eriochrome Cyanine R method, a colorimetric procedure based on the forma-

TABLE 3.—*Chemical analyses of sodium perchlorate solutions in contact with fluorite at 25°C after aging for 1103 days*

Solution	pH	Concentrations (mg/L) Ca	Mg	Na	K	pF	Ionic strength (μ)	$\frac{\sqrt{\mu}}{1+1.97\sqrt{\mu}}$	Ca^{2+} activity coefficient ($\gamma_{Ca^{2+}}$)	pCa	pQ[1]	pQ'[2]
Ontario fluorite												
1	4.89	7.8	0.0	0.2	0.3	3.36	6.00×10^{-4}	0.0233	0.897	3.76	10.48	10.43
2	5.00	7.5	.0	4.2	.2	3.37	7.49×10^{-4}	.0273	.880	3.78	10.52	10.47
3	5.10	7.5	.0	27	.2	3.35	1.74×10^{-3}	.0386	.835	3.81	10.51	10.43
4	5.16	9.2	.0	240	.2	3.26	.0111	.0873	.665	3.82	10.34	10.16
5	5.74	11.7	.0	2,200	.4	3.22	.0966	.193	.406	3.93	10.37	9.97
Illinois fluorite												
6	7.87	24.8	0.2	0.8	0.1	3.43	1.92×10^{-3}	0.0404	0.828	3.29	10.15	10.07
7	7.69	20.6	.2	4.2	.2	3.45	1.75×10^{-3}	.0386	.835	3.37	10.27	10.19
8	7.96	25.5	.2	27	.1	3.42	3.11×10^{-3}	.0502	.791	3.30	10.14	10.04
9	7.91	24.2	1.4	235	.1	3.39	.0122	.0908	.654	3.40	10.18	10.00
10	7.67	22.6	.3	2,200	.2	3.36	.0974	.193	.405	3.64	10.36	9.97

[1] $pQ = -\log_{10}(a_{Ca^{2+}}a_{F^-}^{2})$.
[2] $pQ' = -\log_{10}(m_{Ca^{2+}}a_{F^-}^{2})$.

TABLE 4.—*Negative logarithms of activity and hybrid products for fluorites from Madoc, Ontario, and Rosiclare, Ill.*

Solution	2 days	14 days	20 days	34 days	1103 days
ONTARIO FLUORITE					
Activity products $a_{Ca^{2+}}a_{F^-}^{2}$					
1	11.52	11.11	11.01	10.81	10.48
2	11.52	10.96	10.86	10.70	10.52
3	11.44	11.08	10.98	10.84	10.51
4	11.35	10.94	10.85	10.70	10.34
5	11.68	11.28	11.19	11.01	10.37
Mean	11.48	11.07	10.98	10.81	10.44
Standard deviation	.13	.14	.14	.13	.08
Hybrid products $m_{Ca^{2+}}a_{F^-}^{2}$					
1	11.49	11.08	10.97	10.76	10.43
2	11.38	10.91	10.82	10.66	10.47
3	11.37	11.00	10.90	10.77	10.43
4	11.18	10.77	10.68	10.53	10.16
5	11.29	10.89	10.80	10.62	9.97
Intercept[1]	11.40	10.98	10.88	10.72	10.51
Slope	.891	.760	.701	.732	2.96
Correlation	.571	.474	.464	.530	.967
ILLINOIS FLUORITE					
Activity products $a_{Ca^{2+}}a_{F^-}^{2}$					
6	11.24	10.92	10.74	10.76	10.15
7	11.05	10.87	10.66	10.69	10.27
8	10.94	10.75	10.72	10.57	10.14
9	11.11	10.87	10.83	10.70	10.18
10	11.27	11.06	10.97	10.828	10.36
Mean	11.12	10.89	10.78	10.71	10.22
Standard deviation	.14	.11	.12	.09	.09
Hybrid products $m_{Ca^{2+}}a_{F^-}^{2}$					
6	11.20	10.87	10.69	10.71	10.07
7	11.00	10.81	10.60	10.63	10.19
8	10.86	10.67	10.64	10.49	10 04
9	10.94	10.70	10.65	10.53	10 00
10	10.88	10.67	10.58	10.43	9.97
Intercept[1]	11.05	10.80	10.66	10.68	10.13
Slope	.994	.797	.382	2.18	.935
Correlation	.526	.624	.626	.607	.718

[1] Intercept at $\mu=0$ for logarithms of hybrid products plotted as a function of $\sqrt{\mu}/(1+1.97\sqrt{\mu})$ theoretically should equal the activity product at equilibrium. Theoretical slope is 2.030 at 25°C.

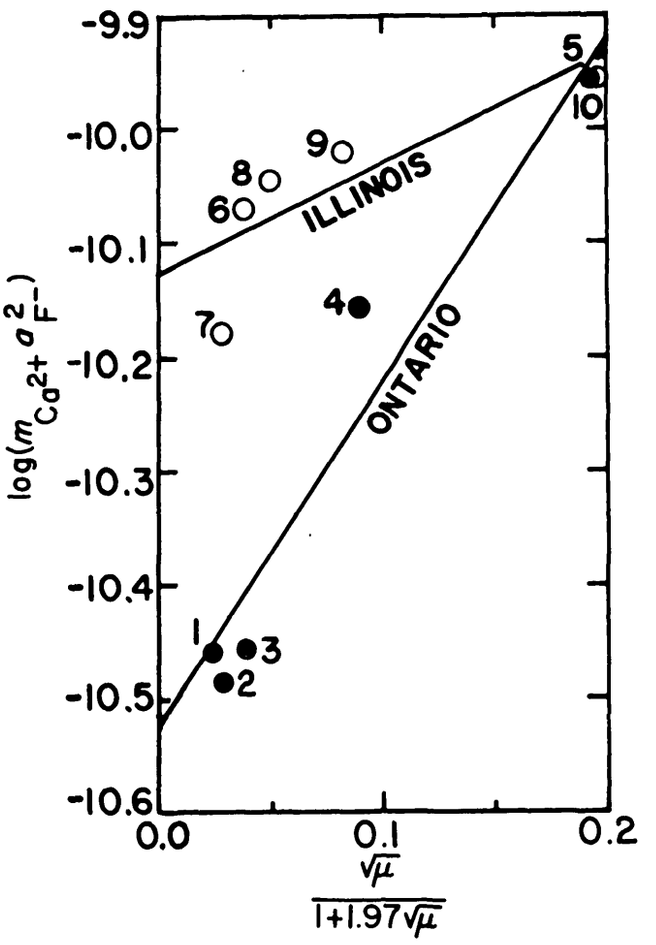

FIGURE 1.—Hybrid product logarithms versus $\sqrt{\mu}/(1+1.97\sqrt{\mu})$ for Ontario (dots) and Illinois (circles) fluorites at 1103 days.

tion of the colorless ZrF_6^{2-} complex at the expense of a colored organic zirconium complex (Brown and others, 1970). The results of these analyses and the corresponding concentration products Q'' and calculated activity products Q are shown in table 5. Typi-

TABLE 5.—*Chemical analyses of sodium perchlorate soluttions in contact with fluorite at* BE°*C after aging for 1118 days*

Solution	Ca	F	HCO_3	Ionic strength (μ)	Ionic strength function [1]	pCa [2]	pF	pCO_3 [3]	pQ [4]	pQ'' [4]	$-\log_{10}(a_{Ca^{2+}}a_{CO_3^{2-}})$
Ontario fluorite											
1	8.3	7.25	<5	6.54×10^{-4}	0.147	3.73	3.43	>9.5	10.59	10.52	>13
2	8.4	7.50	<5	8.17×10^{-4}	.164	3.73	3.42	>9.4	10.57	10.48	>13
3	8.5	7.55	<5	1.82×10^{-3}	.239	3.75	3.42	>9.3	10.59	10.48	>13
4	10.0	8.45	<5	.0112	.539	3.78	3.40	>9.2	10.58	10.31	>13
5	12.5	13.05	<5	.0966	1.229	3.90	3.28	>8.6	10.46	9.83	>12
Illinois fluorite											
6	23.3	5.75	56	1.81×10^{-3}	0.238	3.32	2.54	5.48	10.40	10.27	8.80
7	20.2	5.75	55	1.72×10^{-3}	.233	3.38	3.53	5.67	10.44	10.31	9.05
8	23.9	6.15	57	2.99×10^{-3}	.300	3.32	3.52	5.38	10.36	10.20	8.70
9	24.5	6.25	58	.0122	.559	3.40	3.53	5.40	10.46	10.18	8.80
10	21.6	9.80	60	.0974	1.232	3.66	3.17	5.56	10.00	9.84	9.22

[1] The ionic strength function is $(4\sqrt{\mu})/(1+1.97\sqrt{\mu})+(2\sqrt{\mu})/(1+1.15\sqrt{\mu})$.
[2] Values of pCa and pF are calculated using the Debye-Huckel ion-activity coefficients, and are used for calculating pQ.
[3] Values of pCO_3 are calculated from bicarbonate concentrations and from pH at 1103 days using $K_2=10^{-10.33}$.
[4] $pQ=-\log_{10}(a_{Ca^{2+}}a_{F^-}{}^2)$ and $pQ''=-\log_{10}(m_{Ca^{2+}}m_{F^-}{}^2)$.

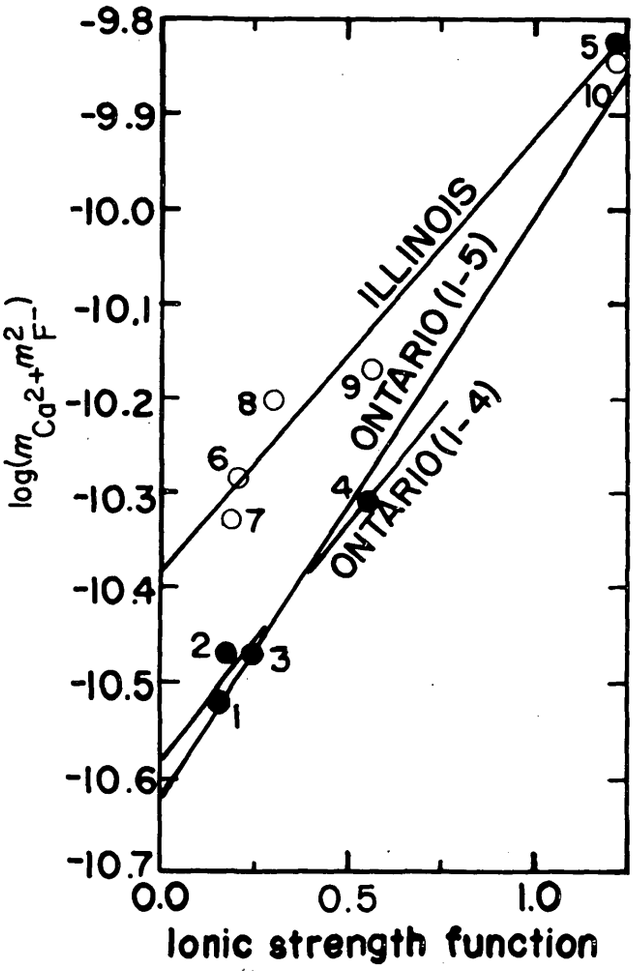

FIGURE 2.—Concentration product logarithms versus ionic strength $(4\sqrt{\mu})/(1+1.97\sqrt{\mu})+(2\sqrt{\mu})/(1+1.15\sqrt{\mu})$ for Ontario (dots) and Illinois (circles) fluorites at 1118 days.

cal standard deviations for the atomic absorption calcium measurements and for the fluoride electrode emf measurements are approximately 10 percent of the mean (International Association of Geochemistry and Cosmochemistry, 1975). A similar percentage standard deviation is reported by Brown and others (1970) for the colorimetric fluoride determination. Given these standard deviations, the difference in calcium and fluoride concentrations at 1103 and 1118 days are not significant and are attributable to analytical error. The logarithms of the concentration products Q'' are plotted versus the ionic strength function $(4\sqrt{\mu})/(1+1.97\sqrt{\mu})+(2\sqrt{\mu})/(1+1.15\sqrt{\mu})$ for both fluorites in figure 2, which shows a linear relationship. The linear correlation coefficients for the data from Ontario and Illinois fluorites are, respectively, 0.996 and 0.981, much better than any correlation of the logarithms of the hybrid products with $\sqrt{\mu}/(1+1.97\sqrt{\mu})$, and the respective slopes of 0.629 and 0.431 are reasonably close to the theoretical value of A at 25°C, 0.5085. These slopes and excellent linear correlations agree with theory, which is valid only at equilibrium, and therefore suggest attainment of equilibrium. These results also suggest that perhaps the colorimetric fluoride determinations were more accurate than those obtained by electrode emf measurements. The intercepts, which are theoretically equal to $\log K_{s0}$ at equilibrium are -10.62 for the Ontario fluorite and -10.38 for the Illinois variety.

Figure 3 shows the classical plots of $\log_{10}Q''$ versus $\sqrt{\mu}$. The intercepts are here calculated by the least-squares-fit method for the first four solutions in contact with each fluorite, excluding solutions 5 and 10, and are equal to -10.57 for Ontario fluorite and -10.33 for Illinois fluorite. The respective correlation coefficients, however, are 0.985 and 0.544, the latter

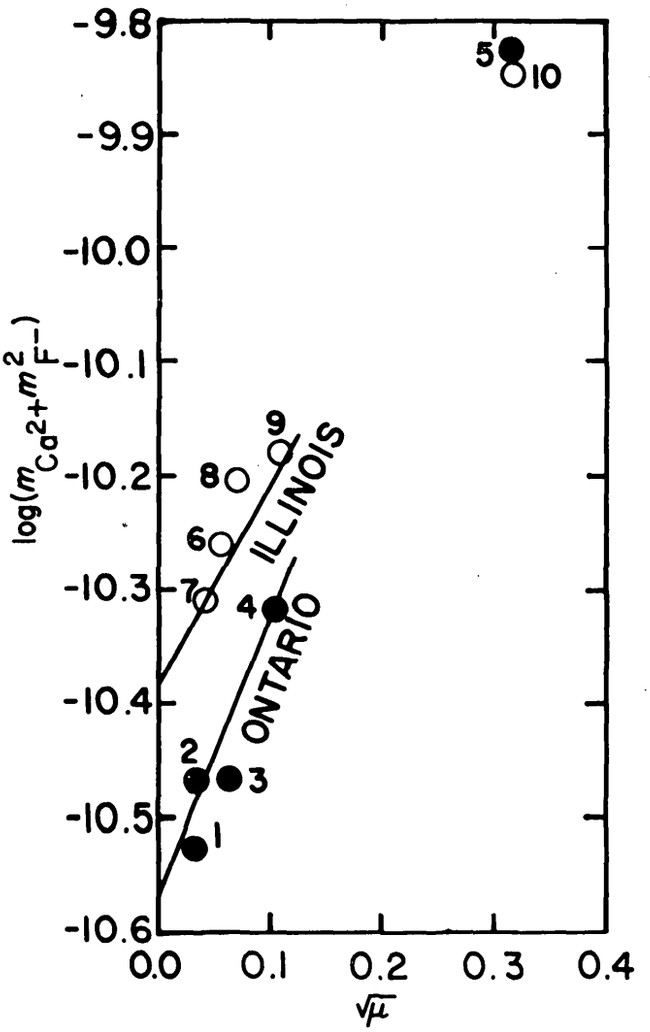

FIGURE 3.—Concentration product logarithms versus square root of ionic strength for Ontario (dots) and Illinois (circles) fluorites at 1118 days.

value indicating an extremely poor linear relationship for the Illinois fluorite data. In addition, the theoretical slope in this type of plot is equal to 6A, or 3.05 at 25°C. The Ontario fluorite data gives a least-squares slope of 2.46, but the Illinois fluorite data gives a slope of 0.74, which is in extremely poor agreement with theory. Final solubility data for Illinois fluorite will be viewed as less accurate than similar data for Illinois fluorite for this reason and for other reasons discussed below.

The reason for discounting solutions 5 and 10 is that the approximation $\log_{10}\gamma_i = -Az^2_i\sqrt{\mu}$, on which this type of plot is based, no longer holds well at a high ionic strength of 0.1. For example, at this ionic strength and 25°C, $\gamma_{Ca^{2+}}$ can be incorrectly calculated, using this relation, as equal to 0.23, while the more correct extended Debye-Hückel relation gives 0.40. Yet another reason why the concentration products from solutions 5 and 10 should perhaps be regarded as less significant than those obtained from the other eight solutions is that the large concentrations of perchlorate represent positive interferences in the colorimetric fluoride determinations. High concentrations of strong oxidizing agents, such as perchlorate, bleach the colored Zirconium Eriochrome Cyanine R complex by oxidizing it, and this cannot be differentiated from the normal fluoride bleaching of the colored complex. The fluoride concentrations listed in table 5 for solutions 5 and 10 may therefore be overestimated, and this would depress values of pQ'' and the resulting calculated pK_{s0} values. Comparisons of the calculated activity products of solutions 1–4, with that from solution 5, and of solutions 6–10, with that from solution 10, show that this is what may have occurred. The means and standard deviations of the logarithms of the calculated activity products shown in table 5 are -10.56 ± 0.06 (Ontario) and -10.42 ± 0.04 (Illinois).

When solutions 5 and 10 are excluded from consideration, the standard deviations are greatly reduced, and these results are -10.58 ± 0.01 (Ontario) and -10.42 ± 0.04 (Illinois). This means K_{s0} for Ontario fluorite also agrees with the values obtained by extrapolation of $\log_{10}Q''$ to zero ionic strength when plotted versus the ionic strength function and when data from solution 5 is excluded. This intercept ($\log_{10}K_{s0}$) is -10.59 and the correlation coefficient is 0.984. The slope of 0.505 agrees very well with the theoretical slope of 0.5085 at 25°C. The corresponding results for the Illinois fluorite data are intercept -10.34, slope 0.310, and correlation coefficient of 0.789. The solubility product of the Ontario fluorite will therefore be taken as $10^{-10.58\pm0.01}$.

From inspection of the data in table 5 it can be observed that there is only a very slight stoichiometric excess of calcium over fluoride in all the Ontario fluorite solutions except solution 5, where instead there is a slight fluoride excess over stoichiometric proportions, perhaps due in part to perchlorate inferference. These excesses, however, are within one standard deviation for the analytical methods used, and so are not significant. In the Illinois fluorite solutions, however, there is a great stoichiometric excess of calcium over fluoride, and this is due to dissolution of a sufficiently large amount of calcite present in the Illinois sample as confirmed by X-ray diffraction. Inspection of intact Illinois fluorite crystals from the same sample batch showed that small veinlets of calcite were present on some crystal faces so that some calcite had been introduced into the samples used for these solubility studies. Analyses of bicarbonate ion by titration with

standard acid are given in table 5, and concentrations were found to be less than 5 mg/L HCO_3^- in the Ontario fluorite solutions, but were 55 to 60 mg/L HCO_3^- in the Illinois fluorite solutions.

The pH values taken at 1103 days were higher in the Illinois fluorite solutions (7.7 to 8.0) than in the Ontario fluorite solutions (4.9 to 5.7). The solubility product of calcite of 25°C is given as $10^{-8.52}$ by Christ, Hostetler, and Siebert (1974). Calculated values for the calcite activity products in table 5 are mostly less than 10^{-13} for the Ontario fluorite solutions, but range from $10^{-9.22}$ to $10^{-8.70}$ for the Illinois fluorite solutions. This indicates that some calcite had already gone into solution in the latter, but that equilibrium with respect to calcite had not yet been attained.

Calculations using $K_{CaHCO_3^+}=10^{1.26}$ (Sillén and Martell, 1964) show the $CaHCO_3^+$ complex to form less than 2 percent of the total calcium concentration. Since this is less than normal analytical error, this complex is not considered in the equilibrium calculations. The relatively high concentrations of calcium in the Illinois fluorite solutions were due to the high solubility of calcite in a system from which atmospheric carbon dioxide had not been excluded over the 3 years aging.

CONCLUSIONS

Owing to the somewhat different solubility products obtained from the data for Illinois and Ontario fluorite, we are faced with choosing between the more correct of the two. Since the activity product of the Illinois fluorite is apparently raised in the presence of calcite, the more correct value of K_{s0} should be $10^{-10.58\pm0.01}$, that given by the Ontario fluorite. The solubility products obtained from fluoride electrode (emf) measurements at 1103 days are summarized in table 6 with those obtained using colorimetric fluoride analysis at 1118 days. It is apparent from standard deviations or from correlation coefficients and slopes

TABLE 6.—*Summary of data obtained from analyses of sodium perchlorate solutions after aging for 3 years*

Method of calculation of solubiity product	Solutions considered	pK_{s0} (from intercept) or mean)	Least-squares data		Notes
			Linear correlation coefficient	Slope	
Ontario fluorite					
Extrapolation of $\frac{\sqrt{\mu}}{1+1.97\sqrt{\mu}}$ to zero	1–5	10.51	0.967	2.96	Fuoride (emf) at 1103 days. Theoretical slope is 4A=2.034.
Mean and standard deviation of calculated activity products.	1–5	10.44±0.08	----	---	Fluoride (emf) at 1103 days.
Extrapolation of $\frac{4\sqrt{\mu}}{1+1.97\sqrt{\mu}}+\frac{2\sqrt{\mu}}{1+1.15\sqrt{\mu}}$ to zero.	1–5	10.62	.996	0.629	Fluoride (colorimetric) at 1118 days. Theoretical slope is A=0.5085.
	1–4	10.59	.984	.505	Do.
Extrapolation of $\sqrt{\mu}$ to zero	1–4	10.57	.985	2.46	Fluoride (colorimetric) at 1118 days. Theoretical slope is 6A=3.051.
Mean and standard deviation of calculated activity products.	1–5	10.56±0.06	----	---	Colorimetric fluoride.
	1–4	10.58±0.01	----	---	Do.
Illinois fluorite					
Extrapolation of $\frac{\sqrt{\mu}}{1+1.97\sqrt{\mu}}$ to zero	6–10	10.13	0.718	0.935	Fluoride (emf) at 1103 days. Theoretical slope is 4A=2.034.
Mean and standard deviation of calculated activity products.	6–10	10.22±0.09	----	---	Fluoride (emf) at 1103 days.
Extrapolation of $\frac{4\sqrt{\mu}}{1+1.97\sqrt{\mu}}+\frac{2\sqrt{\mu}}{1+1.15\sqrt{\mu}}$ to zero.	6–10	10.38	.981	.431	Fluoride (colorimetric) at 1118 days. Theoretical slope is A=0.5085.
	6–9	10.34	.789	.310	Do.
Extrapolation of $\sqrt{\mu}$ to zero	6–9	10.37	.544	.737	Fluoride (Colorimetric) at 1118 days. Theoretical slope is 6A=3.051.
Mean and standard deviation of calculated activity products.	6–10	10.33±0.19	----	---	Colorimetric fluoride.
	6–9	10.42±0.04	----	---	Do.

that the data for Ontario fluorite is more in agreement with theory than that for the Illinois fluorite. Also it is apparent that smaller standard deviations and larger correlation coefficients are typical of the Ontario fluorite data where fluoride was measured colorimetrically rather than by electrode. These results indicate that, for even a simple system such as CaF_2–H_2O, equilibrium is reached with great difficulty and minor impurities can cause significant errors which may also help explain the discrepancies among the results of earlier investigations.

In summary we believe the pK_{s0} of 10.58 obtained from colorimetric analyses of Ontario fluorite solutions to be the most accurate. The very small standard deviation of ± 0.01 does not reflect the standard deviations of ± 10 percent for the determinations of calcium by atomic absorption and fluoride by colorimetry. In order to gage the magnitude of the effects of calcium and fluoride analytical error on the final pK_{s0} obtained from such data, mean pK_{s0} values were calculated from calcium and fluoride data that were raised or lowered by the 10-percent standard deviation. At one extreme, positive errors of 10 percent in both calcium and fluoride would give a pK_{s0} of 10.47 for Ontario fluorite. At the other extreme, negative errors of 10 percent in both species would yield a pK_{s0} of 10.73. It can be shown that the standard deviation of pK_{s0} is ± 0.17 so that, on the basis of possible analytical error, $pK_{s0} = 10.58 \pm 0.17$.

REFERENCES CITED

Brown, Eugene, Skougstad, M. W., and Fishman, M. J., 1970, Methods for collection and analysis of water samples for dissolved minerals and gases: U.S. Geol. Survey Techniques Water Resources Inv., book 5, chap. A1, 160 p.

Butler, J .N., 1964, Ionic equilibrium—a mathematical approach: Palo Alto, Addison-Wesley, Inc., 547 p.

Christ, C. L., Hostetler, P. B., and Siebert, R. M., 1974, Stabilities of calcite and aragonite: U.S. Geol. Survey Jour. Research, v. 2, no. 2, p. 175–184.

Hamer, W. J., 1968, Theoretical mean activity coefficients of strong electrolytes in aqueous solutions from 0 to 100°C: Natl. Bur. of Standards, Natl. Standard Reference Data Ser., Pub. 24, 271 p.

Helgeson, H. C., 1969, Thermodynamics of hydrothermal systems at elevated temperatures and pressures: Am. Jour. Sci., v. 267, p. 729–804.

International Association of Geochemistry and Cosmochemistry, 1975, Report of the international cooperative study on water analysis, sample no. 6: IAGC Working Group on the Geochemistry of Natural Waters, 31 p.

Klotz, I. M., 1964, Chemical thermodynamics: New York, W. A. Benjamin, Inc., 468 p.

Latimer, W. M., 1952, Oxidation potentials [2d ed.]: Englewood Cliffs, N.J., Prentice Hall, 393 p.

Lingane, J. J., 1967, A study of the lanthanum fluoride membrane electrode for end point detection in titrations of fluoride with thorium, lanthanum, and calcium: Anal. Chemistry, v. 39, p. 881–887.

Linke, W. F., 1958, Solubilities of inorganic and metal-organic compounds, v. 1 [4th ed.]: Princeton, N.J., D. Van Nostrand Co., 1,487 p.

Mougnaud, M. P., 1931, Sur le dosage du fluor: Acad. Sci. Comptes Rendus, v. 192, p. 1.733–1.735.

Roberson, C. E., and Schoen, Robert, 1973, Fluorite equilibria in thermal springs of the Snake River Basin, Idaho: U.S. Geol. Survey Jour. Research, v. 1, no. 3, p. 367–370.

Sillen, L. G., and Martell, A. E., 1964, Stability constants of metal-ion complexes: Chem. Soc. [London] Spec. Pub. 17, 754 p.

Smyshlyaev, S. I., and Edeleva, N. P., 1962, Determination of solubility of minerals. I. The solubility product of fluorite: Vyssh. Izv., Ucheb. Zaxedneiy Izv., Khim. Tekhunologia, v. 5, p. 870–874; abs, *in* Chem. Abs., 1963. 58:12010b.

Stephen, H., and Stephen, T., 1964, Solubilities of inorganic and organic compounds, v. 2: New York, The MacMillan Co., 768 p.

Strubel, Gunther, 1965, Quantitativ Untersuchungen uber die hydrothermale Loslichkeit von Flusspat (CaF_2): Neues Jahrb. Mineralogie Monatsh., p. 83–95.

Jour. Research U.S. Geol. Survey
Vol. 5, No. 4, July–Aug. 1977, p. 519–527

BENTHIC INVERTEBRATES IN AN ARCTIC MOUNTAIN STREAM, BROOKS RANGE, ALASKA

By K. V. SLACK, J. W. NAUMAN, and L. J. TILLEY,
Menlo Park, Calif., Anchorage, Alaska, Menlo Park, Calif.

Abstract.—A 1-day, late-summer reconnaissance of the Dietrich River, Alaska, determined species composition and diversity of benthic invertebrates and examined the correlation between stream order and invertebrate distribution. Benthic invertebrates were collected by dip net, drift net, and 10-rock collections, and results were combined for each station. Forty-nine taxa were identified from 5 stations representing stream orders 1 through 5. Aquatic insects comprised 88 percent of all taxa and 97 percent of all individuals from the Dietrich River. Diptera, especially Chironomidae, was the most abundant, followed by Plecoptera. Diamesinae was abundant at the headwaters, decreasing downstream; Orthocladiinae exhibited the reverse distribution pattern. Diversity of collections generally increased downstream. The station collections were compared using coefficients of similarity, cluster analysis, and taxonomy. Collections from adjacent stations were most similar and similarity decreased with increasing distance. The fauna was tentatively divided into zones with characteristic communities: a Diamesinae-Simuliidae fauna in zone I (stream order 1), zone II, a region of transition (orders 2–4), and an Orthocladiinae-Plecoptera-Ephemeroptera fauna in zone III (order 5). The fauna compares closely with that of other arctic streams. Although not conclusive, the benthic invertebrate results are consistent with the hypothesis that stream order is related to lotic biological communities.

Knowledge of arctic limnology is increasing at an unprecedented rate, although our understanding of streams has lagged that of standing waters (Hobbie, 1973). Despite the research that has accompanied recent resource development in Alaska, little predevelopment baseline information is available for the more than 300 streams crossed by the trans-Alaska pipeline corridor (Nauman and Kernodle, 1974). Limitations of time and logistics generally have precluded intensive studies in these remote areas. The present investigation was conducted to test the value of a 1-day reconnaissance of the benthic invertebrate fauna of an arctic stream. The specific objectives were to evaluate a 1-day reconnaissance trip by determining species composition and diversity of benthic invertebrates in the Dietrich River and examining the correlation between stream order and faunal distribution. Results of this synoptic view of the structure and distribution of the benthos in late summer (August 23, 1971) are compared with results from more intensive investigations of arctic streams. This study contributes to the meager baseline information available for the Dietrich River basin prior to road and pipeline construction.

Sampling was designed on the basis of stream order, a system in which the smallest headwater streams are designated order 1, the junction of two order-1 streams forms an order-2 segment, and so on (Horton, 1945; Strahler, 1957). When any two streams of the same order join, they form a stream of the next higher order. The rank of a stream segment is not increased by the junction of lower order streams. Because order is related to many other properties of drainage basins (Leopold, and others, 1964), stream order has been proposed as an objective basis for classifying streams in biological studies (Abell, 1961; Kuehne, 1962, 1970).

Acknowledgments.—We gratefully acknowledge the technical assistance of S. S. Hahn and H. E. Jeavons in processing the benthic samples and R. J. Madison for nutrient analyses. We are indebted to the following taxonomic specialists for classifying specimens: Dr. H. Daly, Ephemeroptera, Tipulidae; V. Landwehr, Collembola; Dr. E. D. Mitchell, aquatic Acarina; Dr. B. V. Peterson, Simuliidae; and Dr. O. A. Saether, Chironomidae.

SETTING

The study area is in the Arctic Mountains Physiographic province, 64 km north of Wiseman, Alaska, or about 390 km north of Fairbanks. This is the northern limit of the interior white spruce-birch forest (Sigafoos, 1958). An open forest of white spruce, birch, cottonwood, alder, and willow extends up the Dietrich River to above station 4 (fig. 1), but

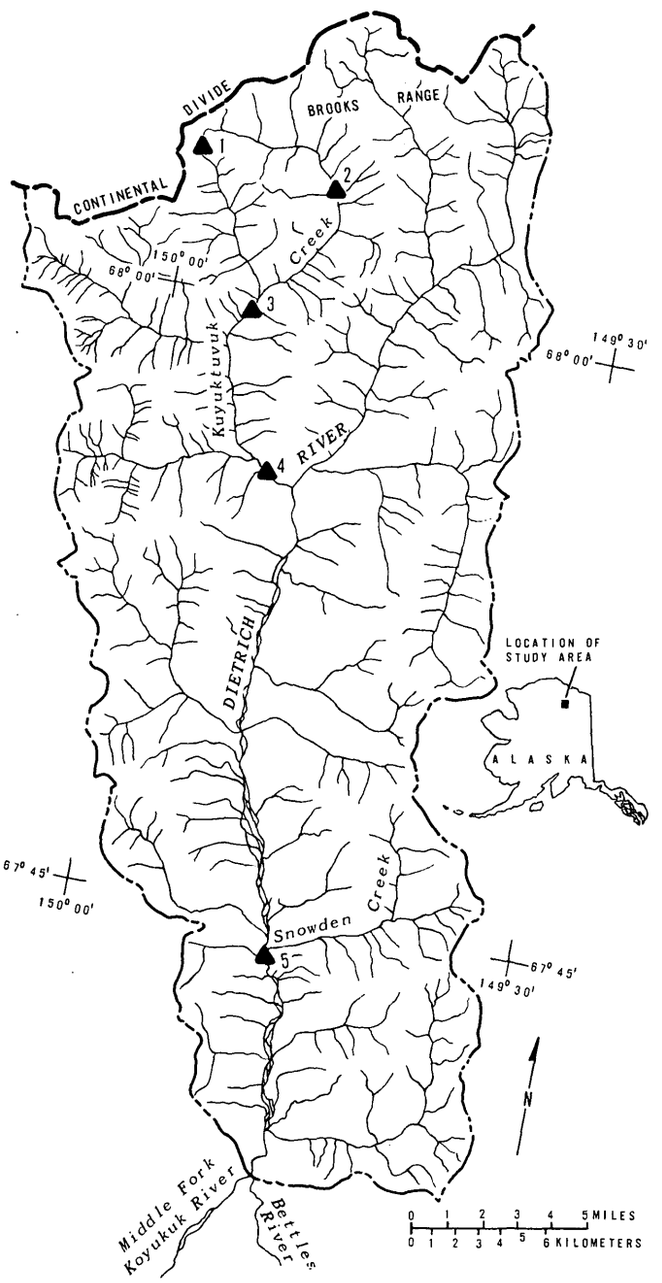

FIGURE 1.—Location of study area and map of Dietrich River drainage basin with sampling stations (solid triangles).

the flood plain is largely bare of plants because of the meandering of the braided channel (Sigafoos, 1972). Upstream from station 4, alpine vegetation prevails. Bedrock, of Late Devonian age, consists of slate, phyllite, and siltstone with scattered exposures of dolomite and limestone (Ferrians, 1971; Kachadoorian, 1971). Pleistocene glacial erosion widened and straightened the valleys into U-shaped cross profiles with steep walls and broad gentle floors (Wahrhaftig, 1965). Winters are dark and cold, but summers are mild. Air temperature during the 12-hr study ranged between 7° and 15°C, and day length was approximately 16 hr. Day length varies from 53 days of continuous sunlight (May 27 to July 18) to 28 days of darkness (December 8 to January 4) (U.S. Department of Commerce, 1970).

The Dietrich River is a fifth order stream in the Yukon drainage basin. It arises south of the Continental Divide in the east central Brooks Range at an altitude of 2041 m above sea level. The headwaters consist of an east branch, the Dietrich River proper, and a west branch, Kuyuktuvuk Creek. For convenience the Dietrich River name will be used to designate the stream studied, including that part on Kuyuktuvuk Creek (fig. 1). The Dietrich River is a typical mountain stream as described by Craig and McCart (1975). Throughout its length, the river may be classified as rhithron (Illies and Botosaneau, 1963). Characteristics of the sampling stations are shown in table 1.

METHODS

Tentative sampling locations representing stream orders 1 through 5 were selected on maps, U.S. Geological Survey topographic quadrangle maps, Philip Smith Mountains and Chandalar quadrangles, scale, 1:250,000, but final sites were selected from a helicopter. Although much of the channel was braided, each station was located where flow was consolidated into a single channel. Time permitted sampling only one stream of each order. The uppermost station, designated order 1, was the most headward reach of continuous flow. When the other stations were plotted

TABLE 1.—*Characteristics of sampling stations, Dietrich River, Alaska, August 23, 1971*
[Gradient, discharge, width, and depth data were estimated]

Station	Stream order	Drainage area (km^2)	Elevation (m)	Gradient [1] (m/km)	Discharge (m^3/s)	Width (m)	Depth (m)
1	1	0.1	1524	ca. 300	0.05	1.6	0.055
2	2	31	915	30	0.5	4.5	.12
3	4 (upper)	90	716	19	1.4	11	.22
4	4 (lower)	223	591	7	2.7	12	.22
5	5	770	462	3	3.5	15	.46

[1] Determined using the nearest upstream and downstream contours on the 1:63,360-scale map (30.4-m contour interval).

on 1:63,360-scale maps, which became available after field work was completed, the original order-3 stream was found to be order 4 and no order-3 stream was sampled.

Chemical properties were determined by the methods of Brown, and others (1970). Samples for total carbon and total organic carbon were preserved with mercuric chloride and analyzed in the U.S. Geological Survey laboratory in Harrisburg, Pa. Water temperature, dissolved oxygen, specific conductance and pH were determined with a Martek Mark II Portable Water Quality Monitor with the sensors placed near midstream.

Benthic invertebrates were collected by three methods at each station. First, a 1-hr drift-net sample was obtained upstream from the area disturbed by other sampling. The net was equipped with nylon screen cloth (Nitex) netting with 471-μm mesh and had a 30×30-cm opening perpendicular to the current. The bottom of the net frame was in contact with the stream bed, and the top extended above the water surface. McLay (1970) and Elliott (1971) showed that organisms in the drift are not carried from far upstream, but as the distance upstream from the sampling point increases, each unit area of bottom contributes a progressively smaller proportion of drifting invertebrates to the total catch. Consequently, drift organisms are assumed to have originated in the same type of environment sampled by the other methods. Second, the stone-dwelling fauna was collected from ten streambed rocks, about 10 to 20 cm in diameter, lifted at random. As each rock was lifted off the bottom it was enclosed in a net to minimize loss of organisms. The rocks were scrubbed with a brush in a bucket of water, and the residue concentrated on a U.S. Standard no. 70 sieve (210-μm mesh). Finally, a D-shaped dip net of nylon screen cloth with 210-μm mesh was used to collect from the major aquatic habitats. Collecting was conducted for 45 min, and the effort in each habitat was approximately in proportion to the amount of that habitat present. For maximum uniformity, all 10-rock and dip-net collections were made by the same individual.

Preserved samples were sorted in the laboratory using the sugar flotation method (Anderson, 1959), and the residue was examined under a dissecting microscope to recover organisms missed. Because the taxonomy of Alaskan freshwater invertebrates is poorly known, it was not possible to assign specific names to many specimens. However, organisms, especially insects, were separated and enumerated to taxa that as nearly as possible correspond to species. Collembola were included because they were locally abundant at the stream margins, and because this group may be important in the aquatic fauna at high latitudes (Folsom, 1919; Mani, 1962; Elgmork and Saether, 1970; Watson, Davis, and Hanson, 1966).

The results of the individual collecting methods were reported by Slack and others, (1976). For this study, however, the data were combined to obtain a total faunal list for each station. Each combined list is considered to be fairly representative of the community at the site of collection, but the extent of the community is not known. It seems best, therefore, to treat each collection as an entity and not as a random sample from a larger parent population (Pielou, 1969). Because the collections differ in size, percentage composition is a convenient basis for comparison.

The essential properties of the collections are the numbers of taxa and their relative abundances. These descriptive properties can be expressed in terms of diversity and evenness (Pielou, 1969). A collection has high diversity if it has many taxa and their abundances are fairly even; diversity is low when the taxa are few and their abundances uneven. Diversity index values in table 4 were calculated using the formula of Brillouin (1962) expressed in bits. Evenness is the ratio of the calculated diversity of a collection to the maximum diversity it could have given the same number of taxa. Maximum evenness is attained when the individuals are divided equally among the taxa (Pielou, 1969).

RESULTS AND DISCUSSION

Environmental Conditions

Tables 2 and 3 show the composition of the stream water during the study. The concentration of dissolved ions increased downstream. Between the order-1 and the order-5 stations, specific conductance increased by a factor of 3.5. The water is a calcium bicarbonate type, and the major cations, in order of decreasing weight concentrations, are calcium, magnesium, sodium, and potassium. The ratios of the cations are nearly constant in downstream order. Of the anions other than bicarbonate, sulfate was most abundant, and its relative abundance increased downstream. Dissolved oxygen was near saturation, and pH ranged from 8.2 to 8.6. Combined nitrogen was relatively abundant (table 3). Nitrate-N was of uniform concentration except for an increase at station 5. There was a shift from organic nitrogen in the headwaters to ammonia downstream. Combined phosphorus was not detected. Both total carbon and total organic carbon increased downstream.

As would be expected for low-flow conditions, seston concentrations were low at all stations, averaging 0.3

TABLE 2.—*Field determinations of water properties, Dietrich River, Alaska, August 23, 1971*

Station	Time[1]	Temperature (°C)	pH	Alkalinity (mg/L)	Dissolved oxygen		Specific conductance (μmho/cm at 25°C)
					Milligrams per liter	Percent	
1	1400	2	8.4	68	11.4	95	120
2	1200	5	8.2	108	11.2	97	185
3	1600	7	8.3	166	10.8	97	310
4	1900	8	8.3	172	10.7	98	380
5	0900	6	8.6	206	11.4	97	420

[1] Alaska daylight time.

TABLE 3.—*Chemical properties of Dietrich River, Alaska, August 23, 1971*

[Concentrations in miligrams per liter]

Station	Time[1]	Calcium	Magnesium	Sodium	Potassium	Bicarbonate	Sulfate	Nitrate (N)	Nitrite (N)	Ammonia (N)	Organic nitrogen (N)	Dissolved ortho-phosphorus (P)	Total phosphorus (P)	Particulate phosphorus (P)	Total carbon[2]	Total organic carbon
1	1400	16	4.6	1.4	0.3	68	6.0	0.2	[3]0	0	0.37	[3]0	[3]0	[3]0	16	1.5
2	1200	21	10	2.2	0.3	108	12	0.2	0	0	.63	0	0	0	31	1.5
3	1600	26	20	8.8	0.6	166	24	0.2	0	.02	.03	0	0	0	34	2
4	1900	42	19	6.3	0.4	172	60	0.2	0	.17	0	0	0	0	34	5
5	0900	52	22	4.2	0.4	206	65	0.5	0	.50	0	0	0	0	38	3

[1] Alaska daylight time.
[2] Total carbonaceous content, including carbon dioxide, alkalinity, and organic carbon.
[3] Not detected.

mg/L total dry weight, 0.2 mg/L inorganic (ash) dry weight, and 0.1 mg/L organic (ash-free) dry weight. Seston values were highest at station 1, intermediate at station 5, and minimal at the intervening stations. The organic fraction ranged from 49 percent at station 1 to 14 percent at station 3. The highest seston concentrations near the stream source apparently resulted from the abundant filamentous alga, *Hydrurus foetidus* which covered rocks in the swiftest current. The alga decreased in abundance downstream. No aquatic macrophytes were found.

Community Structure and Distribution

A total of 49 taxa were identified in the Dietrich River collections, and their abundance and distribution are shown in table 4. Aquatic insects comprised 88 percent of the taxa and 97 percent of the individuals. Diptera was the most abundant order and Chironomidae the most abundant family. The distribution of the fauna can be described in terms of seven of the most abundant groups which together include 73 percent of the taxa and 96 percent of the individuals (figs. 2 and 3). The Chironomidae, of which two subfamilies are designated groups 1 and 2 in the figures, comprised an average of 50 percent of all taxa at the stations. As shown in figs. 2 and 3, the subfamily Diamesinae was abundant at the headwaters and decreased downstream while the Orthocladiinae exhibited the reverse pattern of disbribution. The second most abundant order was Plecoptera which was found in greatest numbers at stations 2 through 4. Thus two insect groups, Chironomidae and Plecoptera, constituted 47 percent of the total number of taxa and 91 percent of the individuals in the collections. The remaining groups were relatively insignificant in abundance. Ephemeroptera and aquatic Acari increased downstream in number of taxa and individuals, whereas Collembola and Oligochaeta decreased downstream.

Diversity and evenness

Diversity and eveness values were lowest at station 4 and highest at station 5, but the range was small. Diversity ranged from 2.60 to 2.98, and evenness ranged from 0.570 to 0.700. Values for other streams are not available for comparison because, as Hughes (1975) showed, diversity may be compared only if sampling methods are the same. Although diversity of the Dietrich River collections increased downstream, except for station 4, neither diversity nor evenness was informative of the considerable qualitative differences between the stations.

Relative similarity and faunal zonation

The degree of taxonomic similarity among the collections was tested by calculating a coefficient of similarity for all combinations of collections using the following expression (Sørensen, 1948):

$$S = \frac{2C}{A+B}$$

where A = number of taxa in collection A,
B = number of taxa in collection B, and
C = number of taxa both collections have in common.

TABLE 4.—*Benthic invertebrates collected by all methods, Dietrich River, Alaska, August 23, 1971*

Organism	Station 1	2	3	4	5
Insecta :					
Diptera :					
Chironomidae :					
Diamesinae :[1]					
Diamesa latitarsis[2]	586	34	16	28	4
Diamesa III	232	93	50	6	----
Diamesa cinerella	199	4	----	1	----
Diamesa nivoriunda	178	9	2	1	----
Diamesa steinböcki	59	5	4	----	----
Diamesa; nr. Colorado, sp. B, Saether (1970)	32	3	14	77	5
Pseudokiefferiella	----	----	1	----	----
Other[3]	12	4	6	4	2
Podonominae :					
Trichotanypus	----	1	----	----	----
Orthocladiinae :[1]					
Eukiefferiella sp.	----	132	178	231	23
Eukiefferiella cyanea	----	44	69	17	67
Eukiefferiella bavarica	----	3	26	5	20
Orthocladius (*Euorthocladius*) I	6	99	5	13	----
Orthocladius (*Euorthocladius*) II	3	7	2	----	2
Orthocladius (*Eurothocladius*) III	----	----	5	2	----
Orthocladius s. str.	----	----	----	1	26
Orthoclaudius sp.	----	----	----	----	1
Parakiefferiella sp.	----	4	----	6	1
Chaetocladius I	1	----	3	----	5
Chaetocladius II	1	----	----	----	----
Other[3]	7	9	23	9	2
Simuliidae :					
Gymnopais dichopticus	116	----	----	----	----
Prosimulium sp.	----	----	----	1	----
Empididae	----	----	1	1	----
Deuterophleblidae	----	----	----	1	----
Tipulidae					
Tipula	----	----	3	1	----
Dicranota	----	1	4	----	1
Heleidae	2	1	----	----	----
Phoridae	----	----	----	----	1
Plecoptera :[1]					
Nemoura spp.	27	253	151	180	54
Capniinae	8	41	11	19	1
Arcynopteryx	----	----	----	----	1
Paraperla or *Utaperla*	----	----	2	5	1
Ephemeroptera :[1]					
Immature Heptageniidae	----	----	----	----	13
Cinygmula	----	1	----	1	----
Iron	----	----	1	----	----
Pseudocloeon	----	----	1	5	----
Baetis	----	----	----	----	1
Ameletus	----	----	----	----	1
Ephemerella (group Serrata)	----	----	----	----	2
Collembola :[1]					
Agrenia bidenticulata	31	----	2	----	----
Hypogastrura nivicola	16	----	----	2	----
Isotoma virdis(?)	1	1	----	----	----
Trichoptera :					
Neothrema	----	----	----	----	4
Coleoptera					
Dytiscidae	----	----	----	----	1
Acarina :[1]					
Sperchon sp.	----	2	5	12	4
Sperchon crassipalpus	----	7	7	4	----
Libertia	----	----	----	1	----
Other[3]	----	----	----	4	----
Oligochaeta :[1]					
Enchytraeidae	55	2	5	1	----
Nematoda	----	----	1	----	----
Gordiida	1	----	----	----	----
Total number of individuals	1573	760	598	639	243
Total number of taxa	19	22	26	26	23
Diversity index	2.79	2.84	2.88	2.60	2.98
Evenness	0.666	0.651	0.634	0.570	0.700

[1] Groups included in figures 2 and 3.
[2] Possibly three varieties.
[3] Not included in diversity caculations.

Values for S lie between 0 and 1, and the higher the number the greater the taxonomic similarity between the entities being compared.

Coefficients of similarity for the Dietrich River collections (table 5) show that, in general, collections from adjacent stations had the highest degree of similarity, and the similarity decreased with increasing distance between stations. Collections from stations 3 and 4 had the highest similarity, and those from stations 1 and 5 had the lowest.

TABLE 5.—*Coefficient of similarity* (S) *for benthic invertebrate collections from the 5 stations on the Dietrich River, Alaska, August 23, 1971*

	1	2	3	4	5
1	----	0.634	0.533	0.478	0.293
2	----	----	0.667	0.653	0.500
3	----	----	----	0.679	0.542
4	----	----	----	----	0.449
5	----	----	----	----	----

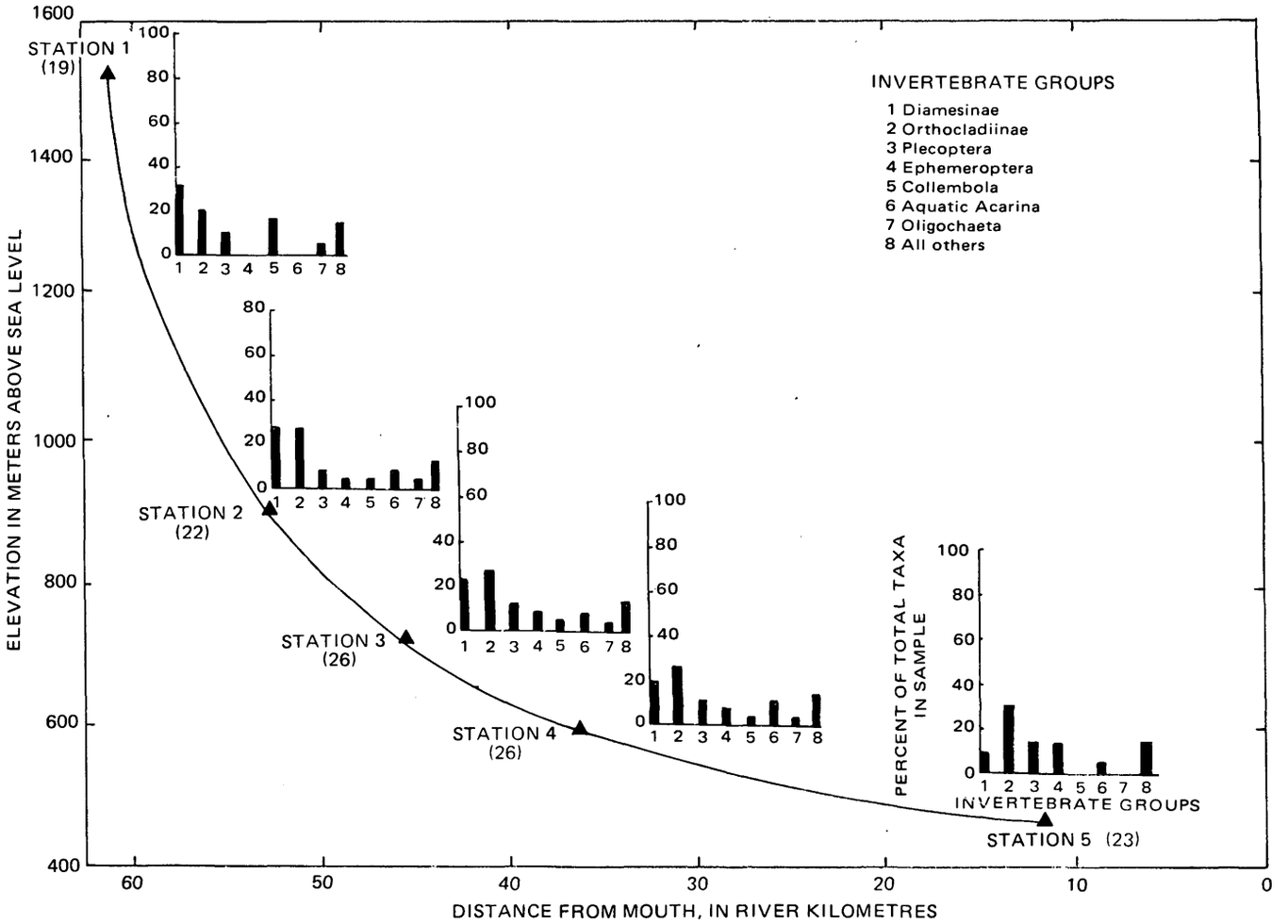

FIGURE 2.—Within-station abundances of taxa of the most common invertebrate groups showing station location and elevation. For each station the number of taxa in each group is plotted as the percentage of the total number of taxa collected at that station. The total number of taxa in the collection appears in parentheses following the station number.

The data in tables 4 and 5 were further examined for evidence of faunal differences between the collections that might be related to stream order. The coefficients of similarity were subjected to cluster analysis using the unweighted pair-group method (Sokal and Sneath, 1963). Visual inspection of the resulting dendrogram (fig. 4) and of the similarity trellis diagram (table 5) suggests a tentative division of the Dietrich River into three faunal zones: I, station 1; II, stations 2, 3, and 4; and III, station 5. Each zone had a characteristic benthic community, all aquatic insects (table 6). In developing the table, taxa which constitute 15 percent or more of the total number of individuals in the collection were defined as dominants. The remaining taxa which constitute at least 5 percent of the total number of individuals were defined as subdominants.

The chironomid subfamily Diamesinae overwhelmingly predominated at faunal zone I. Both dominants and two of the three subdominants belonged to the genus *Diamesa*. The third subdominant was a species of Simuliidae. This community was found in the order-1 stream near the source of flow. The alga, *Hydrurus foetidus*, was abundant, and the subdominant, *D. cinerella*, was reported to be strongly associated with this plant in the Polish High Tatra Mountains (Kownacki, 1971). The dominants of faunal zone II were a chronomid of the subfamily Orthocladiinae and a stonefly. Although the subdominants varied somewhat between the three stations within the zone, all were either Plecoptera or Chironomidae, and both chironomid subfamilies were represented. The dominants of faunal zone III were a species of Orthocladiinae and a stonefly. The subdominants were three Orthocladiinae

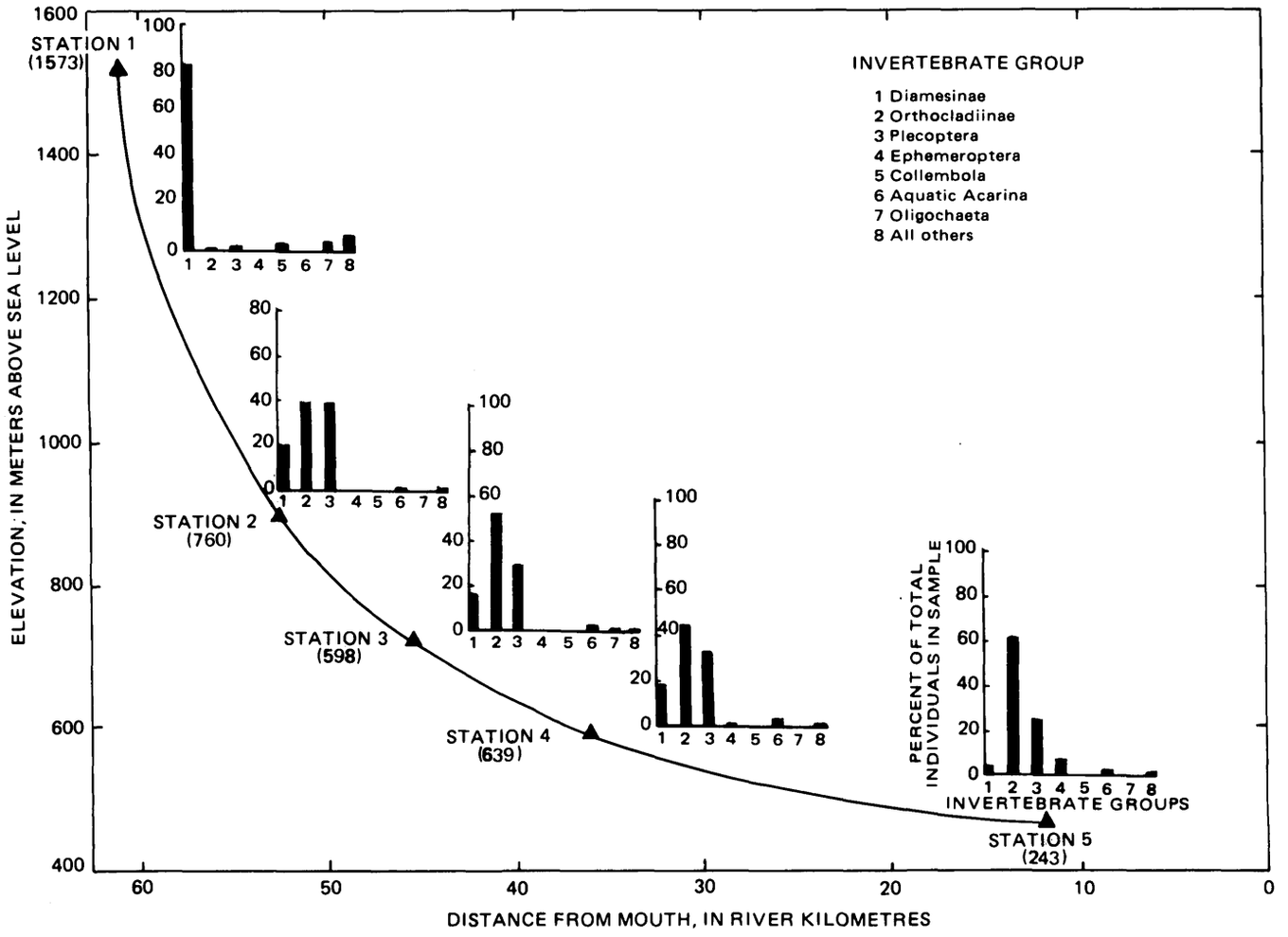

FIGURE 3.—Within-station abundances of individuals of the most common invertebrate groups showing station location and elevation. For each station the number of individuals in each group is plotted as the percentage of the total number of individuals collected at that station. The total number of individuals in the collection appears in parentheses following the station number.

TABLE 6.—*Benthic community zonation in the Dietrich River, Alaska, August 23, 1971*

Zone I (Station 1)	Zone II (Stations 2–4)	Zone III (Station 5)
	Dominants [1]	
Diamesa latitarsis	*Nemoura*-spp.	*Eukiefferiella cynaea*
Diamesa III	*Eukiefferiella* sp.	*Nemoura* spp.
	Subdominants [2]	
Diamesa cinerella	*O.* (*Euorthocladius*) I [3]	*Orthocladius* s. str.
Diamesa nivoriunda	*Diamesa* III [3]	*Eukiefferiella* sp.
Gymnopais dichopticus	*Eukiefferiella cynaea* [3]	*Eukiefferiella bavarica*
	Capniinae [3,4]	Heptageniidae [4]
	Eukiefferiella cynaea [5]	
	Diamesa III [5]	
	Diamesa; nr Colorado sp. B (Saether 1970) [6]	

[1] Taxa constituting 15 percent or more of the total number of individuals in each collection.
[2] Taxa constituting 5 to 14 percent of the total number of individuals in each collection.
[3] At station 2.
[4] Too immature for more adequate identification.
[5] At station 3.
[6] At station 4.

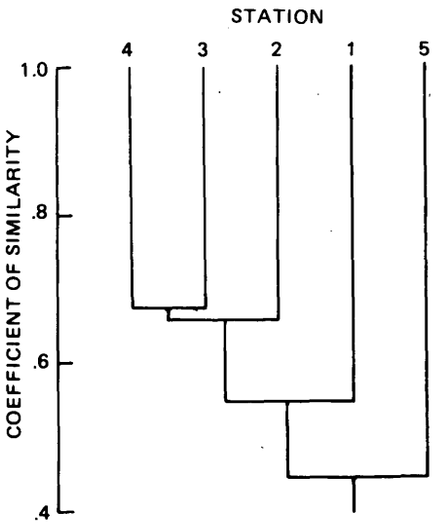

FIGURE 4.—Dendrogram prepared by the unweighted pair-group method with arithmetic averaging showing similarities among Dietrich River benthic invertebrate collections.

taxa and an Ephemeroptera. Thus, a shift in composition of the benthic fauna between the order-1 and order-5 sites is indicated by table 6. The Diamesinae-Simuliidae fauna in zone I (stream order 1) gives way to an Orthocladiinae-Plecoptera-Ephemeroptera fauna in zone III (stream order 5) with zone II being a region of transition spanning stream orders 2 through 4. Because this interpretation is based on limited sampling, both in space and time, further study would be needed to establish the validity and generality of faunal zonation in this stream.

The benthic invertebrate fauna of the Dietrich River as determined in this reconnaissance study compares closely with the fauna of other arctic streams. In Ogotoruk Creek, northwestern Alaska, Chironomidae, Plecoptera, Ephemeroptera, and Oligochaeta were the dominant groups (Watson, Hanson, and others, 1966). In a Canadian arctic stream studied by Hynes and others (1974), Chironomidae comprised 70 to 80 percent of the benthic individuals and Oligochaeta comprised 10 to 20 percent. Moreover, *Diamesa* (Diamesinae) and Orthocladiinae exhibited a tendency toward mutual exclusion similar to that found in the Dietrich River. In mountain streams of the Beaufort Sea drainages, Ephemeroptera, Chironomidae, Plecoptera, and Oligochaeta occurred most frequently (Craig and McCart, 1975). As in the Dietrich River, Trichoptera were rare, occurring in only 1 percent of the samples from mountain streams. The similarity between the Dietrich River fauna and the faunas of more intensively studied streams in the North American arctic lends confidence to the present results.

CONCLUSION

Stream order is a reasonable model for describing the results of physical and chemical sampling in the Dietrich River (tables 2 and 3). Although not conclusive, the benthic invertebrate results are consistent with the hypothesis that stream order is related to lotic biological communities. The collections generally increased in diversity between the order-1 and the order-5 streams (table 4), a result in agreement with findings for benthic invertebrates and fish in temperate-region streams (Kuehne, 1962; Panitz, 1964; Harrel, and others, 1967; Harrel and Dorris, 1968; Lotrich, 1973). The preliminary evidence for faunal zonation in the Dietrich River also seems to be consistent with stream order. Although sampling was not adequate to establish a correlation between stream order and benthic invertebrate communities, the results are suggestive that such a relationship may exist.

The 1-day reconnaissance provided useful information about the benthic fauna of the Dietrich River in its pristine state. Since that visit, the drainage basin has been traversed by a road and an oil pipeline. The results of this study may have additional value as irreplaceable baseline data. Development of the arctic will continue to outstrip the ability of scientists to conduct traditional research in affected areas prior to impact. To supplement traditional research, improved methods are needed for rapid reconnaissance investigations. If future research demonstrates the general applicability of stream order, or some other objective approach to stream ecology, it will be of great value in the design of sampling and monitoring networks in remote areas of the arctic.

REFERENCES CITED

Abell, D. G., 1961, The role of drainage analysis in biological work on streams: Internat. Vereinigung Limnologie Verh., v. 14, p. 533–537.

Anderson, R. O., 1959, A modified flotation technique for sorting bottom fauna samples: Limnolgy and Oceanography, v. 4, p. 223–225.

Brillouin, L., 1962, Science and information theory: Academic Press, New York, 351 p.

Brown, E., Skougstad, M. W., and Fishman, M. J., 1970, Methods for collection and analysis of water samples for dissolved minerals and gases: U.S. Geol. Survey Techniques Water-Resources Inv., book 5, chap. A1, 160 p.

Craig, P. C., and McCart, P. J., 1975, Classification of stream types in Beaufort Sea Drainages between Prudhoe Bay and the Mackenzie Delta, N.W.T., Canada: Arctic Alpine Res., v. 7, p. 183–198.

Elgmork, K., and Saether, O. A., 1970, Distribution of invertebrates in high mountain brook in the Colorado Rocky Mountains: Univ. Colorado Studies, Series in Biol. no. 31, p. 1–55.

Elliott, J. M., 1971, The distances traveled by drifting invertebrates in a Lake District stream: Oecologia (Berlin, Springer-Verlag), v. 6, p. 350–379.

Ferrians, O. J., Jr., 1971, Preliminary engineering geologic maps of the proposed trans-Alaska pipeline route—Phillip Smith Mountain quadrangle: U.S. Geol. Survey Open-File Rept. 71–492, 2 sheets.

Folsom, J. W., 1919, Collembola of the Canadian Arctic Expedition 1913–18: Report of the Canadian Arctic Expedition, v. 3, part A, Collembola: p. 1–29.

Harrel, R. C., Davis, B. J., and Dorris, T. C., 1967, Stream order and species diversity of fishes in an intermittent Oklahoma stream: Am. Midland Naturalist, v. 78, p. 428–436.

Harrel, R. C., and Dorris, T. C., 1968, Stream order, morphometry, physico-chemical conditions, and community structure of benthic macroinvertebrates in an intermittent stream system: Am. Midland Naturalist, v. 80, p. 220–251.

Hobbie, J. E., 1973, Arctic limnology—A review, *in* Britton, M. E., ed., Alaskan arctic tundra: Arctic Inst. North America Tech. Paper, no. 25, p. 127–168.

Horton, R. A., 1945, Erosional development of streams and their drainage basins; hydrophysical approach to quantitative morphology: Bull. Geological Soc. Am., v. 56, p. 275–370.

Hughes, B. D., 1975, A comparison of four samplers for benthic macro-invertebrates inhabiting coarse river deposits: Water Research, v. 9, p. 61–69.

Hynes, H. B. N., Kaushik, N. K., Lock, M. A., Lush, D. L., Stocker, Z. S. J., Wallace, R. R., and Williams, D. D., 1974, Benthos and allochthonous organic matter in streams: Fisheries Research Board Canada Jour., v. 31, p. 545–553.

Illies, J., and Botosaneau, L., 1963, Problemes et methodes de la classification et de la zonation ecolgique des eaux courantes, considerees surtout de point de vue faunistique: Internat. Vereinigung Limnologie Mitteilungen, no. 12, 57 p.

Kachadoorian, Reuben, 1971, Preliminary engineering geologic maps of the proposed trans-Alaska pipeline route—Wiseman and Chandlar quadrangles: U.S. Geol. Survey Open-File Rept. 71–486, 2 sheets.

Kownacki, A., 1971, Taxocens of Chironomidae in streams of the Polish High Tatra Mountains: Acta Hydrobiologia, v. 13, p. 439–464.

Kuehne, R. A., 1962, A classification of streams illustrated by fish distribution in an eastern Kentucky creek: Ecology, v. 43, p. 608–614.

——— 1970, Applications of the Horton stream classification to evaluate faunal studies, *in* Weist, W. G., Jr., and Greeson, P. E., eds., Hydrobiology—Bioresources of shallow water environments: Am. Water Resources Assoc., Proc. Ser. no. 8, p. 367–370.

Leopold, L. B., Wolman, M. G., and Miller, J. P., 1964, Fluvial processes in geomorphology: W. H. Freeman and Co., San Francisco, 522 p.

Lotrich, V. A., 1973, Growth, production, and community composition of fishes inhabiting a first-, second-, and third-order stream of eastern Kentucky: Ecological Monogr., v. 43, p. 377–397.

Mani, M. S., 1962, Introduction to high altitude entomology—Insect life above the timber-line in the North-West Himalaya: London, Methuen and Co., 302 p.

McLay, C., 1970, A theory concerning the distance travelled by animals entering the drift of a stream: Fisheries Research Board Canada Jour., v. 27, 359–370.

Nauman, J. W., and Kernodle, D. R., 1974, Aquatic organisms from selected sites along the proposed trans-Alaska pipeline corridor September 1970 to September 1972: U.S. Geol. Survey open-file rept., 23 p.

Panitz, Eric, 1964, Physical, chemical, and biological data illustrating a stream classification system: Trans. Kentucky Acad. Sci., v. 25, p. 58–64.

Pielou, E. C., 1969, An introduction to mathematical ecology: John Wiley and Sons, New York, 286 p.

Saether, O. A., 1970, Chironomids and other invertebrates from North Boulder Creek, Colorado: Univ. Colorado Studies, Ser. in Biol. no. 31, p. 57–114.

Sigafoos, R. S., 1958, Vegetation of northwestern North America, as an aid in interpretation of geologic data: U.S. Geol Survey Bull. no. 1061E, p. 165–185.

——— 1972, Vegetation, p. 113–145, *in* Environmental impact statement, proposed trans-Alaska pipeline, vol. 2, Environmental setting of the proposed trans-Alaska pipeline system: U.S. Dept. Interior. Available NTIS PB–206–921–2.

Slack, K. V., Nauman, J. W., and Tilley, L. J., 1976, Evaluation of three collecting methods for a reconnaissance of stream benthic invertebrates: U.S. Geol. Survey Jour. Research, v. 4, no. 4, p. 491–495.

Sokal, R. R., and Sneath, P. H. A., 1963, Principles of numerical taxonomy: W. H. Freeman, San Francisco, 359 p.

Sørensen, T., 1948, A method of establishing groups of equal amplitude in plant sociology based on similarity of species content and its application to analyses of the vegetation on Danish commons: Kongelige Danske Videnskabernes Selskab, Biologiske Skrifter, v. 5, no. 4, p. 1–34.

Strahler, A. N., 1957, Quantitative analysis of watershed geomorphology: Trans. Am. Geophys. Union, v. 38, p. 913–920.

U.S. Department of Commerce, 1970, Tide tables, high and low water predictions, 1971, west coast of North and South America, including Hawaiian Islands: U.S. Dept. Commerce, ESSA, Coast and Geodetic Survey, 226 p.

Wahrhaftig, C., 1965, Physiographic divisions of Alaska: U.S. Geol. Survey Prof. Paper no. 482, 52 p.

Watson, D. G., Davis, J. J., and Hanson, W. C., 1966, Terrestrial invertebrates, *in* Wilimovsky, N. J. and Wolfe, J. N., eds., Environment of the Cape Thompson Region, Alaska: U.S. Atomic Energy Commission, PNE–481, p. 565–584.

Watson, D. G., Hanson, W. C., Davis, J. J., and Cushing, C. E., 1966, Limnology of tundra ponds and Ogotoruk Creek, *in* Wilimovsky, N. J., and Wolfe, J. N., eds., Environment of the Cape Thompson Region, Alaska: U.S. Atomic Energy Commission, PNE–481, p. 415–435.

RECENT PUBLICATIONS OF THE U.S. GEOLOGICAL SURVEY

The following books may be ordered from the Branch of Distribution, U.S. Geological Survey, 1200 South Eads Street, Arlington, VA 22202 (an authorized agent of the Superintendent of Documents, Government Printing Office). Prepayment is required. Remittances should be sent by check or money order payable to U.S. Geological Survey. Give series designation and number, such as Bulletin 1368–A, and the full title. Prices of Government publications are subject to change. Increases in costs make it necessary for the Superintendent of Documents to increase the selling prices of many publications offered. As it is not feasible for the Superintendent of Documents to correct the prices manually in all the previous announcements and publications stocked, the prices charged on your order may differ from the prices printed in the announcements and publications.

Professional Papers

P 440–KK. Chapter KK. Compilation of stable isotope fractionation factors of geochemical interest, by Irving Friedman and J. R. O'Neil. 1977. p. KK1–KK12; 49 figs. $2.30. (Professional Paper 440 issued as separate chapters under the general title Data of geochemistry, sixth edition, Michael Fleischer, technical editor.)

P 486–I. Analog simulation of the ground-water system. Yuma, Arizona, by E. P. Patten, Jr. 1977. p. I1–I10; plate in pocket. $1.35.

P 715–B. Combined ice and water balances of Maclure Glacier, California, South Cascade Glacier, Washington, and Wolverine and Gulkana Glaciers, Alaska, 1967 hydrologic year, by W. V. Tangborn, L. R. Mayo, D. R. Scully, and R. M. Krimmel. 1977. p. B1–B20; plates in pocket. $3.90.

P 743–E. Stratigraphic distribution of species of the megaspore genus *Minerisporites* in North America, by R. H. Tschudy. 1976. p. E1–E11; 4 plates. 75¢.

P 835. Quaternary geology of Alaska, by T. L. Péwé. 1975. 145 p.; plate in pocket. $4.60. (Reprint).

P 867–B. Stratigraphy of post-Paleozoic rocks and summary of resources in the Carlin-Pinon Range area, Nevada, by J. F. Smith, Jr., and K. B. Ketner, *with a section on* Aeromagnetic survey, by D. R. Mabey. 1976. p. B1–B48; plate in pocket. $2.50.

P 897. Geology of the western Romanzof Mountains, Brooks Range, northeastern Alaska, by E. G. Sable. 1977. 84p.; plates in pocket. $4.25.

P 902. Precambrian geology of the United States; An explanatory text to accompany the Geologic Map of the United States, by P. B. King. 1976 (1977). 85 p. $2.

P 920. Metamorphism and plutonism around the middle and south forks of the Feather River, California, by Anna Hietanen. 1976 (1977). 30 p.; plate in pocket. 95¢.

P 934. Paleozoic origin of the cycads, by S. H. Mamay, 1976 (1977). 48 p.; 5 plates. $1.65.

P 935–A. The eruption of August 1963 and the formation of Alae lava lake, Hawaii, by D. L. Peck and W. T. Kinoshita, 1976 (1977). p. A1–A33. $1.15.

P 939. Artificial recharge to a freshwater-sensitive brackish-water sand aquifer, Norfolk, Virginia, by D. L. Brown and W. D. Silvey. 1977. 53 p. $1.70.

P 959–H. Alluvial ilmenite placer deposits, central Virginia, by J. P. Minard, E. R. Force, and G. W. Hayes, 1976 (1977). p. H1–H15; plate in pocket. $1.95.

P 971. Structural geology of the Confusion Range, west-central Utah, by R. K. Hose. 1977. 9 p.; plate in pocket. $1.80.

P 980. Effects of the catastrophic flood of December 1966, north rim area, eastern Grand Canyon, Arizona, by M. E. Cooley, B. N. Aldridge, and R. C. Euler. 1977. 43 p.; plate in pocket. $2.70.

P 982. Analog-model analysis of regional three-dimensional flow in the ground-water reservoir of Long Island, New York, by R. T. Getzen. 1977. 49 p. $1.35. (Supersedes Open-File Report 75–617.)

P 985. Biostratigraphy and regional relations of the Mississippian Leadville Limestone in the San Juan Mountains, southwestern Colorado, by A. K. Armstrong and B. L. Mamet. 1976 (1977). 25 p.; 3 plates; plate 3 in pocket. $1.95.

P 989. Plutonism and orogeny in north-central Washington—timing and regional context, by K. F. Fox, Jr., C. D. Rinehart, and J. C. Engels. 1977. 27 p. 75¢.

P 1000. Geological Survey research 1976. 1976 (1977). 414 p. $5.50.

P 1006–A, B. Demand and supply of nonfuel minerals and materials for the United States energy industry, 1975–90—A preliminary report. A, Demand for nonfuel minerals and materials by the United States energy industry, 1975–90, by J. P. Albers, W. J. Bawiec, and L. F. Rooney. p. A1–A19. B, Supply of nonfuel minerals and materials for the United States energy industry, 1975–90, by G. H. Goudarzi, L. F. Rooney, and G. L. Shaffer. p. B1–B37. 1976. $1.70. (Reprint.)

Bulletins

B 1418. Weak-field magnetic susceptibility anisotropy and its dynamic measurement, by W. F. Hanna. 1977. 73 p. $1.

B 1420. Mineral resources of the La Garita Wilderness, San Juan Mountains, southwestern Colorado, by T. A. Steven and C. L. Bieniewski, *with a section on* Geophysical interpretation, by G. P. Eaton. 1977. 65 p.; plates in pocket. $2.

B 1421–C. The volumetric properties of aqueous sodium chloride solutions from 0° to 500°C at pressures up to 2000 bars based on a regression of available data in the literature, by R. W. Potter II and D. L. Brown. 1977. p. C1–C36. 70¢.

B 1422–A. Changes in stratigraphic nomenclature by the U.S. Geological Survey, 1975, by G. V. Cohee and W. B. Wright. 1976. p. A1–A84. $1.15.

B 1422–D. Nomenclature of Precambrian rocks in Colorado, by Ogden Tweto. 1977. p. D1–D22. 45¢.

B 1424. Natural conditions that control landsliding in the San Francisco Bay region—an analysis based on data from the 1968–69 and 1972–73 rainy seasons, by T. H. Nilsen, F. A. Taylor, and R. M. Dean. 1976 (1977). 35 p.; plate in pocket. $1.95.

B 1427. Surficial geologic history of the Canyon Village quadrangle, Yellowstone National Park, Wyoming, for use with Map I–652, by G. M. Richmond. 1976. 35 p. 65¢.

Water-Supply Paper

W 2037. Hydrologic changes after logging in two small Oregon coastal watersheds, by D. D. Harris. 1977. 31 p. 75¢. (Supersedes Open-File Report 76–172).

Back issues of the "Journal of Research of the U.S. Geological Survey" available at reduced prices—for limited time only. Copies of individual issues of volumes 1, 2, 3, and 4, published in 1973–76, are available at $1.25 per issue until December 31, 1977, or sooner if stocks become depleted. Order from U.S. Geological Survey, Branch of Distribution (Book Sales), 1200 South Eads Street, Arlington, VA 22202. Prepayment is required. Make check or money order payable to U.S. Geological Survey.

TECHNICAL INFORMATION OFFI
U S GEOLOGICAL SURVEY TOPO DI
NATIONAL CENTER STOP 520
RESTON VA 22092